Calcium signalling and calcium pools in a *Drosophila* epithelium

A thesis submitted for the degree of
Doctor of Philosophy at the University of Glasgow

By

Tony David Southall

Division of Molecular Genetics

Institute of Biomedical and Life Sciences

University of Glasgow

Glasgow

G11 6NU

UK

November 2003

ProQuest Number: 10800580

ProQuest 10800580

Published by ProQuest LLC (2018). Copyright of the Dissertation is held by the Author.

ProQuest LLC.
789 East Eisenhower Parkway
P.O. Box 1346
Ann Arbor, MI 48106 – 1346

The research reported within this thesis is my own work
except where otherwise stated, and has not been
submitted for any other degree

Tony David Southall

Abstract

The *Drosophila* Malpighian tubule is an ideal model epithelium for the study of fluid transport and cell signalling. The tubule is the primary osmoregulatory tissue in the fly and Ca^{2+} signalling plays a critical role in controlling the fluid secretion rate of this organ. This project describes the use of powerful transgenic and fluorescent reporter techniques to further understand the mechanics of Ca^{2+} signalling in the cells of this tissue. In particular, the contribution of internal Ca^{2+} stores to the diuretic peptide-induced Ca^{2+} signals has been investigated.

In an attempt to unravel the role of the ER in these signals, an approach involving the Ca^{2+} sensitive photoprotein aequorin was undertaken. Transgenic flies were generated that could express ER-targeted aequorin; this in theory would have allowed real-time measurements of $[Ca^{2+}]_{ER}$ in tubules during agonist stimulation. Unfortunately this method is presently not achievable in *Drosophila*, due to problems with targeting signals and the retention properties of the insect ER. As an alternative strategy a fluorescent Ca^{2+} reporter was developed that is targeted and functional in the ER. Transgenic flies were generated that could express this new reporter, ERpicam, in a cell specific manner. This has allowed real-time monitoring of $[Ca^{2+}]_{ER}$ levels in a live intact tissue during stimulation with neuropeptides. The results were surprising, as they imply that the ER plays no role in the generation of IP_3-induced Ca^{2+} signals in some cells of the tubule.

The impact of these Ca^{2+} signals on mitochondrial Ca^{2+} levels was also investigated using targeted aequorin and new improved targeted fluorescent reporters. Mitochondria in the tubule do take up Ca^{2+} during the signalling events, however, the dynamics of this uptake are in contrast with the majority of data collected in other cell systems. Both the aequorin and fluorescent reporter techniques revealed that $[Ca^{2+}]_{mt}$ levels in both cell types of the tubule do not increase in conjunction with the primary IP_3-induced component of the signal but instead with the slower secondary response.

This project also describes the identification and characterisation of the *Drosophila* secretory pathway Ca^{2+}/Mn^{2+} ATPase (SPCA). The discovery that this multiply-spliced ATPase is targeted to multiple organelles will have important implications for further understanding of Ca^{2+} and Mn^{2+} transport in all cellular systems. Furthermore, it has uncovered roles for this protein in tubule function and has proved to be a powerful tool for dissecting the Ca^{2+} signals in this tissue through overexpression studies. Most interestingly, overexpression of a Golgi-localised SPCA results in a potentiation of IP_3-induced Ca^{2+} increases in cells of the tubule, implying that this organelle plays a significant role in generating these responses.

During the initial investigation of the *Drosophila* SPCA, development of a new gene knock-in method for *Drosophila* was theorised in an attempt to elucidate the expression and function of the SPCA. This technology is based on spliceosome-mediated *trans-splicing*. It can allow specific targeting of pre-mRNAs in transgenic *Drosophila* and enable reprogramming of the mature mRNA. The system has been adapted and successfully demonstrated in transgenic flies, however further work and refinement is needed before it can be used as a generic tool.

These approaches have made significant advances into understanding the unusual Ca^{2+} signalling events of this epithelium and this work can be continued to gain further insight into how renal function is controlled in *Drosophila* and higher organisms.

Abbreviations

Ach	acetylcholine
AEQ	aequorin
APS	ammonium persulphate
ATP	adenosine triphosphate
ATPase	adenosine triphosphatase
BDGP	Berkeley *Drosophila* Genome Project
BHQ	tert-butylhydroquinone
BLAST	basic local alignment search tool
bp	base pairs
BSA	bovine serum albumin
C-	carboxy-
Ca^{2+}	calcium
$[Ca^{2+}]$	calcium concentration
$[Ca^{2+}]_{ER}$	endoplasmic reticulum calcium concentration
$[Ca^{2+}]_{Golgi}$	Golgi apparatus calcium concentration
$[Ca^{2+}]_i$	intracellular calcium concentration
$[Ca^{2+}]_{lysosome}$	lysosomal calcium concentration
$[Ca^{2+}]_{mt}$	mitochondrial calcium concentration
CAP_{2b}	cardioacceleratory peptide 2b
CCE	capacitative calcium entry
CICR	calcium induced calcium release
CNG	cyclic nucleotide gated channel
CPA	cyclopiazonic acid
CTS	calreticulin signal
CRF	corticotropin-releasing factor
CTP	cytosine triphosphate
cAMP	3'-5' cyclic adenosine monophosphate
cDNA	complementary DNA
cGK	cGMP-dependent kinase
cGMP	3'-5' cyclic guanosine monophosphate
cpGFP	circularly permuted GFP
DAB	3,3-diaminobenzamidine
DAG	diacylglycerol
DAPI	4,6-diamidino-2-phenylindole, dilactate

DEPC	diethyl pyrocarbonate
DIG	digoxigenin
DMF	dimethylformamide
DMSO	dimethylsulfoxide
DNA	deoxyribonucleic acid
DTT	dithiothreitol
dATP	2' deoxyadenosine triphosphate
dCTP	2' deoxycytosine triphosphate
dGTP	2' deoxyguanosine triphosphate
dLKR	*Drosophila* leucokinin receptor
dNTP	2' deoxy (nucleotide) triphosphate
dTTP	2' deoxythymidine triphosphate
dUTP	2' deoxyuridine triphosphate
EC_{50}	concentration for 50% excitation
ECFP	enhanced yellow fluorescent protein
EYFP	enhanced cyan fluorescent protein
EDTA	ethylenediamine tetra acetic acid
EGTA	ethylene glycol bis tetracetic acid
ER	endoplasmic reticulum
EST	expressed sequence tag
EtBr	ethidium bromide
FCS	foetal calf serum
FRET	fluorescence resonance energy transfer
g	gram
g	centrifugal force equal to gravitational acceleration
GFP	green fluorescent protein
G-protein	guanine nucleotide-binding protein
GPCR	G-protein-coupled receptor
h	hours
HBS	HEPES buffered saline
HEPES	N-((2-hydroxylethyl) piperazine-N'-(2-ethanesulphonic acid))
HRP	horseradish peroxidase
I_{ARC}	arachidonate-regulated Ca^{2+} channel
ICC	immunocytochemistry
IP_3	inositol 1,4,5-trisphosphate
IP_3R	inositol 1,4,5-trisphosphate receptor

IPTG	isopropyl β-D-thiogalactoside
Kb	kilobases
kDa	kiloDaltons
lacZ	β-galactosidase
M	molar
MBSU	Molecular Biology Support Unit
MOPS	3-(N-morpholino)propane-sulphonic acid
mg	milligram
min	minutes
MIP	major intrinsic family
ml	millilitre
mm	millimetre
mM	millimolar
Mn^{2+}	manganese
MPS	mitochondrial pre-targeting sequence
mRNA	messenger RNA
N-	amino-
NHE	Na^+/H^+ exchanger
NMDA	N-methyl-D-aspartic acid
NO	nitric oxide
NOS	nitric oxide synthase
ng	nanograms
nm	nanometre
nM	nanomolar
OD	optical density
ORF	open reading frame
PAGE	polyacrylamide gel electrophoresis
PAT	PBS, Triton X-100, BSA
PBS	phosphate buffered saline
PBT	PBS, Triton X-100
PCR	polymerase chain reaction
PDE	phosphodiesterase
PIP_2	phosphatidylinositol 4,5-bisphosphate
PKC	protein kinase C
PLC	phospholipase C
PMCA	plasma membrane calcium ATPase

PMSF	phenylmethylsulphonylfluoride
PTM	pre-*trans*-splicing RNA molecule
RLU	relative light unit
RNA	ribonucleic acid
RNAi	RNA interference
RNAse	ribonuclease
ROC	receptor-operated calcium channel
RT	room temperature
RT-PCR	reverse transcriptase polymerase chain reaction
RYR	ryanodine receptor
s	second
SDS	sodium dodecyl sulphate
S.E.M.	standard error of the mean
SERCA	sarco(endo)plasmic reticulum
SMaRT	spliceosome-mediated *trans*-splicing
SMOC	second messenger-operated channels
SOC	store-operated calcium channel
SOD	superoxide dismutase
SOCE	store-operated calcium entry
SPCA	secretory pathway calcium ATPase
SR	sarcoplasmic reticulum
ST	sialyltransferase
TBE	tris-borate EDTA
TE	tris-EDTA
TEMED	N,N,N',N'-tetramethylethylenediamine
Tris	2-amino-2-(hydroxymethyl)-1,3-propanediol
TRP	transient receptor protein
U	unit
UAS	upstream activating sequence
UTP	uridine triphosphate
UTR	untranslated region
UV	ultraviolet
V-ATPase	vacuolar-type H^+ adenosine triphosphatase
VOC	voltage-operated channel
X-gal	5-bromo-4-chloro-3-indolyl-β-D-galactopyranoside
μg	microgram

μl	microlitre	
μM	micromolar	
°C	degrees Celsius	
3' ER	3' exon replacement	
5' ER	5' exon replacement	

One and three amino acid codes:

A	Ala	Alanine		N	Asn	Asparagine
C	Cys	Cysteine		P	Pro	Proline
D	Asp	Aspartic acid		Q	Gln	Glutamine
E	Glu	Glutamic acid		R	Arg	Arginine
F	Phe	Phenylalanine		S	Ser	Serine
G	Gly	Glycine		T	Thr	Threonine
H	His	Histidine		V	Val	Valine
I	Ile	Isoleucine		W	Trp	Tryptophan
K	Lys	Lysine		Y	Tyr	Tyrosine
L	Leu	Leucine		*	Stop	
M	Met	Methionine				

Table of Contents

Index of Figures

Chapter 5 Identification and characterisation of the *Drosophila* Secretory Pathway Calcium ATPase

Figure

Chapter 6 Developing a new gene knock-in technology for *Drosophila* based on *trans*-splicing

Chapter 7 Future work and summary

Index of Tables

Acknowledgements

There are many people who I would like to thank for their help and support throughout my time in Glasgow. Firstly I would like to thank my supervisors Shireen Davies and Julian Dow for their advice and encouragement throughout my PhD.

I would also like to thank everyone within the Dow/Davies group, past and present, for their help and also for making my time in and out of the lab so enjoyable. I would particularly like to thank Maria and Big Jon Radford for teaching me molecular biology, Matt for helping me with Ca^{2+} assays and skiing in Italy, Val and Leah for assistance with secretion assays and Tall Jon Day for his general help, advice and excellent singing voice. I also very grateful to Big Jon, Maria and Selim for their time spent reading my thesis.

I would like to thank all of Michael White's group in Liverpool, especially Michael, Dave Spiller and Violaine See for their help and making me feel welcome. Thanks also goes to Godfrey Smith for his help with the reporters and for his advice on aspects of Ca^{2+} signalling.

I am very grateful to the BBSRC for funding my PhD, and also to my assessors, Billy Martin and Graham Brock for their help and advice throughout the 3 years.

I would also like to give a big thank you to my dad and my superb siblings, Slugger, Fat Ted and Birdy for supporting me in everything I have done. A special thanks goes to my mum and dad for bringing me up and for making me who I am today. A huge thanks goes to my brilliant and gorgeous girlfriend Maria for her support, encouragement and love over the last few years. Finally, I would like to dedicate this thesis to my dear mum who sadly passed away during my PhD.

Chapter 1

Introduction

1.1 Ca^{2+} signalling

1.1.1   Ca^{2+} as a signalling molecule

Calcium (Ca^{2+}) is a ubiquitous second messenger involved in numerous cellular responses, such as fertilisation, muscle contraction, proliferation, differentiation, secretion and epithelial renal function (Galione et al., 1991; Ebashi and Endo, 1968; Dolmetsch et al.,1997; Gu and Spitzer, 1995; Petersen, 1992; Rosay et al., 1997). To allow Ca^{2+} to act as a second messenger within the cell for multiple responses, the concentration of Ca^{2+} has to be tightly controlled, both spatially and temporally. This is achieved by Ca^{2+} pumping, Ca^{2+} buffering and the low diffusibility of the molecule. Ca^{2+} concentration at resting state is approximately 100 nM in the cytoplasm ([Ca^{2+}]$_i$), ~500 µM in the endoplasmic reticulum (ER) (Montero et al., 1997; Barrero et al., 1997) and ~300 µM in the Golgi (Pinton et al., 1998). The concentration of external Ca^{2+} is generally within the mM range. As the [Ca^{2+}]$_i$ is so low compared to the extracellular and internal store concentrations, the cell has to continuously pump Ca^{2+} out of the cytoplasm by using Ca^{2+} ATPases on the plasma membrane, the ER and the Golgi.

1.1.2 The control of diverse cellular functions by Ca^{2+} signals

The speed, amplitude and spatio-temporal patterning of Ca^{2+} release/entry allow for the versatility required for a single second messenger to control so many processes. An example of the temporal versatility is the Ca^{2+} triggered exocytosis at synaptic junctions, which occurs within microseconds. This is contrast to the [Ca^{2+}]$_i$ increases that control events such as gene transcription and the cell cycle, which last several minutes. The spatial flexibility of Ca^{2+} events is demonstrated in smooth muscle cells. High [Ca^{2+}]$_i$ increases cause contraction of the cell (Ebashi and Endo, 1968), whereas smaller, more localised 'sparks' of Ca^{2+} activate Ca^{2+}-dependant potassium channels, causing hyperpolarisation and relaxation of the cell (Nelson et al., 1995).

The frequency and amplitude of Ca^{2+} oscillations can control diverse biological systems, such as fluid secretion rate in the salivary gland of *Calliphora erythrocephala* (Rapp and Berridge, 1981), neural differentiation in *Xenopus* embryonic neurons (Gu and Spitzer, 1993) and has been implicated in memory and learning behaviour in *Drosophila* (Rosay et al., 2001). The single secretory granule (acrosome) in human sperm has been shown to act as a functional Ca^{2+} pool (De Blas et al., 2002). The acrosome causes a localised [Ca^{2+}]$_i$ increase, by releasing internal stores to activate its own exocytosis upon interaction with the oocyte. Furthermore, B-lymphocytes respond to antigens with different amplitudes of Ca^{2+} responses with respect to whether they have encountered it before (Healy et al., 1997). Whether it is a large (naive B lymphocyte) or a small (tolerant B lymphocyte)

$[Ca^{2+}]_i$ increase determines which specific transcription factors are activated for the appropriate cellular response.

It is evident that cellular machinery can manipulate $[Ca^{2+}]_i$ spatially and temporally to control a vast array of different biological processes. These control mechanisms are discussed in the next section.

1.1.3 Mechanisms of Ca^{2+} signalling

The Ca^{2+} ATPases and Ca^{2+} buffering proteins (such as calreticulin) play an important role in the 'off' reactions within a cell to remove Ca^{2+} from the cytoplasm. Conversely the inositol 1,4,5–trisphosphate receptor (IP_3Rs) channels, ryanodine receptor (RyRs) channels and plasma membrane Ca^{2+} channels all contribute to 'on' reactions to allow Ca^{2+} to enter the cytoplasm, either from internal stores or the external medium (see figure 1.2).

A typical cellular Ca^{2+} response involves an extracellular ligand (such as a hormone/ peptide/ neurotransmitter) binding to a receptor on the plasma membrane. This induces a conformational change in the receptor thus activating a heterotrimeric G-protein, which then goes on to activate phospholipase C (PLC). PLC catalyses the hydrolysis of phosphatidylinositol 4,5-bisphosphate (PIP_2) to diacylglycerol (DAG) and inositol 1,4,5-trisphosphate (IP_3). IP_3 then binds to IP3R channels on the ER, causing release of Ca^{2+} into the cytoplasm (for review see Berridge, 1993, also see figure 1.1).
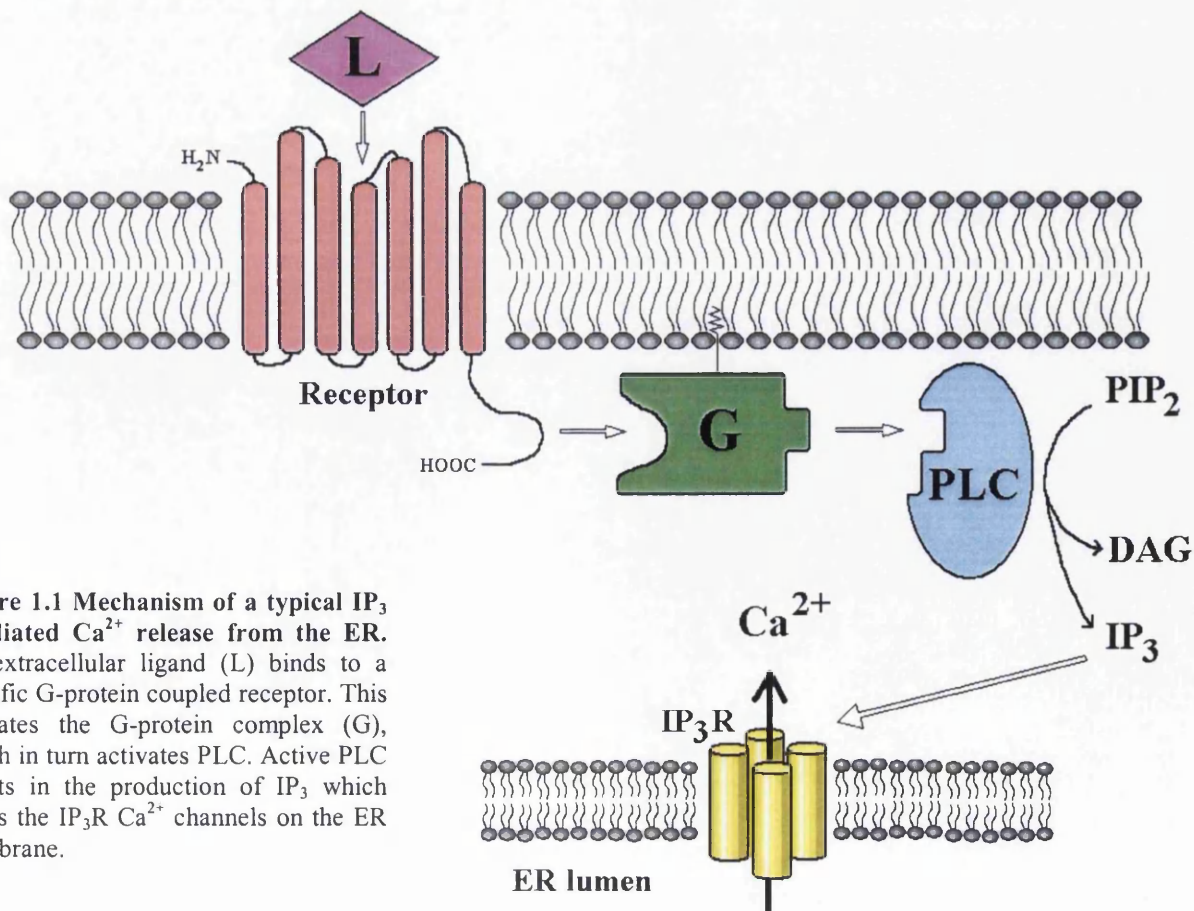
Figure 1.1 Mechanism of a typical IP_3 -mediated Ca^{2+} release from the ER. An extracellular ligand (L) binds to a specific G-protein coupled receptor. This activates the G-protein complex (G), which in turn activates PLC. Active PLC results in the production of IP_3 which opens the IP_3R Ca^{2+} channels on the ER membrane.
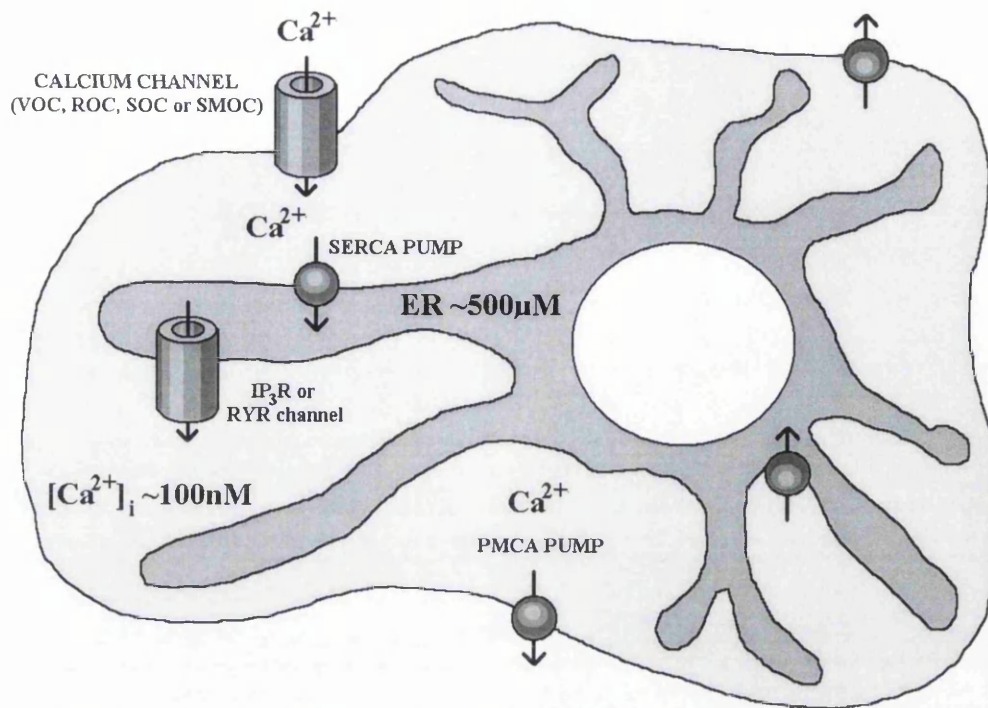
Figure 1.2 The basic elements that control $[Ca^{2+}]_i$. The plasma membrane Ca^{2+} ATPase (PMCA) pumps Ca^{2+} from the cytoplasm into the extracellular space. The sarco/endoplasmic reticulum Ca^{2+} ATPase (SERCA) pumps Ca^{2+} from the cytoplasm into the endoplasmin reticulum (ER). The voltage-operated (VOC), receptor-operated (ROC), store-operated (SOC) and second messenger-operated (SMOC) channels allow influx of extracellular Ca^{2+}. Inositol 1,4,5-trisphosphate receptor channels (IP_3Rs) and ryanodine receptor channels (RyRs) allow release of ER Ca^{2+}.
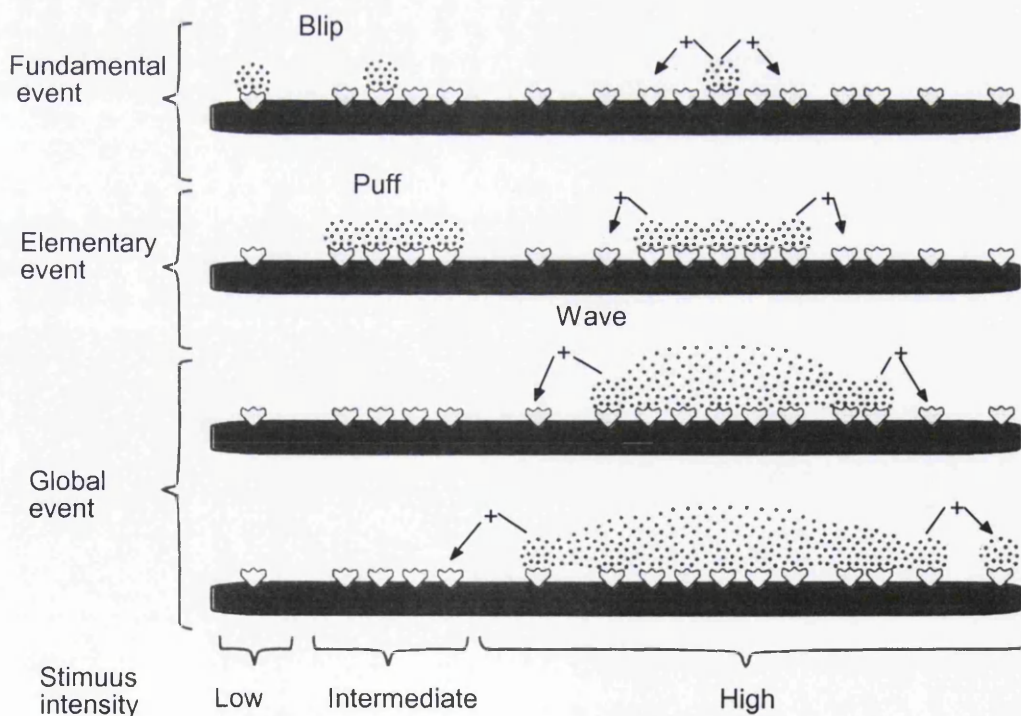
Figure 1.3 A hierarchical organisation of intracellular calcium signalling.
The stimulus intensity seems to determine which events are elicited. Fundamental events are the consequence of opening single intracellular channels to give blips. Elementary events, represented by puffs, result from the concerted opening of small groups of IP_3Rs. These elementary events appear to be the building blocks of the global events, which develop as a wave resulting from the progressive recruitment of neighbouring receptors through a process of Ca^{2+}-induced Ca^{2+} release (CICR). [Figure is taken from Berridge, 1997.

This depletion of Ca^{2+} from intracellular stores invariably leads to an influx of Ca^{2+} from the extracellular medium. The process by which this store depletion activates Ca^{2+} entry has been termed capacitative Ca^{2+} entry (CCE) (Putney, 1986) or store operated Ca^{2+} entry (SOCE) (for review see Berridge, 1995). In excitable cells, an interaction between the RyR on the sarcoplasmic reticulum (SR) and the voltage-operated channel (VOC) on the plasma membrane initiate the Ca^{2+} influx (Chavis et al., 1996). Surprisingly, the mechanism of SOCE in non-excitable cells has yet to be elucidated, though several models have been proposed. These include the small diffusible messenger model (Randriamampita et al, 1993; Parekh et al., 1993), functional interaction between the IP_3R channel and the store-operated Ca^{2+} channel (SOC) (Kiselyov et al, 1998) and the vesicle insertion model (Yao et al., 1999; Patterson et al., 1999). The small diffusible messenger model suggests that a messenger molecule is released from the depleted store, which activates opening of plasma membrane channels. The vesicle insertion model suggests that active Ca^{2+} channels are present in vesicular structures close to the plasma membrane and upon depletion of stores, they insert the channels into the membrane. There is evidence supporting all three of these models in various cell systems; however there is mounting evidence against a diffusible messenger model and now more evidence to support the functional interaction model (for review see Elliot, 2001).

Influx of extracellular Ca^{2+} occurs through plasma membrane channels and some of the various methods of activation are mentioned above. Voltage-operated channels (VOCs) are generally located in neural or innervated muscle tissues, they generate the rapid Ca^{2+} influxes that control fast cellular processes like muscle contraction and exocytosis at synaptic endings (for review see Weiss and Burgoyne, 2002). The receptor-operated channels (ROCs) act in a very direct manner, opening of the channel is triggered by binding of an extracellular ligand such as glutamate (MacDermot et al., 1986) or ATP (Valera et al., 1994). There are also the second messenger-operated channels (SMOCs), which include cyclic nucleotide gated channels (for review see Broillet and Firestein, 1999) and the arachidonate-regulated Ca^{2+} channel (I_{ARC}) (Mignen and Shuttleworth, 2000). Furthermore, the diverse transient receptor protein (TRP) ion-channel family are Ca^{2+} channels that can be activated by stimuli such as temperature, cell stretching or internal Ca^{2+} store depletion (SOCE) (for reviews see Minke and Cook, 2002; Montell et al., 2002).

The hierarchical organisation of intracellular Ca^{2+} signalling is shown in figure 1.3. These events occur and propagate due to the process of Ca^{2+} induced Ca^{2+} release (CICR), which is dependant on the IP_3Rs and RyRs being sensitive to Ca^{2+} itself (for review see Berridge, 1997). A fundamental event is due to the opening of a single IP_3R channel to give a 'blip'

of Ca^{2+} release from the ER. Elementary events arise from the opening of small groups of channels to give 'puffs' of Ca^{2+} release. These elementary events can instigate Ca^{2+} waves because of the activation of channels by Ca^{2+}, these waves can pass through the whole cell in a global event. These events were first observed in HeLa cells (Bootman et al., 1997) and this mechanism of CICR explains the Ca^{2+} wave that propagates through the well studied polarised pancreatic acinar cell (Osipchuk et al., 1990; Kasai et al., 1990; Bird et al., 1991). Ca^{2+} can enter the cell through dynamically controlled channels, other second messengers can trigger Ca^{2+} release from intracellular pools and even Ca^{2+} itself can trigger its own release from these stores. The nature of these Ca^{2+} stores is discussed in the next section.

1.1.4   Intracellular Ca^{2+} pools

1.1.4.1 ER Ca^{2+} pool

The ER is a dynamic signalling organelle, that in addition to controlling the entry and release of Ca^{2+}, plays an important role in protein synthesis, sterol biosynthesis and apoptosis (for review see Berridge, 2002). The high $[Ca^{2+}]_{ER}$ is maintained by Ca^{2+}-transporting ATPases of the sarco(endo)plasmic reticulum Ca^{2+}-ATPase (SERCA) family (Lytton et al., 1991). Ca^{2+}-binding proteins such as calreticulin reside in the ER to assist in storing the high quantity of Ca^{2+}, to buffer levels and also to control Ca^{2+} uptake and release proteins on the ER membrane (for review see Johnson et al., 2001). The high Ca^{2+} is required to provide a releasable pool (through IP$_3$Rs and RyRs) for signalling events and to provide the correct environment for protein folding.

The Ca^{2+} signalling role of the ER has been extensively studied in pancreatic acinar cells; the organelle resides predominantly in the basolateral region of the cell with fine tendrils of ER extending into the apical side (for review see Ashby and Tepikin, 2002). The ER is able to provide localised agonist-induced $[Ca^{2+}]_i$ increases in the apical region by specific localisation of IP$_3$Rs on its membrane. Additionally, it has been demonstrated that the ER (at least in pancreatic acinar cells) is a functionally continuous Ca^{2+} pool; Ca^{2+} released from the apical region of ER can be replenished from the larger basolateral region of the ER (Park et al., 2000).

1.1.4.2 Golgi apparatus Ca^{2+} pool

The Golgi apparatus was first observed to contain high Ca^{2+} levels by Chandra et al., 1994 and it was demonstrated by Pinton et al., 1998, using a targeted aequorin approach, that it was a functional IP$_3$-sensitive intracellular Ca^{2+} store. It was shown that the Golgi had resting levels of Ca^{2+} of ~300µM, which were only partially sensitive to thapsigargin (a

potent SERCA inhibitor). Furthermore, calreticulin was not acting as a Ca^{2+} storage protein in the Golgi. CALNUC (nucleobindin) is a resident Golgi protein that has been shown to involved in Ca^{2+} storage and release (Lin et al., 1999) and has a similar role to that of calreticulin in the ER. Moreover, it has been reported that Golgi luminal Ca^{2+} participates in controlling key processes that occur in the organelle, such as post-translational modification and protein sorting and trafficking (Carnell and Moore, 1994; Duncan and Burgoyne, 1996).

Maintenance of Golgi Ca^{2+} levels appears to be in part dependent on SERCA activity (Pinton et al., 1998). There is growing evidence that the other thapsigargin insensitive component of Golgi Ca^{2+} uptake may be a homologue of the yeast Ca^{2+}/Mn^{2+} ATPase, PMR1. These Ca^{2+} ATPases are similar to the SERCA and PMCA pumps, however they form a discrete group known as the secretory pathway Ca^{2+} ATPases (SPCA). All studies, to date have shown that these ion pumps localise to the Golgi apparatus and possess distinct biochemical and functional properties (for more detail see chapter 5).

1.1.4.3 Mitochondrial uptake of Ca^{2+}

Mitochondria and Ca^{2+} have an intimate relationship, while Ca^{2+} signals can control mitochondrial activity (Jouaville et al., 1999), mitochondria play an important role in shaping and controlling intracellular Ca^{2+} signalling (Gilabert and Parekh, 2000). Uptake of Ca^{2+} into mitochondria is not reliant upon ATP but occurs through an electrogenic transporter (Gunter et al., 1990). This 'Ca^{2+} uniporter' has not yet been characterised at a molecular level. Export of Ca^{2+} from the mitochondria is via a Na^{+}/Ca^{2+} exchanger (Jung et al., 1995). Targeted aequorin and luciferase were used to measure Ca^{2+} levels and ATP levels in mitochondria (Jouaville et al., 1999). It was shown that accumulation of Ca^{2+} in the mitochondria activates the metabolic machinery, therefore increases the levels of ATP. Additionally, the amount of ATP produced was dependant on the amount of Ca^{2+} accumulated, which is probably related to the Ca^{2+} sensitivity of the matrix dehydrogenases. Mitochondria also buffer and redistribute Ca^{2+} within the cell; Gilabert and Parekh (2000) elegantly demonstrated how mitochondria are important in the process of store operated Ca^{2+} entry. The mitochondria are coupled or in very close proximity to the ER (Rizzuto et al., 1998) and upon release of Ca^{2+} from the ER store, the mitochondria accumulate a lot of this released Ca^{2+}. SOCE is activated by store levels depleting below a certain threshold; however, if the mitochondria are blocked from taking up Ca^{2+} then the released Ca^{2+} is immediately recovered by the store and the levels do not deplete sufficiently to activate SOCE. More recent work has demonstrated a more complex interaction between mitochondria and SOCE (Glitsch et al., 2002). Evidence against the

control of SOCE by increased ER refilling and Ca^{2+}-dependent negative feedback was shown and a model was proposed that involved the Ca^{2+}-dependent release of a mitochondrial factor that can control SOCE.

1.1.4.4 Lysosomal Ca^{2+} pool

Lysosomes and lyosomal-related organelles have recently emerged as functional Ca^{2+} stores in various cell types. There is an IP$_3$-sensitive lysosomal Ca^{2+} in Madin-Darby canine kidney (MDCK) cells (Haller et al., 1996), an agonist and thapsigargin insensitive lysosomal store in *Drosophila melanogaster* S2 cells (Yagodin et al., 1999), the acrosomal Ca^{2+} in human sperm (De Blas et al., 2002) and the lysosome-related reserve granules in sea urchin eggs (Churchill et al., 2002). The uptake and release mechanisms for these pools vary between cell types, though generally uptake of Ca^{2+} into these acidic organelles generally appears to be via a Ca^{2+}/H^+ exchanger that is driven by a proton V-ATPase (Yagodin et al., 1999; Churchill et al., 2002).

It is evident that various intracellular organelles act as dynamic Ca^{2+} pools, that can functionally interact with each other to control and shape the Ca^{2+} signalling events which control a vast array of cellular functions.

1.2 Ca^{2+} reporters

1.2.1 Synthetic Ca^{2+} indicators

The first rationally designed fluorescent reporters for Ca^{2+} were synthesised by Roger Tsien (Tsien, 1980). The design was based on the Ca^{2+} chelator EGTA, in which the methylene groups of EGTA were replaced with two benzene rings, allowing it to function as a chromophore. The conformational change caused by the Ca^{2+} binding altered the chromophore, therefore altering the excitation and/or emission of the dye. Improved derivatives of this design evolved to give quin-2 (Tsien et al., 1982), the ratiometric fura-2 (Grynkiewicz et al., 1985) and other variants with different Ca^{2+} sensitivities. The development of polycarbonate dyes that could be incubated with acetoxymethyl esters allowed the ester-dye complex to be taken up by the cell in a non-invasive manner (intracellular cleavage by cellular esterases releases the hydrophilic dye) (Tsien, 1981). Although these Ca^{2+} indicators are easy to use, they only function transiently, they cannot be targeted to organelles (apart from mitochondrial rhod-2 (Minta et al., 1989)) and in some cases are actively transported out of the cell/tissue e.g., the *Drosophila* Malpighian tubule (Dow and Cheek, unpublished).

1.2.2 The photoprotein aequorin

Aequorin is a chemiluminescent protein from the jellyfish *Aequorea victoria* that emits photons upon binding to Ca^{2+} (Shimomura et al., 1962). Until the cDNA for (apo)aequorin was isolated (Prasher et al., 1985), the protein had to be carefully extracted from the jellyfish and micro-injected into cells. Apoaequorin could then be expressed in cells, incubated with the ligand coelenterazine to form active aequorin (fig.1.4) and then the luminescence measured using a photon-multiplier device. Further understanding of this reaction has been aided by the recent solving of the crystal structure of aequorin (Head et al., 2000). Aequorin was found to be a globular molecule containing a hydrophobic core cavity that holds the ligand coelenterazine-2-hydroperoxide. The structure also showed domains that help stabilise the peroxide and suggest a mechanism for how Ca^{2+} activates the luminescent reaction.

Aequorin allows for monitoring of changes in Ca^{2+} levels; however, it also allows quantitative measurements of Ca^{2+}. During an experiment using aequorin, the Ca^{2+} concentration at a time t is proportional to the light emitted at time t divided by the total remaining luminescence in the sample (for a more detailed description see Button and Eidsath, 1996). This allows retrospective calculation of Ca^{2+} concentrations after all the luminescence has been discharged.

Recombinant expression of aequorin introduced a new concept in the Ca^{2+} reporter field as it allowed intracellular localisation of the reporter, using specific signal sequences to organelles such as the mitochondria (Rizzuto et al., 1992), the ER (Montero et al., 1995) and the Golgi (Pinton et al., 1998). Additionally it has enabled real-time monitoring of $[Ca^{2+}]_i$ in live tissues by using a transgenic approach, in plants (Knight et al., 1991) and in *Drosophila* (Rosay et al., 1997). Due to the limited photon-emitting abilities of aequorin, the amount of photons emitted from a cell population is adequate for fast measurements of Ca^{2+}, however it is not sufficient for single cell imaging of Ca^{2+} events (apart from large cells such as oocytes).

AEQUORIN   **APOAEQUORIN**

$3\ Ca^{2+}$

(very fast)

(slow)

coelenterazine + O_2

$+ CO_2$

$+ h^v{}_{470}$
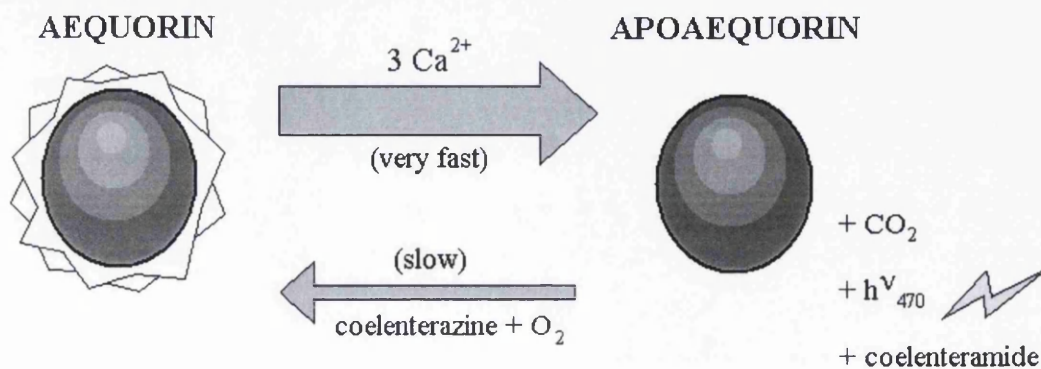
$+$ coelenteramide

Figure 1.4 Aequorin reaction. Reconstitution of apoaequorin with its analogue coelenterazine produces active aequorin. Upon binding of Ca^{2+} ions to aequorin, the molecule reverts back to apoaequorin, producing one photon of light, coelenteramide and CO_2.

1.2.3 Genetically encoded fluorescent indicators for Ca^{2+}

The advantages of using a genetically encoded fluorescent Ca^{2+} reporter to measure intracellular Ca^{2+} levels include the ability to target the reporter to specific cells and to specific organelles. The photoprotein aequorin can also be targeted in this manner; however an encoded fluorescent reporter does not require a co-factor and can also give a strong enough signal to allow fast real-time imaging of Ca^{2+} changes in a single cell.

The first of these reporters to be developed were the 'cameleons'. They consist of tandem fusions of the cyan-emitting mutant of the green fluorescent protein (ECFP), calmodulin, the calmodulin-binding peptide M13 and the enhanced yellow-emitting mutant of GFP (EYFP) (Miyawaki et al., 1997). Binding of Ca^{2+} to the calmodulin EF hands causes calmodulin to wrap around the M13 domain, which causes an increase in FRET (fluorescence resonance energy transfer) between the two GFPs (see figure 1.5A). As the Ca^{2+} concentration is proportional to the ratio of fluorescence emitted at two different wavelengths, it is possible to quantify Ca^{2+} concentrations using this reporter as well as just observing Ca^{2+} changes. However the cameleons have limited signal intensity and the signal-to-noise ratio is low. Truong et al., 2001 developed an improved cameleon that possessed a greater FRET dynamic range, again though the signal-to-noise ratio is not exceptional. Transgenic approaches have allowed the utilisation of cameleons to study Ca^{2+} transients in C. elegans (Kerr et al., 2000) and also Drosophila (Fiala et al., 2002).

The second form of encoded Ca^{2+} reporter to be developed was 'Camgaroo' by Baird et al., 1999. This reporter consists of a circular permuted version of EYFP with calmodulin inserted between the two halves. The reporter's mode of function involves Ca^{2+} binding to the calmodulin domain, this in turn brings the two halves of the permuted EYFP protein closer together, allowing the formation of the fluorophore (see figure 1.5B). This reporter does not allow quantitative measurements (as it had a single excitation and single emission peak spectra) but it does show a large change in fluorescence between Ca^{2+}-bound and Ca^{2+}-free states. Camgaroo's disadvantage is that its sensitivity range (~500nM to ~50μM) is higher than the physiologically significant range (~50nM to ~5μM), large increases in cytoplasmic Ca^{2+} concentrations can be seen but any small or secondary responses are not detected. Nonetheless, transgenic expression of camgaroo in Drosophila has allowed visualisation of Ca^{2+} transients in mushroom body neurons (Yu et al., 2003).

The third form of reporter is also based on a circular permuted GFP (cpGFP). The 'pericams' consist of cpGFP fused to calmodulin and the M13 peptide (Nakai et al., 2001;

Nagai et al., 2001). The binding of Ca^{2+} causes calmodulin to interact with M13, this in turn causes a change in the structure of the protein which leads to an alteration of the environment surrounding the chromophore (see figure 1.5C).
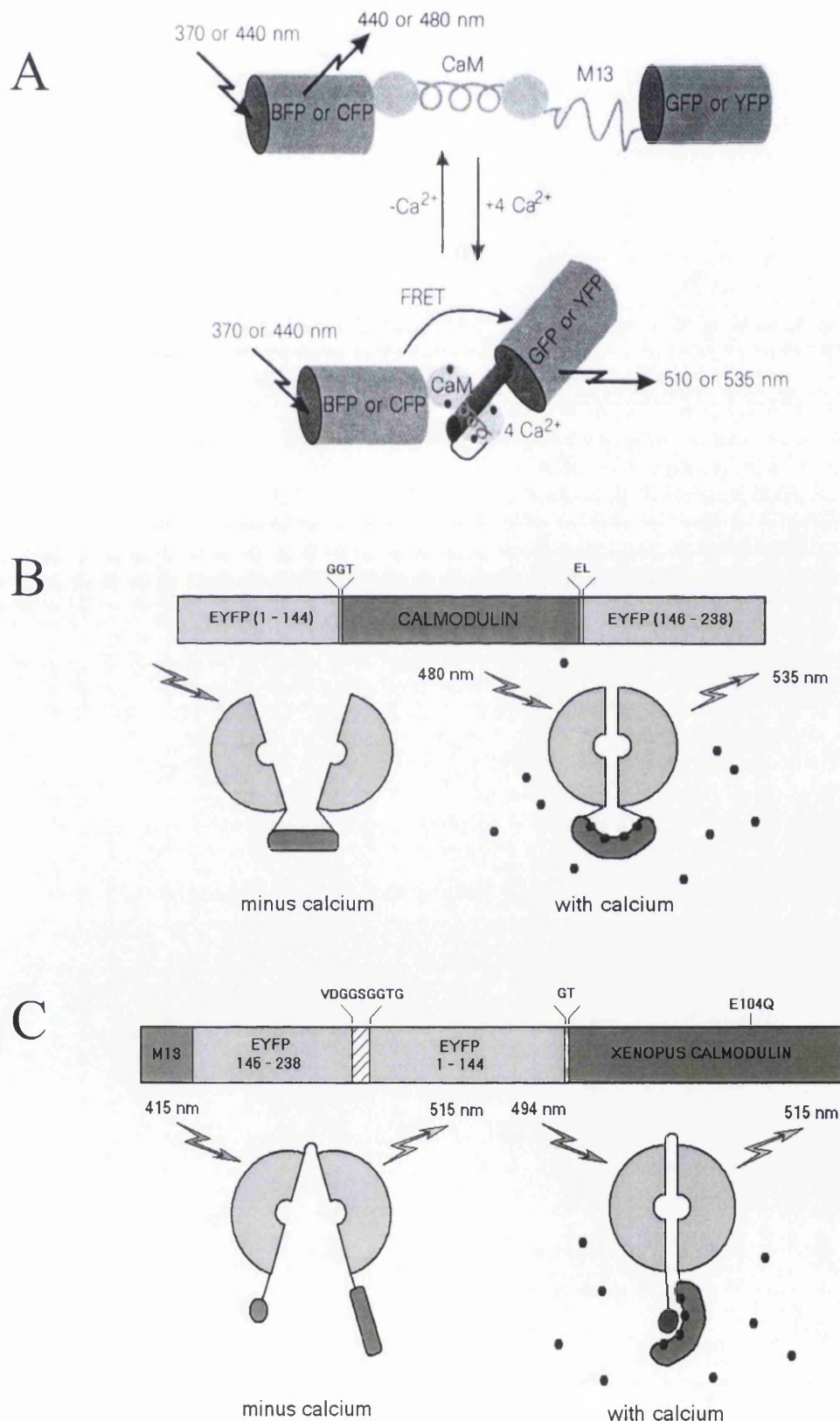
Figure 1.5 Diagrams of the 3 types of genetically encoded fluorescent Ca^{2+} reporters.
(A) cameleon (B) camgaroo (C) ratiometic pericam. Reproduced or modified from Miyawaki *et al.*, 1997; Baird *et al.*, 1999 and Nagai *et al.*, 2001.

Nagai et al. produced pericams that increased in fluorescence when in a Ca^{2+}-bound form (flash pericam), decreased in fluorescence (inverse pericam) and a pericam that changed its excitation wavelength in relation to the Ca^{2+} concentration (ratiometric pericam). The benefit of ratiometric pericam is that it can perform quantitative measurements as well as having a good dynamic range. However, ratiometric pericam, like the cameleons and camgaroo is still very sensitive to pH.

1.3 The *Drosophila melanogaster* Malpighian tubule

1.3.1 *Drosophila* as a genetic model

Drosophila melanogaster is an excellent model organism. Despite its small size, it is an organism that can be easily genetically manipulated and studied, yet still possesses an effective analogy to higher organisms. Due to the short generation time and the ease of culturing, the fruitfly has now been studied extensively for nearly a century. Genetically, *Drosophila* is well defined, with a small (relative to other eukaryotes) genome of approximately 13,600 genes (Adams et al., 2000), arranged in four chromosomes, and a genome project which is complete, covering 120 MB of the *Drosophila* euchromatic portion of the genome (Adams et al., 2000). Polytene chromosomes from *Drosophila* salivary glands make it possible to correlate molecular and cytogenetic maps. Balancer chromosomes can be used to maintain lethal mutations in heterozygotes in a manner that does not require selection in each generation (Rubin and Lewis, 2000).

However the most useful molecular genetic tool available for manipulating *Drosophila* genes, is the presence of transposable elements and especially the use of the P element (Rubin and Spradling, 1982; Spradling and Rubin, 1982). The P element is a transposable element able to mobilise itself within a genome. This transposable element has been modified (O'Kane and Gehring, 1987) and used for a wide variety of applications. These include tagging genes (Lukacsovich et al., 2001, Morin et al.,2001), ectopic expression (Brand and Perrimon, 1994), gene overexpression (Rorth, 1996; Rorth et al., 1998), rescue (Rubin and Spradling, 1982), enhancer trapping (O'Kane and Gehring, 1987), homologous recombination (Rong and Golic, 2000; Rong and Golic, 2001; Rong et al., 2002) and RNAi based gene silencing (Martinek and Young, 2000; Kennerdell and Carthew, 2000; Piccin et al., 2001; Kalidas and Smith, 2002).

This wealth of molecular and genetic tools available for use on *Drosophila* aid researchers in addressing questions of gene identification and function using reverse genetics. Biochemical, cell biology and electrophysiological techniques can also be applied to *Drosophila*, permitting multidisciplinary approaches such as integrative physiology and

functional genomics (Dow and Davies, 2003), developmental biology and neurobiology (Rubin, 1988).

1.3.2 P element technology

1.3.2.1 P element technology and germline transformation

The discovery and utilisation of P elements revolutionised *Drosophila* genetics. They are used as tools in a vast array of genetic, developmental and cell biological studies. The P element is a 2.9kb autonomous transposable element found in natural populations of *Drosophila melanogaster*, with the ability to hop from one chromosomal location to another throughout the genome. Spradling and Rubin were the first to use of P elements to insert recombinant DNA into a random location of the *Drosophila* genome (Spradling and Rubin, 1982). They used a marker gene called *rosy* (ry^+), which encodes for a xanthine dehydrogenase. Mutations in this gene cause an abnormal eye phenotype, which can be easily scored. The idea of this experiment was to introduce a wild-type copy of this gene back into flies with a *rosy* mutant phenotype using P element-mediated transposition. When this P-element vector was injected into syncytial blastoderm embryos that expressed the necessary active transposase enzyme, a high efficiency of transposition was detected by observing a rescue of the eye phenotype. The present method of germline transformation is based on Spradling's and Rubin's work, however the P-element is injected into *white⁻* embryos, the marker gene is the *mini-white⁺* gene and it is usually co-injected with a 'Δ2-3 helper' plasmid that allows transient expression of transposase (see figure 1.6). The use of the helper plasmid enables the P element vector to be injected into embryos that don't express active transposase, ensuring that the P element remains stable after transposition. This technology has led to the development of a wide range of molecular and genetic techniques that were briefly mentioned in the last section.

1.3.2.2 Enhancer trapping

Enhancer trapping is the technique by which a P element with a weak promoter coupled to a reporter gene (eg. *lacZ*), allows the analysis of *cis*-acting patterning information, such as enhancers (Bier et al., 1989; O'Kane and Gehring, 1987). The first generation of enhancer traps involved a weak promoter, such as the P element promoter or the P element transposase promoter coupled to a reporter gene such as the *β*-galactosidase gene (*lacZ*) (O'Kane and Gehring, 1987; Bier et al., 1989). These P elements also have a visible marker such as *rosy⁺* or *mini-white⁺* to permit selection of transformants and plasmid sequences that can be used to rescue flanking genomic DNA from both sides of the P element (Bier et al., 1989). When a P element, such as p{*lacW*} inserts near an enhancer, *lacZ* expression as
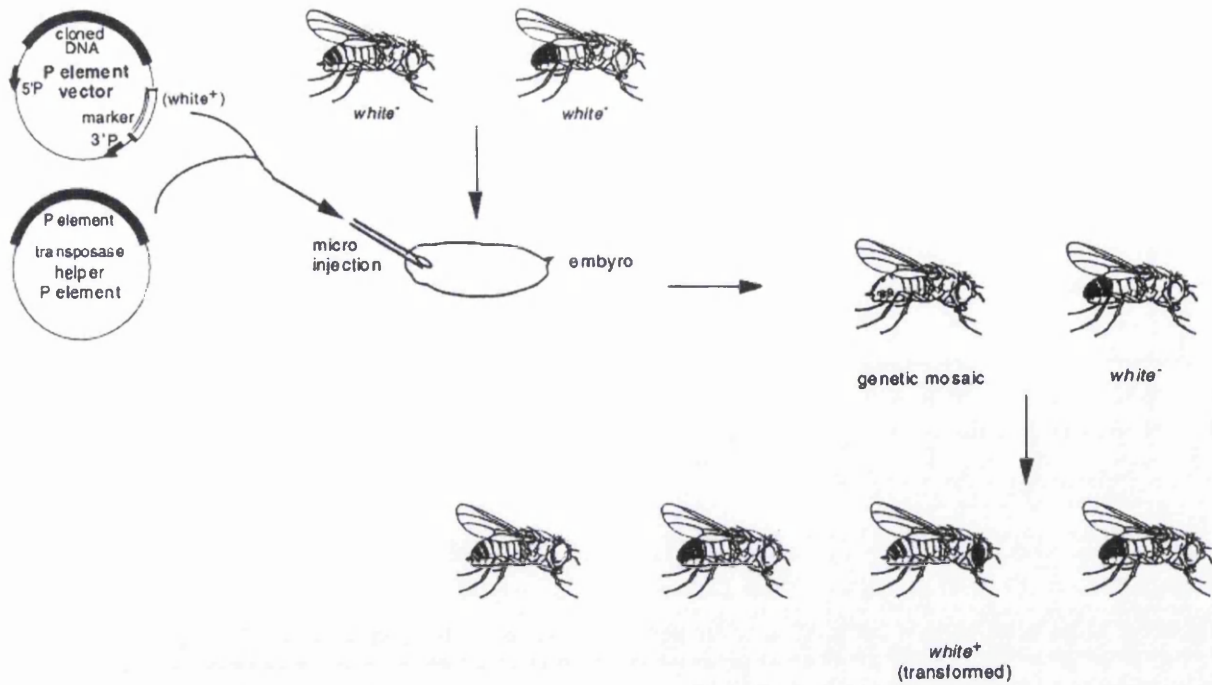
Figure 1.6 Germline transformation of *Drosophila melanogaster*. Reproduced from Guo, 1996. The cloned DNA is inserted into a vector carrying a *white*⁺ marker gene to permit selection of transformed flies. This DNA is then co-injected with a helper plasmid (transposase-producing) into *white* embryos. Adults flies that emerge post injection and potentially have the transposon of interest inserted in their germ cell chromosomes are then crossed back to *white* flies. The progeny of this cross, if transformed have *white*⁺ marker, which gives them red eyes.
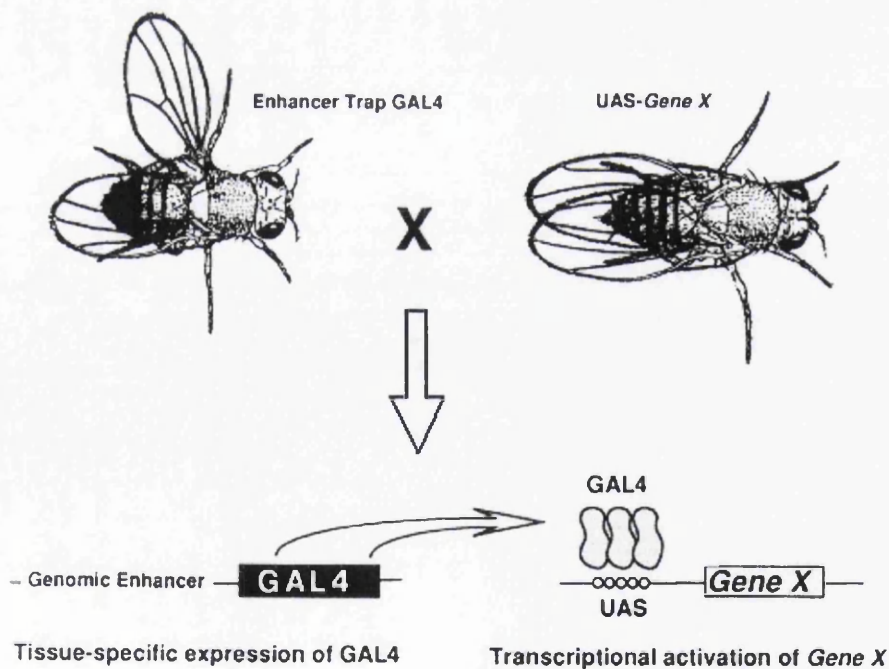
Figure 1.7 Directed gene expression in *Drosophila melanogaster*. Reproduced from Brand and Perrimon, 1993. The GAL4 gene is randomly inserted into the genome, driving GAL4 expression from a number of different enhancers. The GAL4-dependent target gene is constructed by placing the gene sequence behind GAL4 binding sites. The gene is silent in the absence of GAL4. This permits activation of target gene in a cell-specific or tissue-specific manner. Flies carrying the target (*UAS*-Gene X) are crossed to flies carrying the GAL4 transcription factor (enhancer trap GAL4). The progeny of this cross have active GAL4, and this permits expression of Gene X in the same pattern as the enhancer trap GAL4.

33

detected by X-gal staining reveals the endogenous expression of the enhancer. Flanking DNA sequences can be rescued and used to identify the gene involved. However, the pattern detected by the enhancer trap needs to be verified by other means, such as *in situ* hybridisation, as it may be affected by other factors and not reflect the complete expression pattern of the nearby gene.

A second generation of enhancer traps was described, which utilises a binary expression system based on the yeast transcription factor GAL4 (Brand and Perrimon, 1993). GAL4 is a transcriptional activator of genes involved in galactose catabolism in the budding yeast (Gill and Ptashne, 1987). It binds to a specific sequence called UAS$_G$ to activate transcription. Yeast GAL4 was shown to activate gene transcription in *Drosophila melanogaster* in a tissue-specific manner, but only when the *Drosophila* promoter is linked the GAL4 binding sites (Fischer et al., 1988). This observation was utilised by Brand and Perrimon in generating a binary enhancer trap system (Brand and Perrimon, 1993).

GAL4 was inserted randomly into the *Drosophila* genome to drive GAL4 expression by a variety of genomic enhancers, by replacing the *lacZ* gene as the reporter for enhancer-trapping (Bier et al., 1989; Brand and Perrimon, 1993). The gene of interest is then introduced into *Drosophila* in a P element containing GAL4 binding sites in its promoter, or UAS sites (upstream activating sequences) (Brand and Perrimon, 1993) (see figure 1.7). This system permits expression of a gene in a directed and controlled fashion, in a cell-specific or tissue-specific manner. It separates the target gene from its transcriptional activator in two distinct lines, allowing only the progeny of the cross to synthesise the gene product. Lethal or toxic genes can therefore be expressed in a controlled fashion and increase the applications of this system. The UAS sequence can be coupled to *lacZ* to initially determine the expression pattern of the enhancer trap line, and subsequently the enhancer trap line crossed to a variety of UAS-Gene X lines. Another reporter gene widely used for determining enhancer trap patterns is UAS-GFP which permits study of live tissues or organs (Brand, 1995).

A more recent P element trap system has been developed, that allows study of endogenous proteins fused with GFP (Morin et al., 2001). GFP, flanked by strong splice donor and acceptor sites was engineered into a P element. If the element landed in an intron after transposition, then the *cis*-acting splice sites would incorporate the GFP reading frame into the gene mRNA. This element was mobilised in the genome and the progeny screened for fluorescence; the resulting gene trap lines are very useful as they allow study of the intracellular localisation of the respective protein as well as the cell type expression pattern.

1.3.3 The *Drosophila* Malpighian tubule.

The *Drosophila* Malpighian tubule is rapidly becoming recognised as an excellent model epithelium for the study of fluid transport and cell-specific signalling and ion transport pathways (see review, Dow and Davies, 2003). Combined with the robust qualities of the tubule for physiological study and all the genetic and transgenic tools available to the *Drosophila* community, the *Drosophila* Malpighian tubule is an ideal tissue to study cell signalling events in an organotypic context i.e. in a whole, intact organ.

Drosophila melanogaster have four Malpighian tubules, arranged in two pairs, one pointing towards the anterior and one towards the posterior of the fly. The tubules from each pair join to form a common ureter and are joined to the gut at the junction between the midgut and the hindgut (see figure 1.8A). *Drosophila* Malpighian tubules perform analogous roles to the vertebrate kidney and are involved in generation of urine and also selective reabsorption of certain desirable solutes (Dow et al., 1998).

The Malpighian tubules are relatively simple, one cell thick, tubular epithelia, with each tubule comprising of approximately 150 cells (Sözen et al., 1997). The structure of the *Drosophila* Malpighian tubules is shown in figure 1.8, both as described by classical physiology (figure 1.8A) and by molecular genetic analysis (figure 1.8B). Each tubule comprises of six regions with a number of different cell types, two of which appear most important, type (I) or principal cells and type (II) or stellate cells. These regions of the tubule have been shown to be defined genetically and physiologically shown to have different functions (Sözen et al., 1997).

The main segment of the Malpighian tubule is involved in ion and fluid secretion and the lower segment is reabsorptive (O'Donnell and Maddrell, 1995). This correlates with the genetically defined regions within the tubule as identified and characterised using enhancer trapping (Sözen et al., 1997). Fluid secretion is energised by an apical H^+ V-ATPase (proton pump) that is confined to the principal cells of the main segment (Davies et al., 1996). The primary physiological assay for the tubule is the fluid secretion assay (Dow et al., 1994) shown in figure 1.9.

A number of studies on fluid secretion from the *Drosophila* tubule and its neurohormonal control have uncovered the signalling pathways involved and the neuropeptides which are involved in the fluid secretion process. These studies have uncovered the synergistic way in which neuropeptides stimulate fluid secretion, acting via different cell types or through different second messenger pathways.

A

ENLARGED INITIAL SEGMENT

TRANSITIONAL SEGMENT

MAIN SEGMENT

MID·GUT

URETER

HIND·GUT

B

		Stellate	Principal	
Initial segment		7	22	
Transitional segment		6	22	
Main segment		20	77	
	Midgut			
Lower ureter		0	25	Lower tubule
Upper ureter				Upper ureter
Lower tubule		0	23	Lower ureter
	Hindgut			
		20	75	Main segment
		1	3	Transitional segment
		1	4	Initial segment
		Stellate	Principal	

Anterior tubules

Posterior tubules

Principal cell

C

Stellate cell
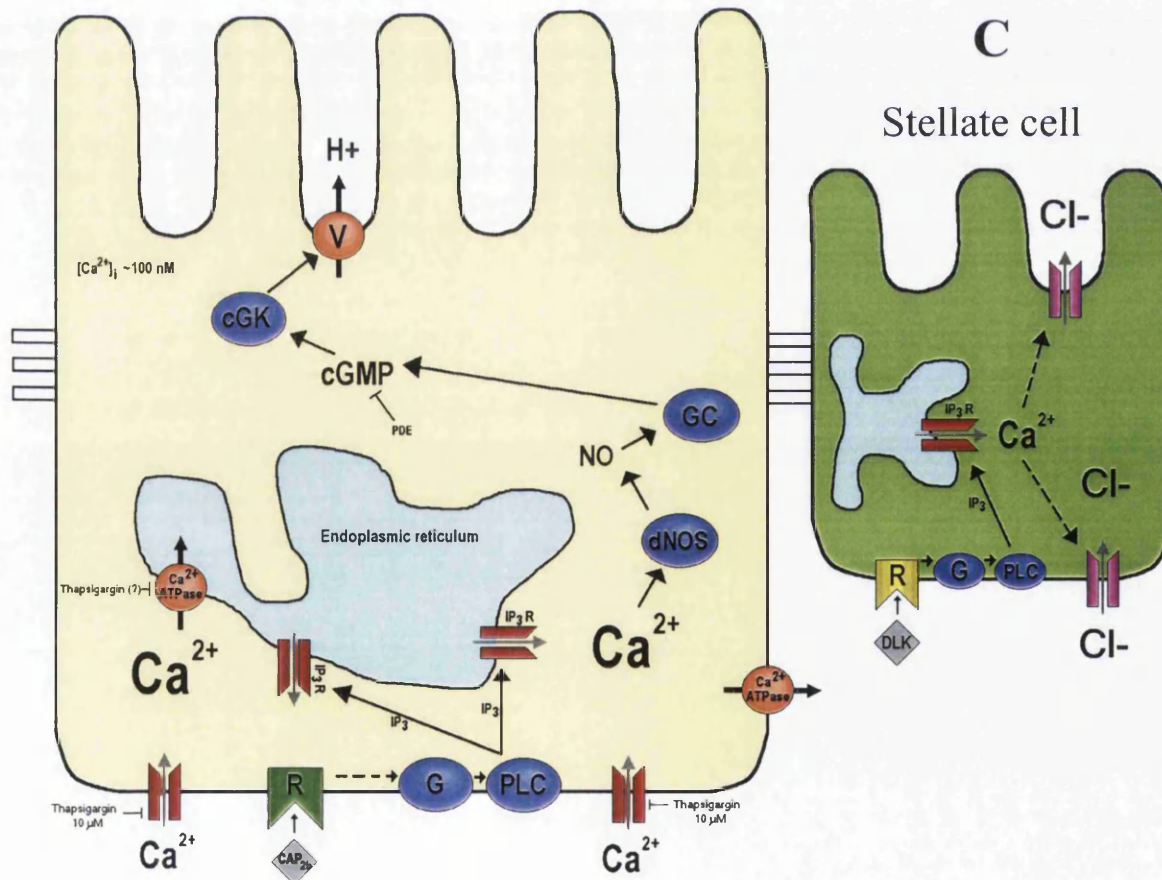
Figure 1.8 *Drosophila melanogaster* Malpighian tubules. (A) Classical morphology of the Malpighian tubules (Wessing and Eichelberg, 1978). (B) Malpighian tubule architecture as shown by enhancer trapping technology. Numbers indicate number of principal and stellate cells in each domain as verified by EtBr staining, standard errors <1 in each case (reproduced from Sözen et al.,1997). (C) Schematic diagram of neuropeptide induced signalling pathways in principal and stellate cells. Abbreviations are as follows: NO, nitric oxide; dNOS, *Drosophila* nitric oxide synthase; GC, guanylate cyclase; PDE, phosphodiesterase; cGK, cyclic G-kinase; V, V-ATPase; DLK, *Drosophila* leucokinin. Diagram was reproduced and adapted from Terhzaz et al., 1999 and Dow and Davies, 2003.

36
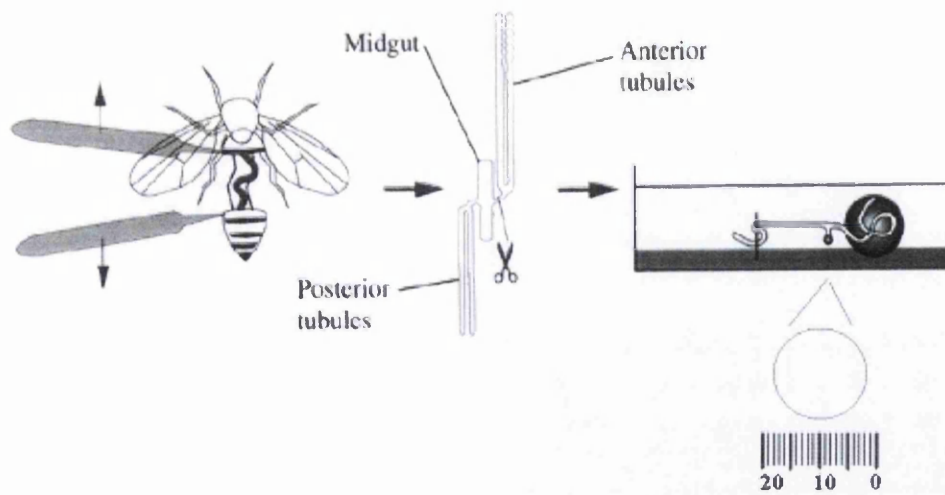
Figure 1.9 The fluid secretion assay. Malpighian tubules were dissected from the fly in Schneider's insect culture medium. Tubules were dissected and separated as pairs by severance of the ureter. One tubule was wrapped around an anchoring pin whilst the other remained in a drop of 1:1 mixture of Schneider's:*Drosophila* saline, under mineral oil. Amaranth is added to the saline to aid visualisation of the secreted fluid. As the tubule secretes, a bubble of secreted fluid is formed at the ureter. This bubble can be removed with a finely pulled glass rod and the diameter measured. The volume of liquid can be calculated from the diameter of the bubble and consequently the fluid secretion rate can be determined.

The two main cell types, principal and stellate cells, and the major signalling pathways in each cell type are shown in figure 1.8C. CAP_{2b} is a cardioacceleratory peptide, originally identified from the tobacco hawkmoth (*Manduca sexta* (Huesmann et al., 1995)). Consequently capa-1 and capa-2, the *Drosophila* homologues of CAP_{2b} have been identified and characterised (Kean et al., 2002). These insect neuropeptides ultimately stimulate the *Drosophila* principal cell V-ATPase via a Ca^{2+}/nitric oxide (NO)/cGMP signalling pathway (Davies et al., 1995; Rosay et al., 1997; Kean et al., 2002). More specifically CAP_{2b}-like peptides activate the capa G-protein-coupled receptor (Iverson et al., 2002; Park et al., 2002) and raise intracellular $[Ca^{2+}]$ via an IP_3 induced release from internal stores (Pollock et al., 2003). This $[Ca^{2+}]_i$ increase activates a *Drosophila* nitric oxide synthase (NOS) which generates NO. NO activates a soluble guanylate cyclase, increasing cGMP levels, which in turn activates cGMP-dependent protein kinases, PKG1/2, which finally is thought to act on the apical H^+-translocating V-ATPase (Davies et al., 1997).

When the V-ATPase activity is up-regulated, the increased proton translocation is proposed to drive greater secondary K^+ transport across the membrane into the lumen via one or more alkali-metal/proton exchangers (in agreement with the Wieczorek model (Wieczorek et al., 1991)). This movement of K^+ produces an osmotic gradient that promotes the flow of water from the extracellular medium into the lumen. Flow of water is

passive, possibly by water channels of the major intrinsic protein family (MIP) localised to the stellate cells (O'Donnell et al., 1998; Dow and Davies, 2002).

A cAMP signalling pathway is also active in the principal cell and is activated by a *Drosophila* homologue of the corticotropin-releasing factor (CRF)-like diuretic peptide (Cabrero et al., 2002) and also the calcitonin-like peptide (Coast et al., 2001). This pathway also activates an increase in fluid secretion, however the downstream components leading to the activation of V-ATPases is not yet understood.

The stellate cells are stimulated by the neuropeptide, *Drosophila* leucokinin (drosokinin). Drosokinin is the most potent diuretic hormone identified in *Drosophila* and it acts through an increase in $[Ca^{2+}]_i$ in stellate cells (Terhzaz et al., 1999). More specifically, drosokinin binds a G-protein coupled receptor (dLKR) (Radford et al., 2002) causing the production of IP_3 (Pollock et al., 2003) and the resultant $[Ca^{2+}]_i$ rise stimulates an increase in chloride shunt conductance (O'Donnell et al., 1998).

1.3.4 Role of Ca^{2+} in the Malpighian tubule

As mentioned in the previous section, Ca^{2+} places an integral role in cell signalling in both the principal cells and the stellate cells. The two characterised neuropeptides, CAP_{2b}-like peptides and Drosokinin both increase fluid secretion via a $[Ca^{2+}]_i$ increase in the respective cell types (Rosay et al., 1997; Terhzaz et al., 1999). Initially, measuring Ca^{2+} concentrations in the tubule appeared difficult. The cells were too small to allow measurement using ion specific microelectrodes; and fluorescent Ca^{2+}-sensitive dyes, such as fura-2, were found to be actively excreted by the tubule (Dow and Cheek, unpublished). However, $[Ca^{2+}]_i$ in the cells of the tubule can be measured by transgenic expression of the Ca^{2+}-sensitive luminescent protein aequorin (see section 1.2.2). In the Malpighian tubule, aequorin expression can be driven in specific regions or cells of the tubule by utilising the GAL4/UAS binary system (Brand and Perrimon, 1993) as was demonstrated by Rosay et al, 1997 (see figure 1.10). Further details of the assay are described in section 2.17.1.
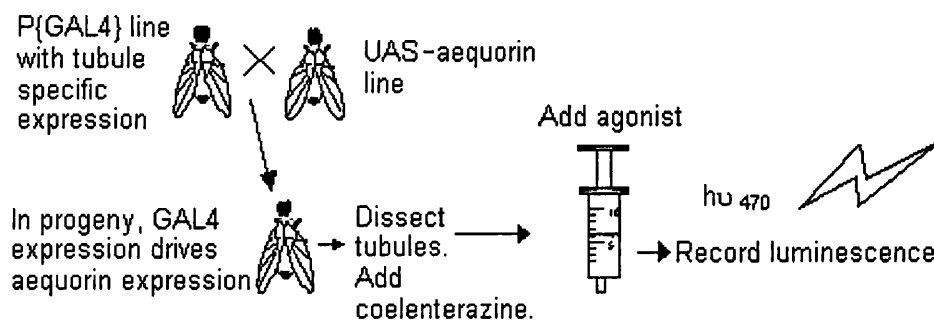
Figure 1.10 Measuring $[Ca^{2+}]_i$ in the tubule using aequorin.

Using such a method it was found that CAP_{2b} caused a rapid, dose-dependent rise in $[Ca^{2+}]_i$ exclusively in the main segment principal cells (Rosay et al, 1997). Experiments performed in Ca^{2+} free medium suggested that this rise is due to an influx of extracellular Ca^{2+} (Rosay et al, 1997). However, the interpretation of these results may be debatable and this is discussed in more detail in chapter 5. More recent experiments revealed a secondary component, consisting of a more sustained rise in $[Ca^{2+}]_i$ (Kean et al., 2002). Furthermore, CAP_{2b}-like peptide stimulated fluid transport is also dependent on extracellular Ca^{2+}, confirming that this pathway acts via a Ca^{2+} signal. It was also found that leucokinin-IV, stimulated a rise in $[Ca^{2+}]_i$ exclusively in the main segment stellate cells (Rosay et al., 1997; O'Donnell et al., 1998). More recently drosokinin has been shown to elicit a biphasic rise in $[Ca^{2+}]_i$ of the stellate cells (Terhzaz et al, 1999), similar to that induced by CAP_{2b} in principal cells (but with a different timecourse).

Stellate and principal cells have been shown to have differing Ca^{2+} cycling mechanisms, evident when the effects of the Ca^{2+}-ATPase inhibitor, thapsigargin are examined (Rosay et al, 1997). Thapsigargin blocks the Ca^{2+} ATPase that actively pumps Ca^{2+} into the endoplasmic reticulum (ER), thus causing a rise in the cytoplasmic Ca^{2+} concentration. In the absence of external Ca^{2+}, thapsigargin stimulates a rise in $[Ca^{2+}]_i$ only in the stellate cells. However, this does not negate a role for internal stores in the principal cells and it is possible that either a thapsigargin induced release is too small to be detected, or the Ca^{2+} pool may be maintained by a thapsigargin insensitive mechanism, or thapsigargin is actively transported out of the cell. It could be possible that there is a *Drosophila* secretory pathway Ca^{2+} ATPase (SPCA) that is maintaining a functional Ca^{2+} store in the principal cell, as SPCAs are insensitive to thapsigargin (Sorin et al., 1997). This is discussed in more detail in chapter 5.

Studies of plasma membrane Ca^{2+} channels in the tubule have implicated their importance in the Ca^{2+} signalling events that lead to increased fluid secretion (MacPherson et al., 2001; MacPherson et al., submitted). The L-type Ca^{2+} channel subunits *Dmca1D* and *Dmca1A* are both expressed in the tubule and inhibitor studies have shown their importance in fluid secretion stimulation (MacPherson et al., 2001). Additionally, mutant studies of the transient receptor potential genes, *trp* and *trpl*, have demonstrated the importance of TRP Ca^{2+} channel function in the tubule (MacPherson et al., submitted). TRP channels act as store-operated Ca^{2+} channels (SOC – see 1.1.3) in *Drosophila* photoreceptor cells (for reviews see Hardie, 2001 and Minke and Cook, 2002). However, it appears that their role in the tubule is different to that in the eye; for example, in tubules TRP and TRPL do not function as SOC channels (MacPherson et al., submitted). Null mutants for *trp* do not

reduce $[Ca^{2+}]_i$ increases in the principal cell. Yet a hypomorphic allele of *trp*, *trp^{365}*, that is functionally disrupted (Yoon et al., 2000) causes a complete ablation of the principal cell secondary $[Ca^{2+}]_i$ increase and prevents a CAP_{2b}-induced fluid secretion increase (MacPherson et al., submitted). It appears that complete loss of one type of TRP channel does not impede Ca^{2+} entry (possibly due to compensation by other channels) but a small amount of dysfunctional TRP has a severe affect on Ca^{2+} entry. TRPL is important in tubule function and unlike TRP it can not be compensated for when knocked out. The *trpl* null tubules do not possess a CAP_{2b} stimulated secondary $[Ca^{2+}]_i$ increase and are unable to be stimulated by CAP_{2b} to increase fluid transport.

The accepted paradigm for hormonally-stimulated increases of $[Ca^{2+}]_i$ in non-excitable cells occurs via G-protein coupled activation of PLC upon ligand-receptor binding, resulting in an intracellular increase of DAG and IP_3 (see 1.1.3). IP_3 binds to IP_3Rs on the ER, resulting in the opening of the channel and release of Ca^{2+}. Mutants for *norpA* (which encodes PLC) prevent CAP_{2b} and drosokinin-induced fluid transport, which suggests a role for PLC in both cell types (Pollock et al., 2003). Additionally hypomorphic mutants for *itpr* (IP_3R) display reduced CAP_{2b} and drosokinin-induced fluid transport and $[Ca^{2+}]_i$ responses (Pollock et al., 2003). This evidence indicates that neuropeptide-induced $[Ca^{2+}]_i$ increases are due to the production of IP_3 in both the principal and stellate cells. Furthermore, it suggests that these responses are releasing Ca^{2+} from an internal store in both cell types.

1.4 Aims and objectives

Given the intriguing possibilities of the role of the ER and other Ca^{2+} stores in fluid secretion, the original aim of this project was to investigate the signalling role of the ER Ca^{2+} stores in the principal and stellate cells. The initial approach involved utilising ER-targeted aequorin; by creating transgenic flies that express this reporter, this could allow the first real-time measurements of $[Ca^{2+}]_{ER}$ in an intact tissue. Furthermore, it was also an objective to investigate how mitochondrial Ca^{2+} levels are affected by the reported neuropeptide-induced $[Ca^{2+}]_i$ increases. This could be achieved by generating transgenic flies that express mitochondrially-targeted aequorin. By using these non-invasive transgenic approaches, it could provide further insight into the Ca^{2+} signalling mechanisms of this intriguing tissue and also provide novel phenotypic assays for studying the effects of mutant alleles.

In addition, this project set out to investigate other intracellular Ca^{2+} stores in the tubule, with respect to how these stores are maintained and how they are involved in Ca^{2+} signalling events.

Chapter 2
Materials and Methods

2.1 *Drosophila melanogaster*

2.1.1 *Drosophila* stocks

Table 2.1 *Drosophila melanogaster* strains used in this study.

Strain	Genotype	Purpose
Oregon R	Wild type	Genomic DNA, cDNA, protein.
w^{1118} (Hazelrigg *et al.*, 1984)	w^{1118}	Microinjection.
c710 (Sözen et al., 1997)	w^-; +/+; c710/c710	GAL4 crosses (drives expression in stellate cells)
c710 marked (Sözen et al., 1997)	w^-; Bl/CyO; c710/TM6	GAL4 crosses
c42 unmarked (Rosay et al., 1997)	w^-; +/+; c42/c42	GAL4 crosses (drives expression in principal cells)
c42 marked	w^-; Bl/CyO; c42/TM6	GAL4 crosses
4534	w^*; +/+; Sb^1/TM3, P{w^{+mC}=ActGFP}JMR2, Ser^1	GFP balancer line on 3rd, for lethal phase studies.
UAS-GFP	w^-; UAS-GFP/UAS-GFP; +/+	GAL4 expression patterns
Marker line	w^-; Bl/CyO; $TM2e^-$/$TM6Tb^-$ Hup^-	Balancing lines and localising P element insertions
aequorin, c42 line (Rosay et al., 1997)	w^- aeq/aeq; +/+; c42/c42	Line expressing aequorin in principal cells.
aequorin, c710 line (Rosay et al., 1997)	w^- aeq/aeq; +/+; c710/c710	Line expressing aequorin in stellate cells.
aequorin marked	w^- aeq/aeq; Bl/CyO; $TM2e^-$/$TM6Tb^-$ Hup^-	For making stable aequorin lines
daG32 kind gift from K.O'Dell (Wodarz et al., 1995)	w^-;+/+;daG32/TM3Sb Canton S	For GAL4 crosses (drives expression in all tissues)
Actin5C GAL4 (Ito et al., 1997)	y^1 w^*; P{w^{+mC}=Act5C-GAL4}25F01/Cyo, y^+; +/+	For GAL4 crosses (drives expression in all tissues)
Actin5C GAL4 (Ito et al., 1997)	y^1 w^*; +/+; P{w^{+mC}=Act5C-GAL4}17bF01 /TM6b, Tb^1	For GAL4 crosses
10205	y^1 w^{1118}; +/+;P{w^{+mC}=lacW}1(3) L7251^{L7251}/TM3, Ser^1	LacZ P-element line, insertion site in the CG32451 gene.
12799	w^{1118}; +/+;P{w^{+mC}=GT1}BG01168	Dual gene trap P-element line, insertion site in the CG32451 gene.

Listed above are various *Drosophila* lines utilised in this study, their genotypes and application. Lines shown in the grey boxes were lab stocks, the rest are from the Bloomington stock centre. The lines from the stock centres were identified by map position using BDGP database or FlyBase Cytosearch.

2.1.2 *Drosophila* rearing

Flies were reared in vials on standard *Drosophila* medium (appendix 1) at 22-25°C in a 12: 12, light: dark cycle. If large quantities of flies were required, rearing was in large bottles on standard medium. For egg collection, flies were reared in cages and egg collection was from standard grape-juice agar plates (appendix 1).

2.2 *Escherichia coli*

2.2.1 *E.coli* strains and plasmids

Table 2.2 *E.coli* strains used in this study.

Strain	Genotype
TOP10 competent cells (Invitrogen)	(F⁻ *mcrA*, Δ(*mrr-hsd*RMS-*mcr*BC), φ80*lacZ* ΔM15, Δ*lac*X74, *rec*A1, *deo*R, *ara*D139, Δ(*ara-leu*)7697,*gal*U, *gal*K, *rps*L, (Str^R), *end*A1,*nup*G).
DH5α^{TM} subcloning efficiency competent cells (Invitrogen)	(F⁻ φ80d*lacZ* ΔM15, Δ(*lac*ZYA-*arg*F), U169, *deo*R, *rec*A1, *end*A1, *hsd*R17 (r$_K$-,m^K+), *pho*A, *sup*E44,λ⁻, *thi*-1, *gyr*A96, *rel*A1).
Rosetta® BL21 pLysS competent cells (Novagen)	*hsdS gal* (λc*I*ts857 *ind*1 Sam7 *nin*5 *lac*UV5-T7 gene *1*)

Table 2.3 Plasmids utilised in this study.

Plasmid	Purpose
pP{UAST}	For germline transformation of cloned sequences under control of the UAS enhancer sequence (Brand and Perrimon, 1993).
pP{Δ2-3}	Transposase source for germline transformation. (Spradling and Rubin, 1983)
pP{CaSpeR-hs-act}	For germline transformation of cloned sequences under heat-shock control. (Thummel *et al.*, 1988)
pCR®2.1 and pCR ®II TOPO	For cloning of PCR products according to the TOPO TA cloning kit protocol (Invitrogen).
pMT/V5-His-TOPO®	For cloning of PCR products for expression in S2 cells (Invitrogen)
pMT/V5-His A	For expression in S2 cells (Invitrogen)
pCR®T7/NT TOPO	For cloning of PCR products for expression in *E.coli*. The vector includes a 6X His-tag at the N-terminus for protein purification purposes. (Invitrogen)
pcDNA3.1/V5-His-TOPO®	For cloning of PCR products for expression in mammalian cells. (Invitrogen)

pEGFP-N1	Contains enhanced GFP sequence. From Clontech, (Prasher *et al.*, 1992)
pEYFP-N1	Contains enhanced YFP sequence (Clontech)
pDsRed2-N1	Contains enhanced DsRed2 sequence (Clontech)
pcDNA3-ratiometric pericam	Contains ratiometric pericam template. Kind gift of A. Miyawaki (Nagai et al., 2001)
pcDNA3-inverse pericam	Contains inverse pericam template. Kind gift of A. Miyawaki (Nagai et al., 2001)
pcDNA3-flash pericam	Contains flash pericam template. Kind gift of A. Miyawaki (Nagai et al., 2001)
LD03227	*Drosophila* EST clone containing the full coding sequence of CG32451-PA
RH52668	*Drosophila* EST clone containing the full coding sequence of CG32451-PB
RE31249	*Drosophila* EST clone containing the full coding sequence of CG32451-PC
pMT/V5-His-aequorin	S2 cell expression vector containing the aequorin template (J. Radford)
pMT/V5-His-drosokinin receptor	S2 cell expression vector containing the drosokinin receptor template (J. Radford)
pWAYGAL4, kind gift of Y. Hiromi (Ito et al., 1997)	pCaSpeR vector containing the actin5C promoter elements, the yellow gene and the GAL4 CDS.
pBluescript (pBS-KS)	Used as a sub-cloning vector (for vector map see www.stratagene.com)

2.2.2 Transformation of *E.coli*

Plasmids were transformed into DH5α™ subcloning efficiency chemically competent cells by the addition of 50-100 ng of plasmid to 50 μl of cells on ice and leaving for 15 min. The cells were then heat shocked at 37°C for 45 s, left on ice for a further 2 min, and 250 μl of L-broth added. This was followed by 30 min incubation at 37°C to allow expression of the amp^R gene. 100 μl of the transformation was then spread onto L-Agar (appendix 2) plates containing 100 μg/ml ampicillin.

Transformation of Invitrogen TOPO® constructs into One Shot® chemically-competent TOP10 cells is described in section 2.6.5.

2.2.3 Plasmid selection

Most plasmids used contained the ampicillin resistance gene encoding β-lactamase, and so were selected for by the presence of 100 μg/ml ampicillin when being grown on L-Agar or in L-Broth. This antibiotic was made as a 100 mg/ml stock solution (w/v) in 50%

H_2O, 50% ethanol) and stored at -20°C. Other antibiotics used for selection of plasmids included chloramphenicol and kanamycin. Chloramphenicol resistance was selected for by the presence of 170 µg/ml chloramphenicol when being grown on L-Agar or in L-Broth. This antibiotic was made as a stock solution of 34 mg/ml in 100% ethanol and stored at -20°C. Kanamycin was purchased in a 50 mg/ml solution from Sigma and stored at 4°C. Selection for kanamycin resistance was performed by the presence of 50 µg/ml kanamycin on L-Agar or in L-Broth.

Selection of pCR®2.1 construct-containing transformants requires further selection using X-gal. Forty µl of a 40 mg/ml (w/v) stock solution in dimethylformamide (DMF) (stored at -20°C) was spread onto an ampicillin or kanamycin L-Agar plate an hour before use.

2.2.4 Storage of bacterial cultures

1 ml of bacterial culture was added to 1 ml of 2 % (w/v) peptone, 40 % (v/v) glycerol solution (in H_2O) before being frozen in liquid nitrogen. Frozen stocks were stored at -70°C.

2.3 Oligonucleotide synthesis

Oligonucleotides were synthesised by the MWG Biotech custom primer service on a 0.01 μmol scale, purified by High Purity Salt Free (HPSF®) technology, and their quality assessed by Matrix Assisted Laser Desorption Ionisation - Time of Flight (MALDI-TOF) analysis. Oligonucleotides were received as a lyophilised pellet, resuspended in H_2O to a stock concentration of 100 μM, and further diluted with H_2O to a working concentration of 6.6 μM. All primers were stored at -20°C. A list of all the primers used in this study is provided in appendix 3

.

2.4 Nucleic acid isolation and quantification

2.4.1 Plasmid DNA isolation

Small scale plasmid DNA preparation was carried out using the Qiaprep Spin Miniprep kit or the Sigma GenElute™ Plasmid purification Miniprep kit. Large scale preparation for germline transformation and cloning was carried out using the Qiagen Plasmid Maxi, Endofree Maxi kit or the Qiagen Hi-Speed™ Plasmid Maxi kit according to the manufacturers' instructions (Qiagen).

2.4.2 Genomic DNA preparation

For inverse PCR and other procedures that required moderate amounts of genomic DNA, the Berkeley *Drosophila* Genome Project Quick Fly Genomic DNA prep, by E. Jay Rehm, was used (see http://www.fruifly.org/about/methods/inverse.pcr.html).

Thirty anaesthetised flies were collected in a 1.5 ml eppendorf tube and briefly frozen at -70°C. The flies were then ground in 200 µl of Buffer A using a disposable tissue grinder (Kontes). An additional 200 µl of Buffer A was then added and grinding continued until only cuticles remained. The suspension was the incubated at 65°C for 30 min. 800 µl of LiCl/KAc solution was then added and the resulting solution incubated on ice for at least 10 min. Spinning followed for 15 min at 13,000 rpm at RT.

1 ml of the supernatant was then transferred into a new tube, avoiding floating crud. 600 µl of isopropanol were then added, the solution mixed, and spinning followed for 15 min at 13,000 rpm at room temperature. The supernatant was aspirated away, and the DNA was then washed with 70 % ethanol (v/v) in H_2O and air-dried. The DNA was then resuspended in 150 µl of TE. DNA was stored at –20°C. Buffers used for 30 fly genomic DNA were as follows:

Buffer A

100 mM Tris-HCl, pH 7.5

100 mM EDTA

100 mM NaCl

0.5 % (w/v) SDS

LiCl/KAc Solution

Mix

1 part 5 M KAc stock: 2.5 parts 6 M LiCl stock

2.4.3 Quantification of nucleic acids

Nucleic acid concentrations were estimated by spectrophotometry at A_{260}/A_{280} (CECIL CE2021 2000 Series Spectrophotometer), where an OD of 1 at 260 nm corresponds to 50 µg/ml of double-stranded DNA and 40 µg/ml of single-stranded DNA and RNA. Readings were zeroed with the solution in which the samples had been diluted. The ratio of A_{260}/A_{280} provided an estimate of nucleic acid purity. Values of 1.8 for DNA and 2.0 for RNA indicated pure preparations. Double-stranded DNA was also semi-quantified by comparison with specific bands of 1kb ladder (Invitrogen) on an agarose gel.

2.5 Restriction digests, electrophoresis and ligations

2.5.1 Restriction digests

DNAs were restricted for 1-2 h at 37°C in single strength REact® buffer (Gibco BRL) appropriate to the restriction enzyme being used (Invitrogen). When double digestion was required the reaction was initiated with the enzyme with the lower strength buffer, and after heat inactivation at 65°C for 20 min, an appropriate amount of salt was added before addition of the second enzyme. When this was not feasible, purification of the first digestion product was performed using the Qiagen PCR purification kit according to the manufacturers' instructions. Amounts of DNA in a restriction digest varied from 200 ng to 4 μg for plasmid DNA or PCR product, dependent on the downstream application.

2.5.2 Agarose gel electrophoresis of DNA

DNAs were separated in 1 % agarose in 0.5x TBE [90 mM Tris, 90 mM boric acid (pH 8.3), 2 mM EDTA] containing 0.1 μg/ml EtBr as described in (Sambrook and Russell, 2001), using 0.5x TBE as the electrophoresis buffer. Sizes were compared to a 1kb ladder (Invitrogen). Prior to loading, 6x loading dye [0.25 % (w/v) bromophenol blue, 0.25 % (w/v) xylene cyanol, 30 % (v/v) glycerol in water] was added to the samples to a final 1x concentration of loading dye in the sample. In cases where UV damage to the DNA needed to be avoided (i.e. in difficult cloning procedures), DNA was separated on a crystal violet gel, crystal violet (Sigma, C 3886) was added to 0.5x TBE at a final concentration of 10 μg/ml. The same concentration of dye is used in the TBE running buffer. DNA samples were loaded in 2% Ficoll 400 with 0.002% xylene cyanol.

2.5.3 Purification of DNA from gels

DNA bands were excised from the gel using a clean scalpel blade and the DNA extracted using the Qiagen Gel Extraction Kit according to the manufacturers' instructions. DNA was typically eluted in 30 μl of H_2O.

2.5.4 DNA ligations

For cloning inserts into vectors, plasmid DNA containing the vector and the insert were digested with appropriate restriction enzymes as described in section 2.4.1. For directional cloning of inserts, two different enzymes were used to restrict the vector and the insert, which permits cloning of the insert into the vector in a directional manner.

When a non-directional ligation was performed, both vector and insert were restricted with a single restriction enzyme and the vector was dephosphorylated prior to the ligation reaction to prevent it from reannealing to itself. Dephosphorylation was carried out during the last 20 min of the restriction digest, by addition of 1 U of calf intestinal alkaline phosphatase (Promega). After the restriction digest, both vector and insert were electrophoresed on a 0.8-1 % agarose gel and the DNA bands excised from the gel and gel-purified. For more challenging cloning strategies (usually involving large vectors) the cut vector DNA would be run out on a crystal violet gel to prevent any damage from UV radiation (see section 2.5.2).

For the ligation reaction, a molecular ration of 3:1 insert: vector was used, typically using 50-100 ng of vector. Ligation reactions were carried out using the Roche Rapid DNA Ligation Kit. The ligation mixture was prepared according to the instructions and the ligation reaction left for 5 to 30 minutes before transformation.

2.6 Polymerase chain reaction (PCR)

2.6.1 Standard PCR

Standard PCR protocols were used in the everyday amplification of DNAs. Amounts of template DNA varied, with 0.5 μg of genomic template DNA used per reaction and 0.1 μg or less of plasmid template. For reactions using Mannheim *Taq* polymerase, dNTPs (Boehringer Mannheim) were added at 200 μM each to single strength PCR buffer, left and right primers at a concentration of 0.5 μM with 1 U of *Taq* polymerase. When Applied Biosystems Reddy Load Mix *Taq* was used, only template and primers (at the same concentration as above) were added to the pre-aliquoted mix.

Cycling was performed in thin walled 0.2 ml PCR tubes in a Hybaid OmnE, Hybaid PCR Sprint or Hybaid PCR Express-Gradient thermocycler.

Cycling procedures were typically:

94°C for 1-3 min to ensure template denaturation.

16-45 cycles; denaturing at 94°C, 15 sec/ annealing at 50-60°C, 30 sec/ extension at 72°C, 1-3 min

72°C, 5 min.

Annealing temperatures depended on the primers used. When multiple PCR reactions were run at the same time or same samples run using different annealing temperatures,

the Hybaid Gradient PCR machine was used and a gradient imposed for the annealing temperatures across the block.

2.6.2 *Pfu* PCR

Pfu DNA polymerase (Promega) is a thermostable enzyme from *Pyrococcus furiosus* which catalyses DNA dependent polymerisation of nucleotides into duplex DNA in the 5'→3' direction, exhibits 3'→5' exonuclease (proofreading) activity and is used for PCR reactions requiring high fidelity synthesis such as expression constructs.

The reaction mix was set up as described in the manufacturers' protocol as follows: single strength *Pfu* DNA polymerase buffer, dNTPs each at 200 µM, primers at 260 nM, DNA template up to 0.5 µg, *Pfu* DNA polymerase 1.25 U, final volume of 50 µl with H_2O. The *Pfu* polymerase was added to the mix last to prevent the polymerase proofreading activity from degrading the primers. Hot start was used to improve the lifespan of the enzyme.

The reaction was cycled as follows:

94°C, 2 min

18-45 cycles; 94°C, 30 sec/ 45-65°C, 30 sec/ 72°C, 2-10 min (*Pfu* amplifies 0.5 kb /min)

72°C, 5 min.

2.6.3 Fusion PCR

This procedure involved fusing up to four different pieces of dsDNA in a PCR reaction. Each piece of DNA was initially amplified using primers designed to overlap with the next piece of DNA. A more detailed description of the process is shown in figure 2.1. All fusion reactions were performed using *Pfu* polymerase (Promega) except when this was unsuccessful and Expand High Fidelity polymerase was used (Roche). 16-45 cycles and annealing temperatures of 45-65°C were used.

2.6.4 Reverse transcriptase (RT) PCR

PolyA$^+$ RNA was obtained using the magnetic Dynabeads mRNA DIRECT kit (Dynal®) according to the manufacturers' instructions. Various tissues of up to three flies were used in the extraction. Tissues were ground in 0.5 ml eppendorf tubes with matching homogeniser. Once the mRNA was extracted a reverse transcription reaction was set up. This reaction contained: 0.2 mM of each dNTP, 40 U RNAseOUT (Invitrogen), 10 mM
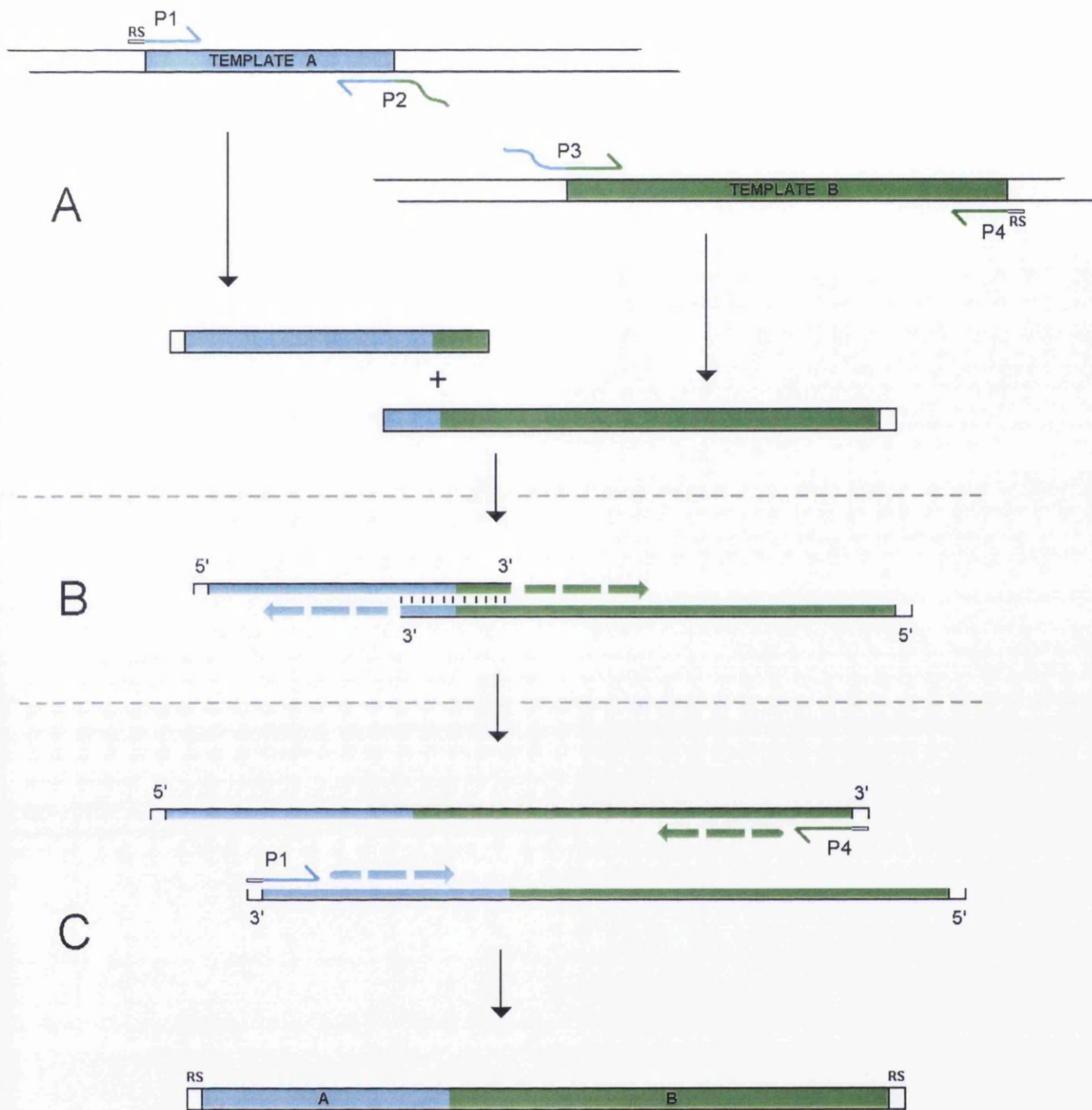
Figure 2.1 Method of fusion PCR. Primers are designed to amplify the DNA sequences that are to be fused together. The primers are designed to overlap with the adjoining sequence (primers P2 and P3) and also can include restriction enzyme sites (RS) for consequent cloning procedures. (A) In separate PCR reactions; template A is amplified using primers P1 and P2 and template B is amplified with primers P3 and P4. The resultant products are purified and used together with primers P1 and P4 in the fusion PCR reaction. (B) In the initial stages of the fusion PCR, single strands of the two DNA templates anneal together at their overlapping regions. The 3' ends of the templates act as primers to allow the polymerase to fill in the rest of the sequence. (C) Once a few fully fused DNA molecules are present, P1 and P4 can amplify them in the standad PCR manner. The resultant DNA can either be digested with restriction endonucleases and cloned, or can be directly TOPO-cloned. For further details of the PCR reactions, see sections 2.6.2 and 2.6.3.

dithiothreitol (DTT), 1x first strand buffer (Invitrogen), final volume 18 μl in H₂O.

After an initial 10 min incubation at 42°C to expose the single-stranded mRNA, 2 μl Superscript™ II RNAse H⁻ Reverse Transcriptase (Invitrogen) was then added to start the reaction. Reactions were incubated at 42°C for 30-50 min, with tapping every 10 min to resuspend the beads. The beads were collected using the Dynal MPC magnet, washed in 50 μl of TE and resuspended in 20 to 50 μl of TE, the suspension being stored at −20°C. 1 μl of the Dynabead solution was sufficient template for a standard PCR reaction.

When previously purified total RNA was used for RT-PCR, the reverse transcription was set up with a few minor changes, 1-5 μg of total RNA was added and 1x hexanucleotide mix (random hexamers, Roche) was used instead of oligo dT beads to prime the reaction. The reaction was terminated by 15 min incubation at 70°C and the RNA in the RNA/DNA duplex degraded using 1 μl RNAse H (Invitrogen) and incubating at 37°C for 20 min, before setting up the PCR reaction using 1 μl of the synthesised cDNA.

2.6.5 Cloning of PCR products

PCR products were directly cloned, using the Invitrogen TOPO TA cloning kits into appropriate TOPO vectors according to the manufacturers' instructions and transformed into TOP10 cells. If there was sufficient PCR product, the PCR product would be digested with the appropriate restriction enzymes and ligated into the vector of choice.

In some cases PCR products were generated using *Pfu* PCR (which does not introduce A overhangs on the 3' end of the PCR product) that required TOPO TA cloning. In these cases, A overhangs were introduced after the PCR reaction. The PCR product was purified using the PCR purification kit, or gel-purified into 30 μl of buffer EB. The volume of the reaction made up to 50 μl in single strength *Taq* buffer, with 20 μM dATP (1μl of 10 mM stock), and 2 U of *Taq* polymerase, incubated at 72°C for 15 min and used as a normal PCR product.

Ligations using TOPO® vectors were done by adding 1-2- μl of the PCR product (gel-purified if necessary) to 0.5 μl of TOPO linearised vector and 0.5 μl of 6x salt solution (1.2 M NaCl, 0.06 M MgCl₂), the volume of the reaction made up to 3 μl with H₂O and the reaction left at room temperature for 5 min.

Transformations were accomplished by adding 3 μl of the ligation reaction and gently stirring on ice. The cells were left on ice for 30 min then heat-shocked at 42°C for 30 sec. The cells were then put back on ice for another 2 min before the addition of 250 μl of SOC medium (appendix 2) then incubated on their side for at least 30 min at 37°C.

100 µl of the transformed cells was then spread onto L-agar plates containing 100 µg/ml ampicillin and incubated overnight at 37°C. These plates sometimes contained X-gal (see section 2.2.3). The transformants were removed as single colonies and grown overnight (with shaking) at 37°C in 5 ml L-broth (appendix 2) containing 100 µg/ml ampicillin.

2.6.6 Targeted PCR mutagenesis

Targeted PCR mutagenesis was performed according to the Stratagene mutagenesis protocol. Primers were designed with the desired mutation and at least 20bp of complementary sequence either side. The plasmid template was PCR amplified using these complementary primers, with *Pfu* enzyme, an annealing temperature of 55°C and 15-22 cycles. The PCR reaction was purified using the Qiagen PCR purification kit and digested with DpnI restriction enzyme (this only digests the template DNA, which is dam-methylated). 3µl of the digest was used to transform chemically competent DH5α cells.

2.6.7 PCR colony screening

To identify the presence and orientation of a DNA insert in a vector, bacterial colonies on a plate could be tested using PCR (before overnight cultures were set up). PCR reactions were set up with one primer that bound to the insert and one primer that bound to the vector (facing into the cloning site). Applied Biosystems Reddy Load Mix was used. The colony was touched with a sterilised tip and then the tip was used to pipette the PCR solution up and down. The PCR program consisted of 30 cycles and an annealing temperature of 55°C.

2.7 Automated DNA sequencing

Automated sequencing was performed at the Glasgow University Molecular Biology Support unit (MBSU), or by Baseclear, in the Netherlands (http://www.baseclear.nl).

Automated sequencing at the MBSU was performed as a single-stranded reaction with template and primer supplied at 1 µg and 3.2 pmol, respectively, with a PCR mix containing fluorescently labelled dideoxynucleotides. Samples were run on an agarose gel with the nucleotides being detected on an ABI automated DNA sequencer. Analysis was performed using a Applied Biosystems automated sequence analysis programme and the sequences were down-loaded from the server onto Editview (version 1.0, free DNA sequencing software from Perkin Elmer) and further analysed.

When samples were sent to Baseclear for sequencing, bacteria containing the plasmid of interest were streaked onto an L-agar plate and sent off for double-stranded sequencing.

2.8 Generation and details of DNA constructs

All the relevant DNA constructs generated are shown in table 2.4. Details of their construction are also displayed in the table. Variants of constructs produced by PCR mutagenesis are not shown.

Table 2.4 Generation and details of DNA constructs. When TOPO® cloning (see section 2.6.5) was not used, the restriction enzymes used for ligation cloning (see section 2.5.4) are shown. Details of the vectors are in table 2.3. For further details on fusion PCR, see section 2.6.3 and figure 2.1. All PCR amplifications and PCR fusions were performed using *Pfu* polymerase, unless stated otherwise. The sequences of the primers can be found in appendix 3. in31, in67 and in140 are all variants of inverse pericam with different calmodulin mutations (see chapter 4). CTS, calreticulin signal. AEQ, aequorin.

Construct	Source/template for insertion	Method of cloning	PCR amplified	Assembly by fusion PCR	Primers used
pBS KS erAEQ	pSVAEQERK	EcoRI & NotI	-	-	-
pP{UAST-erAEQ}	pBS KS erAEQ	EcoRI & XhoI	-	-	-
pP{CaSpeR-hs-act-erAEQ}	pP{UAST-erAEQ}	EcoRI & XbaI	-	-	-
pMT/V5-His A-mtAEQ	pcDNAI-mtAEQ	EcoRI	-	-	-
pP{UAST-mtAEQ}	pcDNAI-mtAEQ	EcoRI	-	-	-
pP{CaSpeR-hs-act-mtAEQ}	pcDNAI-mtAEQ	EcoRI	-	-	-
pCRT7/NT-GolgiAEQ	pMT/V5-His-AEQ & pP{UAST-GolgiECFP} genomic DNA (Taq)	TOPO®	✓	✓	3-6
pP{UAST-GolgiAEQ}	pCRT7/NT-GolgiAEQ	EcoRI & NotI	-	-	-
pCRT7/NT-camgaroo	*Drosophila* CTS & calmodulin (Taq, from genomic). pEYFP-N1	TOPO®	✓	✓	7-14
pCRT7/NT-ER-targeted ratiometric pericam	*Drosophila* CTS & pcDNA3-ratiometric pericam	TOPO®	✓	✓	15-18
pCRT7/NT-ratiometric pericam	pcDNA3-ratiometric pericam	TOPO®	✓	-	19 & 20
pCRT7/NT-flash pericam	pcDNA3-flash pericam	TOPO®	✓	-	19 & 20
pCRT7/NT-inverse pericam	pcDNA3-inverse pericam	TOPO®	✓	-	19 & 20
pMT/V5-His-ERpicam	pCRT7/NT-in31 & pSVAEQERK	TOPO®	✓	✓	21-24
pMT/V5-His-Golicam	pCRT7/NT-in31 & pCRT7/NT-GolgiAEQ	TOPO®	✓	✓	3, 20, 25 & 26
pcDNA3.1-ERpicam	pMT/V5-His-ERpicam	TOPO®	✓	-	21 & 24
pcDNA3.1-Golicam	pMT/V5-His-Golicam	TOPO®	✓	-	3 & 20
pcDNA3.1-in67	pCRT7/NT-in67	TOPO®	✓	-	19 & 20
pcDNA3.1-in140	pCRT7/NT-in140	TOPO®	✓	-	19 & 20
pcDNA3.1-mitycam-1	pCRT7/NT-in67 & pMT/V5-His A-mtAEQ	TOPO®	✓	✓	20, 27-29
pcDNA3.1-mitycam-2	pCRT7/NT-in140 & pMT/V5-His A-mtAEQ	TOPO®	✓	✓	20, 27-29
pP{UAST-ERpicam}	pMT/V5-His-ERpicam	EcoRI & NotI	-	-	-
pP{UAST-Golicam}	pMT/V5-His-Golicam	EcoRI & NotI	-	-	-
pP{UAST-ratiometric	pCRT7/NT-ratiometric pericam	EcoRI & NotI	-	-	-

pericam Q69M}	Q69M				
pP{UAST-in67}	pcDNA3.1-in67	EcoRI & NotI	-	-	-
pP{UAST-in140}	pcDNA3.1-in140	EcoRI & NotI	-	-	-
pP{UAST-mitycam-1 }	pcDNA3.1-mitycam-1	EcoRI & NotI	-	-	-
pP{UAST-mitycam-2}	pcDNA3.1-mitycam-2	EcoRI & NotI	-	-	-
pMT/V5-His-CG32451-PA-c-myc	LD03227	TOPO®	✓	-	73 & 74
pMT/V5-His-CG32451-PB-GFP	RH52668	TOPO®	✓	✓ (Expand)	75-78
pMT/V5-His-CG32451-PC-YFP	RE31249	TOPO®	✓	✓	76-79
pP{UAST- CG32451-PA-c-myc}	pMT/V5-His-CG32451-PA-c-myc	EcoRI & NotI	-	-	-
pP{UAST- CG32451-PB-GFP}	pMT/V5-His-CG32451-PB-GFP & pEGFP-N1	EcoRI & NotI	-	-	-
pP{UAST- CG32451-PC-YFP}	pMT/V5-His-CG32451-PC-YFP & pEYFP-N1	EcoRI & NotI	-	-	-
pMT/V5-His-c-myc-peroxisomal-Dsred2	pDsred2-N1	TOPO®	✓	-	81 & 82
pP{UAST-SPoCk-PTM1}	LD03227, pEGFP-N1 & genomic DNA	EcoRI & NotI	✓	✓	83-90
pP{UAST-SPoCk-PTM2}	LD03227, pEGFP-N1 & genomic DNA	EcoRI & NotI	✓	✓	88-94
pP{UAST-vha55-PTM}	pP{UAST-vha55} (Juan Du), pEGFP-N1 & genomic DNA	EcoRI & NotI	✓	✓	93-99
pP{UAST-2XGFPc-myc}	pEGFP-N1	KpnI, MluI & XbaI	✓		101-104
pP{UAST-dLKR-PTM1-2XGFPc-myc}	pMT/V5-His-dLKR (J. Radford) & genomic DNA	NotI & KpnI	✓	✓	105-108
pP{UAST-irk3-PTM}	cDNA, pEGFP-N1 & genomic DNA	EcoRI & NotI	✓	✓	109-113
Avha55GAL4	pP{UAST-vha55-PTM}	NheI	✓	✓	114-115
ALKRGAL4	Genomic DNA	NheI	✓	✓	116-118

2.9 Detection of β-galactosidase

Flies containing p{*lacW*} insertions were anaesthetised on ice, decapitated and dissected in PBS (130 mM NaCl, 7 mM Na_2HPO_4, 3 mM NaH_2PO_4) then pinned out to display their internal organs onto a Sylgard-coated petri dish. They were fixed with 1 % (v/v) glutaraldehyde in PBS (see appendix 5) for 20 min, washed thoroughly in PBS twice, then stained overnight in Fe-NaP staining buffer [10 mM NaH_2PO_4, 10 mM Na_2HPO_4, 150 mM NaCl, 1 mM $MgCl_2$, 3.1 mM $K_4(Fe^{2+}CN)_6$, 3.1 mM $K3(Fe^{3+}CN)_6$, 0.3 % Triton-X-100, (pH 7.0)], containing 0.2 % (w/v) X-gal (from an 8 % (w/v) stock in DMSO), at 37°C overnight. Flies were then washed three times in PBS then viewed under a light microscope (Leica WILD M3C) and photographed using a Leica WILD MPS 51S camera (WILD Photoautomat MPS 4S shutter release system).

2.10 Germline transformation

2.10.1 Embryo collection and preparation

Several hundred flies (w^{1118}) between 3 and 7 days old were set up in an egg collection cage the day before embryos were required. The day embryos were required, grape-juice agar plates were changed hourly until sufficient eggs were produced for injection (more than 30) in a 30 min period. The eggs were removed to a slide and de-chorionated with fine forceps under a light microscope and lined up on the edge of a slide that had a thin layer of glue (Scotch tape dissolved in heptane) along the edge. The embryos were placed with the posterior pole facing outwards, dehydrated for 5 to 6 min and covered with Halocarbon oil (Sigma).

2.10.2 Needle preparation

Needles were pulled on a Sutter Instrument moving-coil electrode puller, model P-97, from borosilicate glass capillary tubes (Harvard Apparatus Limited) of dimensions 1.0 mm (OD) x 0.78 mm (I.D), with the puller settings on

Heat	580
Pull	100
Velocity	105
Time	150

Needles were filled with the DNA solution. The sealed tip was broken by a slight tap on the edge of the glass slide.

2.10.3 Microinjection

The embryos were injected with a mixture of the pP{UAST} or pP{CaSpeR-hs-act} containing the insert of interest (200 ng/μl) and the helper plasmid pP{Δ2-3} (100 ng/μl), which had been purified on a Qiagen PCR purification column and eluted in filter-sterilised injection buffer (0.1 mM Na_2HPO_4, 0.1 mM NaH_2PO_4, 5 mM KCl, pH 7.8). Embryos were injected with this solution into the posterior end. Embryos were viewed under a Zeiss Axiovert 25 inverted stage microscope. Microinjection was carried out using an Eppendorf rig, consisting of an InjectMan micromanipulator and a Femtojet air supplier. Only undeveloped embryos (syncitial blastoderm or earlier) were injected, and all other (cellularised) embryos were squashed using forceps.

2.10.4 Post-injection care

Slides containing injected embryos were removed to a fresh grape-juice agar plate. The embryos were left to recover for 1-3 days and any hatched larvae were transferred to standard food. Surviving adults were individually crossed back to w^{1118} flies and the progeny screened for eye colour change. Transformants were crossed again to the host strain and transformed progeny of this cross were mated to siblings to generate homozygous transformants for the insertion.

2.10.5 Determining the chromosome of insertion

See figure 2.2 for a summary of the crossing scheme employed in this procedure.

$$UAS ; \frac{+}{+} ; \frac{+}{+}$$

$$w^- ; \frac{Bl}{CyO} ; \frac{TM2e^-}{TM6Tb^-} \quad X \quad w^- ; \frac{UAS}{UAS} ; \frac{+}{+}$$

$$w^- ; \frac{+}{+} ; \frac{UAS}{UAS}$$

$$UAS ; \frac{Bl/CyO}{+} ; \frac{TM2e^-/TM6Tb^-}{+} \qquad w^- ; \frac{Bl/CyO}{UAS} ; \frac{TM2e^-/TM6Tb^-}{+} \qquad w^- ; \frac{Bl/CyO}{+} ; \frac{TM2e^-/TM6Tb^-}{UAS}$$

$$X \quad w^- ; \frac{Bl}{CyO} ; \frac{TM2e^-}{TM6Tb^-}$$

$$UAS ; \frac{Bl}{CyO} ; \frac{TM2e^-}{TM6Tb^-} \qquad w^- ; \frac{Bl/CyO}{UAS} ; \frac{TM2e^-}{TM6Tb^-} \qquad w^- ; \frac{Bl}{CyO} ; \frac{TM2e^-/TM6Tb^-}{UAS}$$

Chromosome 1/X   **Chromosome 2**   **Chromosome 3**

Red eyes, ebony, bristles, and curly wings   Red eyes, ebony, bristles or curly wings   Red eyes, bristles, and curly wings
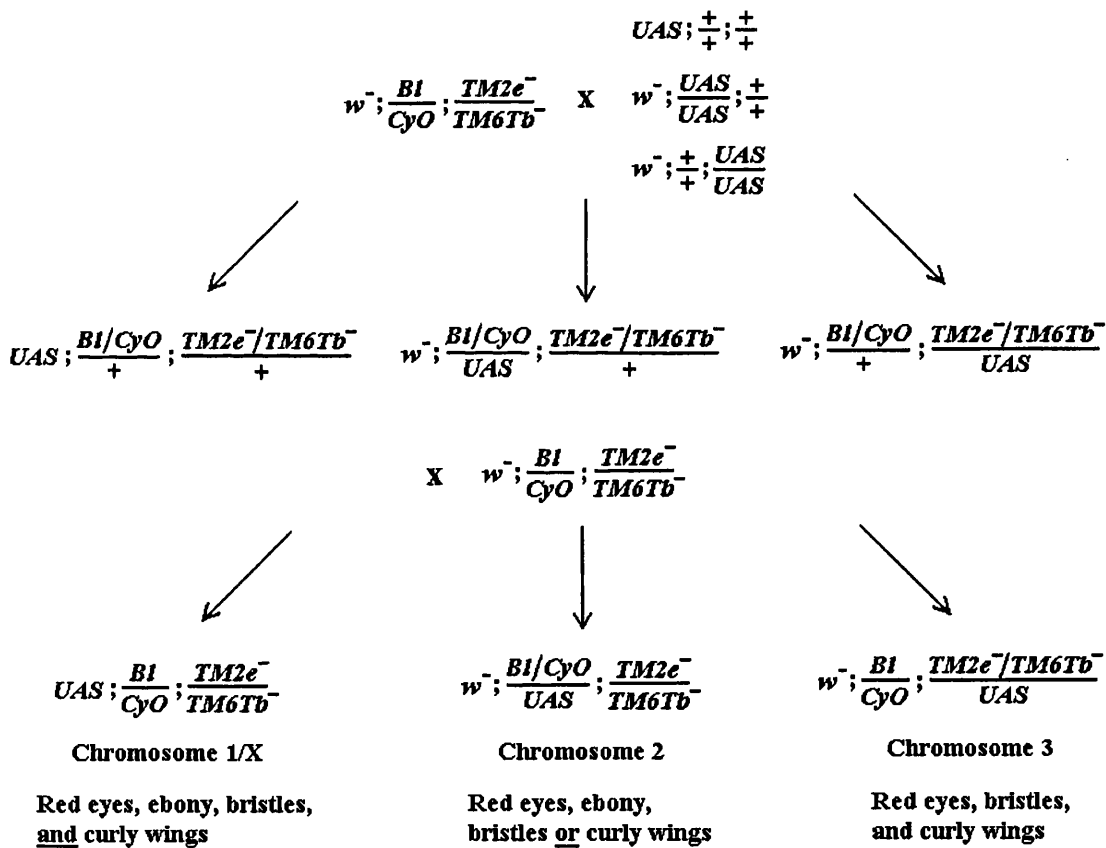
Figure 2.2 The crossing scheme for determining the chromosome of insertion in transgenic fly lines. Lines homozygous for each individual insertion line were crossed to the marker fly line. The f1 progeny of this cross were then back-crossed to the marker line, and the f2 progeny analysed for visible phenotypic markers. *CyO* confers a curly winged phenotype, *Bl* confers a bristled hairs phenotype, *TM6Tb* confers a tubby pupal phenotype, and *TM2e* confers an ebony body phenotype when in combination with *TM6Tb*.

In order to determine which chromosome P-element insertions were on, lines homozygous for each construct were crossed to a marker line (w^-; *Bl/CyO*; *TM2e* /*TM6Tb*). This knowledge is important for creating stable lines containing more than one

ransgene insertion. The *Bl* marker chromosome confers a bristle phenotype on the hairs of the fly, and the *CyO* chromosome confers a curly wing phenotype. The *TM6Tb⁻* chromosome confers a tubby pupal phenotype, whereas the *TM2e⁻* chromosome in combination with the *TM6Tb⁻* chromosome confers an ebony colour on the cuticle. The red-eyed f1 progeny of this cross are then backcrossed to the marker line, and the red-eyed f2 progeny analysed for phenotypic markers. If there are red-eyed f2 progeny with ebony bodies, curly wings <u>and</u> bristles, then the insertion must be on the X (1) chromosome. If there are red-eyed f2 flies with ebony bodies, but only curly wings <u>or</u> bristles, then the insertion is on the 2nd chromosome. If there are red-eyed f2 progeny with bristles and curly wings, but not ebony bodies, then the insertion is on the 3rd chromosome.

2.11 Protein Extraction, electrophoresis and western blotting

2.11.1 Protein extraction from *Drosophila* tissues

Different methods were used for extraction of proteins from *Drosophila* tissues. The simplest protocol consisted of dissecting different organs (eg. 6 bodies, 30 heads) into 400 μl of Tris-Lysis buffer (2 % (w/v) SDS, 70 mM Tris, pH 6.8) containing 2 μl of Sigma protease inhibitor coctail in a 2 ml Nunc tube. The tissues were homogenised using either a Kontes Cordless Motor hand homogeniser or a Microson Ultrasonic Cell Disrupter, until the sample appeared homogeneous. The sample was then centrifuged at 15,000 rpm for 10 min to remove debris and the supernatant transferred into a new tube. A different protocol was used for extracting membrane proteins (Xu et al., 1997) Samples, such as 1000 heads, or bodies were dissected into 400 μl of SMART buffer (0.2 % (w/v) dodecyl-β-maltoside, 2.7 mM KCl, 10 mM NaHPO$_4$, 1.8 mM KH$_2$PO$_4$, 500 mM NaCl, 5 mM EDTA, 5 mM EGTA, 8 mM MgCl$_2$, 2 μg/ml aprotinin, 10 μg/ml leupeptin, 0.1 mM PMSF, 10 mM NaPPi, 50 mM NaF, 1 mM GTP, pH 7.3). Homogenising followed until the sample was homogeneous and the debris then spun down at 15,000 rpm for 10 min. The supernatant was then transferred to a new tube.

2.11.2 Lowry protein assay

The Lowry protein assay (Sanderman and Strominger, 1972) was used to estimate protein concentration of different protein samples. The following reagents were used for the assay:

Reagent 1. 1 % (w/v) $CuSO_4 \bullet H_2O$

Reagent 2. 2 % (w/v) NaK Tartrate

Reagent 3. 2 % (w/v) Na_2CO_3 in 0.1M NaOH

Folin-Ciocalteu reagent (Sigma) 1:1 (v/v) with H_2O

A mix was made up prior to use, taking into account the number of protein samples and standards and for each sample the following amounts of the above reagents were used: 100 µl of reagent 1, 100 µl of reagent 2, 1 ml of reagent 3.

15-25 µl samples of each protein sample and 0-25 µg of BSA (1mg/ml stock made up from 10 mg/ml solution and stored at –20°C) as standards were placed in 1.5 ml eppendorf tubes. 1 ml of the above mix and 100 µl of the Folin Ciocaltau reagent were added to each sample and the solution was mixed. The samples were then left at room temperature for 20 min and the OD read at 750 nm using a no BSA standard as the blank. A standard curve was then plotted using the BSA standards on Cricket Graph, a best fit curve (linear) calculated and the protein concentration of the samples estimated using the resulting equation.

2.11.3 Protein electrophoresis

Protein electrophoresis was performed using either the Novex NuPAGE™, Bio-Rad Ready Gel Mini-PROTEAN II Cell kit, or Bio-Rad Mini-PROTEAN 3 Cell kit Electrophoresis systems. In the case of the Novex electrophoresis system, the Xcell II™ kit was used with 12-well 4-12% Bis-Tris-HCl (Bis(2-hydroxyethyl)imino-tris(hydroxymethyl) methane-HCl) buffered (pH 6.4) polyacrylamide gels. The running buffer used was 1x NuPAGE™ MOPS SDS Running Buffer, diluted from a 20x MOPS SDS Running Buffer stock solution (see appendix 5). The gels were then run at 200 V constant with an expected current of 100-115 mA/gel at the start and 60-70 mA/gel at the end, for approximately 50 min.

When the Bio-Rad Ready Gel Cell kit was used for SDS-PAGE electrophoresis, the gels used were Bio-Rad Ready gels, 4-15% Tris-HCl 10-well gels, and the running buffer used was 1x Tris-Glycine buffer (see appendix 4). When the Mini-PROTEAN 3 Cell system was used, gels were prepared as described in appendix 5, with 10 or 15-well combs. The gels were run at 150 V constant for approximately 1 h.

Using either electrophoresis system, the samples were prepared by adding 6x SDS-PAGE loading buffer to the protein sample (15-60 µg) and then briefly vortexed, heated to 95°C

for 5 min, pulse-spun and vortexed before loading into the well of the gel. Pre-stained Rainbow marker from Amersham Pharmacia was used for sizing the proteins on the gel.

2.11.4 Coomassie staining of SDS-PAGE gels

When required, the gels after running were stained using Coomassie Brilliant Blue (appendix 4). The gel was transferred to a sandwich box and soaked overnight in Coomassie on a horizontal shaker. The gel was then destained using destaining solution (appendix 4) on a shaker. The destaining solution was changed frequently until the bands on the protein gel appeared sharp and the background on the gel clear.

2.11.5 Western blotting

When blotting of SDS-PAGE gels was required, the gels were blotted onto Hybond C or Hybond ECL membrane from Amersham-Pharmacia, using a Bio-Rad Minigel Blotting Kit or a Novex Xcell II™ Blot module. This was done placing the gel and the wet membrane between pieces of Whatmann 3MM paper and in the blot module. The Transfer buffer used is described in appendix 5 and the transfer was done using ice packs to minimise heating up of the blotting apparatus and gels, at 50V constant for 1 h.

2.11.6 Western hybridisation

After transfer the blots were removed from the blotting apparatus and briefly stained with Poncau S staining solution (appendix 4) to check the efficiency of the transfer. After staining, the blots were washed with water to make the bands visible and after visualisation, washed with transfer solution before blocking. Blocking was done in PBS, 0.1 % (v/v) Tween 20, 5 % (w/v) Marvel milk for 1h (at RT) to overnight (at 4°C). The blots were briefly washed for 15 min in PBS, 0.1 % (v/v) Tween 20. The primary antibody (at various concentrations) was then incubated in blocking solution for 3 h (at RT) to overnight (at 4°C). Washes followed in PBS, 0.1 % (v/v) Tween 20, 1x 15 min, 3x 5 min on a horizontal shaker at room temperature. The secondary antibody (at various concentrations) was then incubated in PBS, 0.1 % (v/v) Tween 20 for 1 h at room temperature and the blot washed well for at least 3 h at room temperature in PBS before detection.

2.11.7 Western signal detection

HRP-conjugated (horseradish peroxidase) secondary antibodies were used to detect signals on Western blots. Horseradish peroxidase activity can be detected using either chemiluminescence or DAB substrates.

Chemiluminescence detection, using the ECL™ Western Blotting analysis system (Amersham Pharmacia), was performed by adding equal volumes of reagent 1 and reagent 2 to the filter, incubating at RT for 1 min, and then exposing the blot, covered in Saran Wrap to ECL film (Amersham Pharmacia) for different lengths of time before developing using the X-OMAT film processor.

2.11.8 Primary and secondary antibodies used

The primary and secondary antibodies used for the immunocytochemistry and Western hybridisation are shown in the Table 2.6, along with the dilutions at which they were used.

Table 2.5 Antibodies used for Western hybridisations and immunocytochemistry.

Antibody and Source	Dilution and Use
Anti-Myc-tag (mouse monoclonal, NEB)	1:500 (immunocytochemistry)
Anti-GFP (mouse monoclonal, ZYMED)	1:2000 (Western)
Anti HisG (mouse monoclonal, Invitrogen)	1:5000 (Western)
Anti-GM130 (ML07) (rabbit polyclonal, kind gift from Martin Lowe, Manchester)	1:300 (immunocytochemistry)
Anti-aequorin (rabbit polyclonal, Covalab)	1:2000 (immunocytochemistry)
Anti-discs large (mouse polyclonal, Developmental Studies Hybridoma Bank (DSHB))	1:800 (immunocytochemistry)
HRP labelled anti-rabbit IgG H & L (donkey polyclonal, Amersham)	1:5000 (Western)
HRP labelled anti-rabbit IgG H & L (sheep polyclonal, Amersham)	1:5000 (Western)
Alexa Fluor®568-labelled anti-rabbit IgG H & L (goat polyclonal, Molecular Probes)	1:500 (immunocytochemistry)
Alexa Fluor®568-labelled anti-mouse IgG H & L (goat polyclonal, Molecular Probes)	1:500 (immunocytochemistry)
FITC-labelled anti-rabbit IgG H & L (donkey polyclonal, Diagnostics Scotland)	1: 250 (immunocytochemistry)

2.12 Immunocytochemistry

2.12.1 Intact Malpighian tubules

Malpighian tubules were dissected carefully in Schneider's medium and arranged on pre-treated Poly-L-lysine coated (100 $\mu g/ml$) BDH microscope slides in 100 μl of PBS. The PBS was carefully removed and the tubules were then fixed in 4% (w/v) paraformaldehyde in PBS at RT for 5-30 min. The tubules were washed three times in PBS and permeabilised using PBS, 0.3% (v/v) Triton X-100 (PBT) for 30 min. This was followed by incubation with filter-sterilised PBS, 0.3% (v/v) Triton X-100, 0.5% (w/v) BSA (PAT) for 3 h at RT. Primary antibody, diluted to the desired concentration in PAT, was then applied and the slides incubated in a humidified box overnight at RT.

The following day the tubules were washed in PAT 3x 15 min and incubated in PAT-2% (v/v) goat serum (Diagnostics Scotland) for 3 to 4 h. Secondary antibody, diluted to the desired concentration in PAT-2% goat serum, was then applied and the slides incubated in a dark humidified box overnight at RT. The tubules were then washed in PBT 3x 1 h and in PBS 3x 5 min. Slides were mounted in Vectashield mounting medium (Vector) using 22 mm square BDH coverslips, and sealed with glycerol/gelatin (Sigma).

In some slide preparations, the nuclei were visualised using DAPI staining. Prior to mounting in Vectashield DAPI was applied to slides at 500 ng/ml for 2 min in PBS, diluted from a 10 mg/ml (in H_2O) stock solution. Slides were then washed 3 times in PBS before mounting as normal.

Samples were viewed using either fluorescence microscopy or confocal microscopy.

Fluorescence microscopy was carried out by using a Zeiss Axiophot microscope using either a fluorescein or rhodamine filter. DAPI was visualised using a UV filter. Most images were captured by a Zeiss Axiocam HRC system and processed using Axiovision 3.0.6 software. Confocal microscopy of samples is described in section 2.15.1.

2.12.2 S2 cells

Coverslips were coated with Poly-L-lysine solution (100 $\mu g/ml$) for 30 min, washed with H_2O and allowed to dry. S2 cells were added at a density of $6x10^6$ cells/ml and left for 15 min to allow cells to settle and adhere. Excess solution was removed and the samples washed 3 times with PBS. Samples were then fixed by the addition of 4% (w/v) paraformaldehyde in PBS for 15 min at RT. Samples were then washed 3 times with PBS, and blocked in PBS, 0.2% (w/v) BSA, 0.1% Triton X-100 for 10 min at RT. They were then incubated overnight at RT in a humidified box with primary antibody diluted

61

to the desired concentration in PBS/BSA/Triton X-100. Samples were then washed 3 times with PBS and incubated for 1 h at RT with the appropriate secondary antibody, diluted to the desired concentration in PBS/BSA/Triton X-100. Samples were then washed 3 times in PBS and, if required, DAPI stained as described in section 2.12.1. The coverslips to which samples were attached were then mounted on slides using Vectashield mounting medium and sealed with glycerol-gelatin. Samples were viewed by either fluorescence microscopy or confocal microscopy, as described in section 2.12.1 and 2.15.1.

2.13 Bacterial expression of proteins

2.13.1 pCRT7/NT vectors and constructs

The pCRT7/NT TOPO® vector (Invitrogen) contains an N-terminal tag, which includes a 6X histidine repeat for protein purification purposes. Primers were designed to amplify the chosen sequence for expression, the start of the forward primers were designed to ensure that the sequence would be in frame with the His-tag. PCR products were cloned into pCRT7/NT as described in 2.6.5.

2.13.2 Expression of His-tag fusion proteins

pCRT7/NT constructs were transformed into chemically competent Rosetta® BL21 pLysS cells (Novagen). These cells were plated on 100µg/ml ampicillin and 34µg/ml chloramphenicol (to retain the pLysS plasmid) LB plates. 20ml overnight cultures were used to inoculate 400ml of L broth (ampicillin and chloramphenicol). These were grown for ~3hrs until the culture had an OD_{600} of ~0.5, then induced with 1mM IPTG and then left to express at RT for ~16hrs.

2.13.3 His-tag purification of proteins

The *E. coli* were spun down at 6000 rpm for 15 minutes and resuspended in 40ml of 1X binding buffer (Novagen) containing 10µl of protease inhibitor cocktail (Sigma). This was sonicated on ice (Sonics and Materials Inc. Vibra-cell) for five repeated 10 second intervals and then spun down at 12,000 rpm for 30 minutes. The soluble fraction was purified using the Novagen His•Bind Resin Column Chromatography kit, according to the manufacturers' instructions. Eluted fractions were collected in 200 µl aliquots.

2.14 *In vitro* characterisation of fluorescent reporters

2.14.1 Ca^{2+} calibrations of fluorescent reporters

Purified fluorescent reporter protein was added at a ≥1:100 dilution factor to 250µl of calcium buffered solution (Molecular Probes, Calcium Calibration kits #2 and #3). For free calcium concentrations higher than 1mM (highest concentration available in the kits), solutions were prepared using calculated amounts of $CaCl_2$ (with 100 mM KCl, 30 mM MOPS, pH 7.2). Fluorescent measurements were performed in a Berthold Mithras LB940 96-well plate reader.

2.14.2 pH calibrations of fluorescent reporters

pH buffered solutions (10 mM HEPES, 10 mM K phthalate, 10 mM Na borate, 125 mM KCl and 20 mM NaCl) were prepared, ranging from pH 5.0 to pH 13.0 by dropwise addition of concentrated HCl or NaOH solutions. Purified fluorescent reporter protein was added at a ≥1:100 dilution factor to 250 µl of pH buffered solution. Fluorescent measurements were performed in a Berthold Mithras LB940 96-well plate reader.

2.14.3 Spectral analysis of fluorescent reporters

The excitation spectra of the purified pericam proteins were analysed using a Cairn Optoscan. The purified protein was diluted (at > 100x dilution) in a buffered solution containing either no calcium (EGTA) or 1 mM $CaCl_2$. The samples were scanned from 300 – 550 nm using a 5 nm bandwidth.

2.15 Confocal microscopy

2.15.1 Confocal microscopy of fixed samples

Samples were imaged using a Zeiss Pascal confocal system coupled to a Zeiss microscope. A HeNe1 543nm laser and a 561-625 band pass filter. were used for imaging the Alexafluor® 568 secondary antibody. An Argon 488 laser and a 505-530 band pass filter were used for imaging the FITC antibody or fluorescent proteins. For visualisation of DAPI, a pseudo-DAPI technique was used. The DAPI was excited using the standard UV source (mercury lamp) and the image captured using the confocal photomultipliers. The DAPI image was then merged with the other channels retrospectively, using Adobe Photoshop 7.0. A 63x objective was used in all cases.

2.15.2 Confocal imaging of fluorescent reporters in living tissue

Dissected Malpighian tubules were carefully stuck (in PBS) to the bottom of a glass bottomed dish (Mattek) that had been treated with poly-L-lysine. The PBS was immediately removed and 3ml of Schneider's solution added. The samples were left for at least an hour before imaging. This was to allow the tubules to recover from being in PBS and to prevent the interference of any stimuli that may have occurred within the fly prior to dissection. The imaging was performed using a Zeiss 510 Meta confocal system coupled to an inverted Zeiss microscope. The reporters were excited with an Argon 488 laser and the emission filtered through a 505-530 band pass filter. A 20x objective was used for all live imaging.

2.16 S2 cell culture

2.16.1 Passaging of S2 cells

S2 cells were maintained in DES medium (Invitrogen) supplemented with 10% heat-inactivated foetal calf serum (FCS, Invitrogen). Cells were grown in suspension at 23°C at an initial density of $2\text{-}4\times10^6$ cells/ml. Following the withdrawal of DES medium from production by Invitrogen, S2 cells were maintained in Schneider's medium supplemented with 10% heat-inactivated FCS. Using this medium S2 cells were grown in suspension at 28°C. Cultures were passaged when a density of approximately 1×10^7 cells/ml had been reached. Cell density was determined with the use of a bright line haemocytometer (Hauser Scientific), viewed under an inverted bright field microscope (Olympus Tokyo).

2.16.2 Transient transfection of S2 cells

S2 cells were transfected using a calcium phosphate transfection kit (Invitrogen) according to manufacturer's instructions. Three ml S2 cells were seeded at a density of 1×10^6 cells/ml in a 35 mm culture dish and grown for 16 h or until a density of $2\text{-}4\times10^6$ cells/ml was reached. DNA mix (recombinant DNA and 36 µl of 2 M $CaCl_2$ made up to 300 µl with sterile H_2O) was then added drop-wise to 300 µl 2x HEPES-buffered saline (HBS) (50 mM HEPES, 1.5 mM Na_2HPO_4, 280 mM NaCl, pH 7.1) while continuously mixing with sterile air. The resulting solution was left at RT for 30-40 min, vortexed and added drop-wise to the cells with gentle agitation to mix. Cells were transfected with either 19 µg (single transfection) or 10 µg (co-transfection) of each relevant expression construct. All transgenes used in this study were expressed from the pMT/V5-His vector, which is under transcriptional regulation via a metallothionein promoter. After incubation for 18 h, the transfected cells were washed twice with fresh medium. This was

achieved by harvesting the cells by centrifugation at 1,000 x g for 3 min, followed by resuspension in 4 ml medium. Cells were then re-plated into the original dish in 3 ml fresh medium, immediately induced with 20 μl 100 mM $CuSO_4$ and returned to the incubator. Cells were used 24 h post induction.

2.17 $[Ca^{2+}]_i$ measurements using aequorin

2.17.1 $[Ca^{2+}]_i$ measurements in aequorin expressing tubules

The method for measurement of $[Ca^{2+}]_i$ in aequorin expressing tubules is described in Rosay et al, 1997, and is as follows. For reconstitution of intracellular aequorin, 20-30 tubules from 3-7 day old adults were dissected in Schneider's medium and placed in 160 μl of Schneider with coelenterazine added to a final concentration of 2.5 μM. Samples were then incubated in the dark for 3-4 hours. Bioluminescence recordings were carried out using an LB9507 luminometer (Berthold Wallac). To control for transients due to the injection process itself, samples were 'mock' injected with 25 μl of Schneider's before injection with the appropriate agonist at the desired concentration. At the end of each recording tubules were disrupted with 300 μl lysis solution (1% (v/v) Triton X-100, 100 mM $CaCl_2$), causing discharge of the remaining aequorin and allowing estimation of the total amount of aequorin in the sample by integration of total counts. Ca^{2+} concentrations for each time point in an experiment were calculated by backward integration, using a program written in Perl, based on the method described by Button and Eidsath (1996).

2.17.2 $[Ca^{2+}]_i$ measurements in S2 cells expressing aequorin

Transiently transfected S2 cells were harvested and incubated with 2.5 μM coelenterazine (Molecular Probes) in the dark at room temperature for 1 h. 25000 cells were used per sample tube in DES medium (Invitrogen) supplemented with 10 % FCS. Peptide agonists were diluted to working concentration in DES medium/FCS. At the end of each recording, the cells were disrupted in 300 μl lysis solution (1% (v/v) Triton X-100, 100 mM $CaCl_2$) and the calcium concentrations calculated as described in 2.18.1

2.18 Fluid secretion assays

Malpighian tubules from adult female and male *Drosophila* flies were dissected using forceps under Schneider's *Drosophila* medium (Invitrogen). The fluid secretion assays were performed as described by Dow et al., 1994. A Petri dish was filled with paraffin wax and depressions made for the bathing medium drops. The bathing medium was 1:1

Schneider's and *Drosophila* saline/glucose. *Drosophila* saline consisted of (in mM): NaCl, 117.5; KCl, 20; $CaCl_2$, 2; $MgCl_2$, 8.5; $NaHCO_3$, 10.2; NaH_2PO_4, 4.3; HEPES, 15; glucose, 20. Drops of 9 µl of bathing medium were placed in each depression and the dish filled with mineral oil (to prevent evaporation). A pair of tubules, still linked by the ureter, were placed in the drop using a fine glass rod. One end of the tubule was then pulled out of the drop and wrapped around a thing steel pin, to which it adhered by surface tension. The secreted fluid emerged at the cut end of the ureter and the drops were removed from the ureter at 10 min intervals. The diameter of the droplets was measured using an ocular micrometer and thus the volume of the secreted fluid calculated in nl/min. The data was analysed using Excel 5.0. All data was reported as mean ±SEM and viewed using GraphPad Prism. Statistical significance of differences between treatments was assessed using Student's *t*-test for unpaired sample, taking the critical value of *P* to be 0.05 (two tailed). Cardioacceleratory peptide 2b, CAP_{2b} and *Drosophila* leucokinin were custom-synthesised by Research Genetics, Inc, and added to tubules at 10^{-7} M (diluted to 1 mM in H_2O and then further in Schneider's/saline).

2.19 Cyberscreening and DNA and protein sequence analysis

Cyberscreening was performed using Netscape Communicator on an Apple Macintosh computer or Internet Explorer on a PC. NCBI (http://www.ncbi.nlm.nih.gov/) and BDGP (http://www.fruitfly.org) databases were searched using BLASTN, BLASTP, BLASTX or TBLASTN searches as appropriate.

DNA sequences were viewed and manipulated in MacVector 7.0 (Oxford Molecular Group PLC.). This programme was used to deduce restriction enzyme sites, for primer design and to translate sequences into protein using the open reading frame and translation features.

Protein sequences were aligned either directly in MacVector 7.0 or using ClustalW (http://www.ebi.ac.uk/clustalW/index.html) (Thompson et al., 1994) on the default settings. Bootstrap tree plots were also performed in ClustalW on default settings. Protein alignments were viewed in BioEdit (Hall, 1999) and Tree alignments in Treeview version 1.6.6 (Roderic D. M. Page).

PSORT II (http://psort.nibb.ac.jp/form2.html) (Nakai and Horton, 1999), InterProScan (http://www.ebi.ac.uk/interpro/scan.html) and MacVector 7.0 were used to look at secondary protein structure, targeting and subcellular localisation.

Chapter 3

Measuring organellar Ca^{2+} in the Malpighian tubule using targeted aequorin

3.1 Summary

This chapter discusses the undertaking of a transgenic approach to measure organellar Ca^{2+} in the Malpighian tubule using targeted aequorin. Aequorin is a Ca^{2+} sensitive photoprotein (see section 1.2.2) which, with the addition of encoded targeting motifs, can be localised to specific organelles.

The principal aim of this project was to generate transgenic *Drosophila* that could express ER-targeted aequorin in a cell specific manner and allow real-time monitoring of $[Ca^{2+}]_{ER}$ in the tubule. Transgenic flies were made but it became apparent that the targeting sequences were interfering with the photoprotein's function. Other targeting sequences were investigated, however due to the retention properties of insect ER it seems that the use of aequorin for measuring insect $[Ca^{2+}]_{ER}$ is presently not feasible.

Mitochondrial Ca^{2+} responses in the tubule have been successfully monitored using targeted aequorin. The neuropeptides capa-1 and drosokinin both elicit $[Ca^{2+}]_{mt}$ increases in the respective cell types of the tubule. Typically, an IP_3-induced Ca^{2+} event results in an immediate large uptake of Ca^{2+} into mitochondria. However, the responses in the tubule are different, as they are slower, smaller and appear to correspond to the secondary component of the $[Ca^{2+}]_i$ event, rather than the primary. This data could represent unusual dynamics of Ca^{2+} signalling in the tubule, or could reflect mitochondrial placement within the cells.

Additionally, generation of Golgi-targeted aequorin fly lines has allowed the investigation into a possible means of real-time measurement of $[Ca^{2+}]_{Golgi}$ in the tubule.

3.2 Introduction

3.2.1 ER-targeted aequorin

The ER is the principle Ca^{2+} signalling organelle in non-excitable cells. Upon stimulation of a cell with an IP_3-producing agonist, the ER releases Ca^{2+} into the cytosol to produce a increase in $[Ca^{2+}]_i$. This increase can activate downstream signalling pathways or directly act to change the action of the cell. Measuring Ca^{2+} levels in the ER would provide a greater insight into how this organelle contributes to these signals.

The first attempt to measure $[Ca^{2+}]_{ER}$ with aequorin, involved attachment of the calreticulin targeting sequence at the N-terminus and the KDEL retention sequence at the C-terminus of wild type aequorin (Kendall et al.,1992b) (see figure 3.1 A). They estimated the resting $[Ca^{2+}]_{ER}$ was 1-5 mM in COS cells and also demonstrated a reduction in luminescence when cells were treated with the Ca^{2+} ionophore ionomycin in the absence of external Ca^{2+}. It was also shown that 90% of the active aequorin would be consumed within minutes at resting conditions, due to the high levels of Ca^{2+} in the ER. A strategy to attenuate the rate at which aequorin is consumed in environments of high Ca^{2+}, yielded a mutated version of aequorin (D to A at position 119) (Kendall et al., 1992a). This engineered aequorin possessed a 20-fold reduction in affinity for Ca^{2+}, so would allow a longer period of time to measure $[Ca^{2+}]_{ER}$ before the active aequorin was consumed.

This method of targeting aequorin to the ER was discovered to be flawed with the discovery that any addition of residues (i.e. KDEL) to the aequorin C-terminus causes instability of the protein and drastically alters its luminescent properties (Nomura et al., 1991; Watkins and Campbell, 1993). As the calreticulin sequence alone is not sufficient for efficient targeting of aequorin to the ER (Kendall et al.,1992b), an alternative N-terminal targeting sequence would be required. This problem was solved by Montero et al. (1995), who fused aequorin (D119A) to domains of the Igγ2b heavy chain immumoglobulin (see figure 3.1 B). This is an N-terminal tag that retains aequorin in the ER by interacting with the resident ER protein BiP.

To allow reconstitution of ER-targeted aequorin with coelenterazine, the ER has to be depleted sufficiently of Ca^{2+} beforehand. This is achieved by removal of extracellular Ca^{2+}, addition of Ca^{2+} chelators and use of SERCA inhibitors (Montero et al., 1995). The coelenterazine is then added and after reconstitution the cells are washed and Ca^{2+} reintroduced to the extracellular medium. With available Ca^{2+}, the ER rapidly refills and consequently begins to consume the active aequorin. However, the active aequorin in the ER is consumed within minutes after the beginning of refilling (even with the mutant aequorin) (Montero et al., 1995). The use of a coelenterazine analogue, coelenterazine n (Shimomura et al., 1993) reduces the rate of emission of luminescence by aequorin. This

further extends the ability of aequorin to report high Ca^{2+} levels and using this method, accurate monitoring of $[Ca^{2+}]_{ER}$ has been performed by several groups (Barrero et al., 1997; Montero et al., 1997; Robert et al., 1998). Barrero and colleagues (1997) showed resting $[Ca^{2+}]_{ER}$ levels in HeLa cells are 500-600 µM and that agonists induce a fast but relatively small decrease in $[Ca^{2+}]_{ER}$. Measurements using Mag-Fura-2 in pancreatic acinar cells reported similar values for $[Ca^{2+}]_{ER}$ of 100–300 µM (Mogami et al., 1998).

The ER is the principal IP_3-sensitive, Ca^{2+} releasing store in most cell types. Two of the diuretic hormones that act on the *Drosophila* Malpighain tubule (capa and drosokinin) act via an IP_3/Ca^{2+} pathway. Therefore the ER is the primary intracellular Ca^{2+} store to be investigated as a possible contributable pool in the respective Ca^{2+} responses. Due to the previous development of an aequorin-based Ca^{2+} assay for Malpighian tubules (Rosay et al., 1997), an ER-targeted aequorin approach to measuring $[Ca^{2+}]_{ER}$ in the tubule would be the most practical way forward.

3.2.2 Mitochondrially-targeted aequorin

Mitochondria were effectively put on the shelf, with respect to Ca^{2+} signalling and homeostasis when it became apparent that they only contained minute amounts of Ca^{2+} (Somlyo et al., 1985) and that by indirect measurement of $[Ca^{2+}]_i$ (Grynkiewicz et al., 1985), they released no or marginal quantities of Ca^{2+}. However Rizzuto and colleagues rescued mitochondria from this oblivion when they targeted aequorin to mitochondria and observed the unique $[Ca^{2+}]_{mt}$ response to Ca^{2+} mobilising agonists (Rizzuto et al., 1992). This response is of a similar shape to the bulk cytoplasmic response, however the concentrations reached can be as much as 5 times greater. As mentioned in section 1.1.4.3, this is believed to be due to the close proximity or coupling of the mitochondria to the ER (Rizzuto et al., 1998). The mitochondrial Ca^{2+} uptake machinery (the electrogenic importer of the inner membrane) possesses a low affinity for Ca^{2+} (for review see Benardi, 1999). The paradox of how the mitochondria accumulate the high concentrations of Ca^{2+}, considering the characteristics of the uniporter, is explained by the proximity of the mitochondria to the supramicromolar $[Ca^{2+}]_i$ microdomains next to the release channels on the ER (Rizzuto et al., 1993). In some cells this large mitochondrial uptake has been found to be even higher that first estimated. Montero and colleagues utilised a lower affinity mitochondrially-targeted aequorin (mtAEQmut) to demonstrate stimulated $[Ca^{2+}]_{mt}$ levels of up to 800 µM in chromaffin cells (Montero et al., 2000).

The targeting of aequorin to mitochondria is achieved by addition of the mitochondrial-targeting pre-sequence (MPS) of human cytochrome c oxidase subunit VIII to the N-

terminus of aequorin (see figure 3.1 C). A HA1 epitope is also incorporated to allow immuno-histochemical localisation of the recombinant aequorin.

Real-time measurements of $[Ca^{2+}]_{mt}$ in the *Drosophila* Malpighian tubule with aequorin would help determine the nature of any mitochondrial response to the intracellular Ca^{2+} increases invoked by diuretic hormones such as capa-1 and drosokinin.

3.2.3 Golgi-targeted aequorin

The Golgi apparatus is also emerging as an important and functional Ca^{2+} store (see section 1.1.4.2). Understanding of the Golgi Ca^{2+} pool was greatly enhanced with the real-time measurements of $[Ca^{2+}]_{Golgi}$ with a recombinant targeted aequorin (Pinton et al., 1998). The mutant variant of aequorin (D119A) was targeted to the Golgi by the N-terminal addition of residues 1-69 of the human sialyltransferase (ST) protein (see figure 3.1 D). This region of ST includes a transmembrane domain responsible for retention within the Golgi apparatus. Pinton and colleagues discovered that the resting $[Ca^{2+}]_{Golgi}$ was ~300 μM, which is as almost as high a level as the ER. Due to these high levels of Ca^{2+}, the Golgi apparatus has to be depleted of Ca^{2+} before the recombinant aequorin (D119A) can be reconstituted with coelenterazine *n* (in a similar method to measuring $[Ca^{2+}]_{ER}$ with aequorin).

$[Ca^{2+}]_{Golgi}$ plays a critical role in the processing of proteins (see section 1.1.4.2), therefore will conceivably be tightly regulated for this purpose in the Malpighian tubule. An intriguing possibility though, is whether the Golgi is acting as an IP_3-sensitive Ca^{2+} pool in either of the two main cell types of the Malpighian tubule.
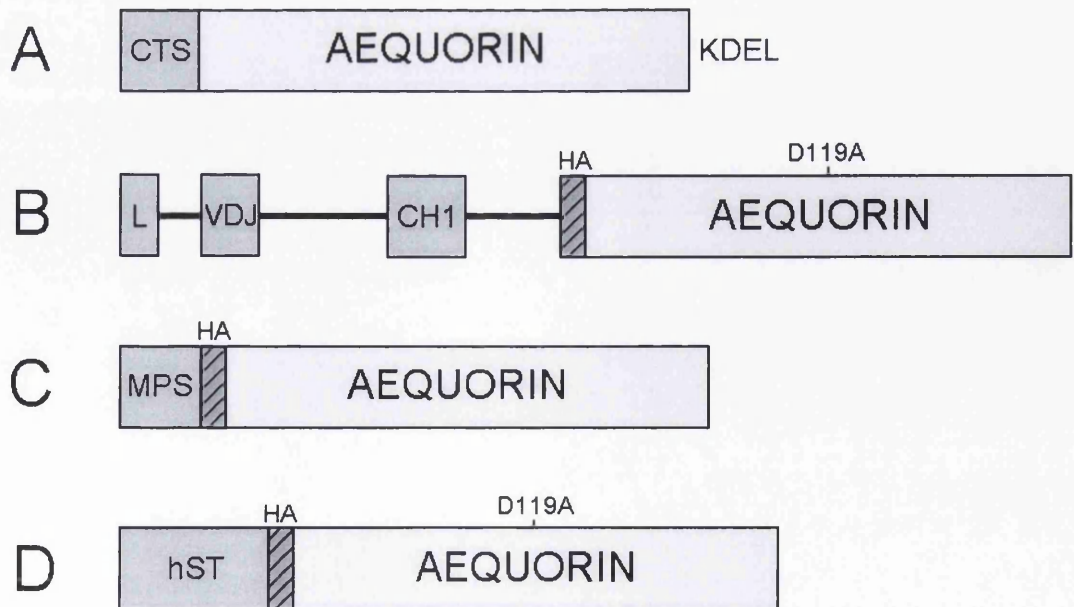
Figure 3.1 Targeted aequorins. (A) The original ER-targeted aequorin. (B) The more recent and functional ER-targeted aequorin. (C) Mitochondrially-targeted aequorin. (D) Golgi-targeted aequorin. D119A is the amino acid substitution that reduces aequorin sensitivity to Ca^{2+}. Abbreviations are as follows: CTS, calreticulin signal; HA, haemaglutinin epitope tag; L, VDJ and CH1 are all components of the Igγ2b heavy chain immumoglobulin; MPS, mitochondrial-targeting pre-sequence of human cytochrome c oxidase subunit VIII; hST, human sialyltransferase region sufficient for targeting to the Golgi.

71

3.3 Results

3.3.1 Problems of using aequorin as a calcium reporter in the ER of *Drosophila*

The initial aim of the project was to generate transgenic *Drosophila* that could express ER-targeted aequorin under the control of the GAL4/UAS system and additionally under heat-shock control. A construct containing an ER-targeted aequorin template (pSVAEQERK) was obtained from Molecular Probes and the template was cut out and cloned into the appropriate P-element vectors (see table 2.4). These constructs were used to produce two separate transgenic lines for both pP{UAST-ERaeq} and pP{CaSpeR-hs-act-ERaeq}.

Initial experiments involved heat-shocking pP{CaSpeR-hs-act-ERaeq} flies, dissecting out tubules and incubating them with coelenterazine *n*. These tubules did emit light and the luminescence increased dramatically when the tubules were exposed to total luminescence (TL) solution. This was encouraging, as there was a luminescent signal, however the TL signal did not decrease immediately but remained high for a considerable amount of time (which was not expected). Consequent experiments involved attempts, using various protocols, to deplete $[Ca^{2+}]_{ER}$ of the tubule sufficiently to allow reconstitution with coelenterazine. This included incubating the tubules in Ca^{2+}-free Schneider's medium (Sigma), using the Ca^{2+} chelator EGTA and also incubating with the reversible SERCA inhibitors tert-butylhydroquinone (BHQ) and cyclopiazonic acid (CPA). This never appeared to be successful, as after washes and addition of Ca^{2+} refilling of the ER store was never observed and the TL response was always unusual (data not shown).

Eventually it became apparent that the ER-targeted cDNA template used, encoded the aequorin targeted with the calreticulin signal and the KDEL motif (see section 3.2.1). As previously mentioned the KDEL sequence destabilises aequorin and affects its luminescent properties. This explained the lack of success and furthermore the template contained the wild-type sequence for aequorin, not the mutant version (D119A) required for successful measurement of $[Ca^{2+}]_{ER}$.

In response to this, I investigated the possibility of using the aequorin targeted to the ER with the Igγ2b heavy chain immumoglobulin (Montero et al., 1995). However, after searching the literature regarding the ER retention of this class of immuoglobulin in insect cells, it became evident that this approach may not succeed in *Drosophila*. Kirkpatrick and colleagues (1995) demonstrated that these immunoglobulins are secreted from insect Sf9 cells, rather than being retained in the ER. Although this could be a unique property of Sf9 cells, there would be high risk of this approach also being unsuccessful due to the possibility of the aequorin not being retained within the ER of the Malpighian tubule.

It appears that with the problem of being unable to use C-terminal retention sequences on aequorin and the retention properties of insect ER, that the present technology cannot allow

us to perform aequorin-based measurements of $[Ca^{2+}]_{ER}$ in insect cells. An alternative strategy was then pursued, the development of an encoded fluorescent reporter that could be targeted to the ER and possessed a suitable sensitivity to Ca^{2+} (see chapter 4).

3.3.2 Measurement of mitochondrial Ca^{2+} in *Drosophila* S2 cells

The cDNA template for mitochondrially-targeted apoaequorin was cloned into the expression vector pMT/V5-His A (Invitrogen) (see table 2.4). This construct was co-transfected in S2 cells, with another construct containing the cDNA for the *Drosophila* leucokinin receptor (Radford et al., 2002). Immunocytochemistry was performed on these cells to check targeting of the aequorin (see figure 3.3). The results show that the localisation is not cytoplasmic, however, co-localisation with a mitochondrial marker would be required for confirmation. Calcium assays were carried out using these cells (as described in 2.17.2), using the drosokinin peptide at a concentration of 10^{-7} M. Control experiments were also performed using a non-targeted cytoplasmic aequorin construct. The results of these experiments are shown in figure 3.3. The $[Ca^{2+}]_{mt}$ response to drosokinin was much larger than the bulk cytoplasmic response, with the maximum level reached being approximately twice the value.

It was additionally noticed that the initiation of the $[Ca^{2+}]_{mt}$ response was delayed by approximately 200 ms, compared to the $[Ca^{2+}]_i$ response (see figure 3.3B).
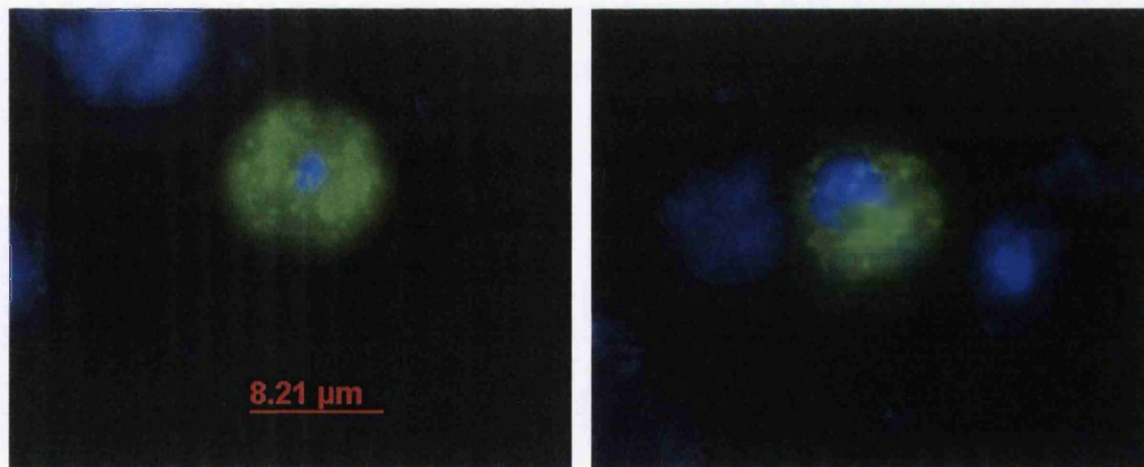
Figure 3.2 ICC localisation of mitochondrially-targeted aequorin in S2 cells. The anti-aequorin antibody was used at 1:2000 dilution and the FITC secondary antibody (green) at 1:2000 dilution. The nuclei are stained with DAPI (blue). Pictures taken on a Zeiss Axiophot microscope (see chapter 2).

Although the kinetics of these responses fully the reporting of $[Ca^{2+}]_{mt}$, it has not been fully confirmed that the aequorin biosensor is localising efficiently in these insect cells. Until the aequorin is co-localised (as mentioned above) and the effect of mitochondrial uncouplers on the signal is observed, it can only be presumed that these are mitochondrial responses. This should be kept in mind throughout the rest of this chapter.
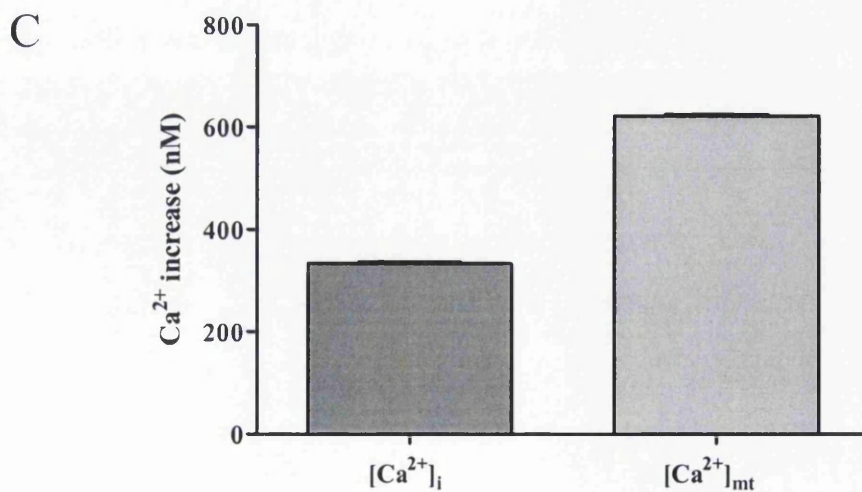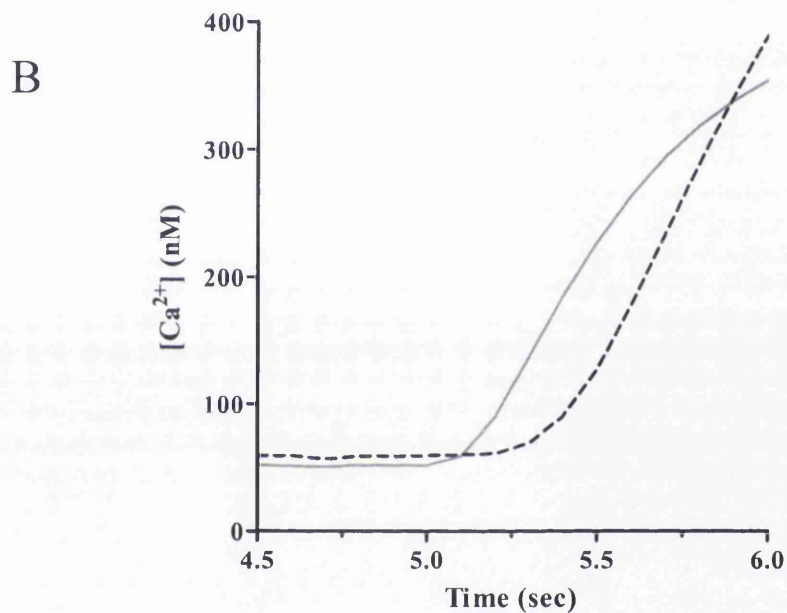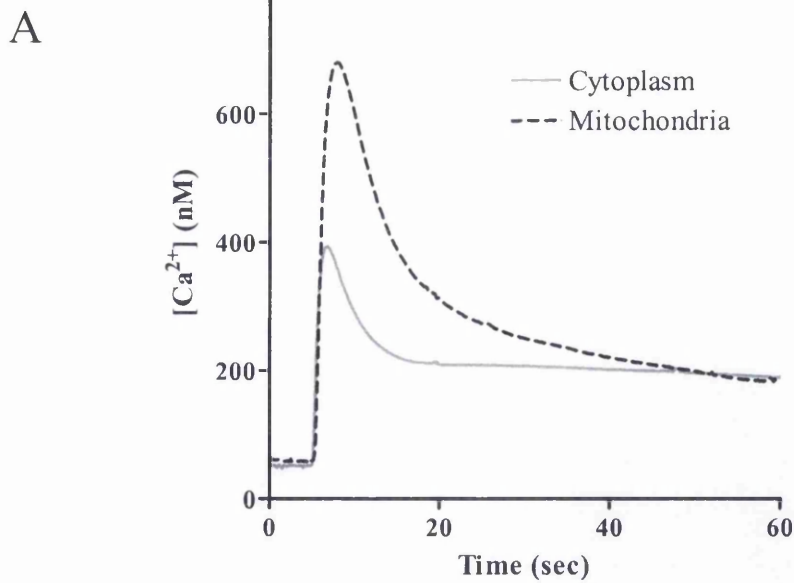
Figure 3.3 Measurement of mitochondrial Ca^{2+} in S2 cells using targeted aequorin. S2 cells expressing both the *Drosophila* leukokinin receptor (dLKR) and mitochondrially-targeted aequorin were stimulated with the drosokinin peptide at a concentration of 10^{-7} at 10 seconds. (A) Averaged [Ca^{2+}]$_{mt}$ and [Ca^{2+}]$_i$ responses. (B) Magnified region, showing the detailed dynamics of the response directly after the addition of the peptide. (C) Bar graph showing the maximum increase above basal levels.

3.3.3 Measurement of mitochondrial Ca^{2+} in the Malpighian tubule using aequorin

To allow real-time measurements of [Ca^{2+}]$_{mt}$ in the tubule, transgenic flies had to be generated. The mitochondrially targeted aequorin template (as used by Rizzuto et al., 1992) was cloned into the P-element vectors pP{UAST} and pP{CaSpeR-hs-act} (see table 2.4). These constructs were micro-injected to produce two separate transgenic lines for both pP{UAST-mtAEQ} and pP{CaSpeR-hs-act-mtAEQ}.

The assays for measuring [Ca^{2+}]$_{mt}$ in the tubule were performed in the same manner as for measuring [Ca^{2+}]$_i$ (see section 2.17.1). The only difference was the quantity of tubules used for each assay; due to the targeting there is less aequorin per cell, therefore more tubules were used to compensate for this. pP{CaSpeR-hs-act-mtaeq} tubules were used in the initial experiments, however even using 60 tubules per sample the luminescent signal was very low. This was partially due to the targeting but in most part due the comparative weakness of the *hsp70* promoter compared to the GAL4/UAS system (general observation and personal communication from Martin Kerr). Therefore all subsequent experiments utilised the pP{UAST-mtaeq} flies.

The pP{UAST-mtaeq} flies were crossed with the GAL4 lines c42 and c710, which are enhancer trap lines (see section 1.3.2.2) that specifically express GAL4 in the principal cells (c42) and the stellate cells (c710) of the tubule (Sözen et al., 1997). The resulting F$_1$ generation specifically expressed mtAEQ, either in the principal or stellate cells. Approximately 30 tubules were used for each sample for the principal cell measurements and 60 for the stellate cell measurements. The experiments were performed as described in 2.17.1. Figures 3.4 and 3.5 show typical measurements of [Ca^{2+}]$_{mt}$ in each cell type and also examples of respective [Ca^{2+}]$_i$ responses for comparison.

As described in section 3.2.2 and demonstrated in the last section, an IP$_3$-mediated [Ca^{2+}] response in most cell types results in a [Ca^{2+}]$_{mt}$ rise that is greater than the bulk [Ca^{2+}]$_i$ rise and occurs within half a second of the stimulus. However, upon addition of capa-1 to the tubule, a principal cell [Ca^{2+}]$_{mt}$ response directly after the stimulus is hardly perceivable, if present at all (see figures 3.4A - D). However there is a delayed (by approximately 30 – 60 seconds), slower and sustained response that coincides with the secondary [Ca^{2+}]$_i$ response. This [Ca^{2+}]$_{mt}$ rise was heterogeneous between samples (as shown by figures 3.4A – D), with respect to the maximum levels reached and the shape of the response.

The stellate cell [Ca^{2+}]$_{mt}$ responses to drosokinin were also delayed, the [Ca^{2+}]$_{mt}$ increase appears to coincide with the secondary response rather than the primary (figure 3.5A). The dynamics of the [Ca^{2+}]$_{mt}$ rise in the stellate cells were more consistent between samples, compared to the principal cell measurements. Figure 3.5B shows a the initial response to drosokinin in more detail; the [Ca^{2+}]$_{mt}$ increase does not start until approximately 1 second
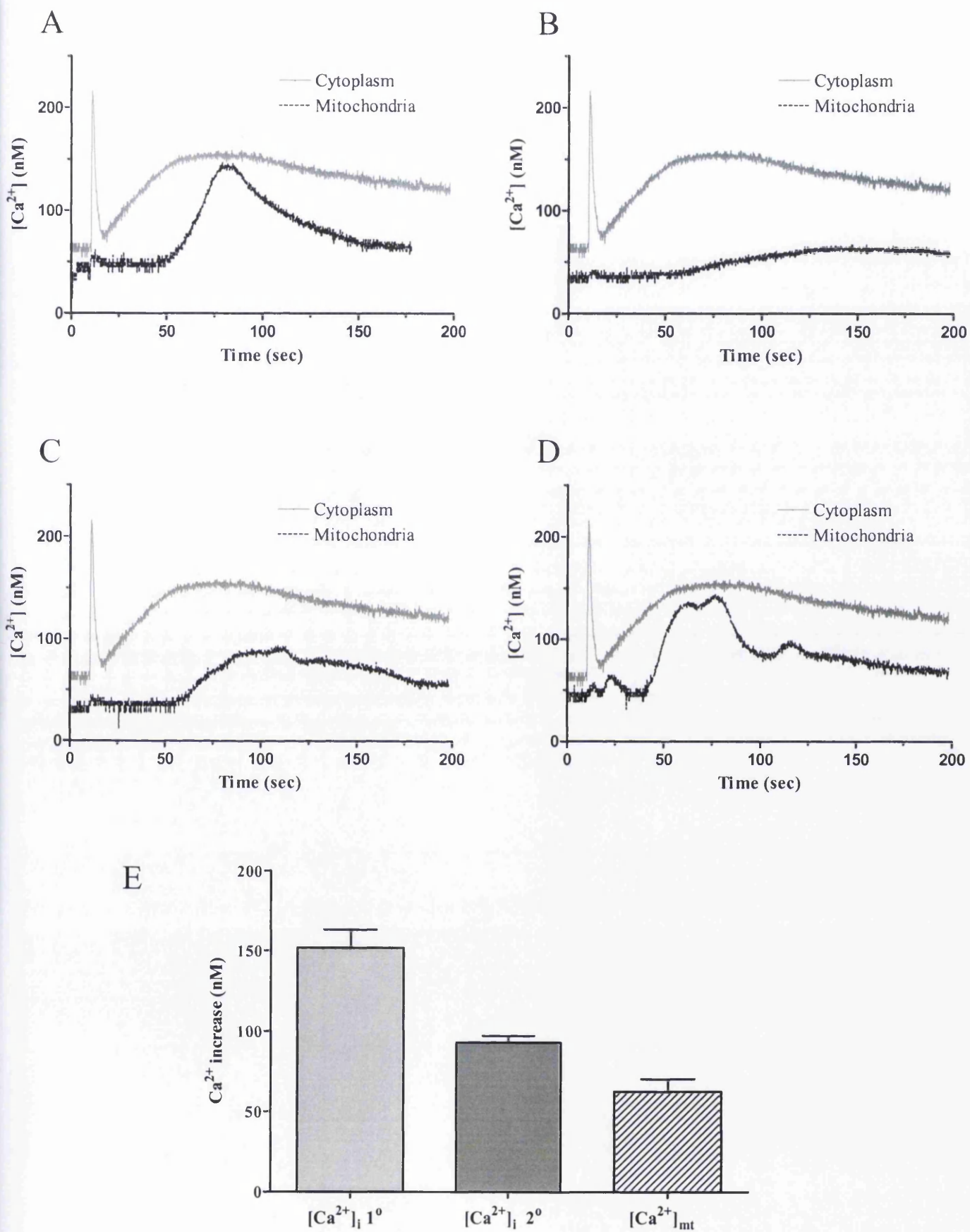
Figure 3.4 Measurement of mitochondrial Ca^{2+} in principal cells using targeted aequorin. The capa-1 peptide was added at 10 seconds at a concentration of 10^{-7} M. (A) – (D) Examples of $[Ca^{2+}]_{mt}$ responses to capa-1 in the principal cell. A typical $[Ca^{2+}]_i$ response is also shown for comparison. (E) Bar graph showing maximum increase above basal levels for the control primary and secondary response and the mitochondrial response (n ≥13).
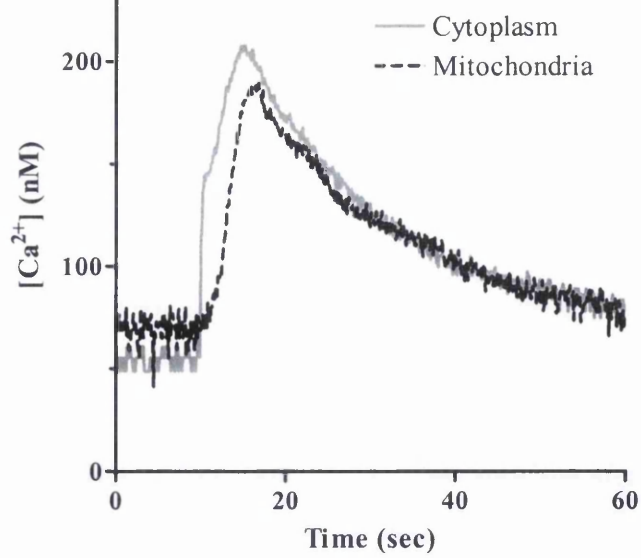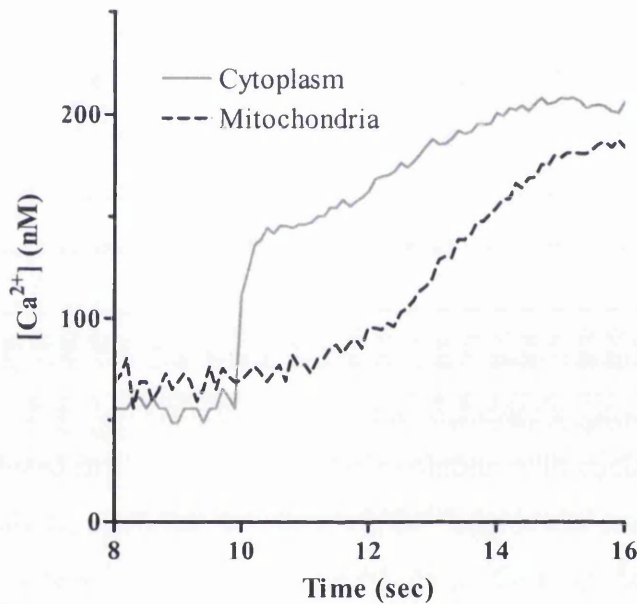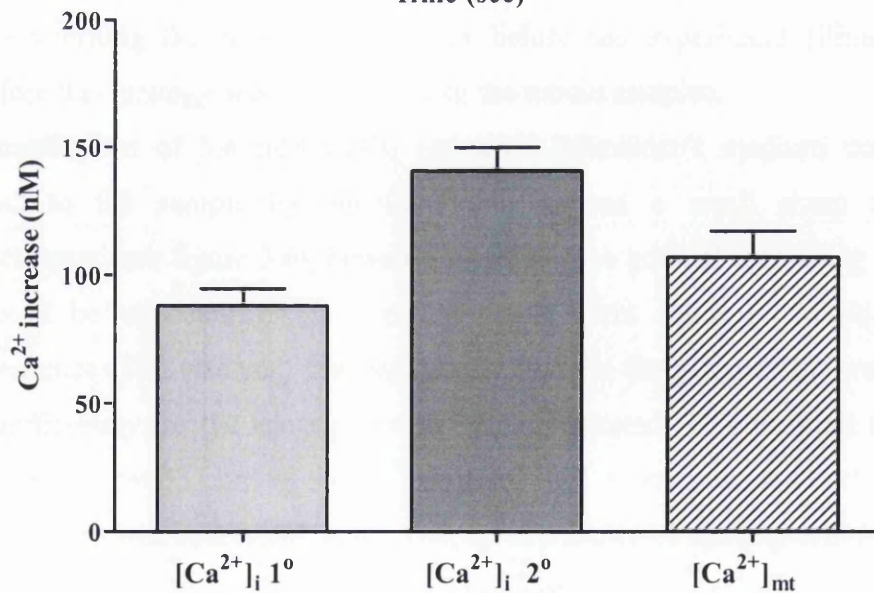
Figure 3.5 Measurement of mitochondrial Ca^{2+} in stellate cells using targeted aequorin. The drosokinin peptide was applied at 10 seconds at a concentration of 10^{-7} M. (A) A typical $[Ca^{2+}]_{mt}$ and control $[Ca^{2+}]_i$ response. (B) Magnified region, showing the detailed dynamics of the response directly after the addition of the peptide. (C) Bar graph showing maximum increase above basal levels for the control primary and secondary response and the mitochondrial response (n ≥10).

after addition of the peptide and the rise in $[Ca^{2+}]_{mt}$ levels are more gradual than the primary $[Ca^{2+}]_i$ increase. Furthermore, in both cell types the $[Ca^{2+}]_{mt}$ response is only equal to or less than the average $[Ca^{2+}]_i$ levels reached. This is in contrast with the $[Ca^{2+}]_{mt}$ response in S2 cells, which was much greater.

3.3.4 Golgi-targeted aequorin in the Malpighian tubule

Due to a template for Golgi-targeted aequorin not being freely available, a suitable cDNA was constructed using fusion PCR (section 2.6.3 and figure 2.1) and targeted mutagenesis (for construction details, see table 2.4). The sialyltransferase sequence (required for targeting) was fused to the 5' end of the aequorin sequence and cloned into pCRT7/NT. This construct was used in PCR mutagenesis to introduce a D119A change into aequorin. The template was then cut out and cloned into pUAST. Four separate transgenic lines were generated. These flies were crossed to the GAL4 line c42 (as described in the last section) to produce flies expressing Golgi-targeted aequorin in the principal cells. Confirmation of the intracellular localisation of the aequorin has not yet been performed; however, this could be achieved by using either an antibody for the sialyltransferase domain or for aequorin.

Approximately 24 tubules were dissected (for each sample) in standard Schneider's medium and then transferred to Ca^{2+}-free Scheider's (Invitrogen). The tubules were initially incubated in Ca^{2+}-free Schneider's solution with coelenterazine for 3 hours. It has been previously reported that depletion of $[Ca^{2+}]_{Golgi}$ in cell lines causes a reorganisation of the Golgi apparatus This can be prevented by performing the incubation step at 4°C and then re-warming the sample 15 minutes before the experiment (Pinton et al., 1998). Therefore this strategy was employed with the tubule samples.

A concentration of 5.4 mM $CaCl_2$ (standard Schneider's medium concentration) was restored to the sample by injection. This caused a small sharp transient rise in luminescence (see figure 3.6), however there was no gradual increasing of luminescence, as would be expected if the depleted stores were refilling. Additionally, the total luminescence (TL) was very low, suggesting that the Golgi apparatus was not depleted of Ca^{2+} sufficiently for the apoaequorin to be reconstituted. To ensure all traces of external Ca^{2+} were removed, 1mM of the Ca^{2+} chelator EGTA was included in the incubation step. This approach was successful in allowing an abundance of apoaequorin to be reconstituted (see TL peak in figure 3.6), but the re-addition of external Ca^{2+} did not elicit a refilling of the store. The addition of Ca^{2+} did cause a large transient increase in luminescence, though this is probably due to aequorin from damaged or expired tubules.

Without refilling of the store it is not possible to perform any functional experiments. Other approaches were attempted to try and overcome this problem, such as using coelenterazine n and shortening the incubation time (in case the prolonged absence of Ca^{2+} was killing the cells). However, so far none of these protocols have succeeded in refilling of the Golgi apparatus.
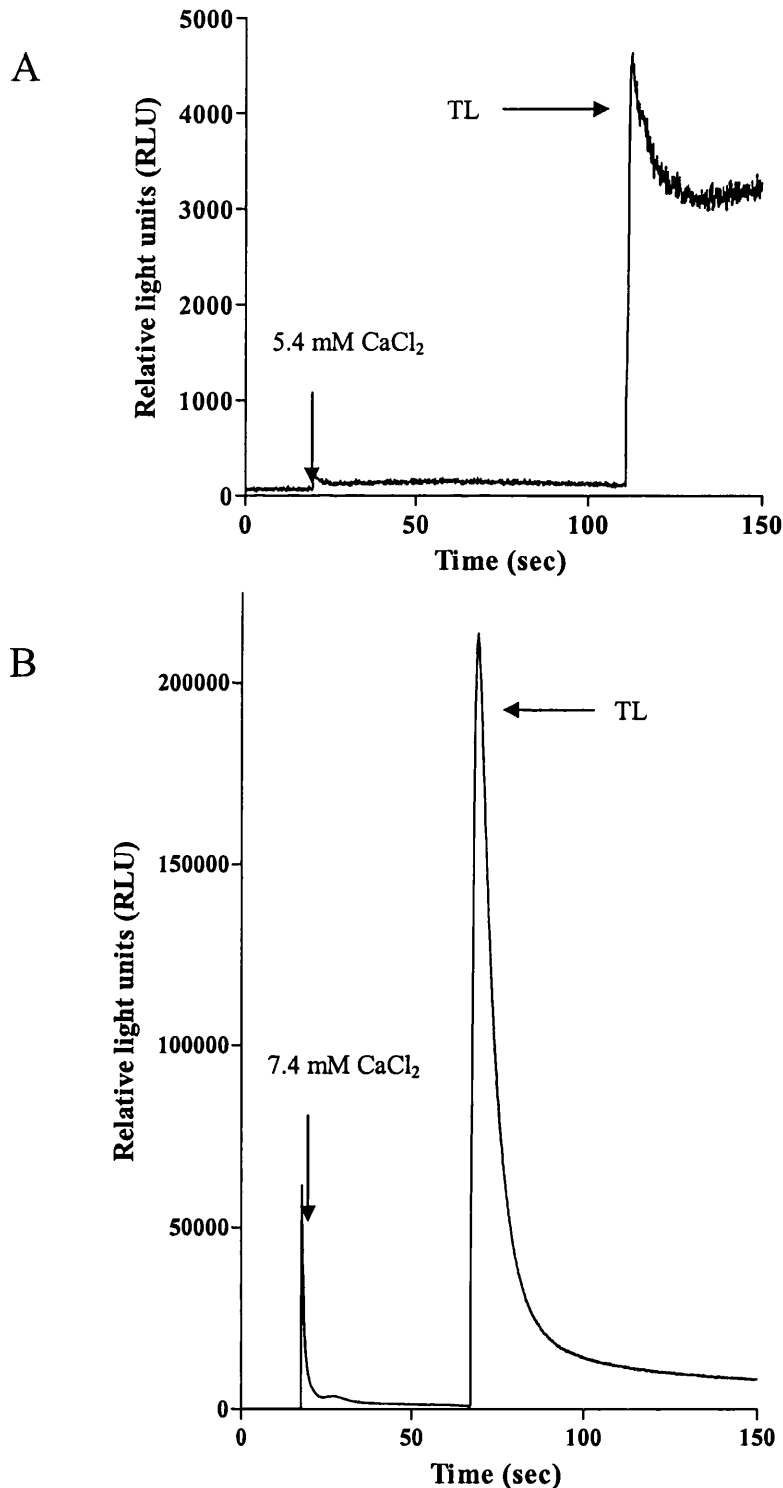
Figure 3.6 Attempts at refilling depleted Golgi Ca^{2+} stores. (A) Tubules incubated in Ca^{2+}-free Schneider's without EGTA. (B) Tubules incubated in Ca^{2+}-free Schneider's with 1 mM EGTA. $CaCl_2$ and total luminescence (TL) were added at times indicated. Standard Schneider's medium contains 5.4 mM $CaCl_2$, hence 5.4 mM $CaCl_2$ was added to Ca^{2+}-free Schneider's and 7.4 mM $CaCl_2$ to Ca^{2+}-free Schneider's containing 1 mM EGTA.

3.4 Discussion

It was unfortunate that the ER-targeted approach was unsuccessful, as it could have enabled real-time, quantitative measurements of $[Ca^{2+}]_{ER}$ in the tubule. This approach may be possible in the future, if an efficient N-terminal ER retention signal is discovered that works in *Drosophila*. Alternatively, an aequorin variant that is not affected by a C-terminal tag could be utilised, as it would allow the addition of the KDEL motif. A variant of aequorin, with no cysteine residues has been reported to function with a C-terminal tag (Deo and Daunert, 2001), however it is not known whether this would work for measuring $[Ca^{2+}]_{ER}$. Due to this method being fruitless, an alternative strategy of developing a fluorescent reporter was undertaken. This is described in chapter 4.

The Golgi-targeted aequorin approach, although it has not yet been successful, should in theory be possible, if the correct conditions can be achieved to allow refilling of the stores after reconstitution. Potential reasons for the inability of the stores to refill are that either the cells are dying because of the removal of external Ca^{2+} or the re-addition of such high levels of Ca^{2+} are in some way inhibiting the Ca^{2+}-ATPases of the cells. Future attempts at refilling the stores could consist of re-introducing the Ca^{2+} at initially very low concentrations and also washing of the tubules after the incubation to remove the EGTA.

The application of mitochondrially-targeted aequorin in S2 cells demonstrated that an IP_3-mediated response elicited a typical $[Ca^{2+}]_{mt}$ rise. This comparatively large $[Ca^{2+}]$ observed in the mitochondria was first described by Rizzuto and colleagues and has been observed in many other cell types (Rizzuto, 1992). As mentioned in section 3.2.2, the large $[Ca^{2+}]_{mt}$ increase is believed to be due to the close interaction of the ER and the mitochondria (Rizzuto et al., 1998). The 200 ms delay before the initiation of Ca^{2+} uptake into the organelle is likely to be due to the time required for activation of the mitochondrial uniporter.

The data obtained from using the mitochondrially-targeted aequorin in the tubule was very different to the S2 cell response. In the principal cells there was no large $[Ca^{2+}]_{mt}$ increase coinciding with the IP_3-mediated primary $[Ca^{2+}]_i$ response, although there was a delayed and slower $[Ca^{2+}]_{mt}$ rise that only reached 63 ± 8 nM above basal levels (see figure 3.4). There are two possible reasons for this lack of an initial mitochondrial Ca^{2+} uptake; either the mitochondria are not coupled or in close proximity to the ER, or the ER is not the IP_3-releasable Ca^{2+} pool. In chapter 4 there is data to support that the ER is not the IP_3-releasable pool in the principal cell and furthermore, chapter 5 provides evidence supporting the involvement of an alternative intracellular pool. Additionally, in the principal cell, a large proportion of the mitochondria are localised in or are in close proximity to the apical microvilli (Eichelberg and Wessing, 1975; general observation).

This distribution of mitochondria will affect Ca^{2+} uptake, especially if the $[Ca^{2+}]_i$ rise is predominantly perinuclear or basolateral.

The beginning of the $[Ca^{2+}]_{mt}$ increase in principal cells does not start until 30-60 seconds after addition of the peptide and the peak usually corresponds to the secondary $[Ca^{2+}]_i$ peak. This suggests that the Ca^{2+} taken up by the mitochondria (after capa-1 stimulation) originates from the same source that provides the secondary $[Ca^{2+}]_i$ rise. The source of the secondary $[Ca^{2+}]_i$ response is still not clarified, although there is strong evidence for an influx of Ca^{2+} from the external medium (see chapter 7 for more details). The observed $[Ca^{2+}]_{mt}$ increase in the principal cell may be due to a subpopulation of plasma membrane-proximal mitochondria that are taking up Ca^{2+} because of the local microdomain of high $[Ca^{2+}]_i$ produced by opening of plasma membrane Ca^{2+} channels. This may be specific to either the basolateral or apical membranes or it may be occurring at both. The alternative possibility is that the long period of the secondary $[Ca^{2+}]_i$ rise could cause a global rise in Ca^{2+} levels (not just in local domains) resulting in a marginal Ca^{2+} uptake by all mitochondria. A similar atypical $[Ca^{2+}]_{mt}$ response has been observed in subpopulations of mitochondria in pancreatic acinar cells (Park et al., 2001). Mitochondria further from the IP_3-releasable apical region of the ER in these cells have an attenuated response to the agonist acetylcholine. However, this response is not delayed like the increase seen in principal cells. This is most likely due to the differences in kinetics of the secondary responses in these two cell types.

The stellate cell $[Ca^{2+}]_{mt}$ response is also atypical; the initiation of the rise is also delayed by more than expected (though only by approximately 1 second) and the rate of increase is also a lot slower than that of the primary $[Ca^{2+}]_i$ increase (see figure 3.5B). The primary $[Ca^{2+}]_i$ peak may be priming the mitochondria for Ca^{2+} uptake, however analogous to the principal cells, the source of the Ca^{2+} appears to be the same as the source driving the secondary $[Ca^{2+}]_i$ rise. Therefore, it again appears that the stellate ER is not the IP_3-releaseable pool or that the mitochondria in the stellate cell are not in close proximity to the ER.

The tubule $[Ca^{2+}]_{mt}$ responses imply that the principal and stellate cells' Ca^{2+} signalling mechanisms do not function in a typical manner. It raises the intriguing questions of how and why these mechanisms are different. This is discussed in more detail in chapter 7. One thing to be noted is that the $[Ca^{2+}]_{mt}$ values were calculated from the raw RLU counts using the same program used for calculating $[Ca^{2+}]_i$ in *Drosophila*. This should still produce accurate values, as the aequorin possesses the same affinity for aequorin. However, there is always the possibility that any pH difference in the mitochondria may effect the calculated values, if it alters the manner in which aequorin binds Ca^{2+}. An important future

experiment will be to verify these calculated results by calibrating the targeted aequorin in conditions representing the internal environment of *Drosophila* mitochondria.

Although the dynamics of $[Ca^{2+}]_{mt}$ in the Malpighian tubules of insects have not been previously studied, there have been studies of mitochondrial movement in the tubules of *Rhodnius prolixus*. Bradley and Satir (1979,1981) used electron microsopy to monitor the movement of mitochondria after the *Rhodnius* tubule had been stimulated with 5-hydroxytryptamine (5-HT). The mitochondria moved from a position below the cell cortex to one inside the microvilli within 10 minutes of stimulation with 5-HT. It is believed that the purpose of this movement is to bring the activated mitochondria in closer proximity to the V-ATPases that drive fluid secretion. It is not unreasonable to propose that a Ca^{2+} response invoked by 5-HT could be stimulating the mitochondria to produce more ATP and to move to the cellular microdomain that is requiring the ATP. The $[Ca^{2+}]_{mt}$ increases in the *Drosophila* tubule may be playing an integral role in stimulating the mitochondria to respond in a similar manner.

Despite the majority of mitochondrial Ca^{2+} studies focusing on the fast and large $[Ca^{2+}]_{mt}$ response associated with close proximity to the ER, several groups have recently investigated the reaction of mitochondria to lower, more sustained $[Ca^{2+}]_i$ rises. Studies in HeLa cells (Collins et al., 2001) and rat adrenal cells (Pitter et al., 2002) have shown that mitochondria will slowly accumulate Ca^{2+} even when the $[Ca^{2+}]_i$ has only risen from 60 – 140 nM. Additionally, they have demonstrated that this slow Ca^{2+} accumulation is sufficient to increase the metabolic activity of the mitochondria (consistent with activation of the Ca^{2+}-dependant mitochondrial dehydrogenases). This information could be important for understanding how mitochondria react in the principal cell to the capa-1 stimulus. The results in this chapter show that the principal cell mitochondria accumulate Ca^{2+} in conjunction with the secondary component of the capa-1 Ca^{2+} signal. This evidence proposes a model in which capa-1 may activate mitochondria (to produce more ATP to drive fluid secretion), via the prolonged characteristics of the secondary $[Ca^{2+}]_i$ response that it generates.

Chapter 4

Development of improved fluorescent calcium reporters and their utilisation in monitoring organellar calcium in the Malpighian tubule

4.1 Summary

This chapter describes the *in vitro* development of a new ER-targeted fluorescent calcium reporter and the generation of transgenic flies which express this reporter, thus allowing real-time monitoring of $[Ca^{2+}]_{ER}$ in an intact tissue. The 'pericam' reporter was used as a template and mutated to lower its sensitivity to Ca^{2+}. Retention signals were also fused to it, which allowed correct targeting. Malpighian tubules, expressing this reporter in either the principal cells or the stellate cells were imaged using confocal microscopy in order to determine the role of the ER in the neuropeptide induced $[Ca^{2+}]_i$ signals. Surprisingly both cell types showed a slight increase in $[Ca^{2+}]_{ER}$ upon stimulation, rather than a typical decrease associated with a release of Ca^{2+} from the ER.

Additionally this chapter describes the generation of transgenic fluorescent reporter fly lines in an attempt to monitor Ca^{2+} levels in other sub-cellular compartments i.e., the Golgi and mitochondria, at a single cell level. Using a novel, highly sensitive pericam, $[Ca^{2+}]_{mt}$ levels were successfully monitored in the tubule during stimulation by neuropeptides.

4.2 Introduction

The aequorin based Ca^{2+} assay has been an excellent tool for understanding Ca^{2+} signalling in the tubule, however, the technology cannot be used for single cell imaging in most systems, as the signal is too weak. One would require an encoded fluorescent reporter to be able to image Ca^{2+} events in a single cell in the tubule. Furthermore, with the available set of targeting tools, fluorescent reporters can be localised to different organelles within the tubule to enable real-time imaging of organellar Ca^{2+}. Due to the technical difficulties of applying aequorin technology to investigate $[Ca^{2+}]_{ER}$ in *Drosophila* (see section 3.3.1), an ER-targeted fluorescent reporter could provide the first insight into the dynamics of *Drosophila* $[Ca^{2+}]_{ER}$.

The various types of encoded fluorescent Ca^{2+} reporters are described in section 1.2.3 and the genetic targeting of these reporters has allowed measurements of Ca^{2+} in various cellular compartments and domains (summarised in table 4.1).

Table 4.1 Genetically encoded fluorescent Ca^{2+} reporters and details of their documented subcellular targeting.

Reporter	Fluorescence source	Excitation λ (nm)	Emission λ (nm)	Subcellular targetting	Reference
Cameleon	CFP/YFP CFP/Venus CFP/Citrine	430	480/535	cytosol	Miyawaki et al., 1997
				ER	
				mitochondria	
				nucleus	
				Golgi	Griesbeck et al., 2001
				caveolae	Isshiki et al., 2002
				plasma membrane	Emmanouilidou et al.,
				secretory granules	1999
Ratiometric pericam	cpYFP	415/490	525	cytosol	Nagai et al., 2001
				mitochondria	
				nucleus	
				subplasmalemmal space	Pinton et al., 2002
Camgaroo	YFP	490	525	cytosol	Baird et al.,1999

Cytoplasmic targeted cameleon, camgaroo and pericam have been expressed in transgenic animals (Kerr et al., 2000; Yu et al., 2002; Wang et al., 2003; Higashijima et al., 2003). However these approaches do have drawbacks; eg., one main concern is that the required high expression of these reporters could interfere with calcium homeostasis. It is likely that the calmodulin domain of these biosensors significantly buffers Ca^{2+} levels (Miyawaki et

al., 1999). Additionally, as mentioned in section 1.2.3, the cameleons have a low signal-to-noise ratio and unfortunately camgaroo's sensitivity range is not optimal for monitoring $[Ca^{2+}]_i$.

In spite of these drawbacks, these reporters have and will contribute a great deal to understanding Ca^{2+} signalling *in vivo*. Progress in this field would benefit from the development of improved reporters and the generation of transgenic animals expressing subcellular targeted reporters.

4.3 Results

4.3.1 Development of a new genetically encoded fluorescent reporter for the ER

Cameleon-based reporters have already been developed for monitoring $[Ca^{2+}]_{ER}$ (Miyawaki et al., 1997). These reporters do have disadvantages; they possess a low signal-to-noise ratio and their Ca^{2+} sensitivity is not adequate to report across the whole range of possible $[Ca^{2+}]_{ER}$ levels. Furthermore, as these were not available to our laboratory, I decided to endeavour to develop an ER reporter based on either camgaroo or the pericams.

The sequence for an ER-targeted camgaroo was assembled in a four-piece PCR fusion reaction. It contained the *Drosophila* calreticulin signal, the two halves of YFP and *Drosophila* calmodulin (figure 4.1 A). The fusion PCR product was TOPO® cloned and fully sequenced by BaseClear. DNA templates for flash, inverse and ratiometric pericams were kindly donated by Dr. Atushi Miyawaki (Riken Institute, Japan). As a putative ratiometric ER reporter would be most practical, the *Drosophila* calreticulin signal and the KDEL sequence were fused to ratiometric pericam (figure 4.1 B). For further details of the construction of these two DNA templates, see table 2.4.

In order to produce a less sensitive Ca^{2+} reporter that would function in the ER, a strategy was undertaken to mutate residues in the Ca^{2+} binding EF hands of the calmodulin domain. Calmodulin has four EF hands, each containing a conserved glutamic acid (E) residue that has a critical role in Ca^{2+} binding (Babu et al., 1988). Mutants of calmodulin with glutamic acid to glutamate (E→ Q) and glutamic acid to lysine (E→ K) substitutions have been demonstrated to affect Ca^{2+} binding (Maune et al., 1988; Maune et al., 1992). The glutamic acid (negatively charged) residue assists binding of the Ca^{2+} ion in an electrostatic manner (see figure 4.2A); therefore a change to glutamate (neutral) will weaken the interaction; while a change to lysine would have a more severe effect due to its positive charge. The approach was to generate mutants of the two types of reporter that had E→ Q and/or E→ K mutations at various EF hand sites. The plan was that the reporters could then be expressed in bacteria, purified and tested *in vitro* for their Ca^{2+} sensitivity.
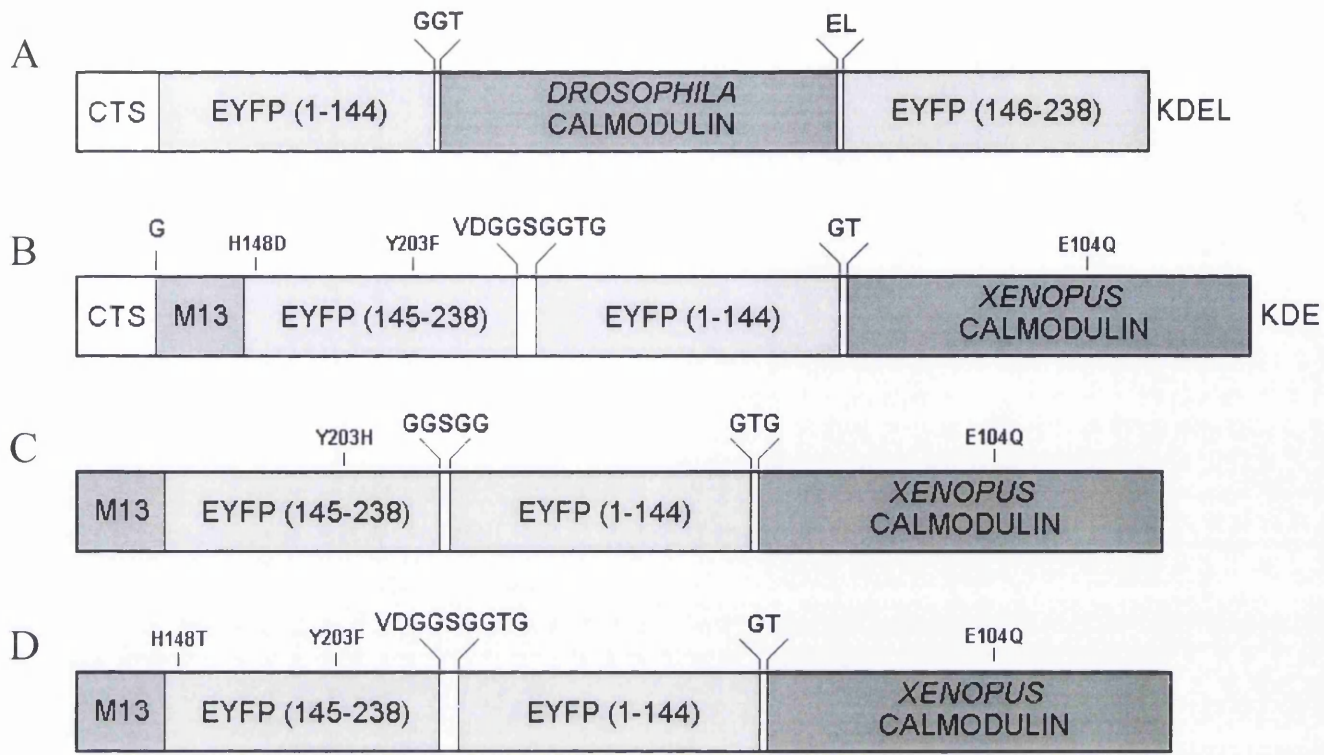
Figure 4.1 Schematic representation of the reporter templates used for mutagenesis. (A) ER-targeted camgaroo. (B) ER-targeted ratiometric pericam. (C) Flash pericam. (D) Inverse pericam. Abbreviations are as follows; CTS, calreticulin signal; EYFP, enhanced yellow fluorescent protein.
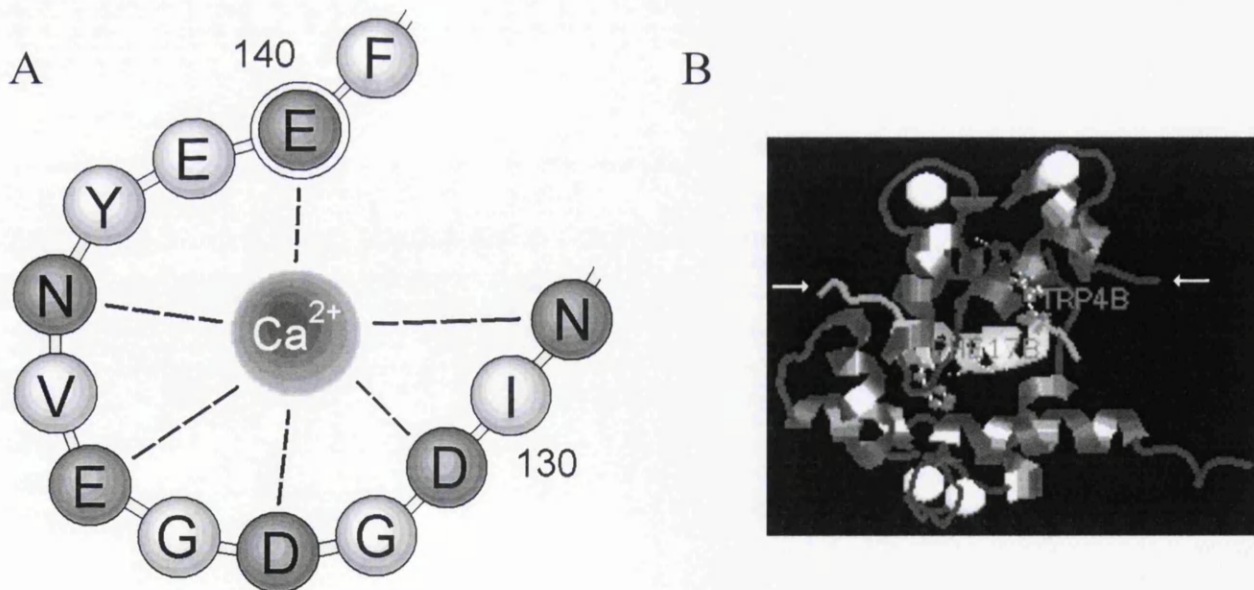
Figure 4.2 Schematic diagram of a calmodulin EF hand binding Ca^{2+} and the structure of calmodulin binding the M13 peptide. (A) The 4th EF hand of calmodulin, residues interacting with the Ca^{2+} ion are shaded in a darker colour. The critical glutamic acid (E) that was mutated in the development of a less sensitive pericam is highlighted. (B) The solved structure of calmodulin binding to the M13 peptide in the presence of Ca^{2+} (Ikura et al., 1992). The N-terminus of M13 and the C-terminus of calmodulin are indicated by white arrows.

87

Figure 4.1 shows a schematic representation of the different reporter templates that were mutated. All the original pericam reporters contain a E104Q mutation in calmodulin (Nagai et al., 2001); therefore before different alternative mutations could be made, this site had to be reverted to wildtype (Q104E). All the changes to calmodulin were produced by targeted PCR mutagenesis (see section 2.6.6 and primers 30-51). The templates were in the pCRT7/NT vector, therefore all subsequent mutated isoforms were ready to be expressed and purified from bacteria (see section 2.13).

The site-mutation strategy for the camgaroo and the pericam was loosely based on the original Ca^{2+} sensitivity of the reporters and predicted severity of each mutation. Table 4.2 displays all the various templates that were generated, including whether expression in bacteria was successful and if so, whether the purified product was fluorescent.

Expression of the ER-targeted camgaroo in bacteria was unsuccessful; only a very faint band was detected on a western (see figure 4.3). This may have been due to the codon usage of the *Drosophila* calreticulin signal and calmodulin domains, though this should have been compensated for by the use of the 'codon preference' Rosetta® cells. Expression of the ER-targeted ratiometric pericam was more successful and the recombinant protein could easily be detected by western analysis using a His-tag antibody. The proteins were expressed and purified as described in sections 2.13.2 and 2.13.3. The purification step had to be optimised because it became apparent that the protein was eluting from the column at low concentrations of imidazole (see figure 4.3).
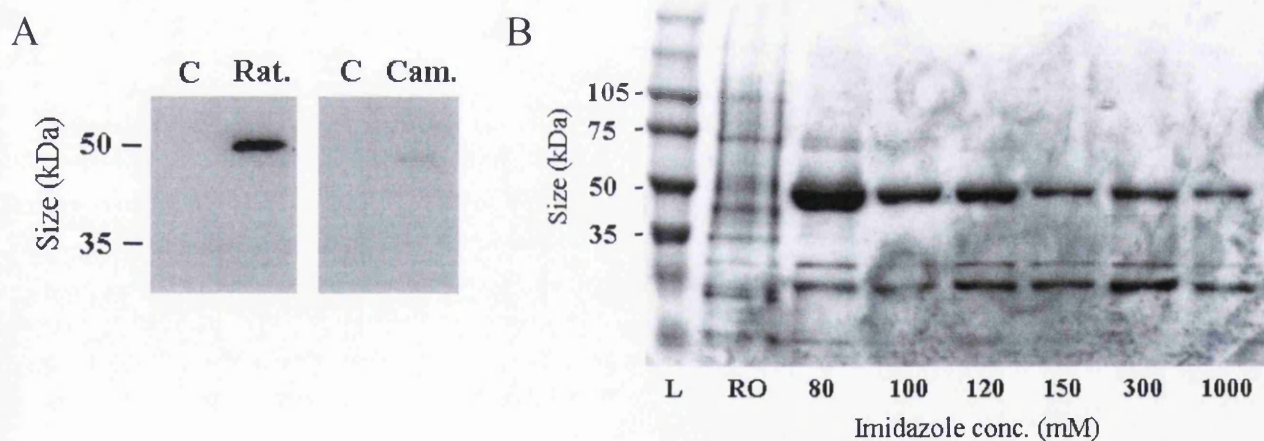
Figure 4.3 Expression of fluorescent reporters in *E. coli.* (A) Western blot showing detection of recombinant reporter protein in the soluble fraction of *E. coli* lysate. Primary antibody, His-G at 1:5000 dilution. Secondary antibody, anti-mouse HRP at 1:5000 dilution. C, control; Rat., ratiometric pericam; Cam., camgaroo. (B) Coomassie gel showing different fractions collected from the His-bind purification column. The majority of the reporter protein is eluted with 80 mM imidazole. L, ladder; RO, run-off from column before elution step.

Unfortunately, the purified proteins were not fluorescent. Considering the possibility that the ER retention signals were interfering with the reporter protein folding or function, non-

Table 4.2 pCRT7/NT constructs generated. For each construct, achievement of bacterial expression and production of a fluorescent protein is indicated.

Template	Calmodulin mutation	Expression in bacteria?	Fluorescent?
Camgaroo with ER retention signals	E31Q	x	-
	E31K	x	-
	E67Q	x	-
	E67K	x	-
	E104Q	x	-
Ratiometric pericam with ER retention signals	E31Q	✓	x
	E31K	✓	x
	E67Q	✓	x
	E67K	✓	x
	E140Q	✓	x
Ratiometric pericam	E31Q	✓	x
	E67Q	✓	x
	E140Q	✓	x
with extended linker 1	E31Q	✓	x
with extended linker 2	E31Q	✓	x
Flash pericam	E31Q	✓	✓
	E67Q	✓	-
Inverse pericam	E31Q	✓	✓
	E67Q	✓	✓
	E140Q	✓	✓
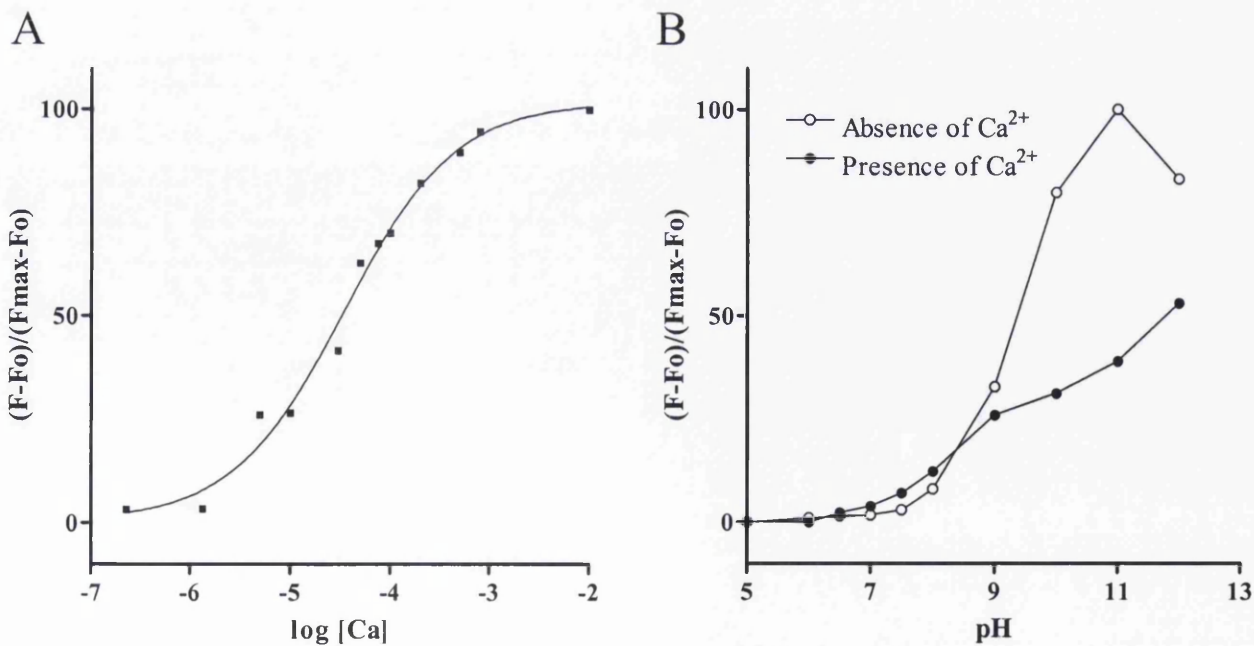
Figure 4.4 Ca^{2+} and pH sensitivity of flash pericam E31Q. (A) Ca^{2+} sensitivity. Kd = $34\mu M$ and Hill coefficient = 0.79. (B) pH sensitivity. (F-Fo)/(Fmax-Fo) allows the fluorescence to be quantified as a percentage of the maximum possible fluorescence.

targeted ratiometric pericam was mutated and purified. Once again though, this yielded non-fluorescent proteins.

It appears that ratiometric pericam can form a fluorophore with the E104Q mutation in calmodulin but if this mutation is exchanged for a similar mutation in any of the other three EF hands, then there is no formation of the fluorophore. It is conceivable that the structural alignment of the two halves of circularly permuted EYFP is critical in the formation of the fluorophore and any change in the structure of the pericam could disrupt this. The alternative mutations in calmodulin are probably affecting the way that the calmodulin and M13 interact, therefore disrupting the alignment between the two halves of EYFP. Based on this interpretation, a possible way to allow the two halves of EYFP to re-align in these mutants would be to make the linkers between the domains more flexible. This was attempted by the addition of a glycine residue in the linker between the two EYFP halves and also between EYFP and calmodulin domains (in separate proteins). Unfortunately, this strategy was also unsuccessful in yielding a fluorescent ratiometric pericam with an alternative calmodulin mutation.

The next step was to investigate whether flash and inverse pericam could be mutated and still retain their fluorescent properties. Inverse pericam is identical to ratiometric pericam, apart from a D148T change in EYFP. This change alters the fluorescent properties of the pericam; therefore there was a possibility that this mutation, in conjunction with a calmodulin mutation, might restore fluorescent properties to the protein. As table 4.2 shows, the mutated flash and inverse pericams that were generated, were all able to form a fluorophore. The fluorescent proteins acquired were then used in *in vitro* Ca^{2+} and pH sensitivity assays (see figures 4.3 and 4.4). The flash pericam containing the E31Q mutation displays a reduced sensitivity to Ca^{2+} (figure 4.4A), which is suitable for measuring $[Ca^{2+}]_{ER}$. Nevertheless, the fluorescent properties of the protein are very sensitive to pH (figure 4.3B) and at pH 7 (the approximate pH of the ER (Kim et al., 1998)) the maximum fluorescence and the fluorescent change between Ca^{2+}-free and Ca^{2+}-bound states is dramatically reduced. The inverse pericam mutants (in31, in67 and in140) are all a lot more robust in terms of pH-sensitivity (figure 4.5) and at pH 7, they operate at near maximum efficiency. These pericams still function in an inverse fashion, ie., an increase in Ca^{2+} results in a decrease in fluorescence. Furthermore the in31 isoform possesses a broad range of Ca^{2+} sensitivity (K_d = 4μM; Hill coeff. = -0.48) which can easily accommodate the full range of possible $[Ca^{2+}]_{ER}$. The in31, in67 and in140 pericams all have a single excitation wavelength peak at ~485 nm (see figure 4.5A-C), which is similar to the published spectra of the original inverse pericam (Nagai et al., 2001). Interestingly, in67 (K_d = 47nM) was in fact more sensitive to calcium than the original
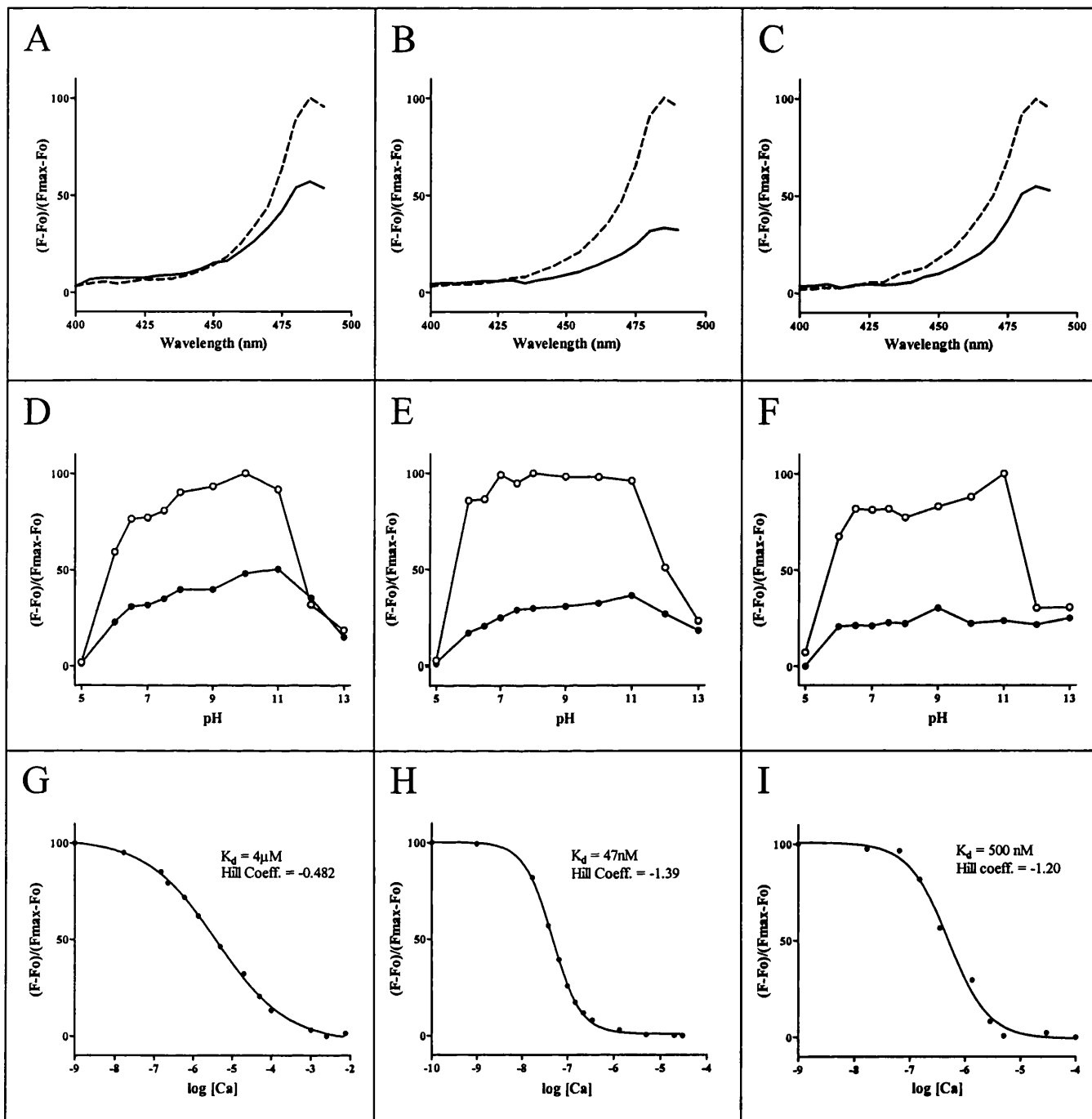
Figure 4.5 *In vitro* **properties of the inverse pericam mutants:** in31 (ERpicam) (A, D and G), in67 (B, E and H) and in140 (C, F and I). Excitation spectra (A-C, dashed lines represent absence of Ca^{2+}), pH sensitivity (D-F, open circles represent absence of calcium), and Ca^{2+} titration (G-I). (F-Fo)/(Fmax-Fo) allows the fluorescence to be quantified as a percentage of the maximum possible fluorescence.

inverse pericam (K_d = 200nM) and in140 was slightly less sensitive (K_d = 500nM). The in31 pericam is an excellent candidate for an ER reporter; however, the only drawback is the fact that the reporter has only one excitation wavelength (therefore ratiometric measurements will not be possible).

A schematic representation of the development of the ER reporter is shown in figure 4.7.

4.3.2 Expression of an ER-targeted pericam in S2 cells and transgenic *Drosophila*

The in31 pericam was fused to the mammalian calreticulin signal and the KDEL sequence (see figure 4.6). It was decided to use the mammalian calreticulin signal, as the reporter could also be tested and used in mammalian cells and it was apparent that this signal was just as effective in *Drosophila* cells (personal communication from Adrian Allan). The structure of calmodulin bound to the M13 peptide has been solved (Ikura et al., 1992) and the N-terminus of M13 and the C-terminus of calmodulin are free from the tertiary structure of the complex (see figure 4.2B). Therefore in theory, the retention signals should not interfere with the function of the pericam. The template for ER-targeted pericam (ERpicam) was TOPO® cloned into the DES expression vector for expression in S2 cells) and the pcDNA3.1 vector (for expression in mammalian cells). From the DES construct, the template was cloned into pUAST (for further details see table 2.4) and six separate transgenic lines were generated.
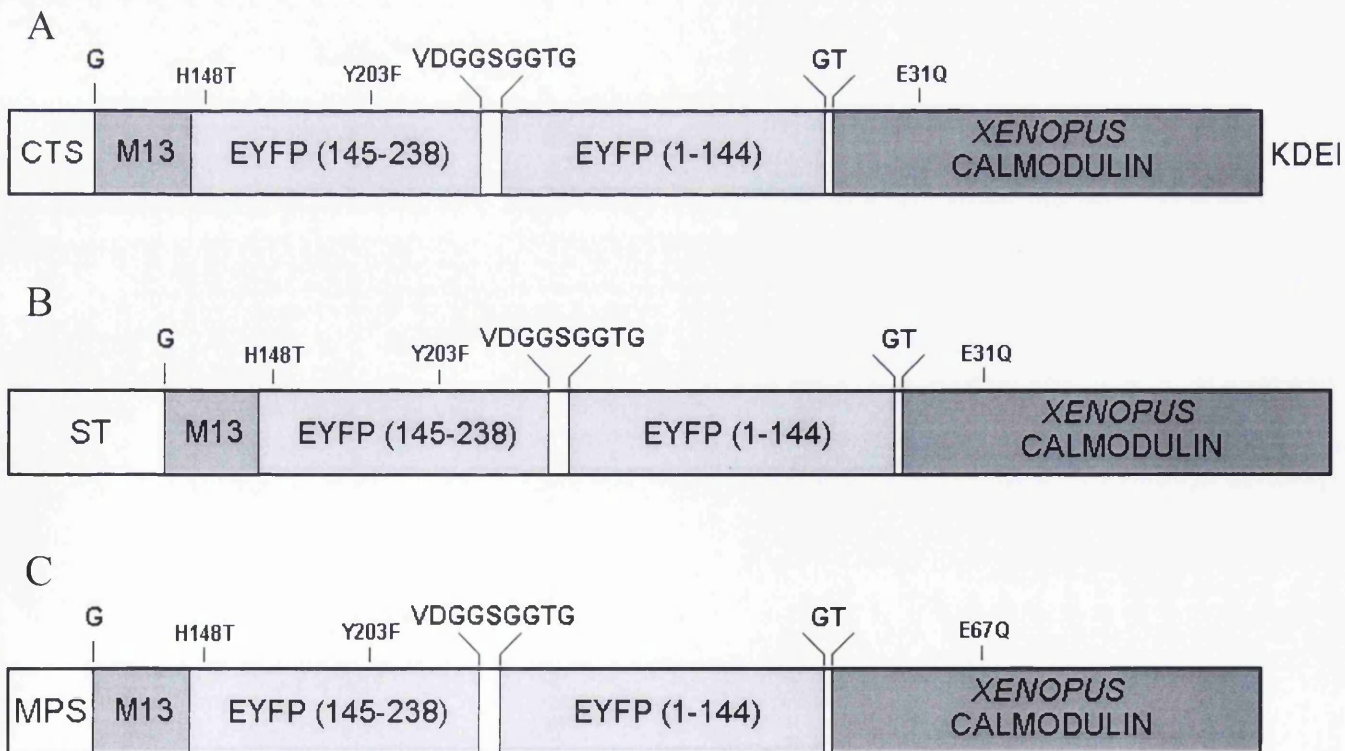
Figure 4.6 Schematic diagram of the new targeted pericams. (A) ERpicam (B) Golicam (C) Mitycam-1. Abbreviations are as follows: CTS, calreticulin signal; EYFP, enhanced yellow fluorescent protein; ST, sialyl transferase signal; MPS, mitochondrial pre-targeting sequence.
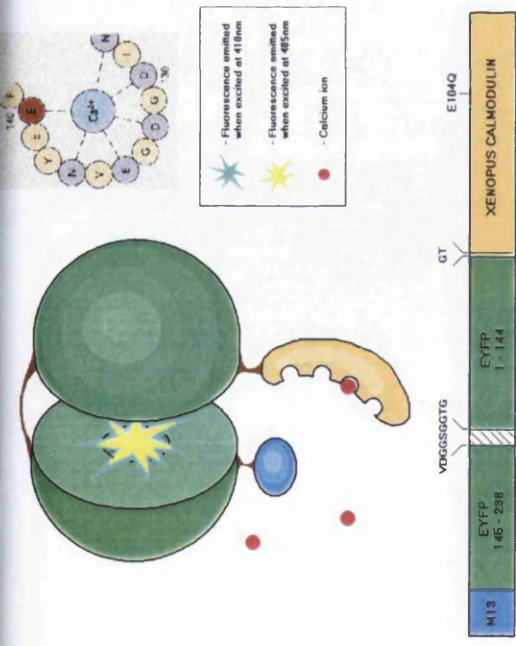
1) **Ratiometric pericam:** Binding of Ca^{2+} ions to calmodulin causes it to bind more tightly to the M13 domain. This changes the structure surrounding the chromophore, resulting in an emission intensity change. This pericam can be excited at two separate wavelengths. The strategy for reducing the Ca^{2+} sensitivity involved mutating the conserved glutamatic acid residue in the EF hands of calmodulin (see inset diagram).
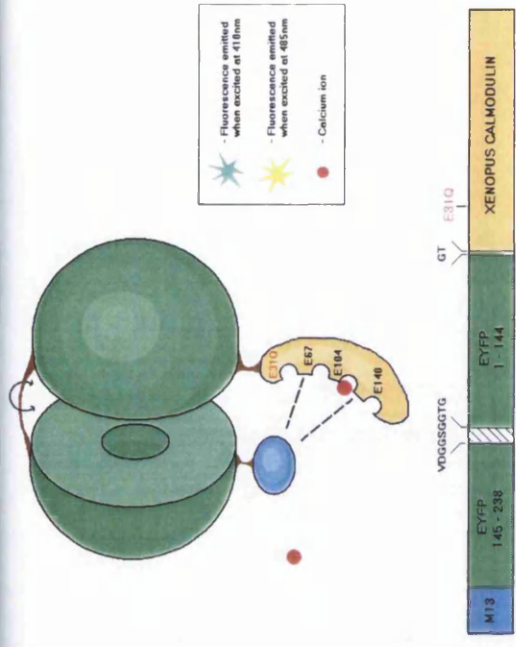
2) **Alternative calmodulin mutations disrupt fluorophore formation:** E31Q, E67Q and E140Q mutations in calmodulin result in a non-fluorescent protein. These changes are possibly altering the interaction between calmodulin and M13, causing an out-of-plane distortion between the two halves of EYFP.
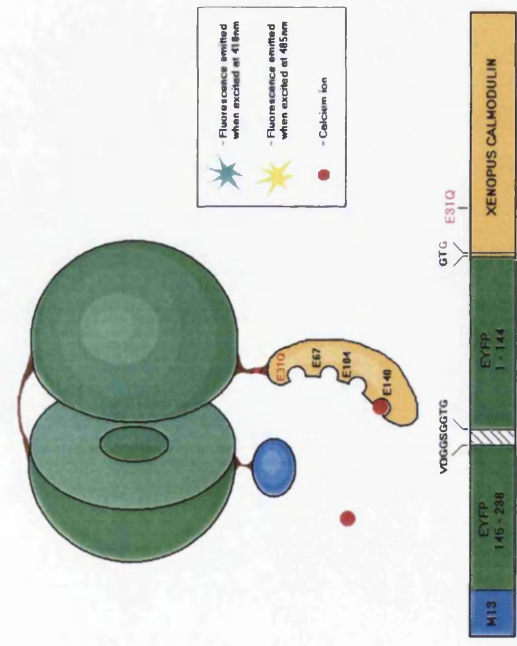
3) **More flexible linkers did not restore fluorophore formation:** Additional glycine residues in the linkers did not allow the two halves of EYFP to interact correctly for fluorophore formation.
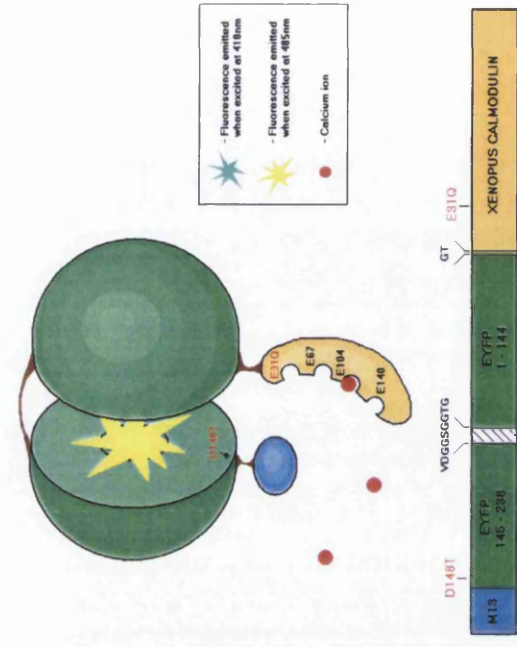
4) **A D148T alteration in EYFP restores fluorescence:** Inverse pericam contains a single residue difference from ratiometric pericam, however this allows formation of the fluorophore in conjunction with the calmodulin mutations. The new proteins, like inverse pericam only have a single excitation wavelength.

Figure 4.7 Schematic representation of the development of a less Ca^{2+}-sensitive pericam.

ERpicam was initially expressed in S2 cells. Transfected cells gave a bright fluorescent signal, which was excluded from the nucleus (see figure 4.8). The fluorescence displayed a predominantly perinuclear localisation and reticular patterns associated with the ER structure. It was not possible to do real-time imaging of ERpicam in S2 cells, as the required confocal microscopy facilities were not available.

4.3.3 Monitoring of $[Ca^{2+}]_{ER}$ in mammalian cell lines

A collaboration was set up with Dr. Michael White's group at the University of Liverpool, enabling us to use their confocal facilities. As part of this collaboration, the group at Liverpool are testing and using the pcDNA3.1 pericam constructs that were made. All the work using ERpicam in mammalian cells was done by Dr.Violaine See at Liverpool. However some of this preliminary work will be mentioned to demonstrate application and functionality of ERpicam.

The pcDNA3.1-ERpicam construct was used to transfect neuroblastoma cells. The fluorescence displayed a clear reticular pattern within the cell (see figure 4.9A). Serum starved neuroblastoma cells elicit an increase in $[Ca^{2+}]_i$ upon addition of serum (personal communication from Violaine See). Cells expressing ERpicam were monitored during the addition of serum and an increase in fluorescence was observed. As the reporter works in an inverse manner, then this increase in fluorescence indicates a decrease in $[Ca^{2+}]_{ER}$ (see figure 4.9B).

4.3.4 Monitoring of $[Ca^{2+}]_{ER}$ in the Malpighian tubule

Homozygous pP{UAST-ERpicam} flies were crossed to the GAL4 lines c42 and c710, and the specific expression of ERpicam in principal and stellate cells was verified (for examples, see figures 4.10B, 4.10D and 4.11C). The signal in principal cells was strong, whereas in the stellate cells it was a lot weaker. This is to be expected, as a stellate cell occupies much less volume than a principal cell and also electron microscopy of principal cell shows them to contain a high density of ER extending to all regions of the cell (Ashburner and Wright, 1978). A reticular pattern of fluorescence is difficult to discern in the principal cells, though is most likely due to the ubiquitous distribution and the high density of ER.

Transgenic tubules expressing ERpicam were imaged in a small glass-bottomed petri dish, on a Zeiss LSM 510 Meta microscope (see section 2.15.2). The real-time images of the tubule expressing ERpicam were captured and average fluorescence values for specified regions of interest (ROI) calculated. These values were subtracted from an arbitrary higher
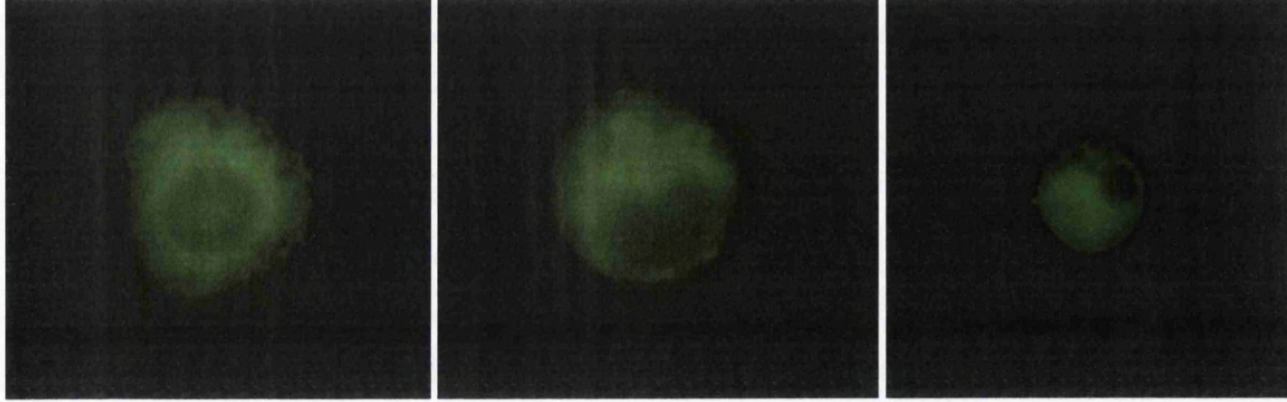
Figure 4.8 Pictures of S2 cells expressing ERpicam. Images were captured with a Zeiss Axiocam system using standard fluorescence microscopy and a 100x objective (see section 2.12.1).

A

B
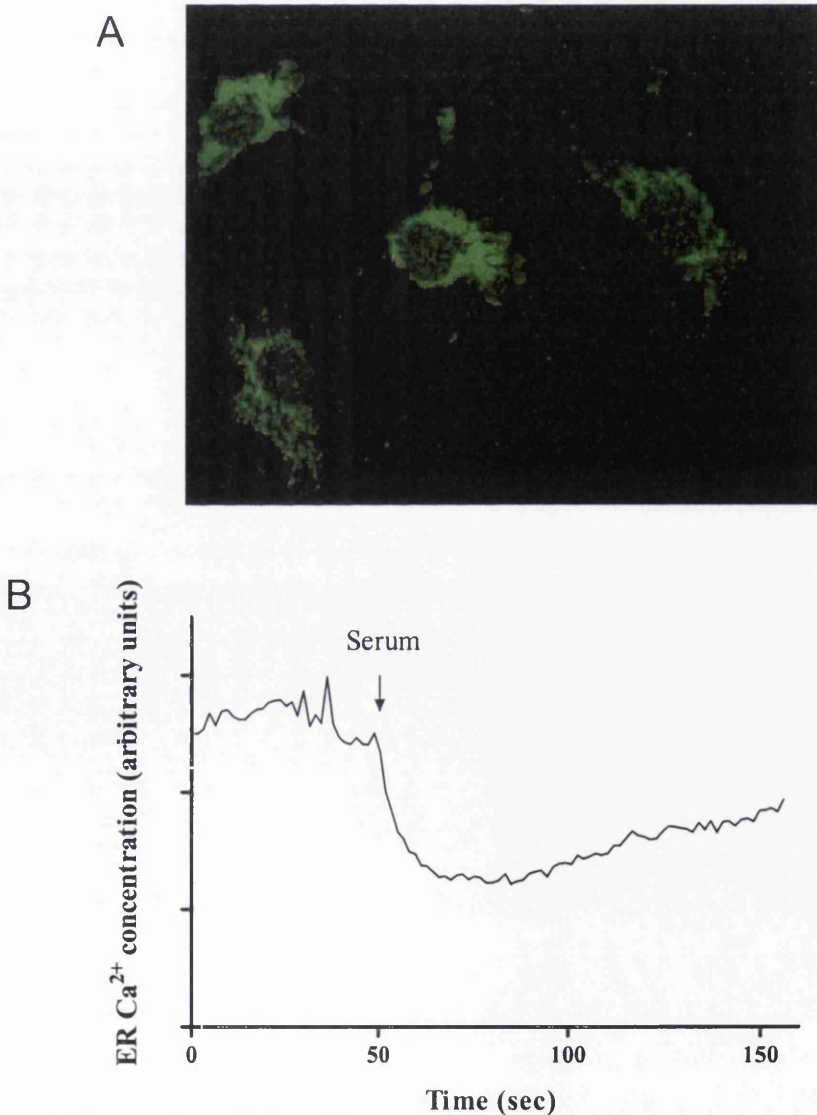
Figure 4.9 Expression of ERpicam in neuroblastoma cells. (A) Picture of neuroblastoma cells expressing ERpicam. Image captured on a Zeiss 510 Meta microscope using a 63x objective. (B) ERpicam reporting ER calcium levels in a single neuroblastoma cell starved of serum. Image and data courtesy of Violaine See, Liverpool University.
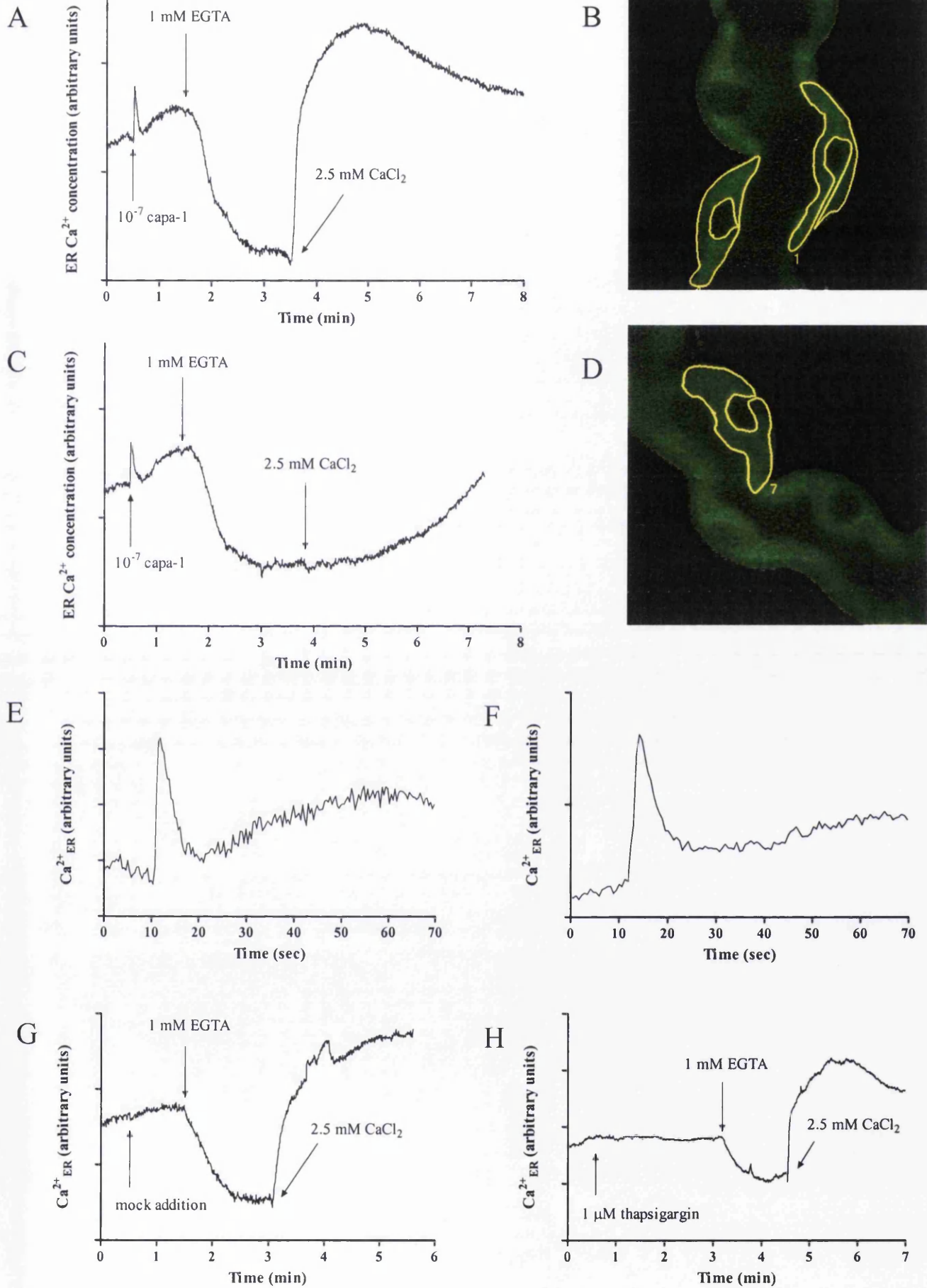
Figure 4.10 Monitoring $[Ca^{2+}]_{ER}$ levels in principal cells using ERpicam. Experiment was performed as described in text and in section 2.15.2. (A) Addition of 10^{-7} M capa-1 peptide (30 sec), 1 mM EGTA (90 sec) and 2.5 mM $CaCl_2$ (210 sec). (B) Typical example of a captured image for (A). (C) Repeat of the same experiment on a separate tubule. (D) Typical example of a captured image for (C). (E) Magnified region of (A), showing the capa-1 response. (F) Another example of a capa-1 response in a separate experiment. (G) The effect of a mock addition of medium. (H) The effect of the addition of 1 μM thapsigargin.

A

B

C
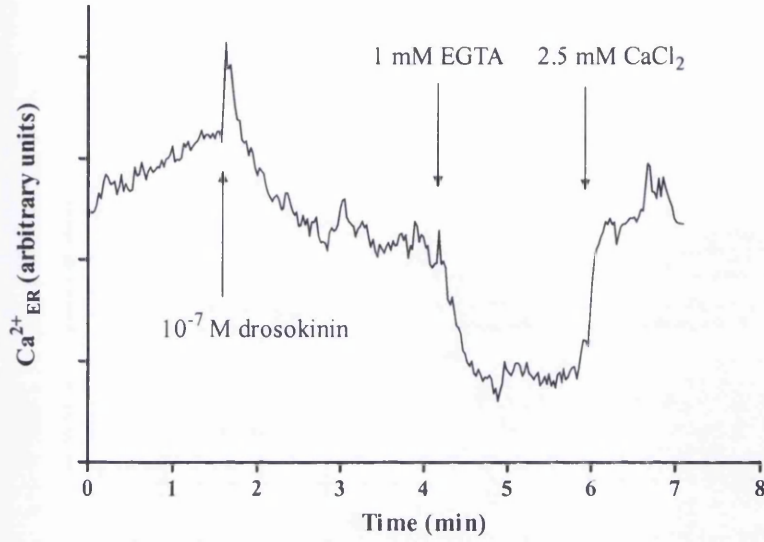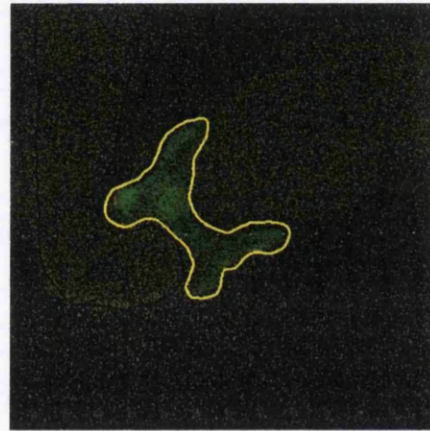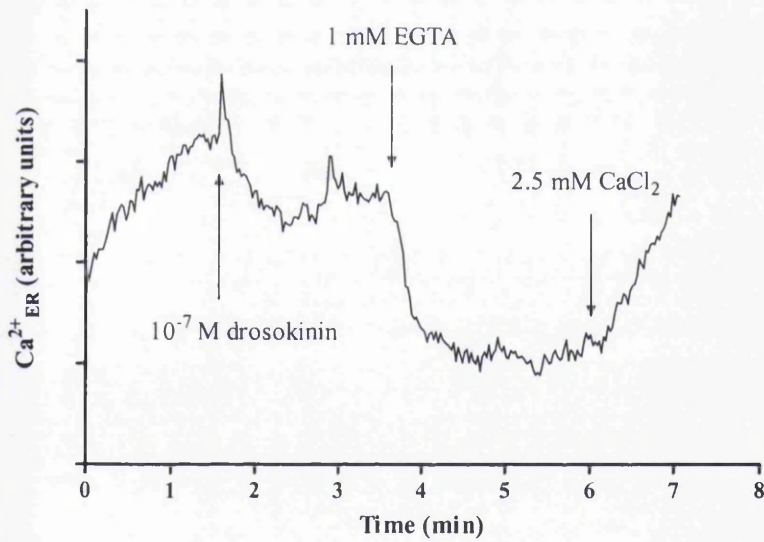
Figure 4.11 Monitoring [Ca²⁺]ᴇʀ levels in stellate cells using ERpicam. Experiment was performed as described in the text and in section 2.15.2. (A) Addition of 10^{-7} M drosokinin peptide (90 sec), 1 mM EGTA (~240 sec) and 2.5 mM CaCl₂ (360 sec). (B) Experiment repeated on a different tubule. (C) Typical example of a captured image for (A). The initial apparent increase in [Ca²⁺]ᴇʀ is actually an artifact, resulting from photoconversion of the probe (see text for further details).

value to give relative values of $[Ca^{2+}]_{ER}$ concentration. Plots of $[Ca^{2+}]_{ER}$ concentration in principal and stellate cells are shown in figures 4.10 and 4.11.

The fluorescence value is not significantly affected by a mock addition of medium (figure 4.10G). Reduction of external Ca^{2+} caused a marked reduction in $[Ca^{2+}]_{ER}$ and this could be restored by the addition of $CaCl_2$ (figures 4.10A, 4.10C, 4.11A and 4.11B). Surprisingly the addition of capa-1 and drosokinin did not show a decrease in $[Ca^{2+}]_{ER}$ in the respective cell types. A decrease in $[Ca^{2+}]_{ER}$ would normally be expected upon stimulation of a cell with a IP_3-producing agonist. Furthermore the level of $[Ca^{2+}]_{ER}$ actually increased slightly upon stimulation and it is apparent from figures 4.10A, 4.10C, 4.10E and 4.10F, that there is a miniature reflection of the principal cell primary and secondary cytosolic responses within the ER. When the dynamics of this $[Ca^{2+}]_{ER}$ increase were compared to the dynamics of the $[Ca^{2+}]_i$ response (measusured with aequorin), they were very similar, apart from the change in the ER being delayed by approximately 1 second and possessing a more prolonged primary increase.

There is also an initial increase in $[Ca^{2+}]_{ER}$ in the stellate cell upon addition of drosokinin, though greater temporal resolution would be required to distinguish whether this was a reflection of the stellate $[Ca^{2+}]_i$ increase. Additionally, in the stellate cells (but not the principal cells) there is a drop in $[Ca^{2+}]_{ER}$ levels immediately after the initial neuropeptide-induced peak (see figure 4.11). Preliminary experiments suggest that the SERCA inhibitors thapsigargin (figure 4.10H) and cyclopiazonic acid (data not shown) have no effect on the resting levels of $[Ca^{2+}]_{ER}$ in both cell types.

During the imaging experiments photobleaching was observed, that resulted in the fluorescence initially decreasing by about 15% and then levelling off after a minute. Importantly the probe still retains its Ca^{2+} sensitivity after this photoconversion event (as shown in figures 4.10 and 4.11). This has been recently reported to occur with the mitochondrially targeted ratiometric pericam (Filippin et al., 2003), therefore is likely to be an intrinisic property of pericams.

4.3.5 Investigation into monitoring cytoplasmic $[Ca^{2+}]$ in the tubule with a fluorescent reporter

The aequorin based Ca^{2+} assay has been an excellent tool for understanding cytosolic Ca^{2+} signalling in the tubule, however as previously mentioned, the technology does not allow imaging of events in a single cell. To be able to image cytosolic $[Ca^{2+}]$ a single cell in the tubule, one would require an encoded fluorescent reporter. Using the pericam templates acquired, separate transgenic fly lines were generated expressing non-targeted flash, inverse and ratiometric pericam under control of the UAS/GAL4 system. Unfortunately

when these lines were crossed to relevant GAL4 lines there was no detectable fluorescent signal in the tubules of the F_1 generation. This was apart from a very weak signal present in the stellate cells of larval tubules expressing inverse pericam. This lack of signal is likely to be largely due to the pH sensitivity of the pericams.

It has been reported that a Q69M mutation in EYFP can reduce its environmental sensitivity to pH and halide ions (Greisbeck et al., 2001). In a strategy to reduce the environmental sensitivity of ratiometric pericam, this mutation was introduced. Protein was purified and transgenic flies generated. Figure 4.12 shows that this change made no difference to the pH sensitivity of the pericam and furthermore the transgenic flies showed no fluorescent signal.
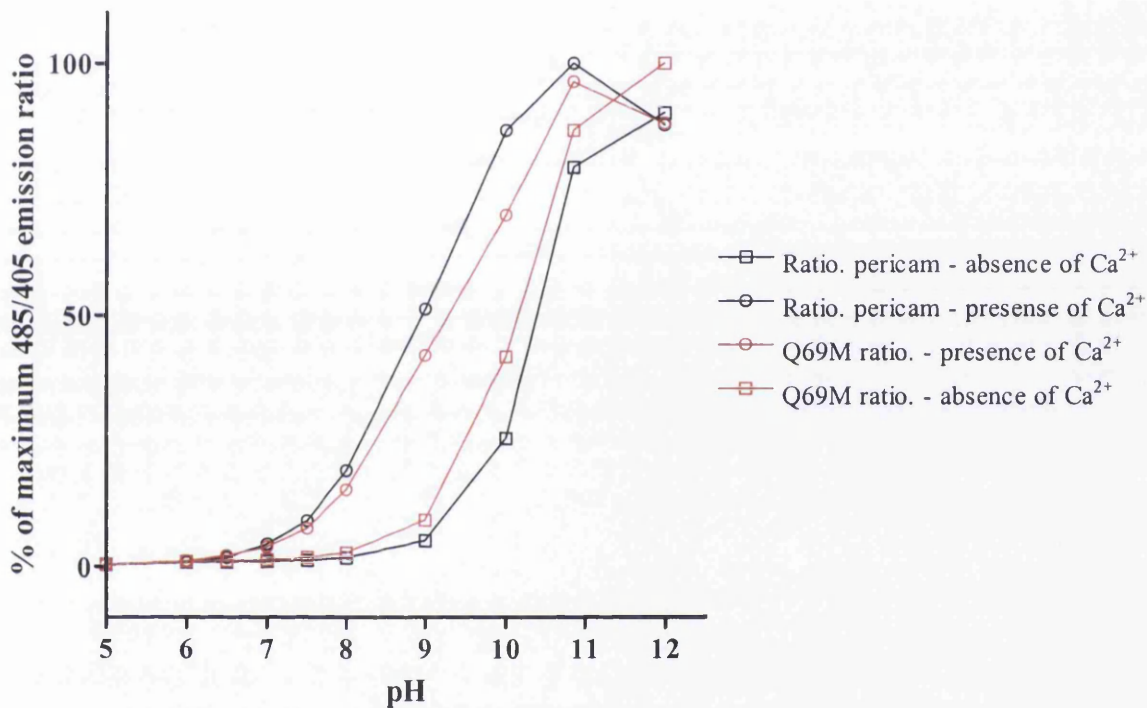
Figure 4.12 Effect of pH on the fluorescence ratio of standard and Q69M ratiometric pericams.

During the development of the ER reporter the pericams in67 and in140 were generated (see section 4.3.1). As these are both relatively insensitive to pH, they were candidates for a cytoplasmic reporter that may actually function *in vivo*. They were both cloned into pUAST (for further details see table 2.4) and transgenic flies generated. Contrary to previous attempts, these reporters produced a fluorescent signal in both cell types of adult tubules. However the signal was still weak and interestingly, the signal from the stellate cells was greater than that from the principal cells. Although the fluorescence can be detected on a fluorescence microscope with a long exposure, it is barely detectable when trying to perform a time series experiment on a confocal microscope. Real-time imaging has been performed using these lines, though only with a high expression level (either with

stable lines or driven by actin-GAL4). These experiments showed no response to neuropeptide stimulation, this could be because of the buffering properties of the pericam calmodulin domain (as mentioned in section 4.2).

The in67 and in140 templates were cloned into pcDNA3.1 and through the collaboration with the University of Liverpool, it has been shown that they work well in mammalian cells (data not shown).

4.3.5 Investigation into monitoring $[Ca^{2+}]_{Golgi}$ in the tubule with a fluorescent reporter

A conceivable method for investigating the role of the Golgi Ca^{2+} store in the signalling pathways of the tubule was to make a Golgi targeted pericam "Golicam". The in31 pericam was fused to the sialyltransferase signal (see figure 4.6) and cloned into the DES, pcDNA3.1 and pUAST vectors (see table 2.4). A very faint signal was detected in S2 cells, however nothing was detected in mammalian cells or in transgenic tubules. This may be due to the low pH of the Golgi apparatus or the processing and folding of the protein.

4.3.6 Monitoring of $[Ca^{2+}]_{mt}$ in the Malpighian tubule at a single cell level

The templates for in67 and in140 were fused to the mitochondrial pre-targetting sequence (see figure 4.6) and cloned into pcDNA3.1 and pUAST (see table 2.4). Transgenic flies were generated that could express mitochondrially-targeted in67 and in140 (mitycam-1 and mitycam-2). Both reporters give a strong signal, when expressed in both cell types (for examples see figures 4.13C and 4.14D). Both mitycam-1 and mitycam-2 were initially used to investigate $[Ca^{2+}]_{mt}$ changes in single principal or stellate cells. However, it became apparent that experiments with mitycam-2 did not show any significant responses to capa-1 or drosokinin. Data shown in chapter 3, using a targeted aequorin approach shows that both the cell types display a relatively small $[Ca^{2+}]_{mt}$ increase in response to the respective neuropeptides. With this in mind, all consequent experiments utilised mitycam-1, as this pericam is more sensitive to small $[Ca^{2+}]$ changes (see section 4.3.1).

Monitoring of $[Ca^{2+}]_{mt}$ in the tubule with mitycam-1 is shown in figures 4.13 and 4.14. The capa-1 response observed with mitycam-1 is similar to ones observed using the aequorin technology (see figure 3.4), with a slow increase that peaks approximately 100 seconds after stimulation. The drosokinin response observed with mitycam-1 is also similar to aequorin-based data, however the dynamics of the increase appear different. The peak appears to take longer to reach and the levels decrease at a slower rate.
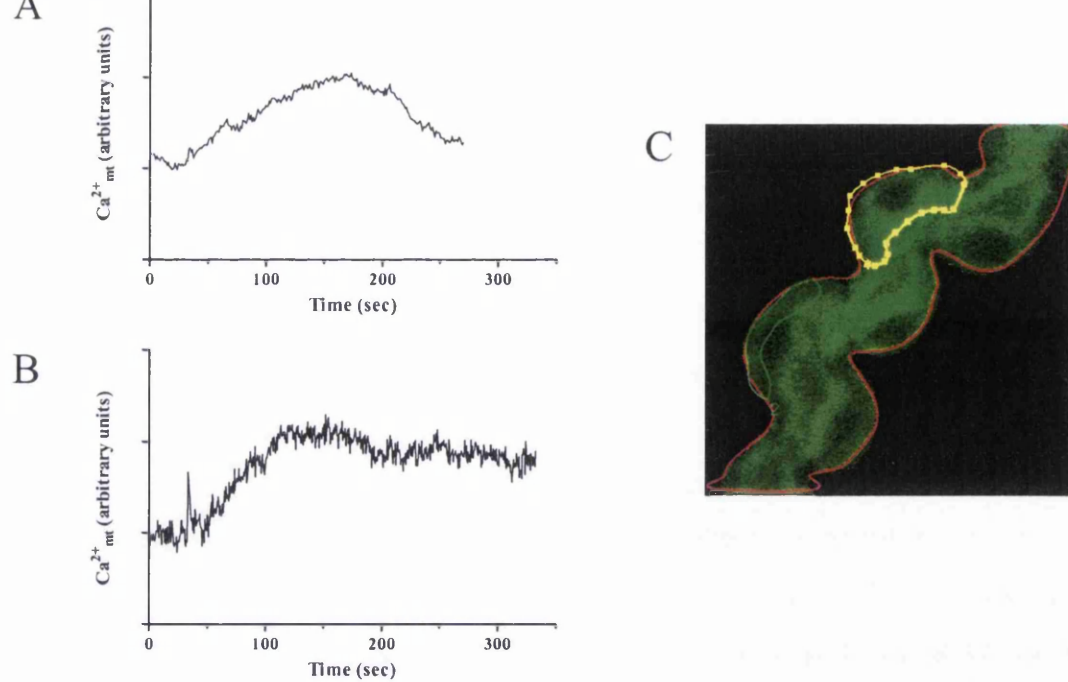
Figure 4.13 Monitoring [Ca^{2+}]$_{mt}$ levels in principal cells using mitycam-1. Experiment was performed as described in the text and in section 2.15.2. The peptide capa-1 was added at 30 seconds at a concentration of 10^{-7} M. (A) First example of a typical experiment. (B) Second exampleof a typical experiment. (C) Typical example of a captured image.
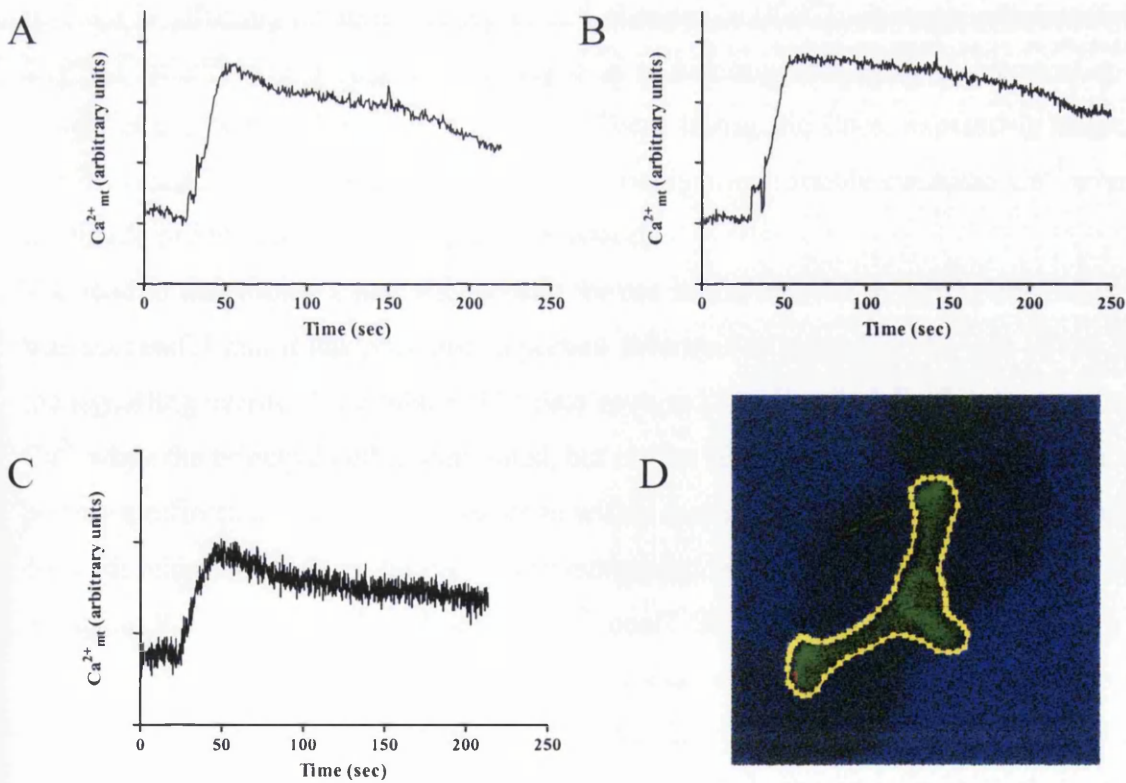
Figure 4.14 Monitoring [Ca^{2+}]$_{mt}$ levels in stellate cells using mitycam-1. Experiment was performed as described in the text and in section 2.15.2. The peptide drosokinin was added at 30 seconds at a concentration of 10^{-7} M. (A) First example of a typical experiment. (B) Second example of a typical experiment. (C) Third example of a typical experiment. (D) Typical example of a captured image.

4.4 Discussion

The new reporters based on inverse pericam are useful tools for studying Ca^{2+} signalling. As demonstrated, in31 can be targeted to provide a high signal, pH-robust ER reporter with good signal-to-noise ratio. in67 and in140 provide new cytoplasmic and mitochondrial reporters that are pH-robust and appear to function better than previous pericams in transgenic tissues. Additionally in67 and in140 have different sensitivities to Ca^{2+}; in67 (more sensitive) can be used for studying smaller, more delicate Ca^{2+} transients, while in140 can be used for looking at larger increases.

Even though many reporters were tried, real-time imaging of $[Ca^{2+}]_i$ in the tubule was elusive. Refinement of the confocal settings may allow this to be possible in the future. No signal from Golicam was detected in the tubule, nevertheless further improvements of these reporters may yield a more robust version that could be targeted in the same manner.

Application of mitycam-1 in the tubule has confirmed the unusual $[Ca^{2+}]_{mt}$ responses described in chapter 3. This is also a good example of how the sensitive in67 pericam can be put to use.

The differences in the kinetics of the responses observed with aequorin and mitycam-1 in the stellate cell are difficult to explain. This may be due to differences in looking at a single cell, rather than a population of cells. Another possibility is that the targeting of the pericam is affecting its ability to report fast changes in $[Ca^{2+}]$, although mitochondrially-targeted ratiometric pericam has been reported to function adequately in mammalian cells (Nagai et al., 2001; Filippin et al., 2003). These transgenic lines, expressing mitycam-1 and mitycam-2, could also be put to use for investigating possible circadian Ca^{2+} events in the tubule or for studying $[Ca^{2+}]_{mt}$ in other tissues.

The road to developing a new ER reporter for use in the tubule was a long one, however it was successful and it has provided important information regarding the role of the ER in the signalling events of the tubule. The data acquired, implies that the ER does not release Ca^{2+} when the principal cell is stimulated, but in fact takes up some of the cytosolic Ca^{2+} to portray a reflection of the $[Ca^{2+}]_i$ response within the ER. The fact that the elevation of IP_3 does not release Ca^{2+} from the ER is very intriguing; firstly, why are the cells in the tubule not using the ER as the IP_3-releasable Ca^{2+} pool? Secondly, where is IP_3 releasing Ca^{2+} from, if it is not the ER? It maybe that because these cells are highly specialised and form a highly active transporting epithelium, that the ER is not a practical Ca^{2+} pool to be released. It is conceivable, with the densely packed ER in the principal cell, that a release from this organelle would create a damagingly high increase in $[Ca^{2+}]_i$ and $[Ca^{2+}]_{mt}$. This is in contrast with other secreting polarised epithelial cell types; the ER in the pancreatic acinar cell plays an integral role in the tightly controlled, spatial Ca^{2+} signalling events that

regulate secretion (for review, see Petersen et al., 1999). With regards to where the IP_3 could be acting, there have been reports of IP_3-mediated release from the Golgi (Pinton et al., 1998), lysosomes (Haller et al., 1996) and a suggested localisation of the IP_3R on the plasma membrane (Putney, 1997). Evidence in the next chapter implicates the Golgi apparatus as being an IP_3-releasable pool in the tubule.

The effect of reducing the external $[Ca^{2+}]$ and then restoring it with an excess of $CaCl_2$, unmasked some interesting properties of the principal cell ER Ca^{2+} pool. Figures 4.10A and 4.10H show that the addition of the $CaCl_2$ appears to cause the store to overcompensate with its uptake of Ca^{2+} and to overfill. This store refilling reaches a peak and then the levels begin to return to normal. This may be due the time taken for negative feed back mechanisms to act upon the ER Ca^{2+} uptake machinery. This could alternatively be due to a phenomenon seen in heart tissues called the Ca^{2+} paradox. Reperfusion of the heart with a Ca^{2+} -containing solution after a period of extracellular Ca^{2+} -free perfusion produces irreversible tissue damage (Zimmerman and Hulsmann, 1966). According to the 'Na$^+$ hypothesis' (Chapman and Tunstall, 1987); upon removal of extracellular Ca^{2+}, Na^+ enters the cell via L-type Ca^{2+} channels resulting in an increase in Na^+_i. Then when extracellular Ca^{2+} is reintroduced, Na^+ exits the cell via a Na^+/Ca^{2+} exchanger causing a large increase in Ca^{2+}_i that is believed to cause cell death. The same series of events may also occur in the principal cell, resulting in the overfilling of the ER that is observed upon repletion of extracellular calcium.

The SERCA inhibitors, thapsigargin and cyclopiazonic acid had no effect on the $[Ca^{2+}]_{ER}$ levels in the principal cell. This data can be interpreted in different ways; firstly it may be possible that the entourage of transporters on the principal cell plasma membrane are removing the inhibitor before it could reach and effect any putative SERCA pumps present on the ER. Secondly, it could be argued that if the ER in the principal cell is not leaky, then blocking the uptake with thapsigargin will not effect $[Ca^{2+}]_{ER}$ resting levels. However, this argument is discredited by the data shown in figure 4.10H, as the thapsigargin does not prevent the uptake of Ca^{2+} after the addition of $CaCl_2$. Thirdly, it may be that there are no thapsigargin-sensitive SERCA pumps resident on the ER membrane. If this is the case, alternative uptake mechanisms might include a thapsigargin-insensitive ATPase or a Ca^{2+}-exchanger of some description. The presence of a thapsigargin-insensitive store is supported by previous experiments on the tubule by Rosay and colleagues (1997); they demonstrated that 1 μM thapsigargin cannot elicit an increase in $[Ca^{2+}]_i$ in principal cells with the external Ca^{2+} removed. Preliminary experiments using ERpicam in stellate cells, also suggest that these SERCA inhibitors have no effect on the stellate $[Ca^{2+}]_{ER}$ levels, although more experiments will be required to confirm this.

Due to its simplicity (single excitation and single emission) and robustness (insensitivity to pH and bright signal), ERpicam could be useful in many different systems. This could include utilisation in mammalian cell lines (already underway at the University of Liverpool), investigation into the $[Ca^{2+}]_{ER}$ levels in other tissues of *Drosophila*, application in other transgenic animals and also for examining $[Ca^{2+}]_{SR}$ (sarcoplasmic reticulum) at a single cell level. Furthermore, we are investigating using this reporter as a basis for a high-thoughput cell-based assay for screening drugs/receptors that act through an IP_3 pathway.

Chapter 5

Identification and characterisation of the *Drosophila* Secretory Pathway Calcium ATPase

5.1 Summary

This chapter describes the identification and characterisation of the *Drosophila* Secretory Pathway Calcium ATPase. Additionally, this chapter investigates the role of this ATPase in the Malpighian tubule. Previous data in our laboratory suggested the possible involvement of a thapsigargin-insensitive Ca^{2+}-ATPase in tubule function. The yeast Ca^{2+}-ATPase, Pmr1 is thapsigargin-insensitive and since its discovery, homologues have been identified that form the new separate SPCA subgroup of Ca^{2+}-ATPases. Using the protein sequences of the yeast Ca^{2+}-ATPase PMR1 and the human SPCA1, the completed *Drosophila* genome database was searched and the gene CG7651 (now CG32451) was identified as possessing high similarity to these SPCAs. The *Drosophila* Flybase database has annotated this gene as having three alternative transcripts, however this study has uncovered another three transcripts. In tradition with previous nomenclature of *Drosophila* genes, I have decided to name this gene *SPoCk* (Secretory Pathway Ca^{2+}-ATPase) as it sits next to a gene called *Jim*.

Surprisingly, the protein products of transcripts A, B and C all possess different intracellular localisations. The translated product of SPoCk-trA localises to the Golgi apparatus, SPoCk-trB to the ER and SPoCk-trC localises to vesicular bodies resembling peroxisomes. The tubule expresses two transcripts, SPoCk-trA and SPoCk-trC. Transgenic overexpression of tagged versions of SPoCk-trA, SPoCk-trB and SPoCk-trC in the tubule has an impact on the dynamics of the neuropeptide induced Ca^{2+} signals. Most interestingly, overexpression of SPoCk-trA in the principal cells results in a potentiated primary Ca^{2+} response to capa-1 and also increases the basal and stimulated fluid secretion rate of the tubule. Additionally, overexpression of SPoCk-trA and SPoCk-trB in stellate cells results in an increased primary Ca^{2+} response to drosokinin.

This is the first demonstration of the localisation of a Ca^{2+}/Mn^{2+}-ATPase to a vesicular body and of a Ca^{2+}/Mn^{2+}-ATPase (distinct from the SERCA pump) localising to the ER in *Drosophila*. Furthermore, studying the localisation and overexpression of these proteins has begun to shed light on the importance of this gene in tubule function. It appears that they play a significant role in maintaining an IP_3-releasable Golgi Ca^{2+} pool. Additionally they may have a role in Ca^{2+} storage and Mn^{2+}-mediated removal of superoxide radicals.

5.2 Introduction – Secretory Pathway Calcium ATPases (SPCAs)

5.2.1 Identification of SPCAs

The ER has been the principally studied intracellular Ca^{2+} store. However more recently it has become apparent that the Golgi is also an important functional Ca^{2+} store that requires high levels of Ca^{2+} for protein processing and can release Ca^{2+} in response to IP$_3$-producing agonists (Zha et al., 1995; Pinton et al., 1998; Van Baelen et al., 2001).

The P-type ATPase that primarily maintains the Golgi apparatus calcium store was first identified by Antebi and Fink (1992). They identified a gene *Pmr1* in the yeast *Saccharomyces cerevisiase* that is required for normal Golgi functions. They showed the *Pmr1* gene product was required for normal secretory processes and that it localised to the Golgi apparatus. However it was Sorin and colleagues (1997) who identified PMR1 as a calcium transporting ATPase.

The first mammalian homologue was cloned from rat (Gunteski-Hamblin et al., 1989) and since its discovery in yeast, PMR1 homologues have been identified in many other species. It is apparent from their amino acid sequence difference and biochemical properties (see next section) that they form a discrete Ca^{2+}-ATPase subgroup.

5.2.2 Biochemical and structural characteristics of SPCAs

The yeast PMR1 pump is insensitive to the potent SERCA inhibitor thapsigargin and is only inhibited by very high concentrations (K_i of 200 µM) of another SERCA inhibitor, cyclopiazonic acid (Sorin et al., 1997). Evidence for a PMR1 homolog in HeLa cells was indirectly shown by Pinton et al. (1998) who identified the Golgi apparatus as being a IP3-sensitive calcium store that was predominantly insensitive to thapsigargin. Like other P-type ATPases, SPCA pumps are sensitive to vanadate (K_i of 130 µM) and are also inhibited by the calcium channel blocker lanthanum (K_i of 55 µM) (Sorin et al., 1997). A specific inhibitor of SPCAs is still yet to be found.

Interestingly, SPCAs can also transport manganese (Mn^{2+}) and the first evidence for this was the ability of *Pmr1* mutants to rescue superoxide dismutase (SOD) mutants in yeast (Lapinskas et al., 1995). It was suggested that PMR1 was maintaining Mn^{2+} homeostasis in the cell by pumping it into the Golgi; when this was disrupted, the cytoplasmic Mn^{2+} levels increased and these elevated Mn^{2+} (or Mn^{2+}-complex) levels scavenged superoxide radicals, therefore compensating for the loss of SOD. It was later shown that the residue Gln^{783}, in the sixth transmembrane domain of yeast PMR1 was a critical residue for the selectivity and transport of Mn^{2+} (Mandal et al., 2000). Additionally, there are packing interactions between the 4th and 6th transmembrane segments which are crucial for Mn^{2+}

transport, it has been proposed that this region is a gate for access of Mn^{2+} ions (Mandal et al., 2003).

Van Baelen et al. (2001) cloned and characterised the C. elegans SPCA and demonstrated that this too was localised to the Golgi, was thapsigargin insensitive and transported both calcium and manganese. This was the first time a PMR1 homologue from a multi-cellular organism had been demonstrated to actively transport Ca^{2+} and to have an equal affinity for transporting both calcium and manganese.

The structure of the SERCA pump is well characterised (Toyoshima et al., 2000; 2002) and though the sequence of the human SPCA1 is shorter than SERCA, the alignment between the two indicates that all 10 membrane segments are present (see figure 5.2). Additionally the alignment shows the presence of residues crucial for pump function, such as the phosphorylation site and the ATP-binding and FITC-binding regions. It is also apparent that, like in PMCA (plasma membrane calcium ATPase) that there is only one site for coordinating binding of calcium, therefore it is likely that only one calcium ion is transported per ATP molecule hydrolysed (Wei et al., 2000). In yeast Saccharomyces cerevisiase, the N-terminus of PMR1 appears to modulate ion transport (Wei et al.,1999), however whether this is the case in other species is yet to be confirmed.
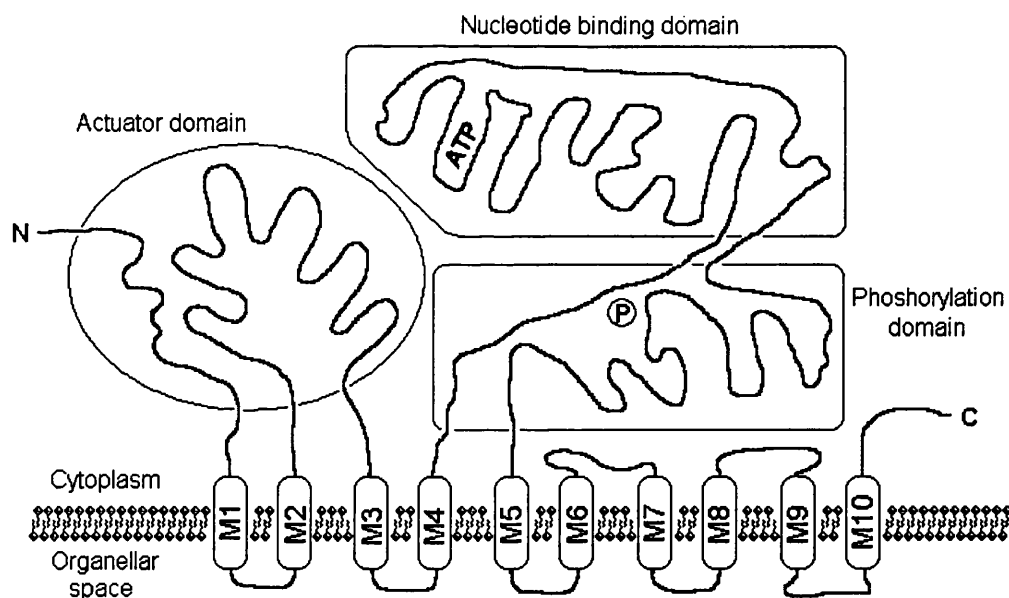
Figure 5.1 Predicted structure of the secretory pathway ATPase (SPCA). Based on the structure of SERCA, taking into account the sequence similarity between SPCA and SERCA (see fig. 5.2). 'ATP' shows the area of ATP binding and 'P' is the area of phosphorylation. Adapted from Wuytack et al., 2002. The actuator domain is believed to move relative to the rest of the protein, to aid in the movement of the Ca^{2+} ion in to the lumen (Xu et al., 2002).

5.2.3 SPCA expression and physiological roles

In yeast the PMR1 pump maintains both Ca^{2+} and Mn^{2+} levels, which is important for providing the correct ionic environment for maturation of secretory products in the lumen

```
ATP2C1     1   ------MKVAR----------------------------QKIPNGENETMIPVLTSKKAS------------ELPLSLV    34
ATP2C2     1   MLHFHLLKFKTRVIFSAVIIMVTGLCLFLLSLPHLHGVEQVPAPWWTSLCPWPIMEAAAFQSGSLYPVASFLAAPMSLL    80
PMR1       1   ------MSDNP----------------------------NASLLDE-DSNREREILDATAEALSKPSPSLEYCTLSLDEA   46


SERCA2a   13   LGH--FGVNESTGLS-LEQVKKLKERWGSNELPAEEGKTLLELVIEQFEDLLVRILLLAACISFVLAWFEEGEETITAFV   89
ATP2C1    35   AS--ILQALLQNGLN-KCEVSHRRAFHGWNKFDISEDEPLWKKYISQFKNP-LIMLLLASAVISVLMHQ---------FD  101
ATP2C2    81   VPDLSFQVTLHTGLS-EFSVTQRRLAHGWNEFVADNSEPVWKKYLDQEKNP-LILLLLGSALVSVLTKE---------YE  149
PMR1      47   LEK--LDTTKNGGLRSSNEANNRRSLYGPWEITVEDDZSLFKKFLSNEIEDRMILLLIGSAVVSLFMGN---------ID  115
                                                                        M1

SERCA2a   90   EPFVILLILVANAIVGVWQERNAENAIEALKEYEPEMGKVYRQDRKSVQRIKAKDIVPGDIVEIAVGDKVPADIRILSIK  169
ATP2C1   102   DAVSITVAILIVVTVAFVQEYRSEKSLEELSKLVPPECCHLEHTLARDLVPGDTVCLSVGDRVPADLRLF--E         177
ATP2C2   150   DAVSIATAVLVVVTVAFIQEYRSEKSLEELTKLVPPECNCLREGK--LQHLLARELVPGDVVSLSIGDRIPADIRLT--E  225
PMR1     116   DAVSITLAIFIVVTVGFVQEYRSEKSLEAINKLVPAECHLMECGQ--ESHVLASTLVPGDLVHFRISDRIPADIRII--E  191
                            M2

SERCA2a  170   STTLRVDQSILTGESVSVIKHTDPVPDPRAVNQDK-------KNMLFSGTNIAAGKAMGVVVATGVTEIGKIRDEMVA    241
ATP2C1   178   AVDLSIDESSLTGETTPCSKVTAPQPAATNGOLAS-------RENIAFMGTLVRCGKAKGVVIGTGENSEFGEVFKMMQA  250
ATP2C2   226   VTDLLVDESSFTGEAEPCSKTDSPLTGG--GDLTT------LSNIVFMGTLVQYGRGCGVVIGTGESSQFGEVFKMMQA   296
PMR1     192   AIDLSIDESNLTGENEPVHKTSQTIEKSSFNLQPNSIVPISERECIAYMGTLVKEGHGKGIVVGTGTVTSFGAVFEMMNN  271

SERCA2a  242   TFQERTPLQQKLDEFGEQLSKVISLICIAVWIINIGHFNDPVHGGSWIRGAIYYFKIAVALAVAAIPEGLPAVITTCLAL  321
ATP2C1   251   EEAPKTPLQKSMDLLGKQLSFYSFGIIGIIMLVGWLLG----------KDILEMFTISVSLAVAAIPEGLPIVVVTLAL   320
ATP2C2   297   EETPKTPLQKSMDRLGKQLTLFSFGIIGLIMLIGWSQG----------KQLISMFTIGVSLAVAAIPEGLPIVMMTLVF   366
PMR1     272   IEKPKTPLQLTMDKLGKDLSLVSFIVIGMICLVGIIQG----------RSWLEMFQISVSLAVAAIPEGLPIIVTVTLAL  341
                         M3              P                                  ▲▲▲ ▲   M4

SERCA2a  322   GTRRMAKKNAIVRSLPSVETLGCTSVICSDKTGTLTTNQMSVCRMFILDRVEGDTCSLNEFTITLSTYAPIGEVHKDDKP  401
ATP2C1   321   GVMRMVKKRAIVKKLPIVETLGCCNVICSDKTGTLTKNEMTVTHIFTSLGLH------TEVTGVGYNQFGEVIVDG--DV  392
ATP2C2   367   GVLRMAKKRVIVKKLPIVETLGCCSVLCSDKTGTLTANEMTVTQLVTSDGLR------ALVSGVGYDGQGTVCLLPSKEV  440
PMR1     342   GVLRMAKKAIVRRLPSVETLGSVNVICSDKTGTLTSNHMTVSKLWCLDSMS------NKLNVLSLDKNKKTKNSN--GN   413

SERCA2a  402   VNCHQYDGLVELATICALCNDSALDYNEAKGVYEKVGEATETALTCLVEKMNVFDTELKGLSKIERANACNSVIKQLMKK  481
ATP2C1   393   VHGFYNPAVSRIVEAGCVCNDAVIRNN------TLMGKPTEGALIALAMKMGLDG------------------LQQDYIR  448
ATP2C2   441   IKEFSNVSLGKLVEAGCVANNAVIRKN------AVMGQPTEGALMALAMKMDLSD------------------IKNSYIR  496
PMR1     414   LKNYLTEDLRETLTIGNLCNNSFSQEHA----IFLGNPTDVALLEQLANFEMPI------------------IRNTVQK   471
                        ATP                  FITC

SERCA2a  482   EFTLEFSRDRKSMSVYCTPNKPSRTSMSKMFVKGAPEGVIDRCTHIRVGSTKVPMTSGVKQKIMSVIREWGSGSDTLRCL  561
ATP2C1   449   KAEYPFSSEQKWMAVKCVHRTQQ-DRPEICFMKGAYEQVIKYCTTYQS--KGQTLTLTQQQRDVYQQEKARMGSAGLRVL  525
ATP2C2   497   KKEIPFSSEQKWMAVKCSLKTE--DQEDIYFMKGALEEVIRYCTMYNN--GGIPLPLTPQQRSFCLQEEKRMGSLGLRVL  572
PMR1     472   VQELPENSKRKLMATKILNPVD---NKCTVYVKGAFERILEYSTSVLKSKGKKTEKLTEAQKATINECANSMASEGLRVF  548
                                              N-P loop

SERCA2a  562   ALATHDNPLRREEMHLEDSANFIKYETNLTFVGCVGMLDPPRIEVASSVKLCRQAGIRVIMITGDNKGTAVAICRRIGIF  641
ATP2C1   526   ALASGPE-----------------LGQLTFLGLVGIIDPPRTGVKEAVTTLIASGVSIKMITGDSQETAVAIASRLGL-   586
ATP2C2   573   ALASGPE-----------------LGRLTFLGLVGIIDPPRVGVKEAVQVLSESGVSVKMITGDALETALAIGRNIGL-   633
PMR1     549   GFAKLTLSD-------SSTPLTEDLIKDLTFTGLIGMNDPPRPNVKFAIEQLLQGGVHIIMITGDSENTAVNIAKQIGIP  621

SERCA2a  642   GQDEDVTSKAFTGREFDELNPSAQRDACLNARCFARVEPSHKSKIVEFLQSFDEITAMTGDGVNDAPALKKAEIGIAMG-  720
ATP2C1   586   ---YSKTSQSVSGEEIDAMDVQQLSQIVPKVAVFYRASPRHKMKIIKSLQKNGSVVAMTGDGVNDAVALKAADIGVAMGQ  663
ATP2C2   633   ---CNGKLQAMSGEEVLSVEKGELADRVGKVSVFFRTSPKHKLKIIKALQESGAIVAMTGDGVNDAVALKSADIGIAMGQ  710
PMR1     622   V--IDPKLSVLSGDKLDEMSDDQLANVIDHVNIFARATPEHKLNIVRALRKRGDVVAMTGDGVNDAPALKLSDIGVSMGR  699

SERCA2a  721   SGTAVAKTASEMVLADDNFSTIVAAVEEGRAIYNNMKQFIRYLISSNVGEVVCIFLTAALGFPEALIPVQLLWVNLVTD   800
ATP2C1   664   TGTDVCKEAADMILVDDDFQTIMSAIEEGKGIYNNIKNFVRFQLSTSIAALTLISLATLMNFPNPLNAMQILWINIIMDG  743
ATP2C2   711   TGTDVSKEAANMILVDDDFHAIMNAVEEGKGIFYNIKNFVRFQLSTSISALSLITLSTVFNLPSPLNAMQILWINIIMDG  790
PMR1     700   IGTDVAKEASDMVLTDDDFSTILTAIEEGKGIFNNIQNFLTFQLSTSVAALSLVALSTAFKLPNPLNAMQILWINILMDG  779
                Mn2+                                        M5      ▼  ▼                    ▲ ▲▲

SERCA2a  801   LPHTALGFNPPDLDIMNKPPRNPKEPLISGWLFFRYLAIGCYVGAATVGAAAWWFIAADGGPRVSFYQLSHFLQCKEDNP  880
ATP2C1   744   PPAQSLGVEPVDKDVIRKPPRNWKDSILTKNLILKILVSSIIIVCGTL------------------IVBWRELR-       799
ATP2C2   791   PPAQSLGVEPVDKDAFRQPPRSVRDTLLSRALILKILMSAAIIISGTL------------------IIWKEMPE        847
PMR1     780   PPAQSLGVEPVDHEVMKKPPRKRTDKILTHDVMKRLLTTAACIIVGTV------------------YIFVKEMAE       836
                M6                          M7

SERCA2a  881   DFEGVDCAIFESPYPMTMALSVLVTIEMCNALNSLSENQSLLRMPPWENIWLVGSICLSMSLHFLILYVEFLPLIFQITP  960
ATP2C1   800   ENVIT-------PRDTTMTFTCFVFFDMFNALSSRSQTKSVFEIGLCSNRMFCYAVLGSIMGQLLVIYFPPLQKVFQTES  872
ATP2C2   848   ERASP------PRTTTMTFTCFVFFDLFNALTCRSQTTLIFEIGFLRNHMFLYSVLGSILGQLAVIYIPPLQRVFQTEN   920
PMR1     837   DGKVT-------ARDTTMTFTCFVFFDMFNALACRHNTKSIFEIGFFTYKMFNYAVGLSLLGQMCAIYIFFFGSIPFKTEK 909
                        M8                          M9

SERCA2a  961   LNVTQWLMVLKISLPVILMDETLKFVARNYLEPAILE-------------  997
ATP2C1   873   LSILLFLFLGLTSVCIVAHIIKKVEP---SREKIQKHVSSTSSSFLEV    919
ATP2C2   921   IGALLEFLTGLASSVFILSELLKLCEKYCCSPKRVQMHPEDV-------  963
PMR1     910   IGISSILLLLISSSVFIVDELRKLWTRK--KNEEDSTYFSNV-------  950
                M10
```

Figure 5.2 Alignment of the amino acid sequences of human SERCA2a, ATP2C1, ATP2C2 and *S. cerevisiae* PMR1 (PID accession no.4502285, 7656910, 7662256 and 172199). Alignment made with ClustalW and similarity shading with BioEdit. The SERCA transmembrane domains are underlined. The phosporylation site (P), residues involved in ATP binding and FITC binding are indicated. Ca^{2+}-coordinating residues on SERCA are indicated by triangles (▼: site I; ▲: site II) below the alignment. "Mn^{2+}" indicates the Gln residue contributing to Mn^{2+} selectivity in the SPCA pumps. Adapted from Wuytack *et al.*, 2002.

of the Golgi (Antebi et al., 1992) as well as helping to prevent Mn^{2+} toxification (Axelsen and Palmgren, 2001). There is evidence that there is an independent requirement for Mn^{2+} in protein glycosylation (Ton et al., 2002). In mammals the SPCA pump plays two significant roles in the mammary gland; it is thought to be responsible for the increased Ca^{2+} transport required for the high concentration of Ca^{2+} in milk (Reinhardt et al., 2000) and the pumped Mn^{2+} is critical for the Golgi-based lactose synthase (Powell and Brew, 1976).

Analysis of the subcellular localisation of SPCA pumps has presently only indicated a Golgi localisation (Van Baelen et al., 2001; Missiaen et al., 2002). However, it has been proposed that a PMR1 homologue is responsible for maintaining a thapsigargin-insensitive store in dense core secretory vesicles of pancreatic cells (Mitchell et al., 2001). The most abundant human SPCA, ATP2C1, is considered to be a housekeeping gene, while human ATP2C2 (60% homology to ATP2C1) has a more restricted expression pattern (Ton et al., 2002). This suggests that SPCA plays a universal role in maintaining Golgi calcium levels as well as possibly performing more specialised roles in specific tissues, either by alternative subcellular localisation or by altered ion transport properties.

Another possible physiological role of the SPCA pump could be its involvement in producing baseline Ca^{2+} oscillations. COS-1 cells overexpressing SPCA display cytoplasmic Ca^{2+} oscillations upon stimulation with ATP (Missiaen et al., 2002). The model proposed for the presence of these oscillations involves the Golgi being a second (the ER being the first), less sensitive IP_3-releasable store. After an agonist induced response, the elevated $[Ca^{2+}]_i$ is partially extruded by the SPCA into the Golgi. When the store's limit is reached, a small $[Ca^{2+}]_i$ increase occurs, which activates the IP_3R on the Golgi causing a calcium spike (Wuytak et al., 2003). The model infers that these oscillations require an increased transport of Ca^{2+} into the Golgi, mediated by SPCA. This maybe the endogenous method of producing Ca^{2+} oscillations in specialised cell types, either the SPCA could be up regulated or a more actively transporting SPCA variant may be present.

5.2.4 SPCA and disease phenotypes

Hailey-Hailey disease (HHD) is keratinocyte disorder characterised by incomplete cell adhesion. Two separate reports identified that mutations in the human SPCA cause HHD (Hu et al., 2000; Sudbrak et al., 2000), these mutations result in defective desmosomes, which normally ensure epidermal keratinocyte adhesion. With the identification that mutations in the SERCA protein ATP2A2 cause another keratinocyte disorder (Darier's

disease (Sakuntabhai et al., 1999)), it is evident that calcium homeostasis is critical for epithelial integrity.

Additionally SPCA may play a role in amyloidoses in mammals (such as Alzheimer's disease), as endoproteolytic convertases (Davidson et al., 1988) and secreatases (LaFerla, 2002) are dependant on calcium homeostasis in the Golgi and secretory vesicles.

5.2.5 Role of a SPCA in the Malpighian tubule?

As mentioned in section 1.3.4, there is evidence from experiments performed by Rosay and colleagues (1997) that suggests the involvement of a thapsigargin-insensitive store in the principal cells. If there is such a store in these cells, it is conceivable that a member of the SPCA family is maintaining this Ca^{2+} store. Furthermore, the tubule is the principal Ca^{2+} storage organ in the fly (Dube et al., 2000), therefore it is possible that a SPCA -like pump is playing a role in the accumulation of Ca^{2+} into organelles.

To answer these questions, the existence of a *Drosophila* SPCA has to be established. Once identified, the expression, intracellular localisation and physiological role of this Ca^{2+}-ATPase can be investigated using molecular techniques and reverse genetics.

5.3 Results

5.3.1 Identification of *Drosophila SPCA* by *in silico* methods

The *S. cerevisiae* PMR1 (accession 6321271) and human ATP2C1 (accession 12644373) amino acid sequences were used separately to blast the *Drosophila* predicted proteins database (BDGP). The top match in both cases was the gene product of CG7651 (chromosome 3L, 80A2), having a 48% identity (65% positives) with PMR1 and 59% identity (72% positives) with ATP2C1. The next closest match, in both cases was the *Drosophila* SERCA gene Ca-P60A. The FlyBase report had automatically identified the gene as encoding for a protein with calcium-transporting ATPase activity.

The sequence similarity strongly suggested that this was the *Drosophila* SPCA gene, however further sequence analysis would be required for confirmation.

5.3.2 Alignment and phylogenetic relationships

For further support that CG7651 was a member of the SPCA family and also to analyse its similarity to other SPCAs and other Ca^{2+} ATPases, a sequence similarity tree was constructed (see figure 5.3). The tree shows the three subtypes of Ca^{2+}-ATPases; the SERCA group, the plasma membrane (PMCA) group and the SPCA group. Each group is distinct with respect to sequence similarity, as well as intracellular localisation and cellular function. The tree also clearly depicts CG7651 as a member of the SPCA group. The closest match to the CG7651 is a protein identified from the recently sequenced *Anopheles gambiae* genome.

Most of the predicted structure and function of SPCA proteins have been based on their sequence similarity to the well studied SERCA proteins (see figure 5.2). Figure 5.4 shows the alignment of CG7651, PMR1 and ATP2C1 amino acid sequences. All the critical domains for Ca^{2+}-ATPase function are present in CG7651, such as ATP binding sites, the phosphorylation site, a N-P domain connection site and site II Ca^{2+}-coordinating residues. Additionally the 10 membrane domains appeared to be conserved. Also, the SPCA-specific residues that have been shown to be critical for Mn^{2+} transport are present.

This sequence comparison and analysis confirms that CG7651 does indeed encode for the *Drosophila* SPCA. As mentioned in the summary, I have decided to call this gene *SPoCk*.

5.3.3   Predicted structure and localisation of SPoCk isoforms

In August, 2002 the genome annotation database (GADFLY) was updated; new EST sequencing data revealed two more alternatively spliced transcripts for CG7651, one of which included an upstream gene CG14449. The gene was then renamed CG32451. Both of the two new transcripts contained extra coding sequence that would result in proteins
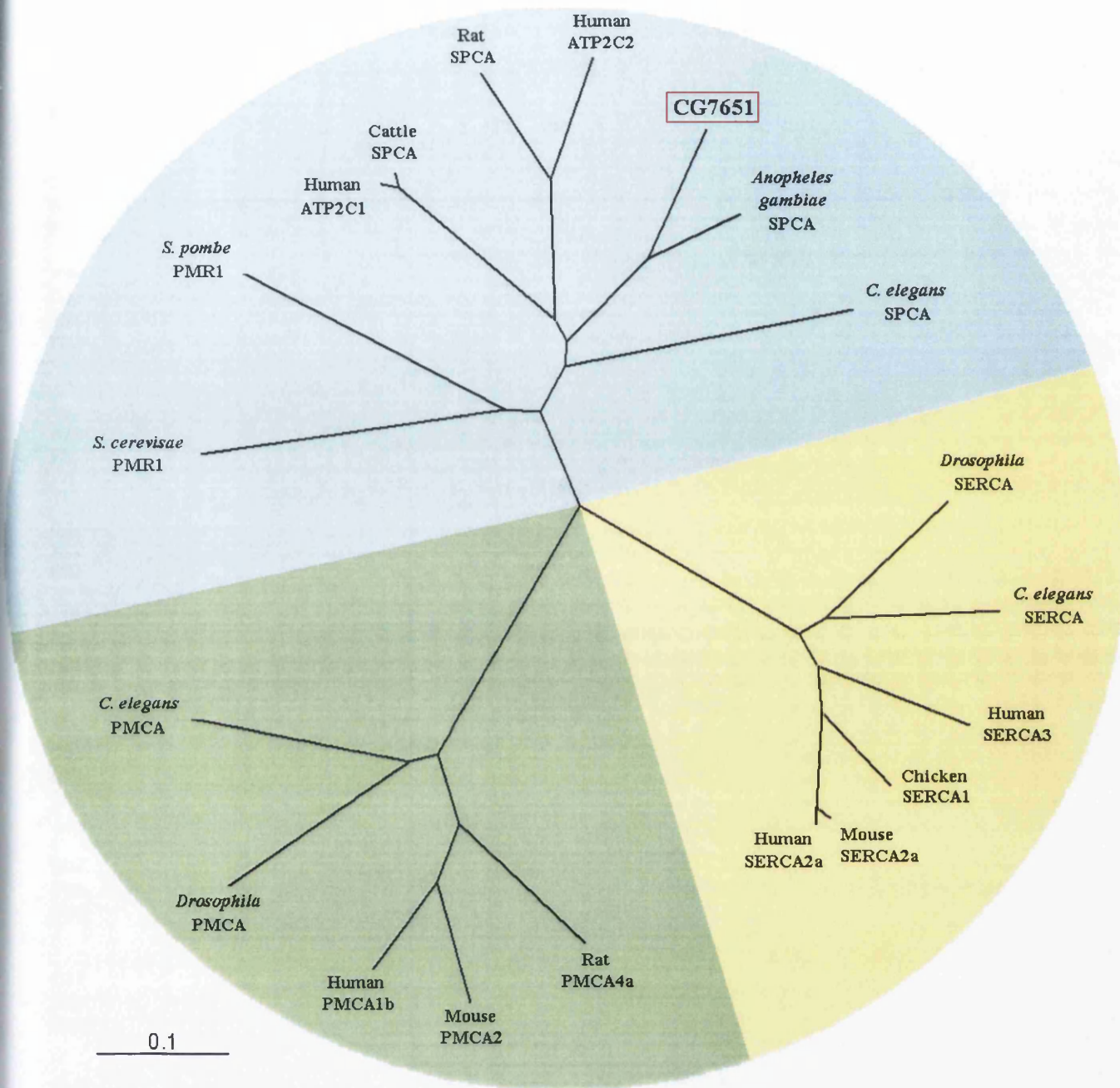
Figure 5.3 Sequence similarity analysis of Ca^{2+}-ATPase protein sequences. The sequences demonstrate the distinct clustering of the three main subtypes of Ca^{2+}-ATPases. These are the secretory pathway Ca^{2+}-ATPases (blue), sarco/endoplasmic reticulum Ca^{2+}-ATPases (yellow) and the plasma membrane Ca^{2+}-ATPases (green). These subtypes are separated by their sequence similarity as well as their intracellular localisation. The *Drosophila* gene CG7651 clearly falls within the SPCA group of Ca^{2+}-ATPases. Sequences were aligned using ClustalW and displayed using TreeView. PID accession numbers, beginning with *S. cerevisiae* PMR1 are given in a clockwise order: 6321271, 3138890, 12644373, 285369, 3327220, 7296577, 21287896, 3875247, 7291680, 3878521, 3211977, 114305, 2826866, 114312, 1083756, 5714364, 14286104, 7304318 and 3549723.

```
PMR1        1    MSDNPFNASLLDEDSNPERELLDATAALSKPSPSLEYCLSVDALEKLDTDKNGGLRSSNRANNEFSL  70

CG32451-PA  40   IGHNELLLVAEDETWKKYIEQFRNP-LILLLLGSALVSVIMKQFDDDAVSITIAILIVVTVAFIQEYRSEK  108
AT?2C1      58   HGWNKFDISEDEPLWKKYISQFKNP-LIMLLLASAVISVLMHQFDDDAVSITVAILIVVTVAFVQEYRSEK  126
PMR1        71   YGPNEITVEDDESLFKKFLSNFIEDRMILLLIGSAVVSLFMGNIDDAVSITLAIFIVVTVGFVQEYRSEK  140
                                            M1                            M2

CG32451-PA  109  SLEELKKLVPPECHCLREGRLDTFLARELVPGDIVHLNVGDRVPADVRLFEAVDLSIDESSFTGETEPAR  178
AT?2C1      127  SLEELSKLVPPECHCVREGKLEHTLARDLVPGDTVCLSVGDRVPADLRLFEAVDLSIDESSLTGETTPCS  196
PMR1        141  SLEALNKLVPAECHLMRCGQESHVLASTLVPGDLVHFRIGDRIPADIRIIEAIDLSIDESNLTGENEPVH  210

CG32451-PA  179  KITDVLLNN------TNVKDHSNMKNIAFMGTLVRCGNEKGIVVSTGERSEFGEVFKMMQAEEAPKTPLQ  242
AT?2C1      197  KVTAPQPAA------TNG-DLASRSNIAFMGTLVRCGKAKGVVIGTGENSEFGEVFKMMQAEEAPKTPLQ  259
PMR1        211  KTSQTIEKSSFNDQPNSIVPISERSCIAYMGTLVKEGHGKGIVVGTGTNTSFGAVFEMMNNIEKPKTPLQ  280

CG32451-PA  243  KSMDILGAQLSFYSFLIIGVIMLLGWLQGKPLSEMENISVSLAVAAIPEGLPIVVTVTLALGVMRMAKFN  312
AT?2C1      260  KSMDLLGKQLSFYSFGIIGIIMLVGWLLGKDILEMFTISVSLAVAAIPEGLPIVVTVTLALGVMRMVKKR  329
PMR1        281  LTMDKLGKDLSLVSFIVIGMICLVGIIQGRSWLEMFQISVSLAVAAIPEGLPIIVTVTLALGVLRMAKRK  350
                              M3 P                         ▲▲▲▲   M4

CG32451-PA  313  SIVKKLPTVETLGCVNVICSDKTGTLTKNEMIAIIITSDGYMADVTCAGVNDQGEIHIRHCNNVEMAKT  382
ATP2C1      330  AIVKKLPIVETLGCCNVICSDKTGTLTKNEMTVHIFTSDGLHAEVTGVGYNQFGEVIVDGDVVHGFYNP  399
PMR1        351  AIVRRLPSVETLGCVNVICSDKTGTLTSNHMTVSKLWCLDSMSNKLNVLSLDKNKKTKNSNGNLKNYLTE  420

CG32451-PA  383  NITNLLEIGAVCNNAYIQNG--TLLGQPTEGALVAVAMKNGMYATAENYVRIQEYPFSSEQKMMAVKCIH  450
ATP2C1      400  AVSRIVEAGCVCNDAVIRNN--TLMGKPTEGALIALAMKMGLDGLQQDMIRKAEYPFSSEQKWMAVKCVH  467
PMR1        421  DVRETLTIGNLCNNASFSQEHAIFLGNPTDVALLEQLANFEMPDIRNTVQKVQELPENSKRKLMATKILN  490
                                                                               ATP

CG32451-PA  451  KYNNNKEEIFFAKGALETLLPQCTKYCF--GTQTVPLTKDNEREFLASKYEIGRKGLRVLALAKGRS---  515
ATP2C1      468  RTQQDRPEICFMKGAYEQVIKYCTTYQS--KGQTLTLTQQRDVYQQEKARMGSAGLRVLALASEPE---  532
PMR1        491  PVDN--KCTVYVKGAFERILEYSTSYLKSKGKKTEKLTEAQKATINECNSMASEGLRVFGFAKLTLSDS  558
                      FITC                          N-P loop

CG32451-PA  515  --------MQDLIYCGLVGITDPPRELVRESIEMLMQSGVRVKMVTGDAQETALAIANLIGIDTIHHST-  576
ATP2C1      532  --------LGQLTFLGLVGIIDPPRTGVKEAVTTLIASGVSIKMITGDSQETAVAIASRLGLYSKTSQS-  593
PMR1        559  STPLTEDLIKDLTFTGLIGMNDPPRENVKFAIEQLLQGGVHIIMITGDSENTAVNIAKQIGIPVLDPKLS  628

CG32451-PA  576  -LSGQEMDQMNEHQLDKVANNVSVFYRVSPRHKLEIVKSLQRSGNILGMTGDGVNDGVALKKADIGIAMG  645
ATP2C1      593  -VSGEEIDAMDVQQLSQIVPKVAVFYRASPRHKMKIIKSLQFNGSVVAMTGDGVNDAVALKAADIGVAMG  662
PMR1        629  VLSGDKLDEMSDDQLANVIDHVNIFARATPEHKLNIVRALRKRGDVVAMTGDGVNDAPALKLSDIGVSMG  698

CG32451-PA  646  KNGTDVCKEAADMILVNDDFHTIIAAIEEGKGIFYNIRNFVRFQLSTSIAALALIALATLMDIANPLNAM  715
ATP2C1      663  QTGTDVCKEAADMILVDDDFQTIMSAIEEGKGIYNNIKNFVRFQLSTSIAALTLISLATLMNFPNPLNAM  732
PMR1        699  RIGTDVAKEASDMVLTDDDFSTILTAIEEGKGIFNNIQNFLTEQLSTSVAALSLVALSTAFKLPNPLNAM  768
                          Mn²⁺                                    M5
                            ↓

CG32451-PA  716  QILWINIIMDGPPAQSLGVEPVDHDVLKQKPRNVKQPMITKSVVVNVLLSASIIVLGTLWVFQREMALGT  785
ATP2C1      733  QILWINIIMDGPPAQSLGVEPVDKDVIRKPPRNWKDSILTKNLILKILVSSIIIVCGTLFVFWRELRDNV  802
PMR1        769  QILWINILMDGPPAQSLGVEPVDHEVMKKPPRKRTDKILTHDVMKRLLTTAACIIVGTVYIFVKEMAEDG  838
                        ▲    ▲  M6                           M7

CG32451-PA  786  LGKIKRDTTMTFTCFVFFDMFNALSCRSQTKSVFTIGLTTNRMFLLAVAFSIIGQMLVVYFPPLQMVFQT  855
ATP2C1      803  I--TPRDTTMTFTCFVFFDMFNALSSRSQTKSVFEIGLCSNRMFCYAVLGSIMGQLLVIYFPPLQKVFQT  870
PMR1        839  K-VTARDTTMTFTCFVFFDMFNALACRHNTKSIFEIGFFTNKMFNYAVGLSLLGQMCAIYIPFFSIEKT  907
                          M8                          M9

CG32451-PA  856  EALTPYDIFFLVSLTSSVLVVSEIKKWFERT---MERKMYSTRSELDFV  901
ATP2C1      871  ESLSILDLLFLLGLTSSVCIVAEIIKKVERSREKIQKHVSSTSSSFLEV  919
PMR1        908  EKLGISDILLLLLISSSVFIVDELRKLWTTK------KNEEDSTYVSNV  950
                      M10
```

Figure 5.4 Alignment of the amino acid sequences of CG32451-PA, human ATP2C1 and *S. cerevisiae* PMR1 (PID accession no.21287896, 7656910 and 172199). Alignment made with ClustalW and similarity shading performed with BioEdit. Predicted transmembrane domains are underlined. The phosporylation site (P), residues involved in ATP binding and FITC binding are indicated. Site II Ca²⁺-coordinating residues are indicated by triangles ▲ below the alignment. "Mn²⁺" indicates the Gln residue contributing to Mn²⁺ selectivity in the SPCA pumps. Sequence annotation based on transmembrane plots (figure 5.7) and alignments by Wuytack *et al.*, 2002 and Van Baelen *et al.*, 2001.

114

Transcript A

Transcript B

Transcript C

Location: 3L 80A1-80A2

Figure 5.5 Annotation of CG32451 transcripts. Adapted from genome annotation figure, FlyBase (Sept. 2002). Shaded areas indicate coding regions.

dPOLYUBIQUITIN	VLRLRGGMQIFVKTLTGKTITLEVE
CG11700	VLRLRGGMQIFVKTLTGKTITLEVE
CG10523	GKTLTHTLSIYVKTNTGKTLTVNLE
SPoCk-trC	MLRARRTISIFIEEQTGLTLTPEML

Figure 5.6 Alignment of the first 25 amino acids of SPoCk-trC with *Drosophila* ubiquitin and 'ubiquitin-like' protein sequences. Dark shading of residues indicates exact matches between all sequences. Lighter shading indicates a majority of the aligned residues being identical to SPoCk-trC or all aligned residues are similar to CG32451-PC. dPOLYUBIQUITIN, *Drosophila* polyubiquitin gene product. CG11700 is predicted to encode for 'ubiquitin-like' protein (FlyBase). CG10523 is the *Drosophila parkin* gene.
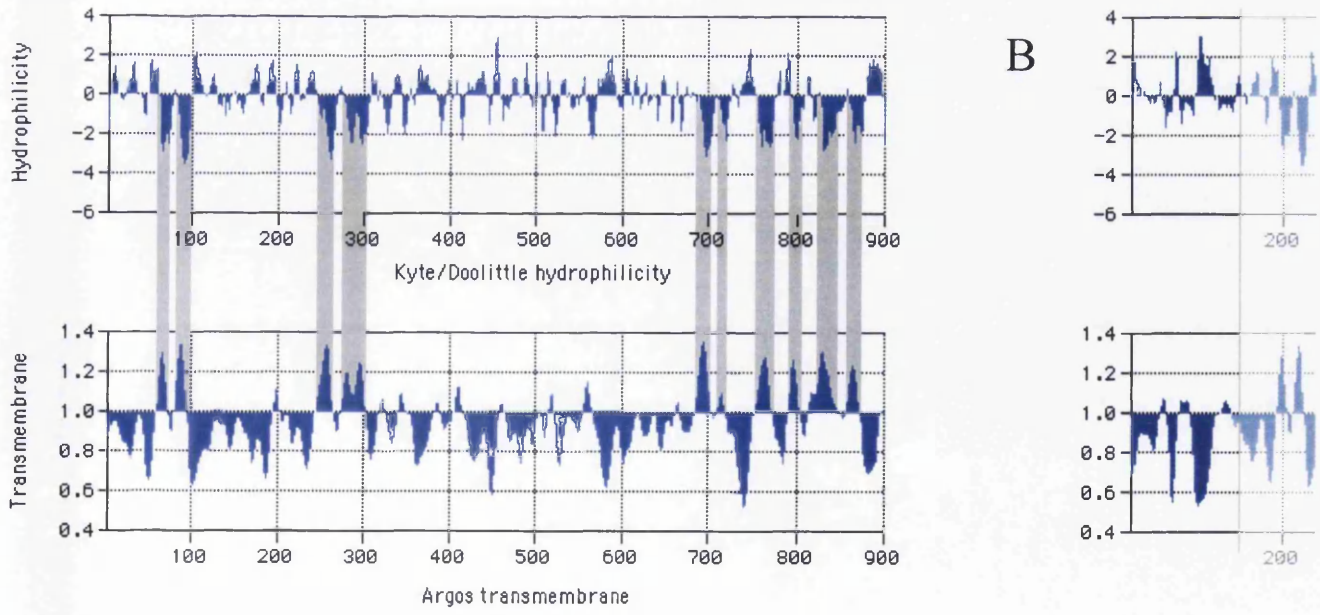
Figure 5.7 Hydrophilicity and transmembrane prediction plots of SPoCk. (A) Plots of SPoCk-trA, shaded regions depict the ten transmembrane domains. (B) Plots of the first 143 amino acids of SPoCk-trB. Window = 7.

115

with an extended N-terminus (see figures 5.5 and 5.9). CG32451-PB (trB) encoded an extra 133 residues, whilst CG32451-PC (trC) encoded an extra 23 residues. The originally identified CG7651 transcript was changed to CG32451-PA (trA).

These extra domains were analysed using PSORTII to determine if there were any obvious localisation signals. The extra 143 residues in trB had a putative vacuolar targeting site (ILPK) at position 109, whilst trC had both an ER-membrane targeting sequence (XXRR (ML<u>RARR</u>TIS....)) and a mitochondria pre-targeting cleavage site (RRT | IS). Furthermore these extra amino acid sequences were taken and submitted into the NCBI standard protein blast server and the BDGP protein blast server. This was to investigate if these domains shared similarity to other proteins and if so, their possible function may be elucidated. The extra trB domain appears to share no sequence similarity with any other protein in the NCBI or the BDGP database, using standard BLAST settings. However, when the protein sequence for trB was submitted into the InterProScan protein analysis program, the first ~140 residues of sequence were identified has possessing similarity to a ATP-binding ABC transporter domain. The trC domain is similar to repeated regions in several *Drosophila* ubiquitin-like proteins (see figure 5.6). These include polyubiquitin and the gene product of *parkin*.

The hydrophilicity and transmembrane prediction plots for SPoCk-trA clearly depict the 10 transmembrane regions of the protein (see figure 5.7A). The hydrophobic domains match up well with the predicted transmembrane domains. The extra N-terminal section in trB was also investigated (figure 5.7B) and this did not show any extra transmembrane regions.

5.3.4   RT-PCR analysis of *SPoCk* transcripts

Before the discovery of alternative splice variants, RT-PCRs had been carried out using primers spanning exons 3 and 4 (primers 64 and 65). This showed expression of the gene at all developmental stages and in all tissues examined (data not shown). When the existence of trB and trC was realised, new primers (primers 66-69) were designed to distinguish between the different splice variants. The binding regions of these primers are shown in figure 5.9 and the results of the RT-PCRs shown in figure 5.8.

The primers designed to detect trB (579 bp product), show that this transcript is expressed throughout the four main developmental stages of the fly and is expressed in all tissues examined, apart from the tubule. The primers designed to detect both trA (350 bp product) and trC (404 bp product) demonstrated the ubiquitous expression of trA, throughout development and in all tissues tested. trC is present throughout development and in every tissue, apart from the testes. Although the RT-PCRs are not quantitative, it is still possible to compare relative amounts of trA with trC between different samples. For example, it is
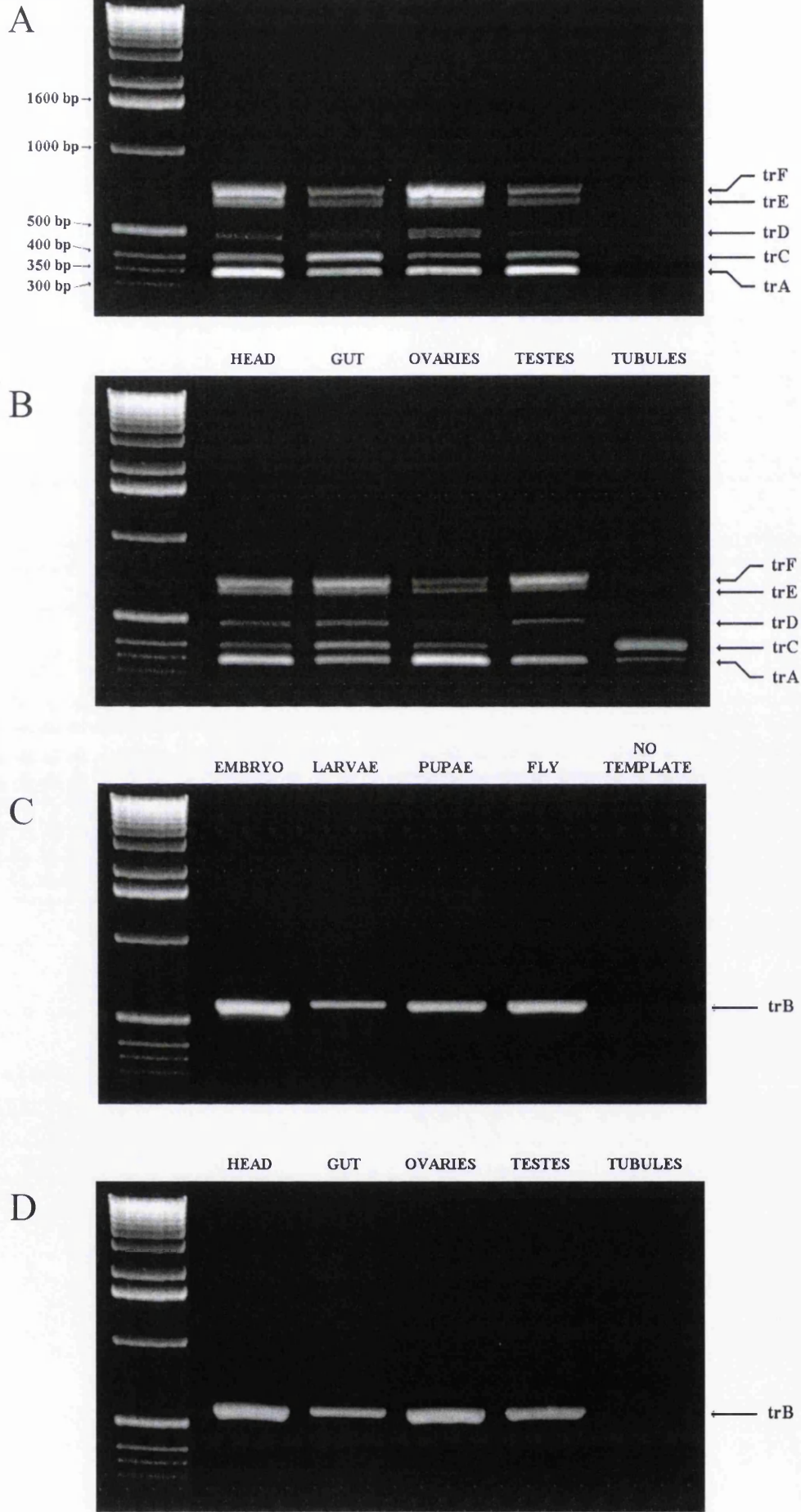
Figure 5.8 RT-PCR analysis of CG32451 transcript expression. (A) and (C) transcript expression through the life cycle of the fly. (B) and (D) transcript expression in various tissues of the fly. trD, trE and trF are extra CG32451 transcripts detected when using primers for trA and trC. RT-PCR was carried out as described in text. Samples were electrophoresed on 1.0% agarose gels. 1kb ladder (Invitrogen) was used.

117
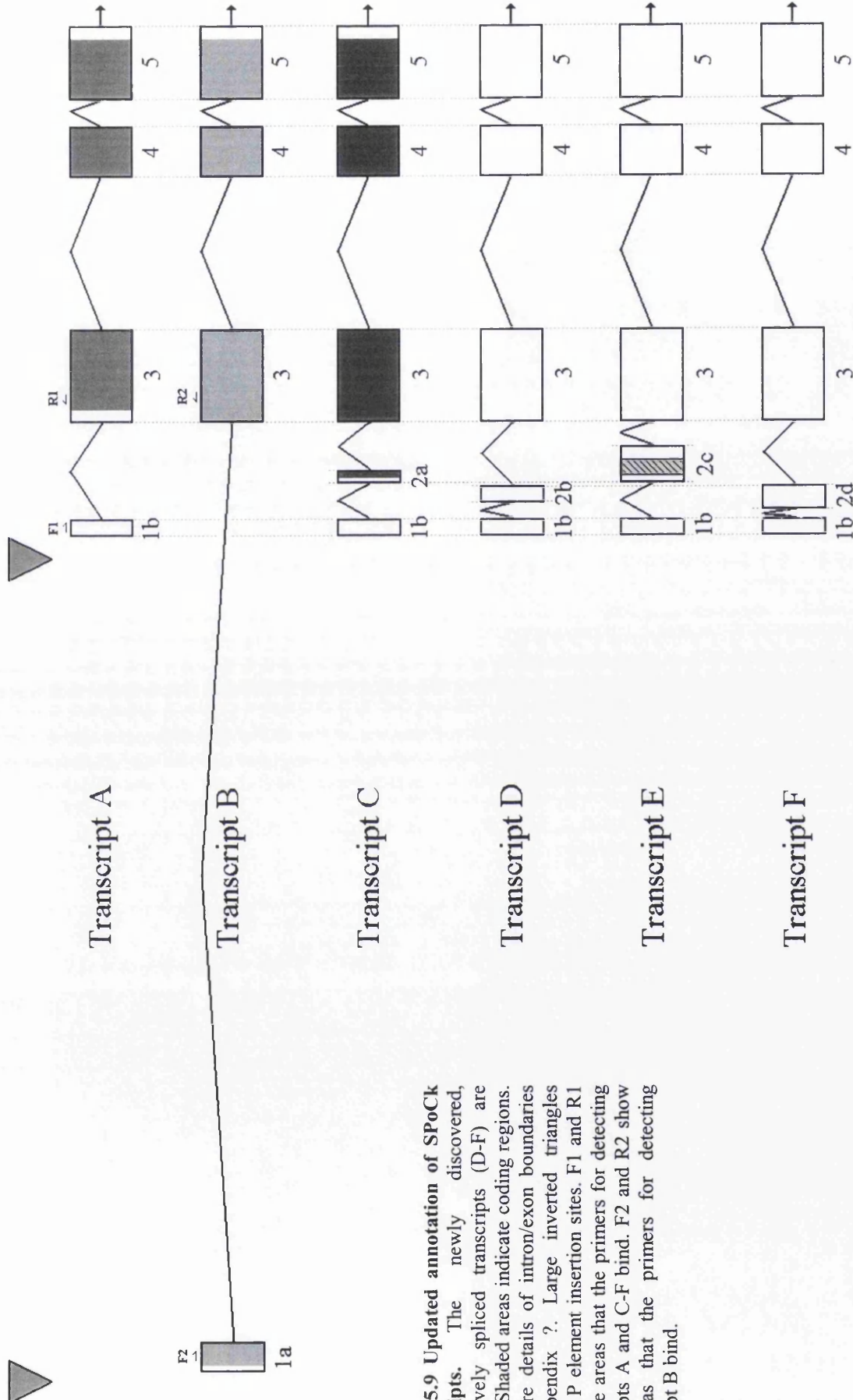
Figure 5.9 Updated annotation of SPoCk transcripts. The newly discovered, alternatively spliced transcripts (D-F) are shown. Shaded areas indicate coding regions. For more details of intron/exon boundaries see appendix ?. Large inverted triangles indicate P element insertion sites. F1 and R1 show the areas that the primers for detecting transcripts A and C-F bind. F2 and R2 show the areas that the primers for detecting transcript B bind.

Location: 3L 80A1-80A2

evident that there is greater expression of trC relative to trA in the tubule compared to the whole fly (see figures 5.8A and 5.8B).

The primers for trA and trC also generated other unexpected products of approximately 500 bp, 650 bp, and 750 bp in size (see figure 5.8A and B). To determine whether these bands indicated extra splice variants, the bands were cut out, TOPO® cloned and sequenced. The sequencing results demonstrated that these bands did indeed represent new, unidentified transcripts of SPoCk. Annotation of these transcripts is shown in figure 5.9 and for exact details of the intron/exon boundries see appendix 6. These extra transcripts do not result in any new SPoCk proteins with different N-terminal domains, however trE does contain a small reading frame that may produce a 35 a.a. protein (see figure 5.9).

5.3.5 *SPoCk* P element mutants

The first P element insertion (in the SPoCk gene region) to be identified was in the 10205 line. The flybase annotation does not show 10205 as an allele of *SPoCk*, however the element was detected on the Flybase Genome Browser as being approximately 100bp from the first exon of trA. These flies were available from the Bloomington stock centre. The insertion site has already been pinpointed using inverse PCR (for protocol, see BDGP site), this sequence data places the insertion 40 bp from the beginning of the first exon of trA. To verify this, PCR was performed on genomic DNA (prepared from 10205 flies) using primers that bound upstream and downstream from the predicted insertion site and the P31 primer (binds the inverted repeats at the ends of P elements). This confirmed the position of the P element (data not shown).

The insertion is a $P\{w^{+mC}=lacW\}$ P element (O'Kane and Gehring, 1987), therefore if it has 'trapped' an enhancer then β-galactosidase will be expressed in the cells specific to that enhancer. LacZ staining (see section 2.9) was performed on the 10205 flies but no staining could be detected. The 10205 insertion is homozygous lethal; so to determine the lethal phase of the homozygotes, a stable line containing the 10205 insertion balanced over a GFP balancer was set up:

$$w^-; +/+; 10205\ P\{w^{+mC}=lacW\}/TM3, P\{w^{+mC}=ActGFP\}JMR2, Ser^1$$

The 10205 homozygous progeny of these flies (from embryo onwards) can be distinguished form heterozygotes, as they are not fluorescent. The homozygotes were found to reach the first instar stage of development, where they stop developing and were observed to live for as long as 2 weeks.
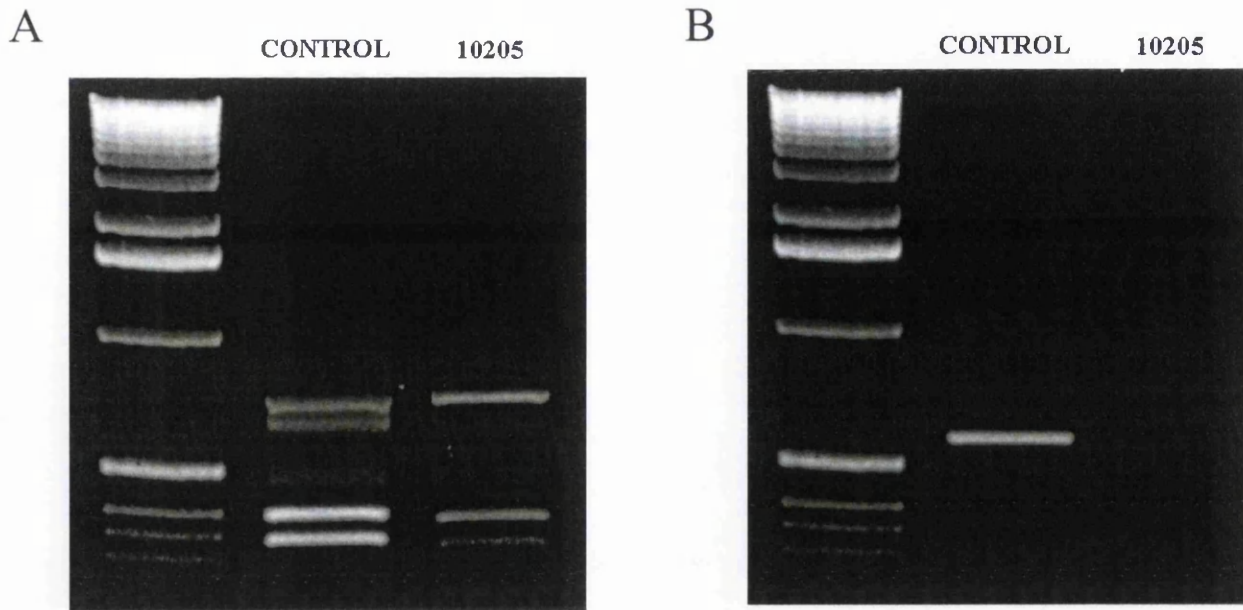
Figure 5.10 RT-PCR analysis of the effect of the P element insertion 10205 on the expression of SPoCk. RT-PCRs were carried out on 1st instar larvae (as homozygote 10205 flies die at 1st instar larvae). (A) Analysis using primers that detect trA, trC, trD, trE and trF. (B) Analysis using primers that detect trB.
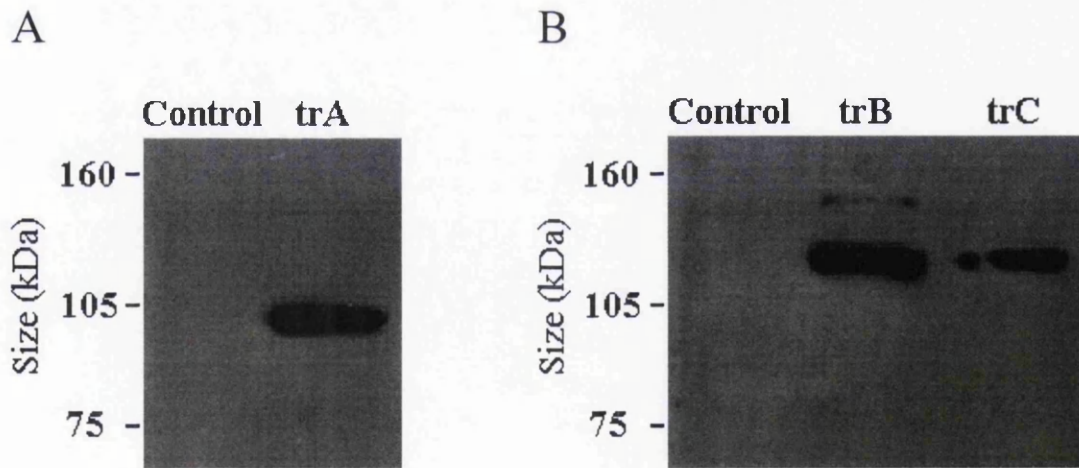
Figure 5.11 Western analysis of flies overexpressing tagged SPoCk isoforms. (A) Western blot showing trA-c-myc expression in *w⁻; trA-c-myc; C42* flies. Mouse monoclonal anti-c-myc antibody was used at a 1:2000 dilution and a anti-mouse HRP secondary at 1:5000 dilution. (B) Western blot showing expression of trC-YFP and trB-GFP in *w⁻; trC-YFP; C42* and *w⁻; trB-GFP; c710* flies. Mouse monoclonal anti-GFP antibody was used at 1:2000 dilution and a anti-mouse HRP secondary at 1:5000 dilution.

120

To determine whether this insertion was preventing expression of any of the SPoCk transcripts, RT-PCR was carried out on the homozygous first instar larvae (see figure 5.10). Transcripts A, C, D, E and F are still present, however trB is completely knocked out. This evidence suggests that it is the lack of trB protein that is causing the phenotype in the homozygous 10205 larvae.

The second P element to be identified in the SPoCk gene region was the homozygous viable 12799 insertion. This line is documented to have an insertion ~100bp upstream of the first exon of trB (by inverse PCR). This is a P{w^{+mGT}=GT1}insertion (Lukacsovich et al., 2001), which functions as a GAL4 enhancer trap. Therefore it is possible that this line can report the expression pattern of trB. When the 12799 line was initially crossed to a UAS-GFP line, fluorescence was observed in the mushroom bodies of the adult brain. However, this fluorescence has not been seen in any consequent experiments. This could be due to the line being unstable or a temporal expression problem.

A recent mutagenesis program using *piggyBac*-based elements (Häcker et al., 2003) has identified an insertion of one of these elements in the intron between exon 1 and exon 2 of trA. However, this line is not yet publicly available.

5.3.6 Generation of *SPoCk* over-expression mutants

For overexpression studies, it is necessary to tag the protein. This is so that overexpression can be confirmed and also the subcellular localisation of the protein can be determined. It was decided to tag SPoCk at the C-terminus. This was based on two pieces of information; firstly Missiaen and colleagues (2002) had shown that a C-terminally GFP-tagged PMR1 appeared to localise and function properly. Secondly, the predicted structure of SPCA depicts the C-terminus on the cytoplasmic side and free from interaction with the rest of the protein (see figure 5.1). trA was tagged with a c-myc epitope, trB with GFP and trC with YFP. trA-c-myc was generated by amplifying the ORF from an appropriate EST using a primer that included the c-myc epitope (see table 2.4). trB-GFP and trC-YFP were made by fusion PCR (see table 2.4).

It has to be noted, that cloning and preparation of the overexpression constructs was very difficult. Once the templates had been cloned into the pMT/V5-His vector, the *E. coli* carrying the plasmid grew slower than normal and the DNA yield was also very poor. It appeared that the plasmids were toxic to the bacteria. Additionally, after ligation and transformation of the template into pUAST, the positive colonies only appeared after being incubated overnight at 37°C AND approximately 3 days at RT! This is likely to be due to low level transcription and translation of the SPCA in the bacteria; even a small amount of

SPCA must have impeded the bacterial growth. Interestingly, the construct carrying trC was observed to be less toxic to the *E. coli*.

The pUAST constructs were used to generate transgenic fly lines. These lines were marked up (see section 2.10.5) and stable lines established, that expressed the tagged transcript in either the principal cells or stellate cells (see table 5.1). It was not possible to create a non-marked stable line for *w⁻; trB-GFP; c42,* as the flies became sterile with increased copies of the transgene and the c42 GAL4 insertion (the separate parental lines are perfectly healthy).

Table 5.1 Stable fly lines expressing *dSPCA* transcripts in the tubule.

Genotype	Expression in tubule
w⁻; trA-c-myc; c42	Principal cells
w⁻; trA-c-myc; c710	Stellate cells
w⁻; trC-YFP; c42	Principal cells
w⁻; trC-YFP; c710	Stellate cells
w⁻; trB-GFP/Cyo; c42/TM6Tb-	Principal cells
w⁻; trB-GFP; c710	Stellate cells

Expression of these transgenes was confirmed by western analysis of the stable fly lines shown in table 5.1. The western blots in figure 5.11 show a specific band for trA-c-myc at the expected size of ~100kDa and a band for trC-YFP at the expected size of ~125kDa. However for trB-GFP there is only a faint band at the expected size of ~140kDa and a much stronger band at ~125kDa. It is possible that the extra 133 a.a. of trB are cleaved off after a processing event.

5.3.7 Subcellular localisation of tagged SPoCk isoforms

Localisation of SPoCk by ICC in *w⁻; trA-c-myc; c42* tubules revealed a punctate and predominantly basolateral pattern in the principal cells (see figures 5.12L → 5.12Q). Furthermore, at high magnification it is possible to see trA-c-myc staining on the periphery of Golgi-like bodies (see figures 5.12L and figure 5.12N). In S2 cells the staining was similar (figures 5.12A, 5.12D and 5.12G), although more perinuclear than in principal cells. As all previously studied SPCA proteins have been shown to localise to the Golgi and the ICC results depict a Golgi-like pattern, it is very likely that trA-c-myc is also localised to the Golgi apparatus. This was verified by expressing trA-c-myc in S2 cells and treating them with 10 μM brefeldin A. Brefeldin A is an antibiotic drug that inhibits the formation of the Golgi apparatus (Mendez, 1995); figures 5.12J and 5.12K show that after
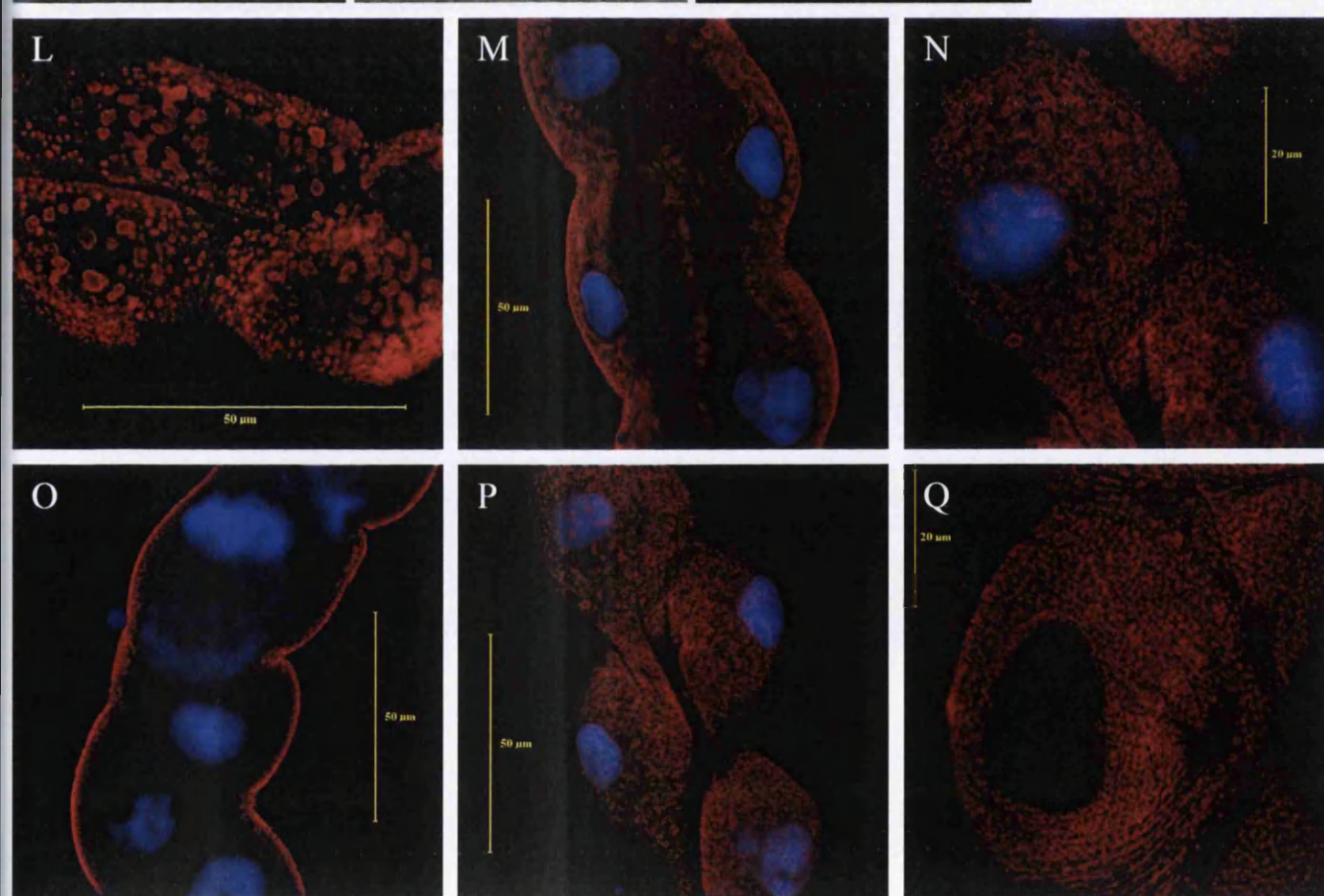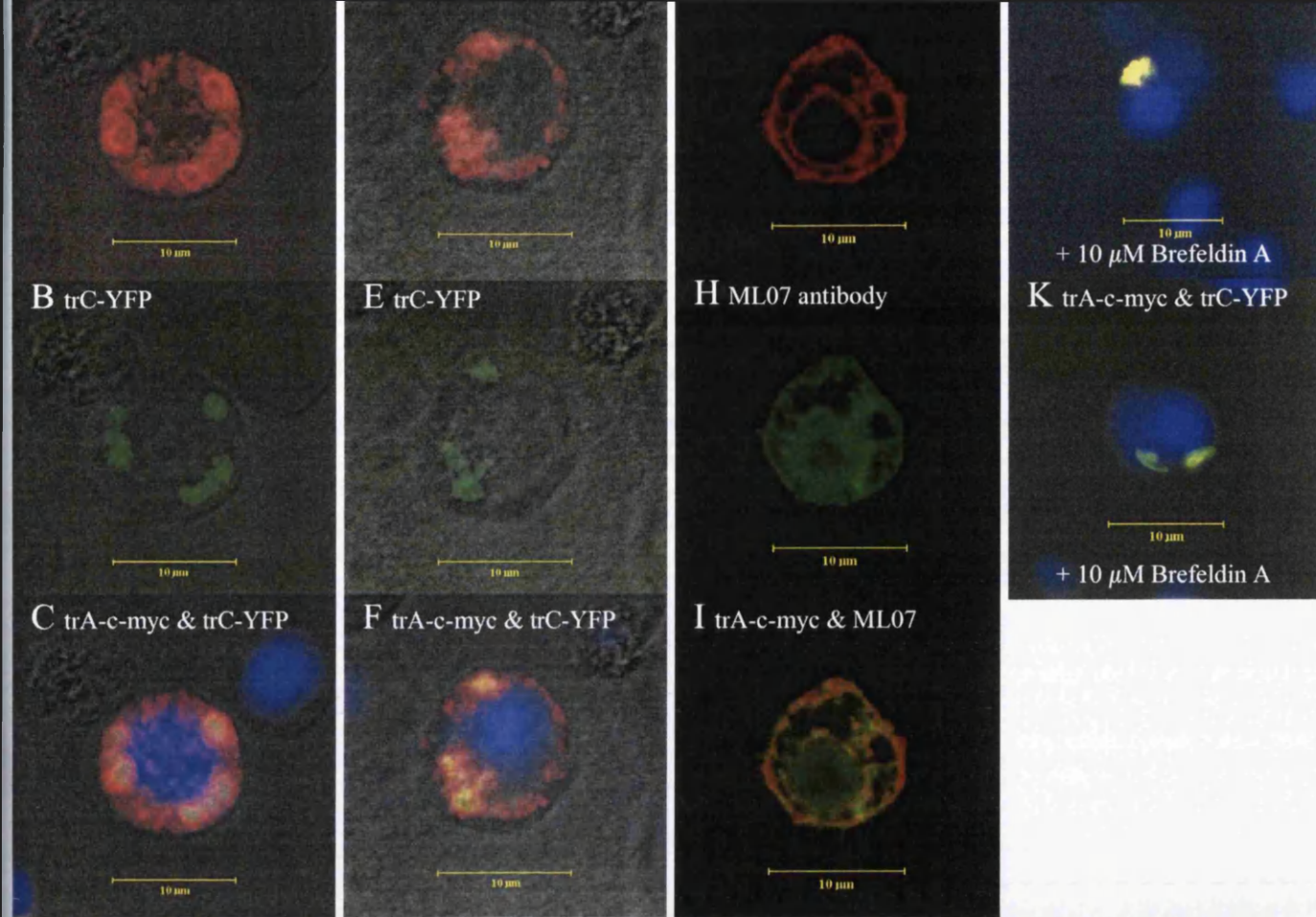
Figure 5.12 Immuno-fluorescence confocal microscopy of S2 cells and Malpighian tubules expressing trA-c-myc.
(A) → (F) trA-c-myc co-expressed with trC-YFP. (G) → (I) Comparison of ML07 Ab staining with trA-c-myc. (J) &
(K) Effect of treatment with brefeldin A. (L) → (Q) Localisation of trA-c-myc, expressed in principal cells (driven by
the c42 GAL4 driver). The bright field channel and pseudo-DAPI (blue nuclei) were included where appropriate (and
possible). All red staining represents trA-c-myc and the green represents trC-YFP (apart from (H) & (I), where green
represents the ML07 Ab). All images were captured on a Zeiss Pascal confocal using a 63x objective.
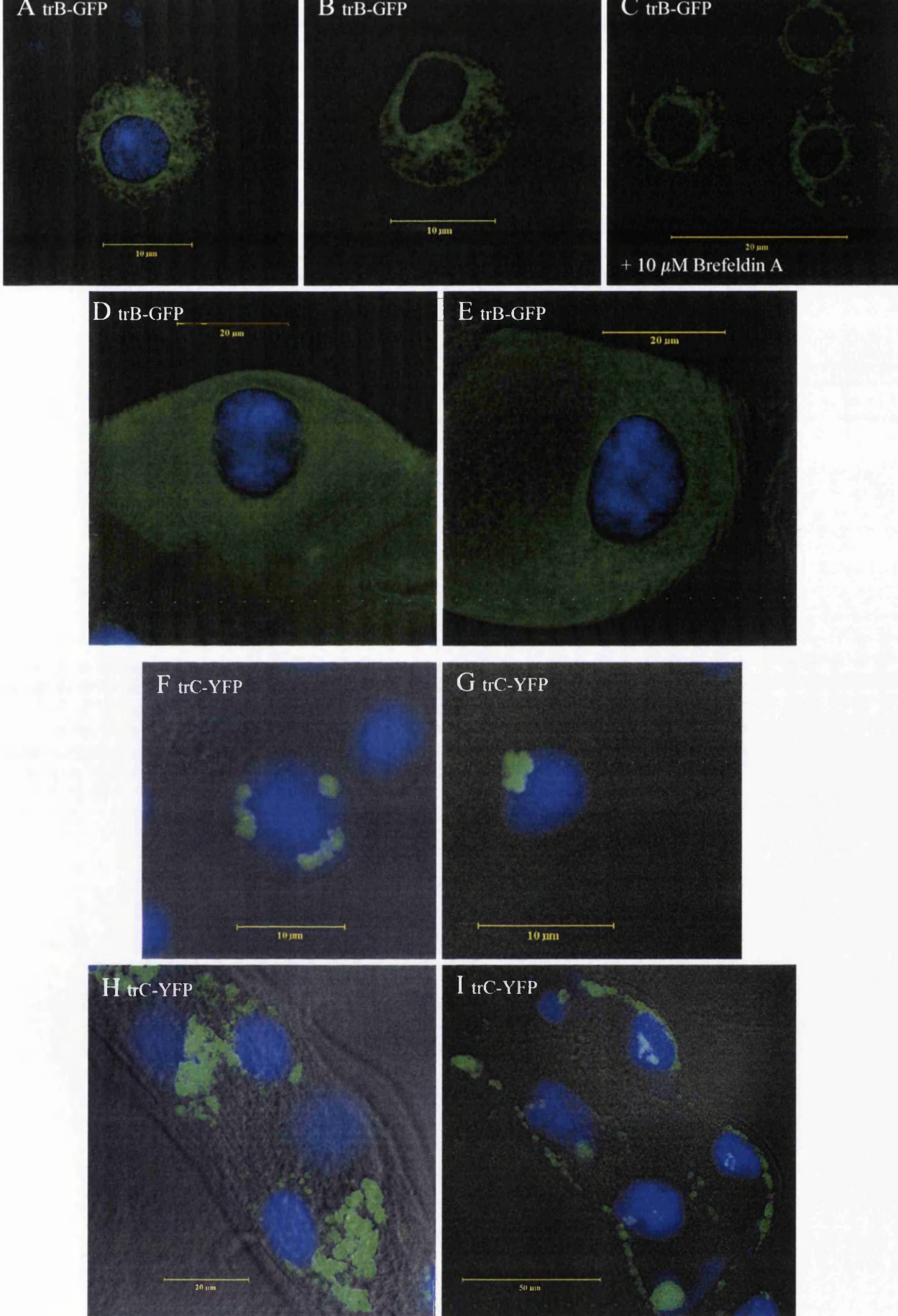
Figure 5.13 Confocal microscopy of S2 cells and Malpighian tubules expressing trB-GFP and trC-YFP.
(A) → (E) trB-GFP. (F) → (I) trC-YFP. (A) → (C), (F) & (G) S2 cells. (D), (E), (H) & (I) principal cells, driven by c42 GAL4. The bright field channel and pseudo-DAPI (blue nuclei) were included where appropriate (and possible). All images were captured on a Zeiss Pascal confocal using a 63x objective.

the cells have been treated for 1 hour and then fixed and ICC performed, that there is very little staining (or none) in the treated cells compared to the control cells. ICC was performed on some of the cells before treatment to confirm expression of trA-c-myc and trC-YFP was also co-expressed to verify that the specific cells being studied (after treatment) had been transfected.

Co-localisation experiments were also performed in S2 cells using the ML07 antibody. This antibody has been previously shown to specifically bind to a Golgi resident protein in *Drosophila* (Kondylis et al., 2001). Figure 5.12I demonstrates the level of co-localisation between the trA-c-myc and ML07 staining; although the ML07 antibody appears to be binding to the same intracellular regions as the c-myc antibody, there are also areas of additional ML07 staining. It is unclear whether this is because of non-specific binding of the ML07 antibody, or because of trA-c-myc only localising to a subcompartment of the Golgi apparatus.

Surprisingly, expression of trB-GFP in S2 cells and principal cells revealed an ER localisation of trB (see figures 5.13A → 5.13E). Although this ER localisation has not yet been confirmed by co-localisation, the confocal images display the reticular pattern typical of an ER resident protein. Additionally, the extent of the ER distribution in the principal cell (as reported by trB-GFP) is consistent with the documented electron microscopy data (as mentioned in chapter 4; Ashburner and Wright, 1978). Treatment of S2 cells with 10 μM brefeldin A for 1 hour did not effect the localisation or presence of trB-GFP (see figure 5.13C).

Analysis of S2 cells and principal cells expressing trC-YFP unveiled yet another distinct intracellular localisation of a SPoCk isoform (see figures 5.13F → 5.13I). trC-YFP localises to some sort of vesicular body; they are relatively large with an approximate diameter of 0.5 - 1 μm and they can also form large conglomerations in both S2 cells and principal cells. When trA-c-myc and trC-YFP were co-expressed in S2 cells, there was an interesting relationship between the localisation of the two isoforms (see figures 5.12A → 5.12F). It appears that the Golgi apparatus envelops the vesicular structures in which trC-YFP is localised.

Initial thoughts on the identity of these organelles included lysosomes and vacuoles. An experiment described later in this chapter (see figure 5.17C) provided evidence against a lysosomal localisation. It then became apparent that the size and distribution of these bodies in S2 cells was similar to the lysosome-related organelle, the peroxisome. To attempt to verify a peroxisomal localisation of trC, a construct was co-transfected with trC-YFP that expresses peroxisomal targeted DsRed2 (for construction details, see table 2.4). Unfortunately the DsRed2 was not localised in S2 cells, it just showed a cytoplasmic

distribution (data not shown). It is possible that the targeting sequence (SKL) is not recognised in *Drosophila* cells.

An unexpected observation when studying overexpression of these isoforms in the tubule was the ubiquitous presence of both trA-c-myc and trC-YFP when driven with the c710 GAL4 driver. trB-GFP is only detected in stellate cells when driven by c710, however trA-c-myc and trC-YFP protein was detected in all cells in the adult tubule. This could be explained by the very high level of expression in combination with a transport system between the stellate cells and principal cells. The tagged ATPases may be carried to the principal cell on the membrane of exocytic components of the secretory pathway, either directly or via the lumen.

5.3.8 The effect of overexpressing SPoCk isoforms on Ca^{2+} signalling in S2 cells

Drosophila S2 cells were transfected with expression constructs for aequorin, the drosokinin receptor and either SPoCk-trA, trB or trC. This would enable investigation into whether overexpression of SPoCk could alter a typical $[Ca^{2+}]_i$ response, by using an aequorin-based Ca^{2+} assay. Cells were challenged with drosokinin (at 10^{-7} M) and the data for each isoform is shown in figure 5.14. There was no detectable change in the maximum $[Ca^{2+}]_i$ response or the dynamics of the response (data not shown) in cells expressing either trA-c-myc or trC-YFP. However, overexpression of trB-GFP resulted in a much larger response (371 ± 4 nM above background) compared to the control response (271 ± 7 nM above background).

5.3.9 The effect of overexpressing SPoCk isoforms on the Ca^{2+} signalling in the tubule

To investigate the effect of overexpression of these SPCA pumps on the dynamics of Ca^{2+} signalling in the tubule, flies were needed that possessed the appropriate GAL4 driver, the UAS-*SPoCk* transgene and the UAS-aequorin transgene. In order to do this, males from the stable lines in table 5.1 were crossed with virgins of the stable aequorin/GAL4 lines.

e.g. *w⁻; trA-c-myc; c42 ♂ x aeq; +; c42 ♀ → aeq/+; trA-c-myc/+; c42* (F₁)

The resulting F₁ generation have one copy of both the UAS transgenes and two copies of the GAL4 driver. Ca^{2+} assays were performed as described in section 2.17.1, apart from the use of 22-26 tubules for principal cell measurements and 40-50 tubules for stellate cell measurements (due to only one copy of the aequorin transgene being present). The tubules were challenged with the appropriate Ca^{2+}-mobilising neuropeptide (either capa-1 or drosokinin) and the results are shown in figures 5.15 to 5.18.
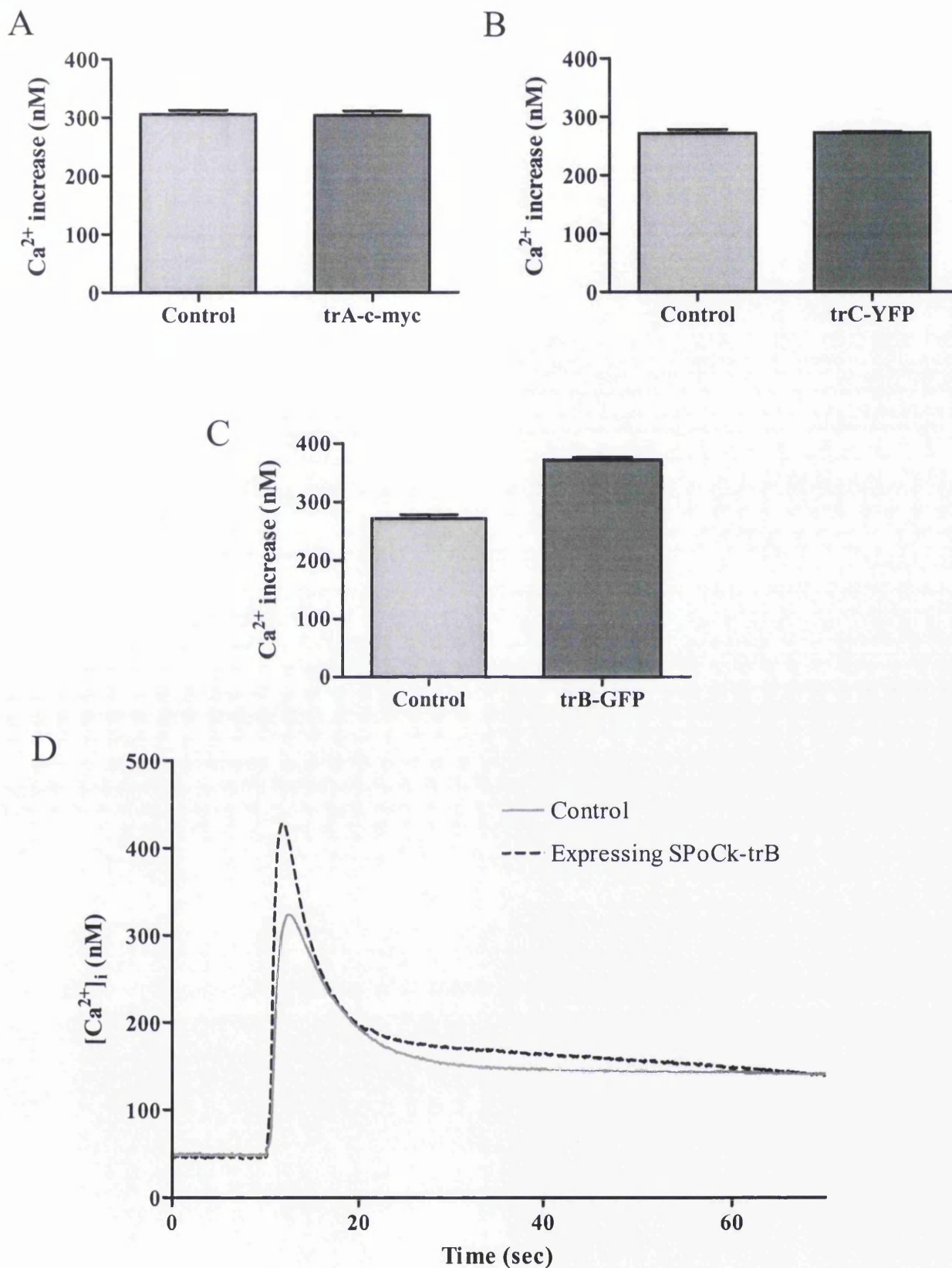
Figure 5.14 Effect of the overexpression of SPoCk isoforms on a neuropeptide-induced $[Ca^{2+}]_i$ response in *Drosophila* S2 cells. S2 cells transfected with expression constructs for aequorin, the drosokinin receptor and a SPoCk isoform were challenged with drosokinin at a concentration of 10^{-7} M. (A) Maximum $[Ca^{2+}]_i$ increase above resting levels in S2 cells expressing SPoCk-trA (n = 10). (B) Increase in cells expressing trC-YFP (n = 10). (C) Increase in cells expressing trB-GFP (n = 10). The increase in cells expressing trB-GFP is significantly greater than in control cells (P < 0.0001). (D) Plots of typical $[Ca^{2+}]_i$ responses on control and trB-GFP expressing cells. Error bars represent S.E.M.

127
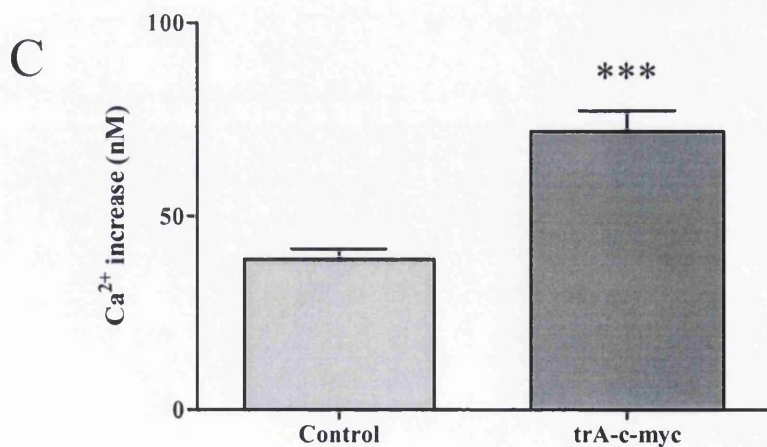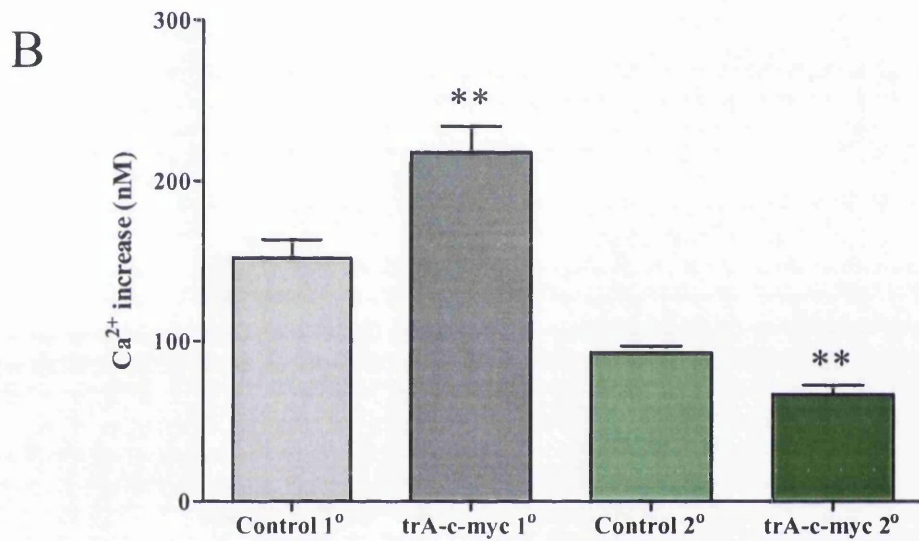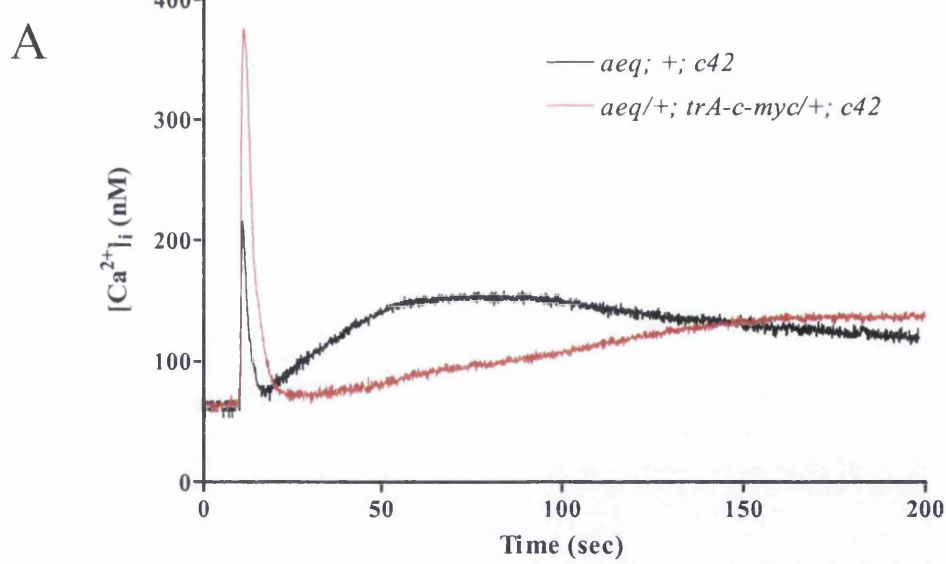
Figure 5.15 Effect of overexpression of trA-c-myc on the capa-1 $[Ca^{2+}]_i$ response in principal cells of intact tubules. The capa-1 peptide was applied at a concentration of 10^{-7} M. (A) Typical capa-1 response in principal cells overexpressing trA-c-myc, compared with a typical control response. (B) Bar graph showing the maximum increase of $[Ca^{2+}]_i$ above resting levels, for both the primary and secondary responses (n = 17). Overexpression of trA results in a significantly higher increase for the primary response (P = 0.0043) and a significantly reduced increase for the secondary response (P = 0.0011). (C) Average $[Ca^{2+}]_i$ increase above background for the first 15 seconds after addition of capa-1 (primary response). The trA-c-myc average is significantly larger than the control (P < 0.0001). Error bars represent S.E.M.

128
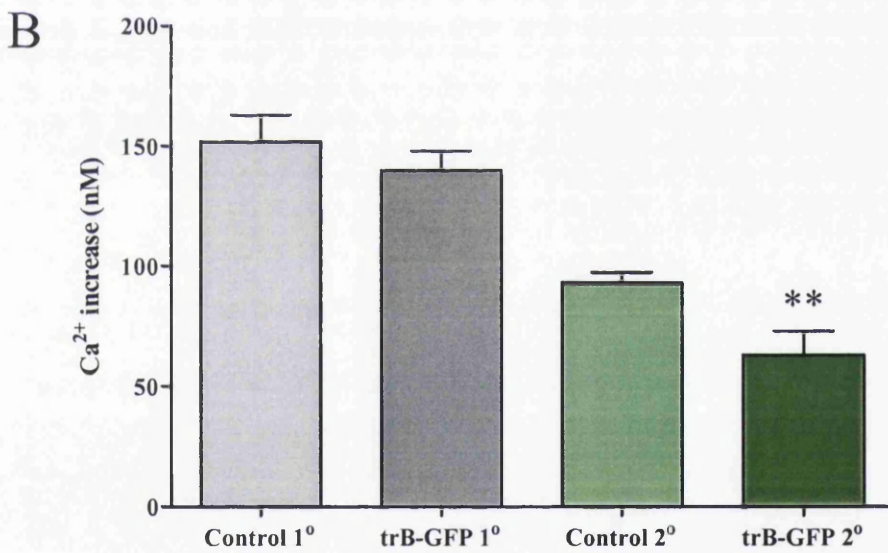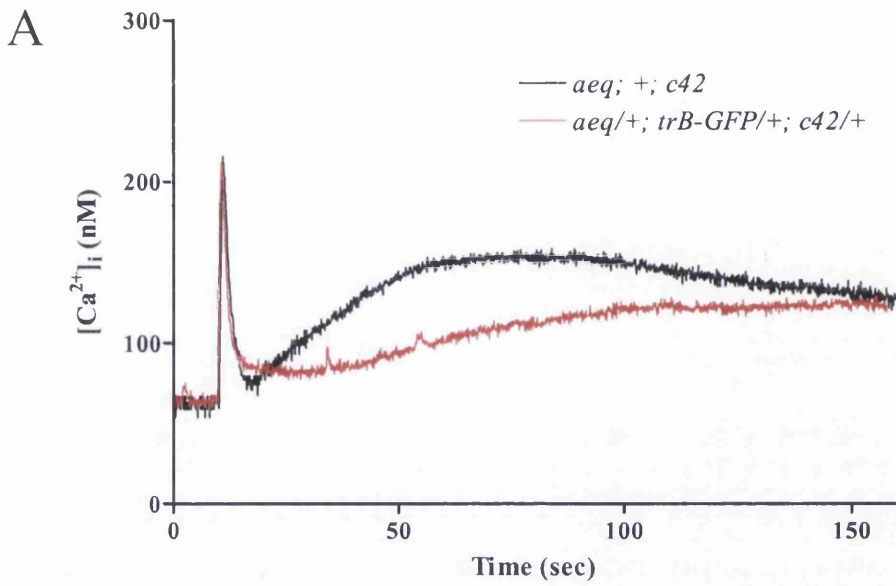
Figure 5.16 Effect of overexpression of trB-GFP on the capa-1 $[Ca^{2+}]_i$ response in principal cells of intact tubules. The capa-1 peptide was applied at a concentration of 10^{-7} M. (A) Typical capa-1 response in principal cells overexpressing trB-GFP compared with a typical control response. (B) Bar graph showing the maximum increase of $[Ca^{2+}]_i$ above resting levels, for both the primary and secondary responses (n ≥ 11). Overexpression of trB results in a significantly reduced secondary response increase (P = 0.0039). Error bars represent S.E.M.
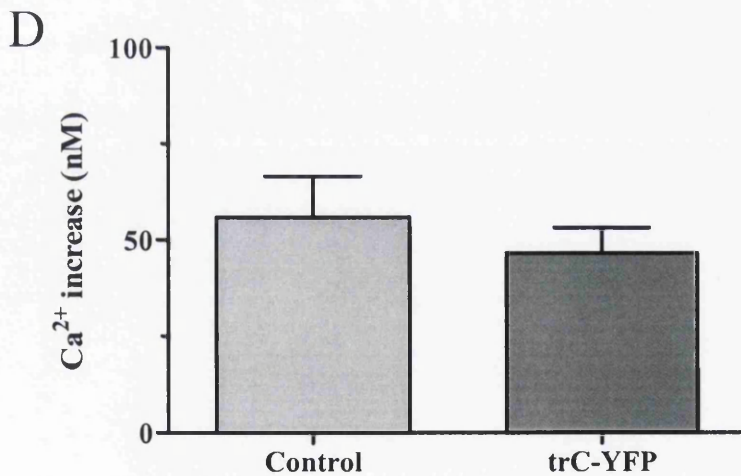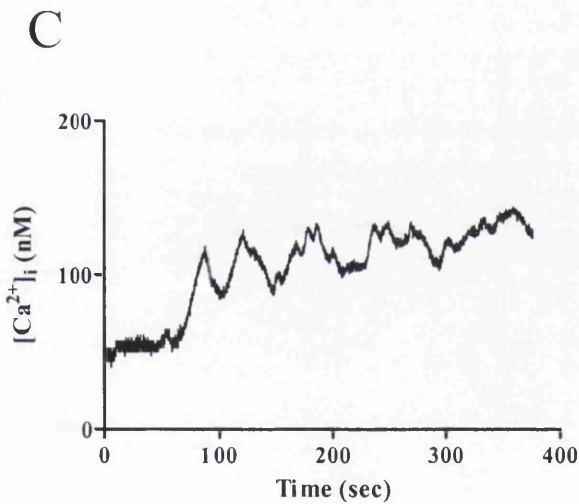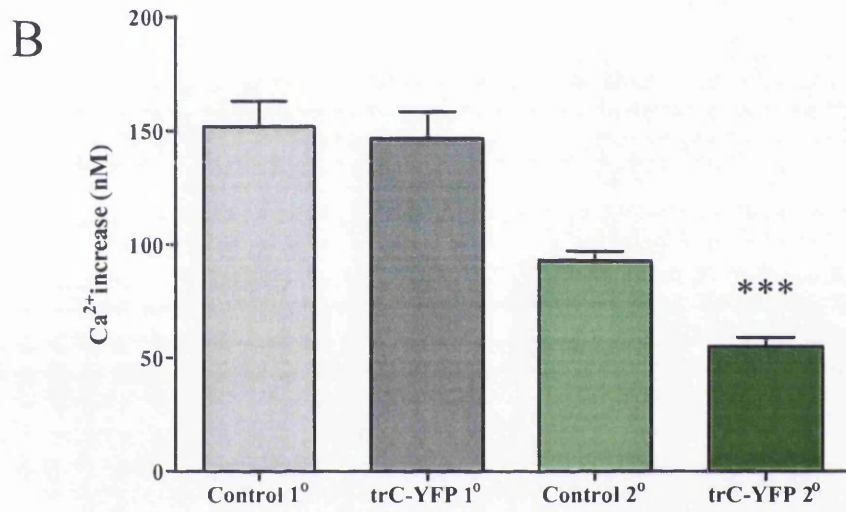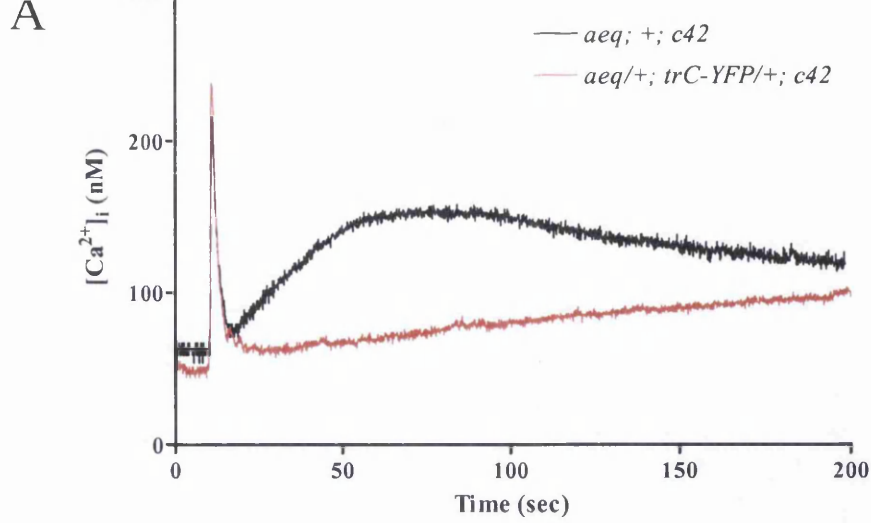
Figure 5.17 Effect of overexpression of trC-YFP on the capa-1 $[Ca^{2+}]_i$ response in principal cells of intact tubules. The capa-1 peptide was applied at a concentration of 10^{-7} M. (A) Typical capa-1 response in principal cells overexpressing trC-YFP compared with a typical control response. (B) Bar graph showing the maximum increase of $[Ca^{2+}]_i$ above resting levels, for both the primary and secondary responses (n = 17). Overexpression of trC results in a significantly reduced secondary response increase ($P < 0.0001$) (C) Typical response of the principal cells to 200µM of the lysosomal disruptor GPN. (D) Comparison of the average increase in response to GPN (above background), between control and trC-YFP overexpressing tubules. Error bars represent S.E.M.

130
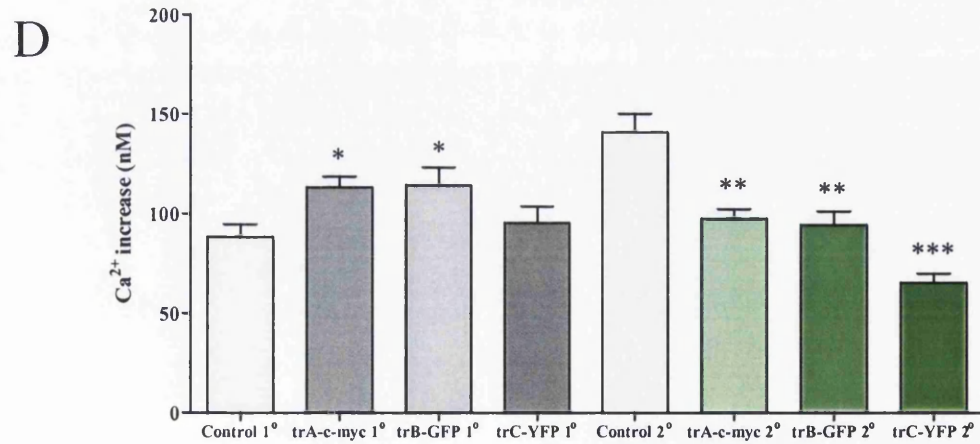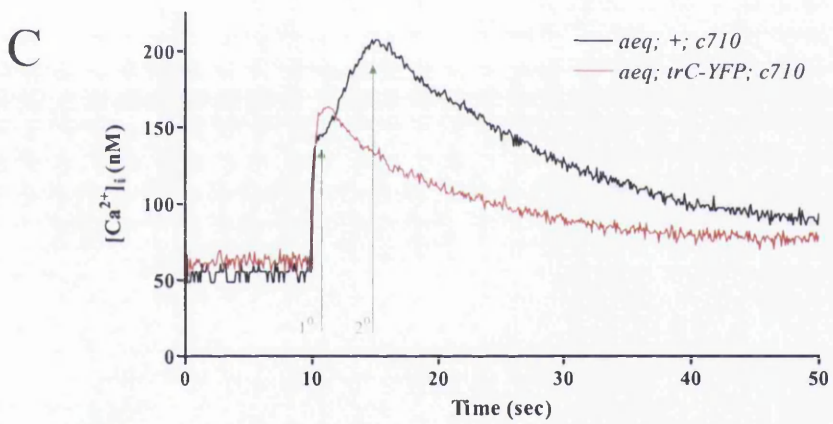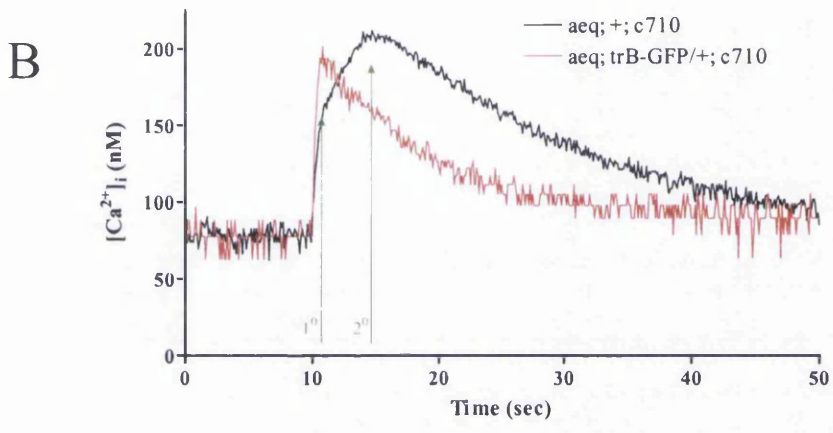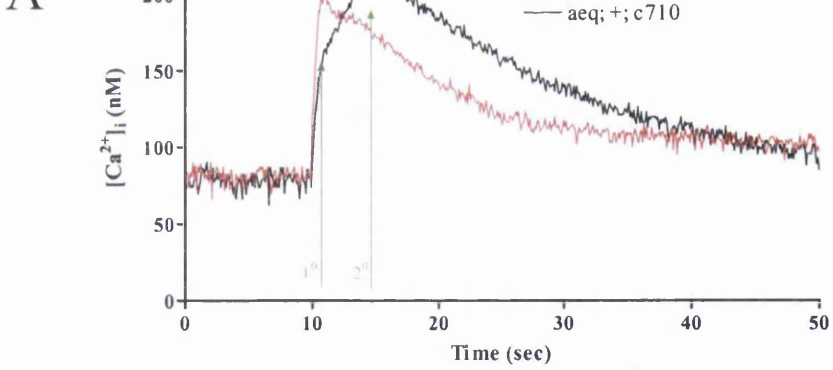
Figure 5.18 Effect of overexpression of SPoCk isoforms on the stellate [Ca^{2+}]$_i$ drosokinin response in intact tubules. The drosokinin peptide was applied at a concentration of 10^{-7} M. The green arrows indicate measurement points for the primary and secondary responses (1° at 1.0 sec. and 2° at 5.0 sec.). (A) Typical response in stellate cells overexpressing trA-c-myc compared with a typical control response. (B) A typical example for trB-GFP. (C) A typical example for trC-YFP. (D) Bar graph showing the increase of the primary and secondary [Ca^{2+}]$_i$ responses above resting levels (n ≥8). Overexpression of trA and trB results in a significantly higher increase for the primary response (P = 0.0112 and P = 0.0264). Overexpression of trA, trB and trC results in a significantly reduced increase for the secondary response (P = 0.0016, P = 0.0014 and P < 0.0001). Error bars represent S.E.M.

Overexpression of these Ca^{2+}-ATPases has a profound effect on the dynamics of the capa-1 and drosokinin $[Ca^{2+}]_i$ responses. Overexpression of all 3 isoforms results in a reduction of the secondary response in the two cell types. Additionally, the secondary response in the principal cells appears to be much more prolonged. Although all isoforms reduced the maximal secondary response, the reduction caused by trC was significantly greater than by trA and trB (data not shown).

Furthermore and most interestingly, overexpression of trA causes an increase in the capa-1 primary response, whereas trB and trC do not. The maximum capa-1 primary peak for trA is significantly larger than the control ($P = 0.0043$), however to confirm this result the $[Ca^{2+}]_i$ for the first 15 seconds after capa-1 addition was averaged to give an indication of the amount of Ca^{2+} released (see figure 5.15). This method of measuring the primary response gave a more significant difference ($P < 0.0001$). For the stellate cells the data is not as clear cut; overexpression of both trA and trB cause an increase in the drosokinin primary response ($P = 0.0012$ and $P = 0.0264$), whereas trC does not (see figure 5.18).

Figures 5.17C and 5.15D show the results of the treatment of tubules with 200 μM glycyl-L-phenylalanine-β-naphthylamide (GPN). GPN is a substrate for the lysosomal protein cathespin C and GPN causes permeabilisation of lysosomes by osmotic swelling. Investigating a possible lysosomal localisation of trC, the Ca^{2+} responses of *aeq; +; c42* and *w⁻; trC-YFP/+; c42* tubules were monitored after the addition of GPN. If trC was localised to the lysosomes, then overexpression would increase the $[Ca^{2+}]_{lysosome}$, therefore GPN treatment would result in a higher $[Ca^{2+}]_i$ response. However the average $[Ca^{2+}]_i$ increase was not different between the two sets of samples. This is evidence against a lysosomal localisation of trC.

5.3.10 The effect of overexpressing SPoCk isoforms on the fluid secretion rate of the tubule

Secretion assays were performed on the *w⁻; trA-c-myc; c42* and *w⁻; trC-YFP; c42* lines, using the parental UAS and GAL4 lines as controls (see figure 5.19). Overexpression of trA in the tubule causes an increase in basal levels and an increase in the maximum stimulated rate upon addition of capa-1. Although the *w⁻; trC-YFP; c42* line showed increased secretion rates compared to the *w⁻; +; c42* line it was not different from the *w⁻; trC-YFP; +* line. This suggests an insertional effect of the trC-YFP transgene and that overexpression does not have an impact on fluid secretion rates.

As the c710 driven overexpression of the transgenes did not result in a stellate cell specific localisation of the tagged protein (see section 5.3.7), secretion assays were not performed on these lines, as the results would be difficult to interpret.

A
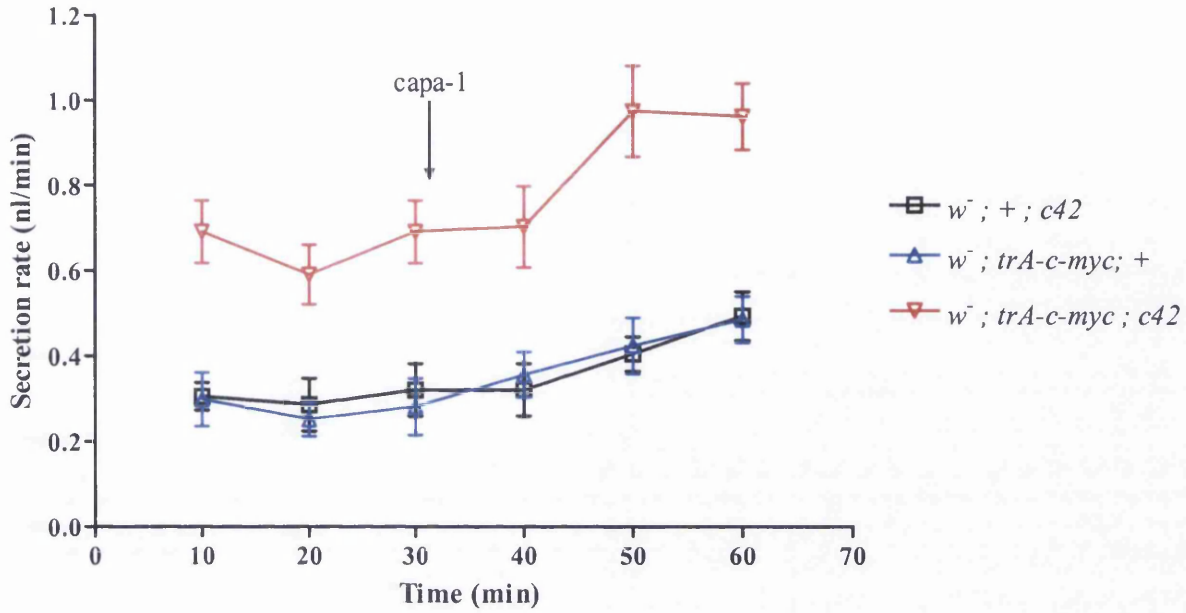
B
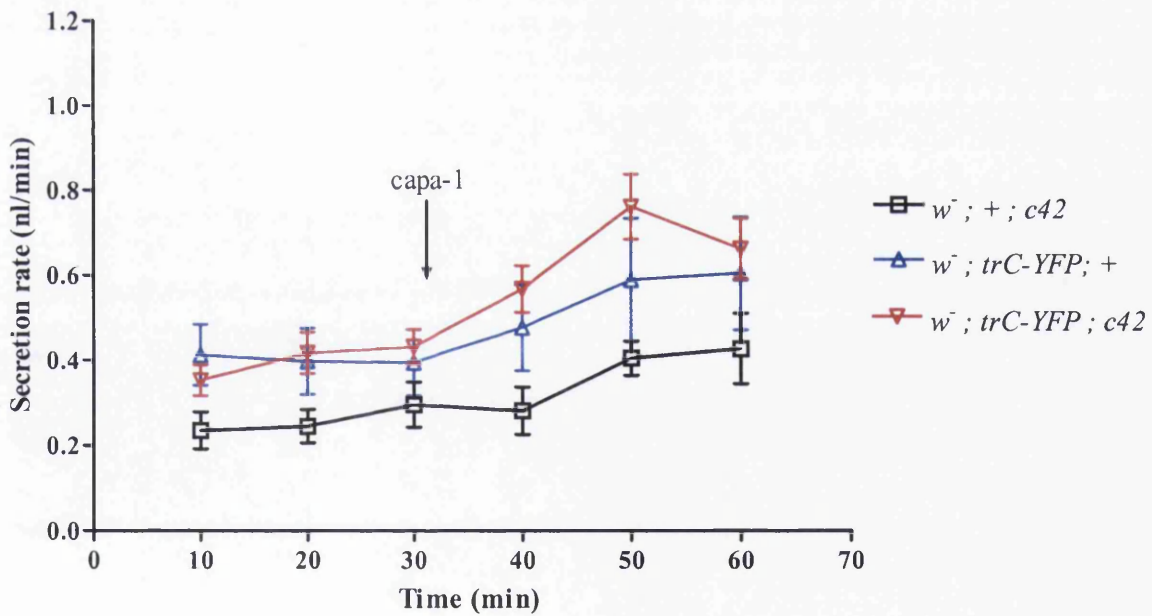
Figure 5.19 Effect of the overexpresion of SPoCk-trA and SPoCk-trC on capa-1 stimulated fluid secretion. Secretion assays on tubules overexpressing trA and trC in the principal cells. The neuropeptide capa-1 was added at a concentration of 10^{-7} after the 30 minute reading. Details of the assay are described in sections 1.4.3 and 2.19. Error bars represent S.E.M.

5.4 Discussion

Using the protein sequences of the yeast PMR1 and the human SPCA1, the *Drosophila* SPCA gene (*SPoCk*) was successfully identified. Further protein analysis clearly groups SPoCk with the SPCA family of ATPases and identifies the product of an *Anopheles gambiae* gene as the closest known homologue. This is not to be unexpected, as *Anopheles* is closely related to *Drosophila* and this protein is presumably the *Anopheles* SPCA.

When the genome annotation was updated, it revealed two extra transcripts (trB and trC) that encoded for SPCA proteins with extra N-terminal domains. This was intriguing, as it would seem very likely that these extra domains must have a purpose, either to alter the localisation of the pump or to change its functional properties. Additionally, alternatively spliced transcripts that contain these accessory domains have not been identified for any other SPCAs studied in other organisms. The *in silico* investigation into these extra regions was confusing; it appeared that the extra 23 amino acids of trC might target the ATPase to the ER membrane, mitochondria or possibly interact with the ubuiquitination machinery in the cell. However the extra 143 residues of trB did not match to any sequence in the NCBI database, had a putative vacuolar targeting site and possesses similarity to the ABC transport family of proteins. To truly understand the function of these regions, these proteins were tagged and overexpressed in S2 cells and in transgenic *Drosophila*.

Overexpression revealed that trA possessed a Golgi apparatus localisation. This was predicted, due to the previous studies of SPCAs in other organisms. trA is presumably playing a house-keeping role, in maintaining $[Ca^{2+}]_{Golgi}$ at the required level for Ca^{2+}-dependent protein processing events. Additionally, as the Golgi has been shown to be a functional IP_3-releasable Ca^{2+} pool (Pinton et al., 1998), trA will be playing a role in maintaining this pool (this is discussed in greater detail later on). The predominantly basolateral localisation of trA-c-myc in the principal cell is interesting; either all the Golgi apparatus is restricted to this region or trA is specifically targeted to a sub-compartment of the Golgi. Co-localisation experiments with well characterised Golgi-markers could help to determine this.

SERCA pumps are absent from a large number of eukaryotes, including fungi, protozoans and plants. The question of how these organisms maintained their $[Ca^{2+}]_{ER}$ levels was unanswered until recently. It appears that the ER is maintained by ATPases distinct from the PMCA, SERCA and SPCA groups (Liang et al., 1997; Furuya et al., 2001; Vashist et al., 2002), that are possibly more related to more primitive Ca^{2+}-ATPases. However, in insect and vertebrate organisms, it is well documented that $[Ca^{2+}]_{ER}$ is maintained by the SERCA pump. Therefore the ER localisation of trB was surprising because there is an existing mechanism for pumping Ca^{2+} into the ER in *Drosophila* (the SERCA pump,

encoded by the *Ca-P60A* gene). Nevertheless, the discovery of a Pmr1-like ATPase in the ER is not wholly unprecedented; overexpression studies of calreticulin in HEK-293 cells have implied the additional presence of a thapsigargin-insensitive Ca^{2+}-ATPase in the ER (Arnaudeau et al., 2002). Arnaudeau and colleagues suggested that this may be a member of the PMR1 family of Ca^{2+}-ATPases. The discovery of the ER-targeted SPCA in *Drosophila* (trB) sheds light on this mystery; it is likely that HEK-293 cells (and other cells in insects and vertebrates) possess an ER-targeted thapsigargin-insensitive Ca^{2+}-ATPase that is either the product of an alternatively spliced transcript from a *SPCA* gene (like trB) or is the product of a second *SPCA* gene (e.g. the *ATP2C2* gene in humans).

The subcellular localisation studies for trC are the first demonstration of the existence of a Ca^{2+}-ATPase targeted to either lysosomes or peroxisomes. The initial prediction, as to the identity of these organelles, included lysosomes. However, several lines of evidence argue against this hypothesis; firstly lysosomes have been previously studied in S2 cells (Yagodin et al., 1999) and are found to be a lot more abundant and distributed differently compared to the staining pattern of trC-YFP. Secondly, studies on the uptake of Ca^{2+} into lysosomes have all implicated the involvement of a pH sensitive Ca^{2+}/H^+-exchanger rather than an ATPase (Yagodin et al., 1999; Srinivas et al., 2002; Churchill et al., 2002). Finally, experiments (described earlier in this chapter) using the lysosomal disruptor GPN show that overexpression of trC-YFP does not increase the amount of Ca^{2+} released from these organelles.

It then became apparent that trC may be localising to peroxisomes (a lysosome-related organelle). There are various lines of evidence to support this localisation; firstly the abundance and distribution of the trC-YFP fluorescence in S2 cells is similar to that of peroxisomes in yeast (Vizeacoumar et al., 2003). Secondly, peroxisomes have been studied in the *Drosophila* Malpighian tubule (Beard and Holtzman, 1987) using electron microscopy; the organelles were described as 0.2-0.5 μM in diameter, round to oblong in shape and sometimes appeared as multiple, interconnecting bodies. This describes the pattern of fluorescence observed in principal cells expressing trC-YFP (see figures 5.13H and 5.13I). Thirdly, Beard and Holtzman reported that peroxisomes are abundant in the Malpighian tubule and gut of *Drosophila*, which correlates well with the relative of expression of the *SPoCk* trC transcript (see figure 5.8). Finally, the extra 23 residues of trC, that allow the ATPase to be targeted to this organelle are very similar to repeated domains of ubiquitin (see figure 5.6). It has been shown that the peroxisomal protein Pex4p is a ubiquitin-conjugating enzyme that is anchored to the cytoplasmic surface of peroxisomes (Wiebel and Kunau, 1992; Koller et al., 1999) and can couple to ubiquitin *in vitro* (Crane et al., 1994). Pex4p is important for import of proteins into peroxisomes and it

is conceivable that the *Drosophila* homologue of Pex4p binds to the extra region of trC and imports the ATPase into the peroxisome membrane.

Overexpression of the SPoCk variants provided important information, concerning confirmation of SPoCk's Ca^{2+} transporting activity and also the manner in which the Ca^{2+} pools shape neuropeptide $[Ca^{2+}]_i$ responses in the tubule. Ca^{2+} assay studies in S2 cell revealed that overexpression of trA and trC have no effect on Ca^{2+} signalling, while overexpression of trB resulted in a much larger IP_3-mediated Ca^{2+} release from internal stores. This fits well with the ER localisation of trB in the cell; overexpression of trB-GFP in the S2 cells would result in an increase of Ca^{2+} stored in the ER, and upon opening of the IP_3Rs the amount of Ca^{2+} released would be greater.

Overexpression of SPoCk has confirmed and helped to understand the unusual Ca^{2+} signalling mechanisms present in the principal cell. Unlike S2 cells, overexpression of trB did not result in an increased $[Ca^{2+}]_i$ peak in response to an IP_3-generating agonist. However, overexpression of trA (Golgi localisation) does increase this response. This suggests that in the principal cell, the ER is not the IP_3-releasable store and that it is instead the Golgi apparatus. These results fit in well with the data described in chapters 3 and 4. Overexpression in stellate cells also had an impact on the $[Ca^{2+}]_i$ dynamics, both trA-c-myc and trB-GFP increased the primary response. Although statistically significant, the P values (0.0112 and 0.0264) were only just within the acceptable boundaries, therefore concrete conclusions cannot be presently made about the roles of these stores in this cell type. However, these results could imply that both the ER and the Golgi contribute to the primary drosokinin response. Another possibility is that in this cell, these pools are functionally connected and an increase in luminal $[Ca^{2+}]$ in one organelle can increase luminal $[Ca^{2+}]$ in the other.

Evidence for the Ca^{2+} transporting activity of these ATPases was demonstrated by their impact on the secondary $[Ca^{2+}]_i$ response dynamics in the tubule. All 3 isoforms reduced the maximum levels of the secondary response in both cell types. It is also apparent that in the principal cell, the secondary response took longer to reach its maximum. It is conceivable that the influx of Ca^{2+} driving this response, continues until the $[Ca^{2+}]_i$ has reached a specific value. The high Ca^{2+} buffering conditions, resulting from overexpression of these pumps would prevent the $[Ca^{2+}]_i$ from this reaching this value as quickly.

The secretion assay performed on *w⁻; trA-c-myc; c42* tubules revealed an increased basal and capa-1-stimulated secretion rate. This may be due to the modification of the Ca^{2+} signalling dynamics by overexpression of trA or it may be due to altered processing of proteins in the Golgi (because of increased $[Ca^{2+}]_{Golgi}$ or $[Mn^{2+}]_{Golgi}$ levels) that are

important in regulating the secretion rate. Further work would be required to determine exactly how trA-c-myc increases the fluid secretion rate.

In conclusion, this chapter has identified the *Drosophila* secretory pathway Ca^{2+}/Mn^{2+} ATPase and characterised its multi-functionality achieved by its 3 protein coding transcripts. Overexpression studies using the SPoCk isoforms have provided a powerful tool in dissecting the Ca^{2+} signalling mechanisms in the tubule. This has uncovered a role of the Golgi Ca^{2+} pool in the principal cell, it appears that this is the primary IP_3-releasable Ca^{2+} store.

Furthermore, to summarise the role of the SPoCk isoforms; trA looks like a house-keeping protein that is required for maintenance of Golgi $[Ca^{2+}]$ levels necessary for processing of proteins and also for in specialised tissues (i.e. the tubule) where the Golgi is an important signalling organelle. trB is an another ER-targeted Ca^{2+}-ATPase (the other being the well characterised SERCA pump); the function of which is unclear, it maybe required as an alternatively regulated Ca^{2+}-uptake mechanism into the ER or maybe to pump Mn^{2+} ions into the ER lumen. trC appears to be a peroxisomal Ca^{2+}/Mn^{2+} ATPase that may facilitate the storage of Ca^{2+} in these organelles or to possibly provide Mn^{2+} ions for a peroxisomal Mn^{2+} dependant superoxide dismutase. To further understand the roles of these different proteins, antibodies have been generated and work is currently undergoing to determine their expression pattern in the whole fly.

Chapter 6

Developing a new gene knock-in technology for *Drosophila* based on *trans*-splicing

6.1 Summary

This chapter describes the development of a new technology for *Drosophila* research that allows targeting and alteration of endogenous RNA transcripts. This system is based on the elegant spliceosome-mediated *trans*-splicing (SMaRT) technology developed by Puttaraju and colleagues (1999). This method of reprogramming mRNA involves a pre-*trans*-splicing RNA molecule (PTM) that binds in an anti-sense manner to the target gene's pre-mRNA intron. The splicing machinery will then additionally splice into the PTM's acceptor site as well as the gene's endogenous acceptor site.

I have generated transgenic lines expressing PTMs under the control of the UAS/GAL4 system or the actin5C promoter. The advantage of this system is that it may be possible to tag or alter a gene product without altering the gene's expression pattern or level of expression. This has primarily been utilised to tag endogenously expressed proteins with the green fluorescent protein (GFP). Successful *trans*-splicing in the transgenic flies has been demonstrated using RT-PCR.

Although GFP fluorescence has been detected in tissues of these flies, it has become apparent that this is primarily not a result of altered endogenous protein but of leaky translation of the PTM RNA molecule. Despite this, the basic technology has been shown to be successful, and with further development it has the potential to become a very powerful tool in *Drosophila* research.

6.2 Introduction

6.2.1 Endogenous *trans*-splicing in *Drosophila*

Cis-splicing is the process of combining exons from the same pre-mRNA to produce mature mRNA, whereas *trans*-splicing combines exons from separate pre-mRNA molecules. *Trans*-splicing was first discovered in trypanosomes (Murphy et al., 1986; Blumenthal, 1995) and then in mammalian cells (Eul et al., 1995; Li et al., 1999). More recently it has been demonstrated that it occurs naturally in insects (Labrador et al., 2001; Dorn et al., 2001) at the complex *mod(mdg4)* locus in *Drosophila*.

The *mod(mdg4)* locus produces transcripts that all contain the common exons 1-4 from the 5' of the locus. However, the alternatively spliced 3' exons are found in five separate clusters, on both DNA strands. Dorn et al proved that *trans*-splicing was the mechanism for producing many of the different transcripts from this locus, using transgenics and RT-PCR. They showed that the common exons (1-4) could *trans*-splice to an alternative tagged 3' exon being expressed at a different chromosomal location.

With the more detailed study of gene expression in *Drosophila*, this method of producing variation in gene products is becoming more apparent; recently, another gene called *lola* has been identified as naturally utilising *trans*-splicing (Horiuchi et al., 2003).

6.2.2 mRNA alteration using *trans*-splicing ribozymes

Ribozymes (RNAs with catalytic activity) have generated significant interest for the potential genetic and therapeutic use of catalytic RNA molecules. (Cech, 1988; Haseloff and Gerlach, 1988) The hammerhead ribozyme is the smallest of the known ribozyme motifs (Haseloff and Gerlach, 1988) and can cleave a specific RNA target. The hammerhead ribozyme has been utilised in *Drosophila* to knock down levels of *fushi tarazu* mRNA (Zhao and Pick, 1993). Since then RNA interference (RNAi) has become a more effective and easier method of knocking down mRNA levels in *Drosophila* in order to study gene function (Kennerdell and Carthew, 2000; Tavernarakis et al., 2000).

Group I introns were first discovered in *T. thermophila* (Cech et al., 1981); certain rRNA molecules acted as ribozymes as they could self-splice their own introns. Group I introns have also been shown to mediate *trans*-splicing of RNA *in vitro* (Inoue et al., 1986). Continuing this work, the lab of Bruce Sullenger has been developing these ribozymes to alter or repair pre-mRNA *in vivo* (Sullenger and Cech, 1994; Jones et al., 1997; Lan et al., 1998; Watanabe and Sullenger, 2000; Rogers et al., 2002). The engineered ribozyme trans-splices into the target mRNA and replaces the remaining exons with repaired or altered exons. This research has demonstrated the partial repair of sickle β-globin, p53 and chloride channel mRNAs.

Until recently, ribozyme-mediated *trans*-splicing was not very efficient. In cell lines only 1.2% *trans*-splicing of the target mRNAs had been achieved (Rogers et al., 2002). However, Sullenger's group have now developed an improved ribozyme that can repair 10%-50% of sickle beta-globin RNAs in transfected mammalian cells (Byun et al., 2003).

6.2.3 mRNA alteration using spliceosome-mediated *trans*-splicing

Lloyd Mitchell's lab at Intronn, North Carolina, first developed RNA molecules that were capable of effecting spliceosome-mediated RNA trans-splicing reactions with a target messenger pre-mRNA (Puttaraju et al., 1999). The pre-*trans*-splicing RNA molecule (PTM) binds in an antisense manner to the target gene intron. The splicing machinery will then occasionally splice into the PTM's splice acceptor site rather than the gene's endogenous acceptor site (see figure 6.1A).

They developed a system repairing mutated lacZ transcripts in human cells as a tool for the design and *in vitro* evolution of improved PTMs. Using SMaRT technology they were able to correct a CFTR mutation in human cystic fibrosis airway epithelia (Mansfield et al., 2000), and further improved the mechanism to show a 22% restoration of protein function *in vivo* (Liu et al., 2002). This technology has great potential for gene therapy applications, as correction of the gene is achieved without over-expression or mis-localised expression of the respective protein.

More recently this group has developed a 5' exon replacement system based on this technology (Mansfield et al., 2003). This involves expressing a PTM that contains the altered 5' exons followed by a donor splice site and an intron-binding domain (see figure 6.1B).

6.2.4 *Trans*-splicing as a tool in *Drosophila* research

The development of germline transformation in *Drosophila* has provided many useful tools in *Drosophila* research. These include P-element mutagenesis (Rubin and Spradling, 1982) ectopic expression (Brand and Perrimon, 1994), enhancer trap screens (O'Kane and Gehring, 1987), RNAi (Kennerdell and Carthew, 2000), GFP gene trap screens (Morin et al., 2001) and homologous recombination approaches (Rong and Golic, 2000). However, the only strategy to enable a targeted gene knock-in has been the homologous recombination method (Rong and Golic, 2001; Rong et al., 2002), which although a complete knock-in when accomplished, is very complicated and labour intensive.

The possibility of developing a system in *Drosophila* that uses *trans*-splicing to alter or tag endogenous proteins is an attractive one. Although it is unlikely that 100% *trans*-splicing could ever be achieved *in vivo*, the technology could allow tagging of proteins, dominant
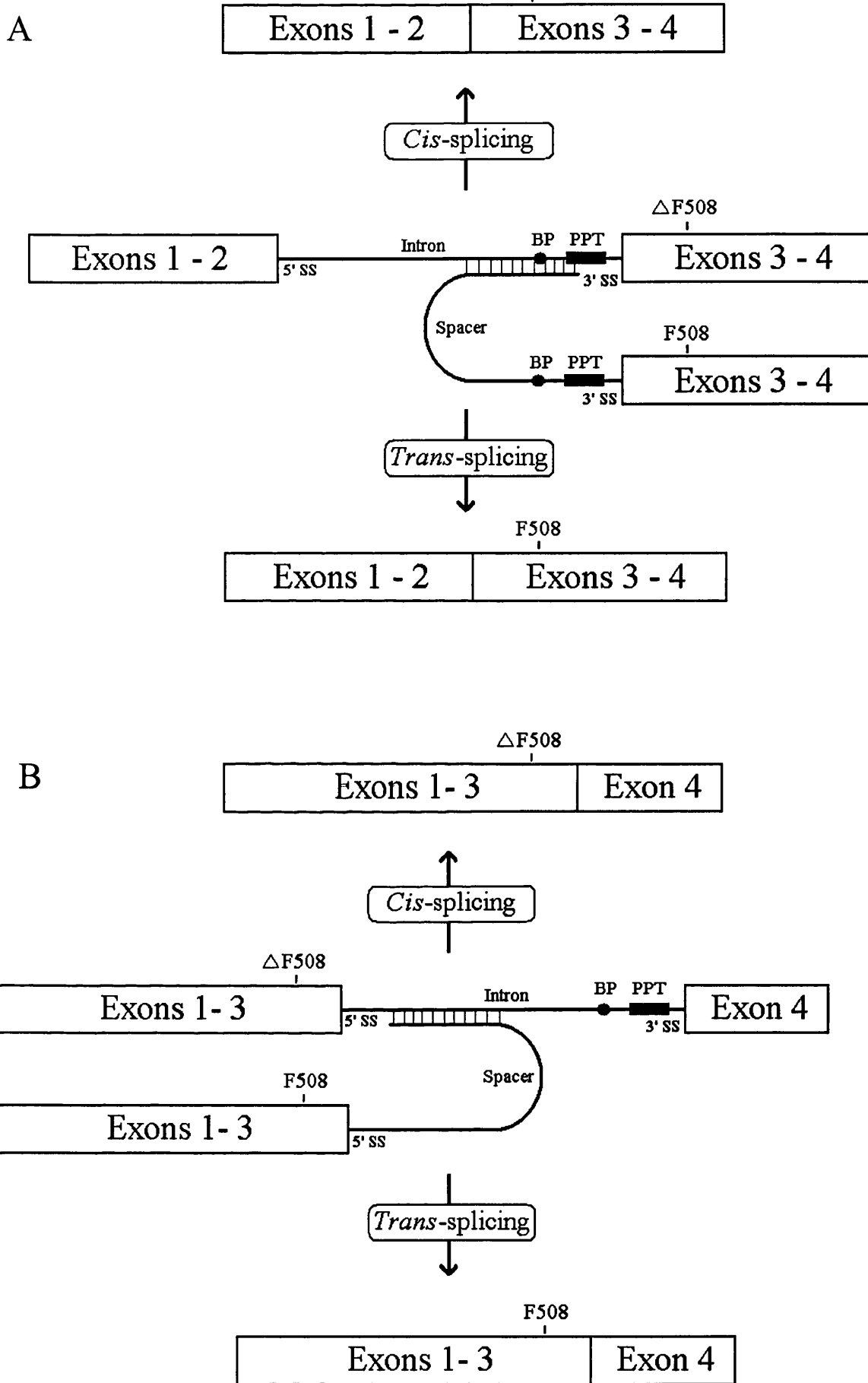
Figure 6.1 Diagram showing the principle of spliceosome–mediated RNA trans-splicing (SMaRT). When *trans*-splicing occurs the wildtype sequence from the PTM is incorporated to form the mature mRNA, thus correcting the DF508 mutation. (A) 3' exon replacement method. (B) 5'exon replacement method. BP, branch point. PPT, polypyrimidine tract. Adapted from Mansfield et al., 2000 and Mansfield et al., 2003.

142

negative mutations, targeting of specific splice-variants, production of hypomorphs and a targeted GAL4 enhancer trap system. Additionally, the constructs are relatively easy to assemble and only a single transgenic fly would be needed to be generated to target a gene. I initially began developing this technology to try and determine the expression pattern and subcellular localisation of the *Drosophila* secretory pathway Ca^{2+}-ATPase (see chapter 5), by reprogramming the pre-mRNA to include the GFP coding sequence.

6.3 Results

6.3.1 Adaptation of SMaRT technology for use in transgenic *Drosophila*

The first attempt to implement SMaRT technology in *Drosophila* involved designing a PTM to target the SPoCk pre-mRNA and reprogram it to include the coding sequence for GFP at the 3' end of the gene's coding sequence. The PTM contained an intron-binding domain (-155 → -15 of exon 4), a spacer and a yeast splice-acceptor site (as used by Puttaraju et al., 1999), the coding regions of exons 4 and 5 and the GFP sequence. To prevent translation of the exons and GFP, the 5' end of the PTM was checked for an early start codon followed by a stop codon. The PTM template was constructed by PCR amplification of the intron-binding domain, exons 4 and 5 and the GFP sequence separately. The intron-binding domain and exons were then re-amplified using primers that included the sequence for the spacer and acceptor site. Finally, the 3 fragments were fused together by PCR to form the complete template (SPoCk-PTM1). The product was then cloned into pUAST (for further details of construction, see table 2.4).

Transgenic flies were generated for this construct and crossed to the c42 GAL4 line and the daG32 (ubiquitous, low level expression) GAL4 line. For both crosses, no fluorescence could be detected in the tubules or in the rest of the fly. Additionally cDNA was prepared from flies crossed to daG32 and RT-PCR performed in order to detect *trans*-splicing. Primers were used that bound to exon 3 (not in the PTM) and GFP (primers 119-107); therefore a PCR fragment could only be produced if targeted *trans*-splicing was occurring (see figure 6.2 for primer binding sites). Various annealing temperatures and cycles were used for the PCR but no product could be detected. This evidence suggested that this particular PTM was not eliciting any *trans*-splicing reactions with the SPoCk pre-mRNA.

The PTM was re-designed so that it had an organism specific splice-acceptor site and an intron-binding domain that covered all the endogenous splice-acceptor site. The acceptor site of the 19th exon of the *Drosophila* myosin heavy chain II gene has been shown to be an efficient and strong splice site (Hodges and Bernstein, 1992; Morin et al., 2001). This site was incorporated into the PTM instead of the yeast acceptor site, in the hope that it would function more efficiently in transgenic *Drosophila*. The intron-binding domain was extended to cover the endogenous acceptor site; this was based on the idea that if this site was covered it would inhibit *cis*-splicing and promote *trans*-splicing. The new PTM template (SPoCk-PTM2) was constructed in the same manner to the previous one, and cloned into pUAST (for more details, see table 2.4). Transgenic flies were generated.

When the flies were crossed to the c42 and daG32 lines, once again there was no detectable fluorescence. However RT-PCR on tubules (primers 106-107) demonstrated successful trans-splicing (see figure 6.2). To confirm this result the PCR product was
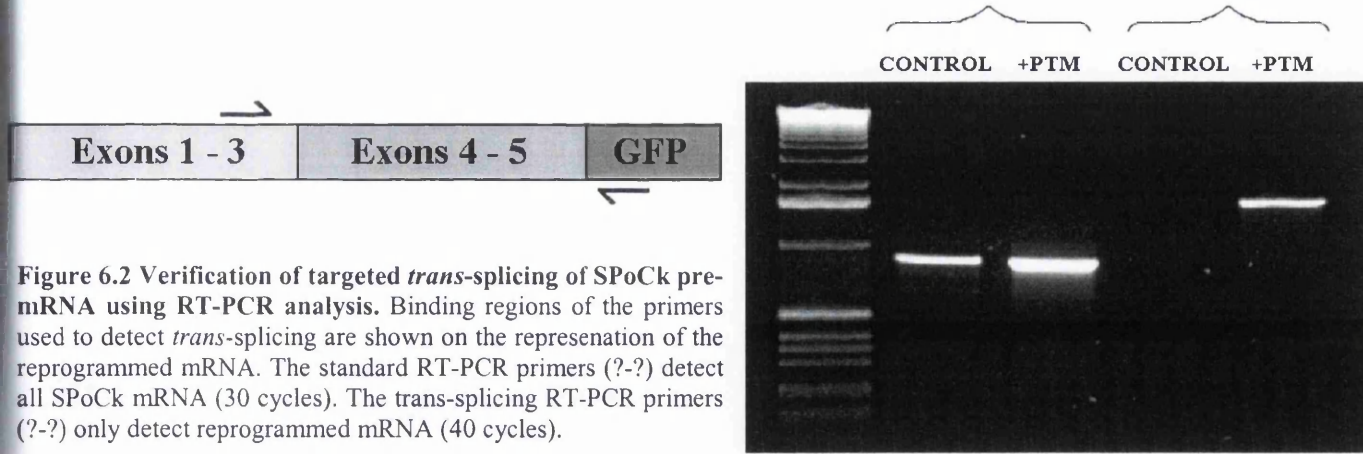
Figure 6.2 Verification of targeted *trans*-splicing of SPoCk premRNA using RT-PCR analysis. Binding regions of the primers used to detect *trans*-splicing are shown on the represenation of the reprogrammed mRNA. The standard RT-PCR primers (?-?) detect all SPoCk mRNA (30 cycles). The trans-splicing RT-PCR primers (?-?) only detect reprogrammed mRNA (40 cycles).
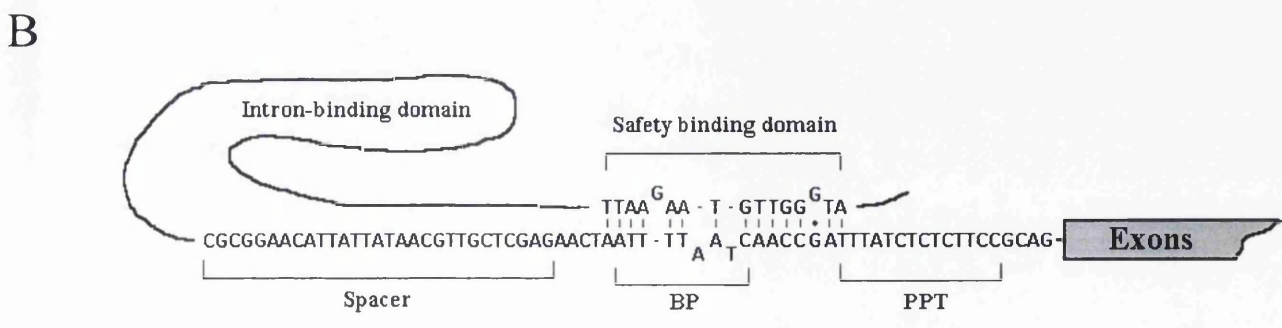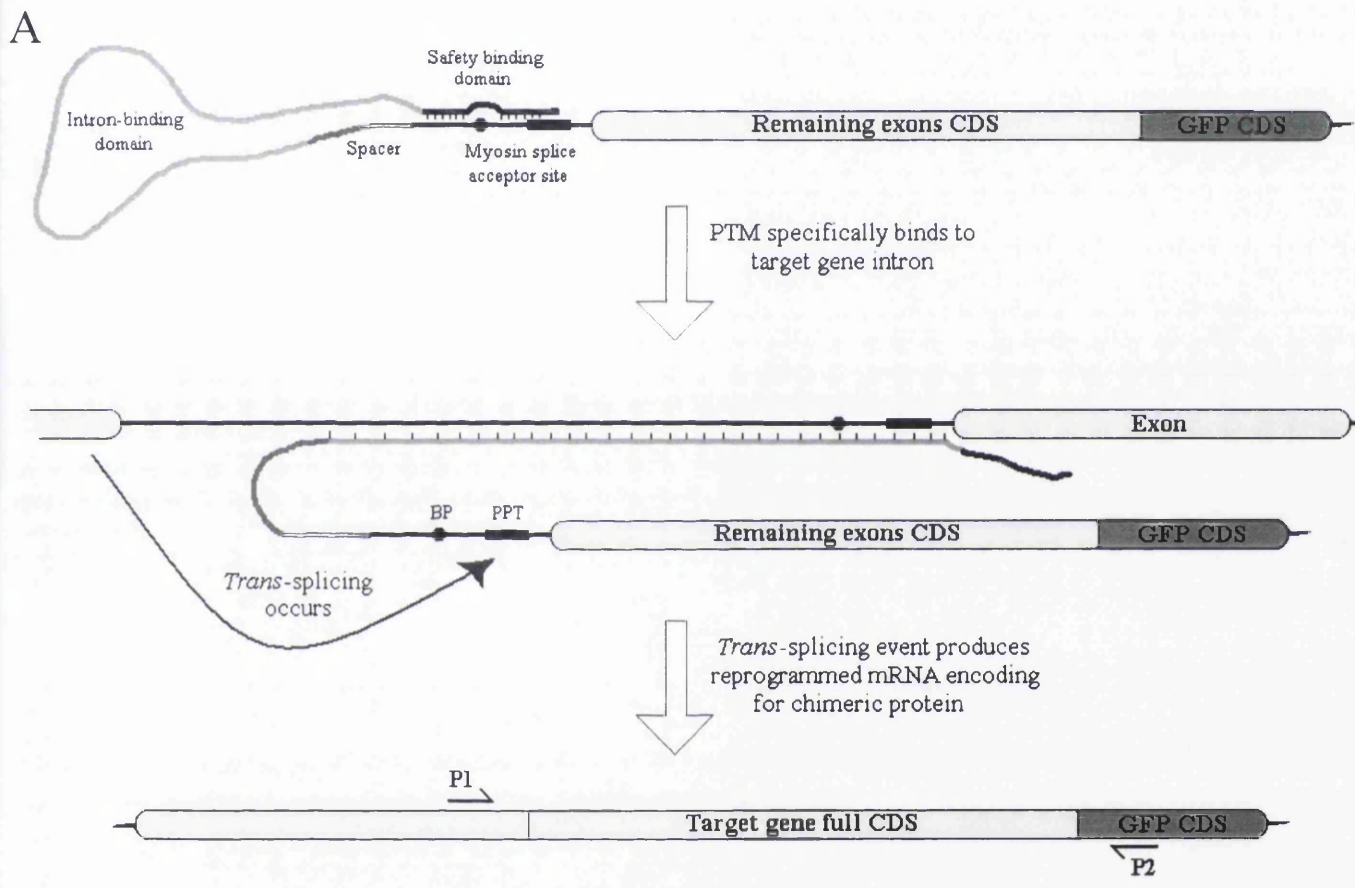
Figure 6.3 Mechanism of mRNA reprogramming using *trans*-splicing in *Drosophila*. (A) Schematic representation of the *trans*-splicing reaction. (B) Sequence of the spacer, the myosin acceptor site and the safety binding domain. CDS, coding sequence; BP, branchpoint, PPT, polypyrimidine tract. P1 and P2 indicate binding regions for primers used for RT-PCR analysis.

TOPO® cloned and sent to be sequenced. The sequencing revealed in-frame *trans*-splicing of the PTM into the endogenous SPoCk transcript, including the GFP coding sequence at the end. This confirms that this technology can work in *Drosophila*. However, it appears that the present efficiency must be low, as the GFP fluorescence cannot be detected and the *trans*-spliced mRNA could only be detected after 40 cycles of PCR. These observations could also be due to a low level expression of this gene or an incompatible PCR primer pair.

The efficiency of *trans*-splicing can be increased by increasing the amount of PTM present (Puttaraju et al., 1999). Therefore, if the expression of the PTM transgene is driven harder, then the efficiency *in vivo* may improve. To do this the pP{UAS-SPoCk-PTM2} line was crossed to two separate actin-GAL4 lines (high, ubiquitous expression of GAL4). Unfortunately this cross did not yield adult flies with both the transgene and the driver, it seems that driving expression of the PTM this high has lethal effects. This may be because of problems with non-specific *trans*-splicing.

The next step was to attempt to target a gene that was known to be expressed at high levels, and also to integrate a mechanism to increase specificity of the targeting. The *vha55* gene was chosen as it is known to be highly expressed in the tubule and has been extensively studied in our laboratory. The strategy behind increasing the specificity involved engineering a sequence at the 5' end of the PTM that would anneal to the myosin heavy chain acceptor site. In theory, this should inhibit the PTM from splicing non-specifically into another pre-mRNA until the target had been bound (see figure 6.3). This modified PTM template was constructed and transgenic flies generated (for details, see table 2.4).

The transgenic flies were crossed to the actin-GAL4 line and the progeny were found to be viable. Additionally fluorescence was observed in specific cells and tissues of the fly, as well as in specific subcellular localisations within the cells. Figure 6.4 shows examples of GFP fluorescence in flies expressing vha55-PTM; fluorescence was observed in apical regions of principal cells of the tubule, and was absent in stellate cells. The fluorescence was also detected in areas of other tissues that are known to express V-ATPases; i.e. the rectal pad and hindgut (see figures 6.4D → 6.4G). This was convincing data to support successful specific *trans*-splicing of the target pre-mRNA, as the fluorescence was only present in cells known to express *vha55*. RT-PCR analysis, using primers (120-121) designed in the same manner as for SPoCk-PTM flies, established successful *trans*-splicing (figure 6.4A). This band was also cloned and sequenced to further confirm this result. Figure 6.4B shows a western blot of control (*vha55*-PTM) whole fly protein and *vha55*-
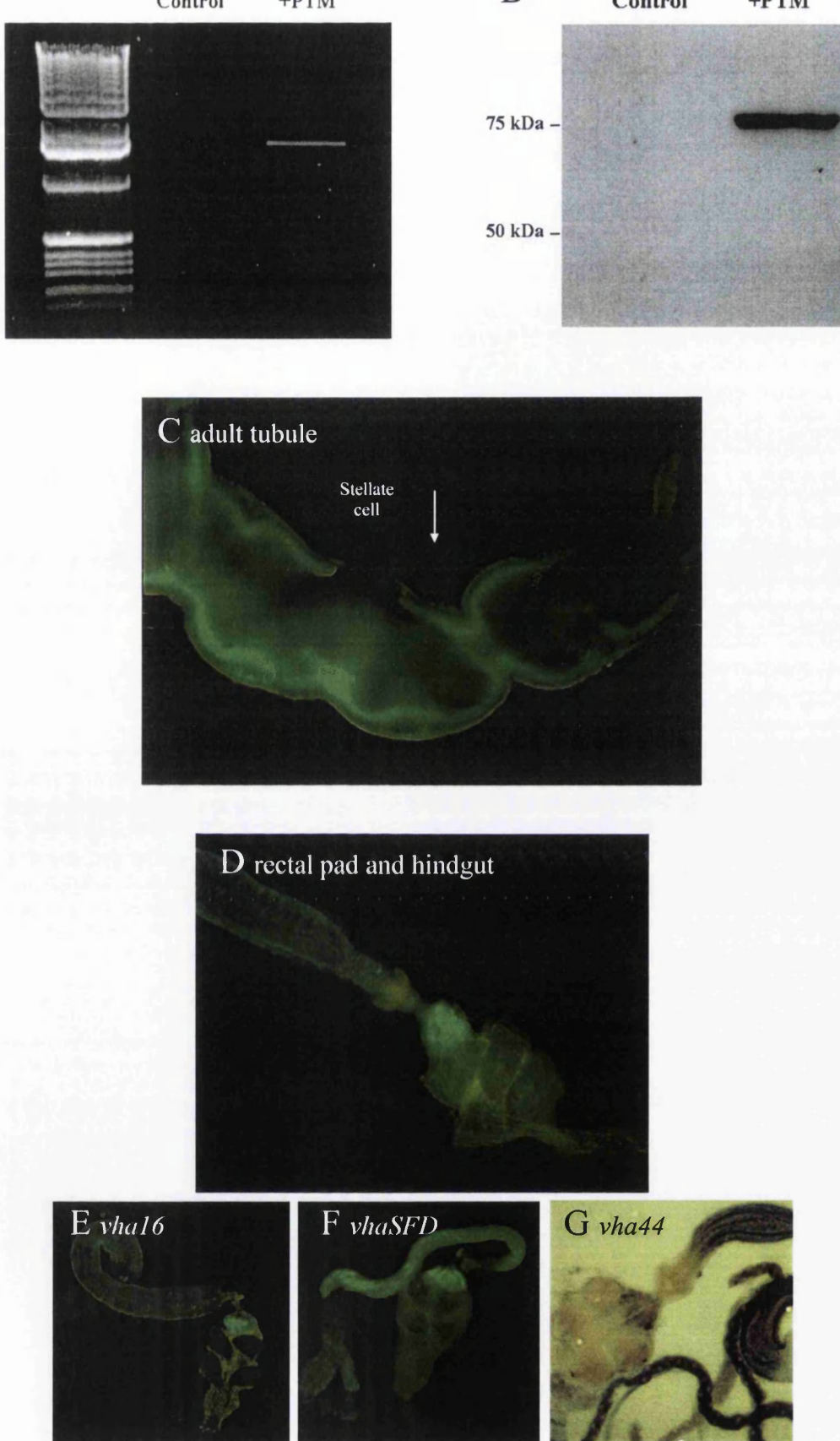
Figure 6.4 Is the *vha55*-PTM eliciting efficient *trans*-splicing? (A) RT-PCR to detect *trans*-splicing. *Trans*-splicing occurs in flies expressing the *vha55*-PTM (1600 bp product). (B) Western blot analysis of flies expressing *vha55*-PTM, using a mouse monoclonal anti-GFP antibody. (C) GFP fluorescence in the adult tubule from a fly expressing *vha55*-PTM. Apically located fluorescence can be seen in the principal cells, with no fluorescence detected in the stellate cells. (D) GFP fluorescence in the adult rectal pad and hindgut from a fly expressing *vha55*-PTM. Images were captured using standard fluorescence microscopy. (E) → (G) expression pattern of other V-ATPase subunits; GFP gene trap data for *vha16* and *vhaSFD*, and in situ data for *vha44* (images kindly provided by Adrian Allan). Scale bars for images are not shown.

PTM + actin-GAL4 whole fly protein. The GFP antibody detects a clear band at an approximate size of 75 kDa.

However, if a successfully GFP-tagged endogenous vha55 protein is being detected, the size of the band should be nearer to 80 kDa (~55 kDa for vha55 and ~25 kDa for GFP). One possible explanation for this is that the size estimation of the detected band is inaccurate (due to irregular separation of the protein on the acrylamide gel). The other less appealing explanation, is that the protein detected did not originate from a *trans*-spliced mRNA, but in fact results from leaky translation of the PTM RNA molecule. After studying the *vha55*-PTM sequence, it is apparent that if the ribosome can bypass the stop codons engineered into the 5' of the PTM; there is an ATG present that will allow translational read-through of the majority of the vha55 coding sequence and GFP. If this did occur it would result in a GFP tagged protein of ~70 kDa in size. The cell specific detection of GFP could then only be explained by degradation of vha55 protein in cells in which it is not required. If the vha55 subunit is expressed in cells where its partner subunits are not present, there will be no V-ATPase complex to integrate with, possibly leaving the subunit prone to ubiquitination and degradation.

It is not presently possible to say conclusively which scenario is happening; however, I believe that there is specific *trans*-splicing occurring, but only at a low level and the majority of the fluorescence observed is due to leaky translation of the PTM. It appears that this may be a inherent problem with this technology due to evidence resulting from other fly lines that have been generated. These included lines designed to tag leucokinin receptor (dLKR), inward rectifying potassium channel 3 (irk3) and IP₃R proteins.

dLKR-PTM1 and irk3-PTM were assembled using fusion PCR and cloned into pUAST (see table 2.4 for further details). These constructs were used to create transgenic lines. Pictures of tubules expressing dLKR-PTM1 and irk3-PTM are shown in figure 6.5. dLKR-PTM1 results in stellate cell specific GFP fluorescence, which is where the receptor is endogenously expressed (Radford et al., 2002). However, the reported expression in the rest of the fly was a lot more ubiquitous than had been shown with an anti-dLKR antibody (Radford et al., 2002). Furthermore, the intracellular localisation shown by the GFP fluorescence includes perinuclear staining. This is not the endogenous localisation of dLKR in the stellate cell (Radford et al., 2002) and may be explained by a lack of the N-terminus of LKR (as it may have been translated from the PTM) or the improper processing of the protein due to the GFP tag.

The GFP fluorescence produced by expression of irk3-PTM was very weak, but it did show fluorescence in stellate cells and possibly principal cells of the tubule (see figure 6.5B). This fits well with *in situ* analysis of *irk3* expression, which indicates expression in
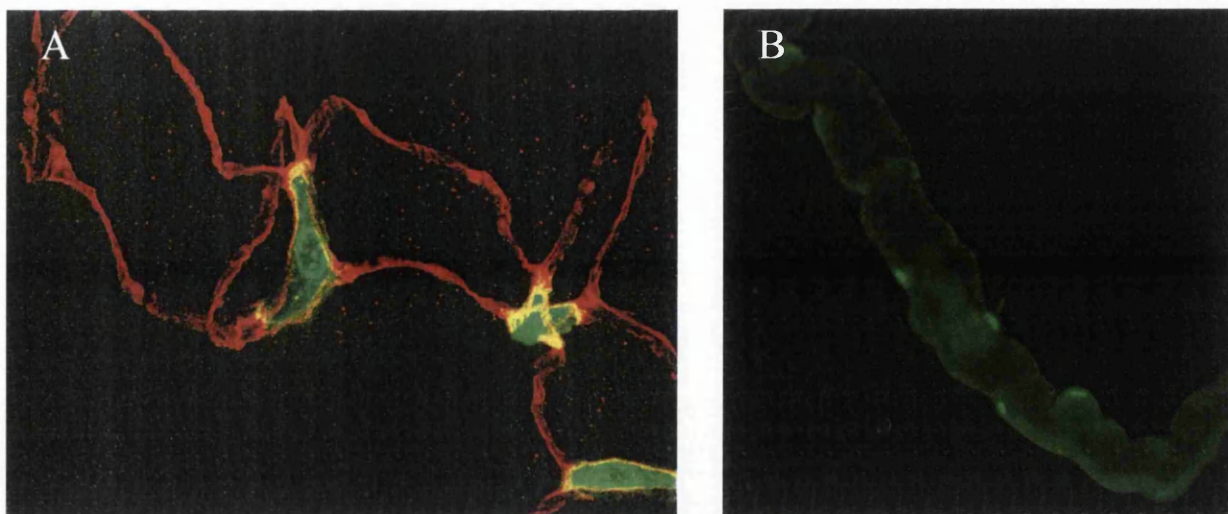
Figure 6.5 GFP fluorescence in tubules expressing dLKR-PTM1 and irk3-PTM. (A) Confocal projection of a tubule expressing dLKR-PTM1 (driven by actin-GAL4). The red staining is the localisation of discs large, a cell junction protein (detected using a anti-discs large antibody at a 1:800 dilution). (B) Fluorescence microscopy of a tubule expressing irk3-PTM (driven by actin-GAL4). Scale bars are not shown.
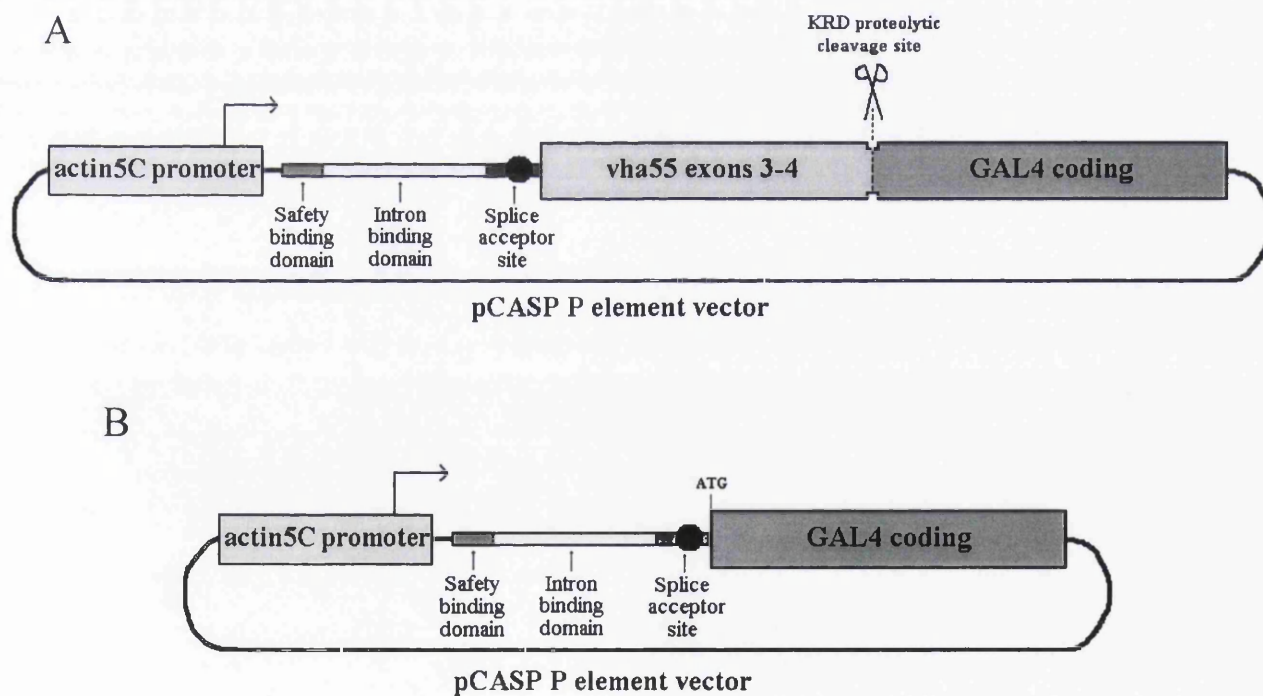
Figure 6.6 Schematic representation of constructs to enable targeted enhancer trapping in *Drosophila*. (A) Construct designed to express GAL4 only in cells where *vha55* is expressed. (B) Construct designed to express GAL4 only in cells where *leucokinin receptor* is expressed. Their design and proposed mechanism of action is described in the text.

both cell types (Adrian Allan, personal communication). As with the targeting of *vha55* pre-mRNA, the degree of GFP fluorescence that is resulting from *trans*-splicing rather than leaky translation of the PTM, has not been determined. Future analysis of these lines could answer this question and also help in the development of a more efficient and practical system.

6.3.2 Development of a targeted enhancer trap system

After realising that targeted *trans*-splicing is achievable in transgenic flies (RT-PCR evidence), I endeavoured to design a targeted enhancer trap system based on this technology. This was undertaken before the discovery of the inherent problems of the system. Two methods were attempted, both involved the incorporation of the GAL*4* coding sequence in the PTM. The designs of these PTMs are shown in figure 6.6. The basic idea is that if you can specifically *trans*-splice into an endogenous pre-mRNA, then it should be possible tag or replace this RNA with the transcription factor GAL4. This would be a powerful technique as it would allow expression of a UAS-transgene in cells specific to the gene in question. This is analogous to the present enhancer trap system in *Drosophila* (see section 1.3.2.2). However, this importantly provides a <u>targeted</u> system which may also be achievable without disruption of the endogenous gene.

The constructs shown in figure 6.6 were assembled using fusion PCR, and non-directionally cloned into the AyGAL4 vector (actin-GAL4) in between the actin promoter and the GAL4 coding sequence (for further details see table 2.4). Figure 6.6A shows the construct that was made in an attempt to try and 'trap' the *vha55* gene's expression pattern. The theory was that the actin promoter would drive high expression of the PTM, which would specifically splice into the endogenous *vha55* pre-mRNA. This would produce a vha55 protein with GAL4 on the C-terminus, which can be cleaved off to allow it to drive the expression of a desired reporter transgene. A known *Drosophila* neuropeptide proteolytic cleavage sequence KRD (Veenstra, 2000) was placed in between vha55 and GAL4 to allow the cleavage of the GAL4 post-translation. Transgenic flies were generated using the construct shown in figure 6.6A. When these transgenic lines were crossed to UAS-GFP no fluorescence was detected. This may be because the splicing is not occurring or that the KRD site is not being cleaved. Processing of the KRD site may require additional factors, including other signal sequences, the presence of necessary processing machinery (such as endoproteolytic convertases) and correct trafficking through the secretory pathway.

A second approach was attempted which involved replacing the ORF with GAL4 (see figure 6.6B). This method is simpler because there is no need for a cleavage site, but the

drawback that it can be only used on a gene that does not have the start codon in the first exon. Additionally, if the achieved splicing efficiency is high, then the levels of expression of the endogenous gene will be affected. The *dLKR* gene (Radford et al., 2002) was targeted, as there is a specific antibody available, the protein has been demonstrated to be expressed in the stellate cells of the tubule. Four transgenic fly lines were generated but unfortunately the transformants either died within a day or two, or if they survived longer, they were sterile. Although this was a hinderance, it was also encouraging as it implied that the PTM was causing this phenotype (it is unlikely that the 4 separate transgenic lines can all give the same phenotype due to random insertion effects). Preliminary western blot analysis performed using the anti-dLKR antibody on protein extracted from one of these flies (data not shown), showed a down-regulation of LKR compared to control flies. Although loading controls were unsuccessful, the western blot suggests that a down-regulation of dLKR protein levels may be eliciting the observed phenotype. The construct was re-injected and the injected flies reared and crossed back at 18°C instead of 22°C. This was successful and new transgenics have recently been generated that are viable and virile at 18°C. Due to time constraints, experiments on these flies have not yet been undertaken.

6.4 Discussion

This chapter has described the initial development of a gene knock-in technology in *Drosophila,* which has the potential to be a very powerful research technique. However, a lot more work and refinement will be required if this is ever to be a generic tool. The two main problems to overcome are to prevent leaky expression of the PTM and to improve the *trans*-splicing efficiency.

To prevent leaky expression of the PTM there are two possible approaches. Firstly, the PTM could be engineered to inhibit translation by the addition of *cis*-acting elements or upstream ORFs. Secondly, the PTM could be engineered so that it is prevented from being exported from the nucleus. The majority of the PTMs described in this chapter were designed with an ATG at the beginning, followed almost immediately by a stop codon. Having such a short reading frame may increase the possibility of the ribosome re-initiating translation. The incorporation of a larger ORF (encoding a nonsense protein) may help the ribosome to terminate translation on a more permanent basis before subsequent ORFs within the PTM are reached. The insertion of *cis*-acting sequences may also be a simple way to prevent translation; RNA sequences that result in stem-loop secondary structures have been shown to repress translation in prokaryotes and eukaryotes (Kosak, 1989; Beuzón et al., 1999; Wang and Wessler, 2001).

Preventing nuclear export of the PTM this would be beneficial in two ways. Firstly, leaky translation would not occur and secondly, it may increase the concentration of the PTM within the nucleus resulting in an increased level of *trans*-splicing. Unfortunately, I have not been able to find a suitable method for achieving this. An obvious approach would be to prevent the addition of a poly-A tail to the PTM. However, if performing 3'exon replacement, the modified mRNA would also be prevented from being exported.

Regarding the improvement of *trans*-splicing efficiency, this could be increased by elevation of PTM concentration, or by inhibition of *cis*-splicing. The use of a strong promoter (i.e. the actin promoter) or, as previously mentioned, preventing nuclear export of the PTM could increase PTM concentration. Puttaraju and colleagues (2001) have already investigated the effects of masking the endogenous acceptor site with an intron binding domain. This was found to enhance *trans*-splicing, and furthermore, creating RNA loop structures in this region increased splicing levels even more. This chapter has described the use of PTMs that cover the endogenous acceptor site, however, future work could include these secondary RNA loop-structures in the PTM design.

There is still more to be learned from analysing the transgenic flies generated to express GAL4 in dLKR cells. This work could include western blot analysis (with loading controls), quantitative RT-PCR and investigation of GAL4 expression within these flies. If the phenotype observed in these flies could be attributed to a knock-down of LKR levels, it will demonstrate that high efficiency targeted *trans*-splicing is achievable in a transgenic organism, and that this technology can also be used to create hypomorphs.

Due to their documented low *trans*-splicing efficiency, ribozymes were not previously considered as an approach to reprogram RNAs in *Drosophila*. However, with recent publications (Byun et al., 2003) demonstrating efficiencies of up to 50%, these self-catalytic RNAs could also be put to use in *Drosophila*. One advantage of a ribozyme-based system is that the target does not just have to be pre-mRNA, ribozymes can also splice into mature mRNA. However, as with the SMaRT technology, leaky translation of the ribozyme would have to be prevented.

The SMaRT technology was originally developed for a gene therapy application. Developing and improving the technology in *Drosophila* will provide a powerful tool for *Drosophila* research, but will act as an excellent model for further advancing gene therapy approachs. The majority of previous work on this technology has been using cell culture techniques to analyse different PTMs. However, the ease of creating transgenic *Drosophila* lines facilitates the development of this system within a multicellular context. Furthermore, with regards to modelling gene therapy approaches in *Drosophila*, it has been recently documented that many disease causing genes in humans have homologues in *Drosophila*

(Reiter et al., 2001; Dow and Davies, 2003). In the post-genomic era, this technology could provide another valuable tool in closing the genotype-phenotype gap, in not just *Drosophila*, but also in other model organisms.

Chapter 7

Future work and summary

7.1 Future work

This thesis has described the development of several new powerful tools and techniques, in addition to the identification of a novel multiply-spliced Ca^{2+}-ATPase in *Drosophila*. This work has opened the door for a host of possible future experiments and projects, the majority of which are described below.

The discovery that SPoCk-trB can be targeted to the ER by a N-terminal 133 amino acid sequence raises the possibility of fusing this sequence to target aequorin to the ER in *Drosophila*, without disrupting its function. Although the ERpicam reporter has allowed monitoring of $[Ca^{2+}]_{ER}$ levels, targeted aequorin could provide quantitative measurements. Regarding the Golgi-targeted aequorin reporter, I believe this can be successfully utilised, requiring only the appropriate conditions to be found in order to allow refilling of the store. An important future experiment, utilising the mitochondrially-targeted aequorin, and possibly mitycam-1, will be to investigate whether Ru360 (a previously documented blocker of mitochondrial Ca^{2+} uptake (Matlib et al., 1998)) can prevent Ca^{2+} uptake into principal cell mitochondria. If this is the case, then it should be possible to determine whether it is the uptake of Ca^{2+} that activates mitochondria to produce more ATP in response to capa. This could be performed by using secretion assays and also by using the mitochondrial redox-state sensitive dye JC-9 (Smiley et al., 1991).

During development of ERpicam, it became evident that residue 148 of YFP in the pericam is a critical 'hinging' residue (see chapter 4). Using site-directed mutagenesis it would be possible to investigate the effect of different amino acids at this position, in conjunction with different calmodulin EF hand mutations. This might result in a combination of mutations that allows alignment of the two halves of YFP in such a way that produces a ratiometric pericam, suitable for use in the ER.

Future work, involving live imaging of the pericams in the tubule, could comprise of refining the procedure to permit higher resolution imaging of single cells. It may then be possible to observe spatial differences within single cells during stimulation with appropriate agonists. Stable fly lines expressing the pericams could also be generated to improve the strength of the fluorescence signal in the tubule. However, the implications of expressing such high levels of a Ca^{2+}-binding protein on Ca^{2+} buffering effects would have to be carefully considered.

There is a great deal of potential future experiments in the SPoCk project. The primary objective will be to confirm the intracellular localisation and determine the cellular expression pattern of the 3 isoforms using antibodies. Specific antibodies have recently been generated and preliminary results look promising (Selim Terhzaz, personal communication). It would also be interesting to look at the impact of overexpressing these

pumps on Mn^{2+} homeostasis. As previously documented (Lapinskas et al., 1995), alterations of Mn^{2+} levels in eukaryotic cells can prevent oxidative damage. Therefore, overexpression of these pumps may alter levels of oxidative damage on an organismal scale, and could have a significant effect on the life span of the fly. Additionally, with the available overexpressing fly lines and the new antibodies, it will be possible to perform co-immunoprecipitation experiments. This may facilitate the identification of proteins that interact with these novel *Drosophila* ATPases.

Regarding SPoCk-trA maintaining the IP_3-releasable Ca^{2+} store in the principal cell, a crucial experiment will be to determine the localisation of IP_3Rs in this cell. Based on the model described in the section 7.2, they should localise to the Golgi apparatus and not to the ER.

Future work on developing the *trans*-splicing gene knock-in technology is discussed in section 6.4.

7.2 Summary

Previous studies in our laboratory have described the cytoplasmic Ca^{2+} responses to the diuretic peptides capa and drosokinin within the principal and stellate cells of the Malpighian tubule (Rosay et al., 1997; Terhzaz et al., 1999; Kean et al., 2002). Both cell types respond in a biphasic manner, with an initial fast primary spike followed by a more prolonged secondary wave. The most plausible model for these responses (based on the majority of previous studies of cellular Ca^{2+} signalling events) would involve the elevation of IP_3 levels upon activation of a receptor. The IP_3 would then elicit a release of Ca^{2+} from an internal store (most probably the ER), producing the primary $[Ca^{2+}]_i$ peak. This would then initiate a Ca^{2+} influx from extracellular sources via plasma membrane channels, producing the secondary response. This basic model is supported by work by Pollock et al (2003), who demonstrated that capa and drosokinin elevate IP_3 levels, and that mutations in the *Drosophila IP_3R* gene reduce the primary Ca^{2+} response. Furthermore, when heteromultimers of TRP channels are disrupted by a mutant channel, the secondary response in the principal cell is almost completely abolished (MacPherson et al., submitted). However, not all the previous work fits with this model. In 1997, Rosay et al. showed that when tubules are incubated in Ca^{2+}-free medium both the primary and the secondary rises in the principal cell were eliminated, suggesting that both aspects of the signal require external Ca^{2+}. However, these experiments have been repeated using EGTA to remove the extracellular Ca^{2+} only minutes before stimulation, in order to minimise depletion of internal stores (Terhzaz et al., unpublished). Using this method, the primary response is still present (although slightly reduced), and the secondary response is very small or completely abolished. Similar experiments in stellate cells demonstrate the same effect; the primary response remains and the secondary response is lost. This is further support for the previously described model of Ca^{2+} signalling in the tubule involving a release from internal stores followed by an influx of external Ca^{2+}.

This evidence provides the first step towards understanding the Ca^{2+} signalling in this renal tissue. However, there are a lot more questions to be answered. For example, whether the ER is the IP_3-releasable pool in the principal and stellate cells; and are other organelles such as the mitochondria involved or affected by these Ca^{2+} signalling events? This thesis has begun to answer these questions by a variety of approaches, including the development and utilisation of targeted genetically encoded Ca^{2+} probes and studying the effects of overexpressing differentially targeted Ca^{2+}-ATPases.

Data from chapters 3, 4 and 5 provide evidence that the principal cell ER plays no role in the capa-induced Ca^{2+} signalling event. Firstly, the application of an ER-targeted fluorescent reporter demonstrated that upon stimulation with capa-1 the $[Ca^{2+}]_{ER}$ levels do

not drop, but instead mimic the cytoplasmic response. Secondly, overexpression of an ER-targeted Ca^{2+}-ATPase (SPoCk-trB), which has been shown to potentiate IP_3-generated Ca^{2+} increases in S2 cells, has no effect on the primary response to capa-1 in principal cells. Thirdly, the mitochondria in this cell do not take up Ca^{2+} during the primary response. Mitochondria have been shown to be coupled or in very close proximity to the ER (Rizzuto et al., 1998), and upon release of Ca^{2+} from the ER they are subjected to a microdomain of high $[Ca^{2+}]$, resulting in a rapid uptake of Ca^{2+}. As this does not occur in principal cells, the primary implication is that the ER is not releasing Ca^{2+} during the primary response. As mentioned in chapter 4, the principal cell is densely packed with ER, and so a possible reason for the lack of participance of the ER in the signalling events may be that a release from this organelle could cause dangerously high of $[Ca^{2+}]_i$ and $[Ca^{2+}]_{mt}$ levels. Another possibility for why the ER plays no role, is that the ER could be acting as a tunnelling system for the movement of ions or organic compounds from the basolateral to the apical membrane. Consequently, a release of Ca^{2+} might impede this function.

The next obvious question is where is the Ca^{2+} being released from, if it is not the ER? The effects of overexpressing a Golgi-targeted Ca^{2+}-ATPase (SPoCk-trA) in the principal cell strongly suggest that it is in fact the Golgi, which is acting as the primary IP_3-releasable pool. Pinton and colleagues (1998) have demonstrated that the Golgi can act as an IP_3-releasable in conjunction with the ER. Nevertheless, these studies in the principal cell have for the fist time shown the Golgi acting as the primary releasable Ca^{2+} pool, with no contribution from the ER. It will be very interesting to see whether this unusual method of Ca^{2+} signalling is present in other renal tissues, such as the proximal convoluted tubule in mammalian kidneys.

The impact of these Ca^{2+} signals on the mitochondria has been studied in the principal and stellate cells using a targeted aequorin and targeted pericam approach. Both methods have shown that in the two main cell types of the tubule, the uptake of Ca^{2+} into the mitochondria upon agonist stimulation is atypical. The uptake occurs in accordance with the secondary cytoplasmic Ca^{2+} event and not the primary. As discussed in chapter 3, it appears that the influx of external Ca^{2+} (secondary response) drives the uptake of Ca^{2+} into mitochondria, and that this uptake should be sufficient to produce an increase in ATP production, via activation of the matrix dehydrogenases. This provides an elegant link between stimulation of the principal cell with capa, and the consequent requirement of ATP for the activated V-ATPase complexes.

The discovery of the alternatively targeted SPCA ATPases (SPoCk-trB and SPoCk-trC) is intriguing and will hopefully lead to a greater understanding of how cells handle Ca^{2+} and Mn^{2+}. As previously discussed in chapter 5, it seems peculiar that a second ER-targeted
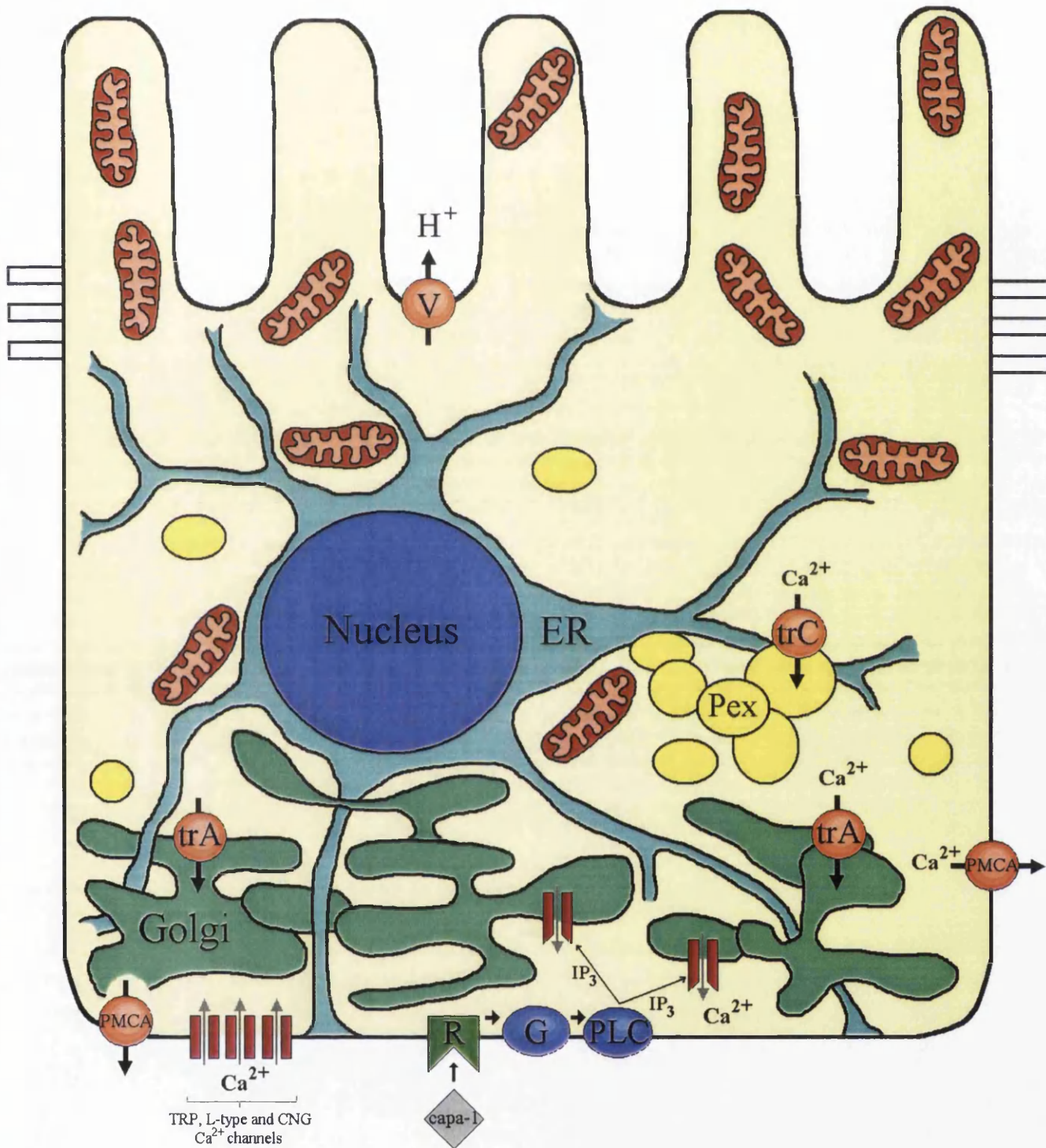
Figure 7.1 Present model for Ca^{2+} signalling and Ca^{2+} pool characteristics in the principal cell. The model is described in the text. Abbreviations are as follows: V, V-ATPase; Pex, peroxisome; ER, endoplasmic reticulum; trA, SPoCk-trA $Ca2+/Mn^{2+}$-ATPase; trC, SPoCk-trC Ca^{2+}/Mn^{2+}-ATPase; R, receptor; G, G protein; PLC, phospholipase C; PMCA, plasma membrane Ca^{2+}-ATPase; TRP, transient receptor potential channel; CNG, cyclic-nucleotide gated channel. Red oval structures represent mitochondria. Electron microscopy has shown that ER channels connect with the infoldings of the basal plasmalemma in the principal cell (Ashburner and Wright, 1978); this is represented by the joining of the ER and the basolateral membrane on the diagram.

Ca^{2+} ATPase (trB) is required in some cell types. However, this may be due to the need for an ER pump with different transporting properties, or possibly one that can supply Mn^{2+} to the ER. If indeed SPoCk-trC does localise to peroxisomes it will raise the question of why this enigmatic organelle requires a Ca^{2+}/Mn^{2+} ATPase. Possible explanations are that peroxisomes may act as functional Ca^{2+} stores and/or that Mn^{2+} is needed for resident peroxisomal enzymes (such as Mn^{2+}-dependent SOD).

Figure 7.1 displays an updated model for Ca^{2+} signalling within the principal cell. This model describes a cell where a predominantly basolateral Golgi Ca^{2+} pool, maintained by SPoCk-trA, releases Ca^{2+} upon an agonist mediated stimulus. Although the ER is extensive throughout the cell, it does not contribute to IP_3-based Ca^{2+} events, and the manner by which its Ca^{2+} levels are maintained is still unclear. Mitochondria are found mainly in the apical region, and peroxisomal Ca^{2+} stores/pools (maintained by SPoCk-trC) are present throughout various regions of the cell. The secondary Ca^{2+} response occurs via an influx of extracellular Ca^{2+}, possibly through a complex of TRP, L-type and/or CNG-gated plasma membrane channels. Whether both the Ca^{2+} signalling events are required for activation of downstream signalling pathways is yet to be resolved. However, the secondary response looks likely to be required for the increase in ATP production via the activation of mitochondria. The work described in this thesis has helped contribute to this model, and, like many models of intracellular systems, it will continue to evolve.

The *Drosophila* Malpighian tubule is an excellent model system for studying the Ca^{2+}-signalling events that control renal function. The application of powerful transgenic and fluorescent reporter techniques has made it possible to alter and observe these signalling events in a live intact tissue. This work has made significant advances into understanding these events, and will hopefully be continued to gain further insight into how renal function is controlled in *Drosophila* and higher organisms.

References

Adams, M. D. Celniker, S. E. Holt, R. A. Evans, C. A. Gocayne, J. D. Amanatides, P. G. Scherer, S. E. Li, P. W. Hoskins, R. A. Galle, R. F. et al. (2000). The genome sequence of Drosophila melanogaster. *Science* **287**, 2185-95.

Antebi, A. and Fink, G. R. (1992). The yeast Ca(2+)-ATPase homologue, PMR1, is required for normal Golgi function and localizes in a novel Golgi-like distribution. *Mol Biol Cell* **3**, 633-54.

Arnaudeau, S., Frieden, M., Nakamura, K., Castelbou, C., Michalak, M. and Demaurex, N. (2002). Calreticulin differentially modulates calcium uptake and release in the endoplasmic reticulum and mitochondria. *J Biol Chem* **277**, 46696-705.

Ashburner, M., Wright, T. R. F. (1978). The Genetics and Biology of Drosophila.

Ashby, M. C. and Tepikin, A. V. (2002). Polarized calcium and calmodulin signaling in secretory epithelia. *Physiol Rev* **82**, 701-34.

Axelsen, K. B. and Palmgren, M. G. (2001). Inventory of the superfamily of P-type ion pumps in Arabidopsis. *Plant Physiol* **126**, 696-706.

Babu, Y. S., Bugg, C. E. and Cook, W. J. (1988). Structure of calmodulin refined at 2.2 A resolution. *J Mol Biol* **204**, 191-204.

Baird, G. S., Zacharias, D. A. and Tsien, R. Y. (1999). Circular permutation and receptor insertion within green fluorescent proteins. *Proc Natl Acad Sci U S A* **96**, 11241-6.

Barrero, M. J., Montero, M. and Alvarez, J. (1997). Dynamics of [Ca2+] in the endoplasmic reticulum and cytoplasm of intact HeLa cells. A comparative study. *J Biol Chem* **272**, 27694-9.

Barrero, M. J., Montero, M. and Alvarez, J. (1997). Dynamics of [Ca2+] in the endoplasmic reticulum and cytoplasm of intact HeLa cells. A comparative study. *J Biol Chem* **272**, 27694-9.

Beard, M. E. and Holtzman, E. (1987). Peroxisomes in wild-type and rosy mutant Drosophila melanogaster. *Proc Natl Acad Sci U S A* **84**, 7433-7.

Bernardi, P. (1999). Mitochondrial transport of cations: channels, exchangers, and permeability transition. *Physiol Rev* **79**, 1127-55.

Berridge, M. J. (1993). Inositol trisphosphate and calcium signalling. *Nature* **361**, 315-25.

Berridge, M. J. (1997). Elementary and global aspects of calcium signalling. *J Physiol* **499** (Pt 2), 291-306.

Berridge, M. J. (2002). The endoplasmic reticulum: a multifunctional signaling organelle. *Cell Calcium* **32**, 235-49.

Beuzon, C. R., Marques, S. and Casadesus, J. (1999). Repression of IS200 transposase synthesis by RNA secondary structures. *Nucleic Acids Res* **27**, 3690-5.

Bier, E., Vaessin, H., Shepherd, S., Lee, K., McCall, K., Barbel, S., Ackerman, L., Carretto, R., Uemura, T., Grell, E. et al. (1989). Searching for pattern and mutation in the Drosophila genome with a P-lacZ vector. *Genes Dev* **3**, 1273-87.

Bird, G. S., Rossier, M. F., Hughes, A. R., Shears, S. B., Armstrong, D. L. and Putney, J. W., Jr. (1991). Activation of Ca2+ entry into acinar cells by a non-phosphorylatable inositol trisphosphate. *Nature* **352**, 162-5.

Blumenthal, T. (1995). Trans-splicing and polycistronic transcription in Caenorhabditis elegans. *Trends Genet* **11**, 132-6.

Bootman, M., Niggli, E., Berridge, M. and Lipp, P. (1997). Imaging the hierarchical Ca2+ signalling system in HeLa cells. *J Physiol* **499** (**Pt 2**), 307-14.

Bradley, T. J. and Satir, P. (1979). Evidence of microfilament-associated mitochondrial movement. *J Supramol Struct* **12**, 165-75.

Bradley, T. J. and Satir, P. (1981). 5-hydroxytryptamine-stimulated mitochondrial movement and microvillar growth in the lower malpighian tubule of the insect, Rhodnius prolixus. *J Cell Sci* **49**, 139-61.

Brand, A. H. and Perrimon, N. (1993). Targeted gene expression as a means of altering cell fates and generating dominant phenotypes. *Development* **118**, 401-15.

Brand, A. H., Manoukian, A. S. and Perrimon, N. (1994). Ectopic expression in Drosophila. *Methods Cell Biol* **44**, 635-54.

Brand, A. H. and Dormand, E. L. (1995). The GAL4 system as a tool for unravelling the mysteries of the Drosophila nervous system. *Curr Opin Neurobiol* **5**, 572-8.

Broillet, M. C. and Firestein, S. (1999). Cyclic nucleotide-gated channels. Molecular mechanisms of activation. *Ann N Y Acad Sci* **868**, 730-40.

Button, D. and Eidsath, A. (1996). Aequorin targeted to the endoplasmic reticulum reveals heterogeneity in luminal Ca++ concentration and reports agonist- or IP3-induced release of Ca++. *Mol Biol Cell* **7**, 419-34.

Byun, J., Lan, N., Long, M. and Sullenger, B. A. (2003). Efficient and specific repair of sickle beta-globin RNA by trans-splicing ribozymes. *Rna* **9**, 1254-63.

Cabrero, P., Radford, J. C., Broderick, K. E., Costes, L., Veenstra, J. A., Spana, E. P., Davies, S. A. and Dow, J. A. (2002). The Dh gene of Drosophila melanogaster encodes a diuretic peptide that acts through cyclic AMP. *J Exp Biol* **205**, 3799-807.

Carnell, L. and Moore, H. P. (1994). Transport via the regulated secretory pathway in semi-intact PC12 cells: role of intra-cisternal calcium and pH in the transport and sorting of

secretogranin II. *J Cell Biol* **127**, 693-705.

Cech, T. R., Zaug, A. J. and Grabowski, P. J. (1981). In vitro splicing of the ribosomal RNA precursor of Tetrahymena: involvement of a guanosine nucleotide in the excision of the intervening sequence. *Cell* **27**, 487-96.

Cech, T. R. (1988). Ribozymes and their medical implications. *Jama* **260**, 3030-4.

Chandra, S., Fewtrell, C., Millard, P. J., Sandison, D. R., Webb, W. W. and Morrison, G. H. (1994). Imaging of total intracellular calcium and calcium influx and efflux in individual resting and stimulated tumor mast cells using ion microscopy. *J Biol Chem* **269**, 15186-94.

Chapman, R. A. and Tunstall, J. (1987). The calcium paradox of the heart. *Prog Biophys Mol Biol* **50**, 67-96.

Chavis, P., Fagni, L., Lansman, J. B. and Bockaert, J. (1996). Functional coupling between ryanodine receptors and L-type calcium channels in neurons. *Nature* **382**, 719-22.

Churchill, G. C., Okada, Y., Thomas, J. M., Genazzani, A. A., Patel, S. and Galione, A. (2002). NAADP mobilizes Ca(2+) from reserve granules, lysosome-related organelles, in sea urchin eggs. *Cell* **111**, 703-8.

Coast, G. M. (2001). Diuresis in the housefly (Musca domestica) and its control by neuropeptides. *Peptides* **22**, 153-60.

Collins, T. J., Lipp, P., Berridge, M. J. and Bootman, M. D. (2001). Mitochondrial Ca(2+) uptake depends on the spatial and temporal profile of cytosolic Ca(2+) signals. *J Biol Chem* **276**, 26411-20.

Crane, D. I., Kalish, J. E. and Gould, S. J. (1994). The Pichia pastoris PAS4 gene encodes a ubiquitin-conjugating enzyme required for peroxisome assembly. *J Biol Chem* **269**, 21835-44.

Davidson, H. W., Rhodes, C. J. and Hutton, J. C. (1988). Intraorganellar calcium and pH control proinsulin cleavage in the pancreatic beta cell via two distinct site-specific endopeptidases. *Nature* **333**, 93-6.

Davies, S. A., Huesmann, G. R., Maddrell, S. H., O'Donnell, M. J., Skaer, N. J., Dow, J. A. and Tublitz, N. J. (1995). CAP2b, a cardioacceleratory peptide, is present in Drosophila and stimulates tubule fluid secretion via cGMP. *Am J Physiol* **269**, R1321-6.

Davies, S. A., Goodwin, S. F., Kelly, D. C., Wang, Z., Sozen, M. A., Kaiser, K. and Dow, J. A. (1996). Analysis and inactivation of vha55, the gene encoding the vacuolar ATPase B-subunit in Drosophila melanogaster reveals a larval lethal phenotype. *J Biol Chem* **271**, 30677-84.

Davies, S. A., Stewart, E. J., Huesmann, G. R., Skaer, N. J., Maddrell, S. H., Tublitz, N. J. and Dow, J. A. (1997). Neuropeptide stimulation of the nitric oxide signaling pathway in Drosophila melanogaster Malpighian tubules. *Am J Physiol* **273**, R823-7.

De Blas, G., Michaut, M., Trevino, C. L., Tomes, C. N., Yunes, R., Darszon, A. and

Mayorga, L. S. (2002). The intraacrosomal calcium pool plays a direct role in acrosomal exocytosis. *J Biol Chem* **277**, 49326-31.

Deo, S. K. and Daunert, S. (2001). An immunoassay for Leu-enkephalin based on a C-terminal aequorin-peptide fusion. *Anal Chem* **73**, 1903-8.

Dolmetsch, R. E., Lewis, R. S., Goodnow, C. C. and Healy, J. I. (1997). Differential activation of transcription factors induced by Ca2+ response amplitude and duration. *Nature* **386**, 855-8.

Dorn, R., Reuter, G. and Loewendorf, A. (2001). Transgene analysis proves mRNA trans-splicing at the complex mod(mdg4) locus in Drosophila. *Proc Natl Acad Sci U S A* **98**, 9724-9.

Dow, J. A., Maddrell, S. H., Gortz, A., Skaer, N. J., Brogan, S. and Kaiser, K. (1994). The malpighian tubules of Drosophila melanogaster: a novel phenotype for studies of fluid secretion and its control. *J Exp Biol* **197**, 421-8.

Dow, J. A., Davies, S. A. and Sozen, A. (1998). Fluid Secretion by the *Drosophila* Malpighian Tubule. *American Zoology* **38**, 450-60.

Dow, J. T. and Davies, S. A. (2003). Integrative physiology and functional genomics of epithelial function in a genetic model organism. *Physiol Rev* **83**, 687-729.

Dube, K., McDonald, D. G. and O'Donnell, M. J. (2000). Calcium transport by isolated anterior and posterior Malpighian tubules of Drosophila melanogaster: roles of sequestration and secretion. *J Insect Physiol* **46**, 1449-1460.

Duncan, J. S. and Burgoyne, R. D. (1996). Characterization of the effects of Ca2+ depletion on the synthesis, phosphorylation and secretion of caseins in lactating mammary epithelial cells. *Biochem J* **317 (Pt 2)**, 487-93.

Ebashi, S. and Endo, M. (1968). Calcium ion and muscle contraction. *Prog Biophys Mol Biol* **18**, 123-83.

Elliott, A. C. (2001). Recent developments in non-excitable cell calcium entry. *Cell Calcium* **30**, 73-93.

Emmanouilidou, E., Teschemacher, A. G., Pouli, A. E., Nicholls, L. I., Seward, E. P. and Rutter, G. A. (1999). Imaging Ca2+ concentration changes at the secretory vesicle surface with a recombinant targeted cameleon. *Curr Biol* **9**, 915-8.

Eul, J., Graessmann, M. and Graessmann, A. (1995). Experimental evidence for RNA trans-splicing in mammalian cells. *Embo J* **14**, 3226-35.

Fiala, A., Spall, T., Diegelmann, S., Eisermann, B., Sachse, S., Devaud, J. M., Buchner, E. and Galizia, C. G. (2002). Genetically expressed cameleon in Drosophila melanogaster is used to visualize olfactory information in projection neurons. *Curr Biol* **12**, 1877-84.

Filippin, L., Magalhaes, P. J., Di Benedetto, G., Colella, M. and Pozzan, T. (2003). Stable interactions between mitochondria and endoplasmic reticulum allow rapid accumulation of

calcium in a subpopulation of mitochondria. *J Biol Chem* **278**, 39224-34.

Fischer, J. A., Giniger, E., Maniatis, T. and Ptashne, M. (1988). GAL4 activates transcription in Drosophila. *Nature* **332**, 853-6.

Furuya, T., Okura, M., Ruiz, F. A., Scott, D. A. and Docampo, R. (2001). TcSCA complements yeast mutants defective in Ca2+ pumps and encodes a Ca2+-ATPase that localizes to the endoplasmic reticulum of Trypanosoma cruzi. *J Biol Chem* **276**, 32437-45.

Galione, A., Lee, H. C. and Busa, W. B. (1991). Ca(2+)-induced Ca2+ release in sea urchin egg homogenates: modulation by cyclic ADP-ribose. *Science* **253**, 1143-6.

Gilabert, J. A. and Parekh, A. B. (2000). Respiring mitochondria determine the pattern of activation and inactivation of the store-operated Ca(2+) current I(CRAC). *Embo J* **19**, 6401-7.

Gill, G. and Ptashne, M. (1987). Mutants of GAL4 protein altered in an activation function. *Cell* **51**, 121-6.

Glitsch, M. D., Bakowski, D. and Parekh, A. B. (2002). Store-operated Ca2+ entry depends on mitochondrial Ca2+ uptake. *Embo J* **21**, 6744-54.

Griesbeck, O., Baird, G. S., Campbell, R. E., Zacharias, D. A. and Tsien, R. Y. (2001). Reducing the environmental sensitivity of yellow fluorescent protein. Mechanism and applications. *J Biol Chem* **276**, 29188-94.

Grynkiewicz, G., Poenie, M. and Tsien, R. Y. (1985). A new generation of Ca2+ indicators with greatly improved fluorescence properties. *J Biol Chem* **260**, 3440-50.

Grynkiewicz, G., Poenie, M. and Tsien, R. Y. (1985). A new generation of Ca2+ indicators with greatly improved fluorescence properties. *J Biol Chem* **260**, 3440-50.

Gu, X. and Spitzer, N. C. (1993). Low-threshold Ca2+ current and its role in spontaneous elevations of intracellular Ca2+ in developing Xenopus neurons. *J Neurosci* **13**, 4936-48.

Gu, X. and Spitzer, N. C. (1995). Distinct aspects of neuronal differentiation encoded by frequency of spontaneous Ca2+ transients. *Nature* **375**, 784-7.

Gunter, T. E. and Pfeiffer, D. R. (1990). Mechanisms by which mitochondria transport calcium. *Am J Physiol* **258**, C755-86.

Gunteski-Hamblin, A. M., Greeb, J. and Shull, G. E. (1988). A novel Ca2+ pump expressed in brain, kidney, and stomach is encoded by an alternative transcript of the slow-twitch muscle sarcoplasmic reticulum Ca-ATPase gene. Identification of cDNAs encoding Ca2+ and other cation-transporting ATPases using an oligonucleotide probe derived from the ATP-binding site. *J Biol Chem* **263**, 15032-40.

Hacker, U., Nystedt, S., Barmchi, M. P., Horn, C. and Wimmer, E. A. (2003). piggyBac-based insertional mutagenesis in the presence of stably integrated P elements in Drosophila. *Proc Natl Acad Sci U S A* **100**, 7720-5.

Haller, T., Volkl, H., Deetjen, P. and Dietl, P. (1996). The lysosomal Ca2+ pool in MDCK cells can be released by ins(1,4,5)P3-dependent hormones or thapsigargin but does not activate store-operated Ca2+ entry. *Biochem J* 319 (Pt 3), 909-12.

Hardie, R. C. (2001). Phototransduction in Drosophila melanogaster. *J Exp Biol* 204, 3403-9.

Haseloff, J. and Gerlach, W. L. (1988). Simple RNA enzymes with new and highly specific endoribonuclease activities. *Nature* 334, 585-91.

Hazelrigg, T., Levis, R. and Rubin, G. M. (1984). Transformation of white locus DNA in drosophila: dosage compensation, zeste interaction, and position effects. *Cell* 36, 469-81.

Head, J. F., Inouye, S., Teranishi, K. and Shimomura, O. (2000). The crystal structure of the photoprotein aequorin at 2.3 A resolution. *Nature* 405, 372-6.

Healy, J. I., Dolmetsch, R. E., Timmerman, L. A., Cyster, J. G., Thomas, M. L., Crabtree, G. R., Lewis, R. S. and Goodnow, C. C. (1997). Different nuclear signals are activated by the B cell receptor during positive versus negative signaling. *Immunity* 6, 419-28.

Higashijima, S. I., Masino, M. A., Mandel, G. and Fetcho, J. R. (2003). Imaging neuronal activity during zebrafish behavior with a genetically encoded calcium indicator. *J Neurophysiol.*

Hodges, D. and Bernstein, S. I. (1992). Suboptimal 5' and 3' splice sites regulate alternative splicing of Drosophila melanogaster myosin heavy chain transcripts in vitro. *Mech Dev* 37, 127-40.

Horiuchi, T., Giniger, E. and Aigaki, T. (2003). Alternative trans-splicing of constant and variable exons of a Drosophila axon guidance gene, lola. *Genes Dev* 17, 2496-501.

Hu, Z., Bonifas, J. M., Beech, J., Bench, G., Shigihara, T., Ogawa, H., Ikeda, S., Mauro, T. and Epstein, E. H., Jr. (2000). Mutations in ATP2C1, encoding a calcium pump, cause Hailey-Hailey disease. *Nat Genet* 24, 61-5.

Huesmann, G. R., Cheung, C. C., Loi, P. K., Lee, T. D., Swiderek, K. M. and Tublitz, N. J. (1995). Amino acid sequence of CAP2b, an insect cardioacceleratory peptide from the tobacco hawkmoth Manduca sexta. *FEBS Lett* 371, 311-4.

Ikura, M., Clore, G. M., Gronenborn, A. M., Zhu, G., Klee, C. B. and Bax, A. (1992). Solution structure of a calmodulin-target peptide complex by multidimensional NMR. *Science* 256, 632-8.

Inoue, T., Sullivan, F. X. and Cech, T. R. (1986). New reactions of the ribosomal RNA precursor of Tetrahymena and the mechanism of self-splicing. *J Mol Biol* 189, 143-65.

Isshiki, M., Ying, Y. S., Fujita, T. and Anderson, R. G. (2002). A molecular sensor detects signal transduction from caveolae in living cells. *J Biol Chem* 277, 43389-98.

Ito, K., Awano, W., Suzuki, K., Hiromi, Y. and Yamamoto, D. (1997). The Drosophila mushroom body is a quadruple structure of clonal units each of which contains a virtually

identical set of neurones and glial cells. *Development* **124**, 761-71.

Johnson, S., Michalak, M., Opas, M. and Eggleton, P. (2001). The ins and outs of calreticulin: from the ER lumen to the extracellular space. *Trends Cell Biol* **11**, 122-9.

Jones, J. T. and Sullenger, B. A. (1997). Evaluating and enhancing ribozyme reaction efficiency in mammalian cells. *Nat Biotechnol* **15**, 902-5.

Jouaville, L. S., Pinton, P., Bastianutto, C., Rutter, G. A. and Rizzuto, R. (1999). Regulation of mitochondrial ATP synthesis by calcium: evidence for a long-term metabolic priming. *Proc Natl Acad Sci U S A* **96**, 13807-12.

Jung, D. W., Baysal, K. and Brierley, G. P. (1995). The sodium-calcium antiport of heart mitochondria is not electroneutral. *J Biol Chem* **270**, 672-8.

Kalidas, S. and Smith, D. P. (2002). Novel genomic cDNA hybrids produce effective RNA interference in adult Drosophila. *Neuron* **33**, 177-84.

Kasai, H. and Augustine, G. J. (1990). Cytosolic Ca2+ gradients triggering unidirectional fluid secretion from exocrine pancreas. *Nature* **348**, 735-8.

Kean, L., Cazenave, W., Costes, L., Broderick, K. E., Graham, S., Pollock, V. P., Davies, S. A., Veenstra, J. A. and Dow, J. A. (2002). Two nitridergic peptides are encoded by the gene capability in Drosophila melanogaster. *Am J Physiol Regul Integr Comp Physiol* **282**, R1297-307.

Kendall, J. M., Sala-Newby, G., Ghalaut, V., Dormer, R. L. and Campbell, A. K. (1992). Engineering the CA(2+)-activated photoprotein aequorin with reduced affinity for calcium. *Biochem Biophys Res Commun* **187**, 1091-7.

Kendall, J. M., Dormer, R. L. and Campbell, A. K. (1992). Targeting aequorin to the endoplasmic reticulum of living cells. *Biochem Biophys Res Commun* **189**, 1008-16.

Kennerdell, J. R. and Carthew, R. W. (2000). Heritable gene silencing in Drosophila using double-stranded RNA. *Nat Biotechnol* **18**, 896-8.

Kerr, R., Lev-Ram, V., Baird, G., Vincent, P., Tsien, R. Y. and Schafer, W. R. (2000). Optical imaging of calcium transients in neurons and pharyngeal muscle of C. elegans. *Neuron* **26**, 583-94.

Kim, J. H., Johannes, L., Goud, B., Antony, C., Lingwood, C. A., Daneman, R. and Grinstein, S. (1998). Noninvasive measurement of the pH of the endoplasmic reticulum at rest and during calcium release. *Proc Natl Acad Sci U S A* **95**, 2997-3002.

Kirkpatrick, R. B., Ganguly, S., Angelichio, M., Griego, S., Shatzman, A., Silverman, C. and Rosenberg, M. (1995). Heavy chain dimers as well as complete antibodies are efficiently formed and secreted from Drosophila via a BiP-mediated pathway. *J Biol Chem* **270**, 19800-5.

Kiselyov, K., Xu, X., Mozhayeva, G., Kuo, T., Pessah, I., Mignery, G., Zhu, X., Birnbaumer, L. and Muallem, S. (1998). Functional interaction between InsP3 receptors and

175

store-operated Htrp3 channels. *Nature* **396**, 478-82.

Knight, M. R., Campbell, A. K., Smith, S. M. and Trewavas, A. J. (1991). Transgenic plant aequorin reports the effects of touch and cold-shock and elicitors on cytoplasmic calcium. *Nature* **352**, 524-6.

Koller, A., Snyder, W. B., Faber, K. N., Wenzel, T. J., Rangell, L., Keller, G. A. and Subramani, S. (1999). Pex22p of Pichia pastoris, essential for peroxisomal matrix protein import, anchors the ubiquitin-conjugating enzyme, Pex4p, on the peroxisomal membrane. *J Cell Biol* **146**, 99-112.

Kondylis, V., Goulding, S. E., Dunne, J. C. and Rabouille, C. (2001). Biogenesis of Golgi stacks in imaginal discs of Drosophila melanogaster. *Mol Biol Cell* **12**, 2308-27.

Kozak, M. (1989). Circumstances and mechanisms of inhibition of translation by secondary structure in eucaryotic mRNAs. *Mol Cell Biol* **9**, 5134-42.

Labrador, M. and Corces, V. G. (2003). Extensive exon reshuffling over evolutionary time coupled to trans-splicing in Drosophila. *Genome Res* **13**, 2220-8.

LaFerla, F. M. (2002). Calcium dyshomeostasis and intracellular signalling in Alzheimer's disease. *Nat Rev Neurosci* **3**, 862-72.

Lan, N., Howrey, R. P., Lee, S. W., Smith, C. A. and Sullenger, B. A. (1998). Ribozyme-mediated repair of sickle beta-globin mRNAs in erythrocyte precursors. *Science* **280**, 1593-6.

Lapinskas, P. J., Cunningham, K. W., Liu, X. F., Fink, G. R. and Culotta, V. C. (1995). Mutations in PMR1 suppress oxidative damage in yeast cells lacking superoxide dismutase. *Mol Cell Biol* **15**, 1382-8.

Li, B. L., Li, X. L., Duan, Z. J., Lee, O., Lin, S., Ma, Z. M., Chang, C. C., Yang, X. Y., Park, J. P., Mohandas, T. K. et al. (1999). Human acyl-CoA:cholesterol acyltransferase-1 (ACAT-1) gene organization and evidence that the 4.3-kilobase ACAT-1 mRNA is produced from two different chromosomes. *J Biol Chem* **274**, 11060-71.

Liang, F., Cunningham, K. W., Harper, J. F. and Sze, H. (1997). ECA1 complements yeast mutants defective in Ca2+ pumps and encodes an endoplasmic reticulum-type Ca2+-ATPase in Arabidopsis thaliana. *Proc Natl Acad Sci U S A* **94**, 8579-84.

Lin, P., Yao, Y., Hofmeister, R., Tsien, R. Y. and Farquhar, M. G. (1999). Overexpression of CALNUC (nucleobindin) increases agonist and thapsigargin releasable Ca2+ storage in the Golgi. *J Cell Biol* **145**, 279-89.

Liu, X., Jiang, Q., Mansfield, S. G., Puttaraju, M., Zhang, Y., Zhou, W., Cohn, J. A., Garcia-Blanco, M. A., Mitchell, L. G. and Engelhardt, J. F. (2002). Partial correction of endogenous DeltaF508 CFTR in human cystic fibrosis airway epithelia by spliceosome-mediated RNA trans-splicing. *Nat Biotechnol* **20**, 47-52.

Lukacsovich, T. and Yamamoto, D. (2001). Trap a gene and find out its function: toward functional genomics in Drosophila. *J Neurogenet* **15**, 147-68.

Lukacsovich, T., Asztalos, Z., Awano, W., Baba, K., Kondo, S., Niwa, S. and Yamamoto, D. (2001). Dual-tagging gene trap of novel genes in *Drosophila melanogaster*. *Genetics* **157**, 727-42.

Lytton, J., Westlin, M. and Hanley, M. R. (1991). Thapsigargin inhibits the sarcoplasmic or endoplasmic reticulum Ca-ATPase family of calcium pumps. *J Biol Chem* **266**, 17067-71.

MacDermott, A. B., Mayer, M. L., Westbrook, G. L., Smith, S. J. and Barker, J. L. (1986). NMDA-receptor activation increases cytoplasmic calcium concentration in cultured spinal cord neurones. *Nature* **321**, 519-22.

MacPherson, M. R., Pollock, V. P., Broderick, K. E., Kean, L., O'Connell, F. C., Dow, J. A. and Davies, S. A. (2001). Model organisms: new insights into ion channel and transporter function. L-type calcium channels regulate epithelial fluid transport in Drosophila melanogaster. *Am J Physiol Cell Physiol* **280**, C394-407.

Mandal, D., Woolf, T. B. and Rao, R. (2000). Manganese selectivity of pmr1, the yeast secretory pathway ion pump, is defined by residue gln783 in transmembrane segment 6. Residue Asp778 is essential for cation transport. *J Biol Chem* **275**, 23933-8.

Mandal, D., Rulli, S. J. and Rao, R. (2003). Packing interactions between transmembrane helices alter Ion selectivity of the yeast Golgi Ca2+/Mn2+-ATPase PMR1. *J Biol Chem*.

Mansfield, S. G., Kole, J., Puttaraju, M., Yang, C. C., Garcia-Blanco, M. A., Cohn, J. A. and Mitchell, L. G. (2000). Repair of CFTR mRNA by spliceosome-mediated RNA trans-splicing. *Gene Ther* **7**, 1885-95.

Mansfield, S. G., Clark, R. H., Puttaraju, M., Kole, J., Cohn, J. A., Mitchell, L. G. and Garcia-Blanco, M. A. (2003). 5' exon replacement and repair by spliceosome-mediated RNA trans-splicing. *Rna* **9**, 1290-7.

Martinek, S. and Young, M. W. (2000). Specific genetic interference with behavioral rhythms in Drosophila by expression of inverted repeats. *Genetics* **156**, 1717-25.

Matlib, M. A., Zhou, Z., Knight, S., Ahmed, S., Choi, K. M., Krause-Bauer, J., Phillips, R., Altschuld, R., Katsube, Y., Sperelakis, N. et al. (1998). Oxygen-bridged dinuclear ruthenium amine complex specifically inhibits Ca2+ uptake into mitochondria in vitro and in situ in single cardiac myocytes. *J Biol Chem* **273**, 10223-31.

Maune, J. F., Klee, C. B. and Beckingham, K. (1992). Ca2+ binding and conformational change in two series of point mutations to the individual Ca(2+)-binding sites of calmodulin. *J Biol Chem* **267**, 5286-95.

Mignen, O. and Shuttleworth, T. J. (2000). I(ARC), a novel arachidonate-regulated, noncapacitative Ca(2+) entry channel. *J Biol Chem* **275**, 9114-9.

Minke, B. and Cook, B. (2002). TRP channel proteins and signal transduction. *Physiol Rev* **82**, 429-72.

Minke, B. and Cook, B. (2002). TRP channel proteins and signal transduction. *Physiol Rev* **82**, 429-72.

Minta, A., Kao, J. P. and Tsien, R. Y. (1989). Fluorescent indicators for cytosolic calcium based on rhodamine and fluorescein chromophores. *J Biol Chem* **264**, 8171-8.

Missiaen, L., Vanoevelen, J., Van Acker, K., Raeymaekers, L., Parys, J. B., Callewaert, G., Wuytack, F. and De Smedt, H. (2002). Ca(2+) signals in Pmr1-GFP-expressing COS-1 cells with functional endoplasmic reticulum. *Biochem Biophys Res Commun* **294**, 249-53.

Mitchell, K. J., Pinton, P., Varadi, A., Tacchetti, C., Ainscow, E. K., Pozzan, T., Rizzuto, R. and Rutter, G. A. (2001). Dense core secretory vesicles revealed as a dynamic Ca(2+) store in neuroendocrine cells with a vesicle-associated membrane protein aequorin chimaera. *J Cell Biol* **155**, 41-51.

Miyawaki, A., Llopis, J., Heim, R., McCaffery, J. M., Adams, J. A., Ikura, M. and Tsien, R. Y. (1997). Fluorescent indicators for Ca2+ based on green fluorescent proteins and calmodulin. *Nature* **388**, 882-7.

Miyawaki, A., Griesbeck, O., Heim, R. and Tsien, R. Y. (1999). Dynamic and quantitative Ca2+ measurements using improved cameleons. *Proc Natl Acad Sci U S A* **96**, 2135-40.

Mogami, H., Tepikin, A. V. and Petersen, O. H. (1998). Termination of cytosolic Ca2+ signals: Ca2+ reuptake into intracellular stores is regulated by the free Ca2+ concentration in the store lumen. *Embo J* **17**, 435-42.

Montell, C., Birnbaumer, L. and Flockerzi, V. (2002). The TRP channels, a remarkably functional family. *Cell* **108**, 595-8.

Montero, M., Brini, M., Marsault, R., Alvarez, J., Sitia, R., Pozzan, T. and Rizzuto, R. (1995). Monitoring dynamic changes in free Ca2+ concentration in the endoplasmic reticulum of intact cells. *Embo J* **14**, 5467-75.

Montero, M., Alvarez, J., Scheenen, W. J., Rizzuto, R., Meldolesi, J. and Pozzan, T. (1997). Ca2+ homeostasis in the endoplasmic reticulum: coexistence of high and low [Ca2+] subcompartments in intact HeLa cells. *J Cell Biol* **139**, 601-11.

Montero, M., Barrero, M. J. and Alvarez, J. (1997). [Ca2+] microdomains control agonist-induced Ca2+ release in intact HeLa cells. *Faseb J* **11**, 881-5.

Montero, M., Alonso, M. T., Carnicero, E., Cuchillo-Ibanez, I., Albillos, A., Garcia, A. G., Garcia-Sancho, J. and Alvarez, J. (2000). Chromaffin-cell stimulation triggers fast millimolar mitochondrial Ca2+ transients that modulate secretion. *Nat Cell Biol* **2**, 57-61.

Morin, X., Daneman, R., Zavortink, M. and Chia, W. (2001). A protein trap strategy to detect GFP-tagged proteins expressed from their endogenous loci in Drosophila. *Proc Natl Acad Sci U S A* **98**, 15050-5.

Murphy, W. J., Watkins, K. P. and Agabian, N. (1986). Identification of a novel Y branch structure as an intermediate in trypanosome mRNA processing: evidence for trans splicing.

Cell 47, 517-25.

Nagai, T., Sawano, A., Park, E. S. and Miyawaki, A. (2001). Circularly permuted green fluorescent proteins engineered to sense Ca2+. *Proc Natl Acad Sci U S A* 98, 3197-202.

Nakai, K. and Horton, P. (1999). PSORT: a program for detecting sorting signals in proteins and predicting their subcellular localization. *Trends Biochem Sci* 24, 34-6.

Nakai, J., Ohkura, M. and Imoto, K. (2001). A high signal-to-noise Ca(2+) probe composed of a single green fluorescent protein. *Nat Biotechnol* 19, 137-41.

Nomura, M., Inouye, S., Ohmiya, Y. and Tsuji, F. I. (1991). A C-terminal proline is required for bioluminescence of the Ca(2+)-binding photoprotein, aequorin. *FEBS Lett* 295, 63-6.

O'Donnell, M. J. and Maddrell, S. H. (1995). Fluid reabsorption and ion transport by the lower Malpighian tubules of adult female Drosophila. *J Exp Biol* 198, 1647-53.

O'Donnell, M. J., Rheault, M. R., Davies, S. A., Rosay, P., Harvey, B. J., Maddrell, S. H., Kaiser, K. and Dow, J. A. (1998). Hormonally controlled chloride movement across Drosophila tubules is via ion channels in stellate cells. *Am J Physiol* 274, R1039-49.

O'Kane, C. J. and Gehring, W. J. (1987). Detection in situ of genomic regulatory elements in Drosophila. *Proc Natl Acad Sci U S A* 84, 9123-7.

Osipchuk, Y. V., Wakui, M., Yule, D. I., Gallacher, D. V. and Petersen, O. H. (1990). Cytoplasmic Ca2+ oscillations evoked by receptor stimulation, G-protein activation, internal application of inositol trisphosphate or Ca2+: simultaneous microfluorimetry and Ca2+ dependent Cl- current recording in single pancreatic acinar cells. *Embo J* 9, 697-704.

Parekh, A. B., Terlau, H. and Stuhmer, W. (1993). Depletion of InsP3 stores activates a Ca2+ and K+ current by means of a phosphatase and a diffusible messenger. *Nature* 364, 814-8.

Park, M. K., Petersen, O. H. and Tepikin, A. V. (2000). The endoplasmic reticulum as one continuous Ca(2+) pool: visualization of rapid Ca(2+) movements and equilibration. *Embo J* 19, 5729-39.

Park, M. K., Ashby, M. C., Erdemli, G., Petersen, O. H. and Tepikin, A. V. (2001). Perinuclear, perigranular and sub-plasmalemmal mitochondria have distinct functions in the regulation of cellular calcium transport. *Embo J* 20, 1863-74.

Petersen, O. H. (1992). Stimulus-secretion coupling: cytoplasmic calcium signals and the control of ion channels in exocrine acinar cells. *J Physiol* 448, 1-51.

Petersen, O. H., Burdakov, D. and Tepikin, A. V. (1999). Polarity in intracellular calcium signaling. *Bioessays* 21, 851-60.

Piccin, A., Salameh, A., Benna, C., Sandrelli, F., Mazzotta, G., Zordan, M., Rosato, E., Kyriacou, C. P. and Costa, R. (2001). Efficient and heritable functional knock-out of an

adult phenotype in Drosophila using a GAL4-driven hairpin RNA incorporating a heterologous spacer. *Nucleic Acids Res* **29**, E55-5.

Pinton, P., Pozzan, T. and Rizzuto, R. (1998). The Golgi apparatus is an inositol 1,4,5-trisphosphate-sensitive Ca2+ store, with functional properties distinct from those of the endoplasmic reticulum. *Embo J* **17**, 5298-308.

Pinton, P., Tsuboi, T., Ainscow, E. K., Pozzan, T., Rizzuto, R. and Rutter, G. A. (2002). Dynamics of glucose-induced membrane recruitment of protein kinase C beta II in living pancreatic islet beta-cells. *J Biol Chem* **277**, 37702-10.

Pitter, J. G., Maechler, P., Wollheim, C. B. and Spat, A. (2002). Mitochondria respond to Ca2+ already in the submicromolar range: correlation with redox state. *Cell Calcium* **31**, 97-104.

Pollock, V. P., Radford, J. C., Pyne, S., Hasan, G., Dow, J. A. and Davies, S. A. (2003). norpA and itpr mutants reveal roles for phospholipase C and inositol (1,4,5)- trisphosphate receptor in Drosophila melanogaster renal function. *J Exp Biol* **206**, 901-911.

Powell, J. T. and Brew, K. (1976). A comparison of the interactions of galactosyltransferase with a glycoprotein substrate (Ovalbumin) and with alpha-lactalbumin. *J Biol Chem* **251**, 3653-63.

Prasher, D., McCann, R. O. and Cormier, M. J. (1985). Cloning and expression of the cDNA coding for aequorin, a bioluminescent calcium-binding protein. *Biochem Biophys Res Commun* **126**, 1259-68.

Prasher, D. C., Eckenrode, V. K., Ward, W. W., Prendergast, F. G. and Cormier, M. J. (1992). Primary structure of the Aequorea victoria green-fluorescent protein. *Gene* **111**, 229-33.

Putney, J. W., Jr. (1986). A model for receptor-regulated calcium entry. *Cell Calcium* **7**, 1-12.

Putney, J. W., Jr. (1987). Formation and actions of calcium-mobilizing messenger, inositol 1,4,5-trisphosphate. *Am J Physiol* **252**, G149-57.

Puttaraju, M., Jamison, S. F., Mansfield, S. G., Garcia-Blanco, M. A. and Mitchell, L. G. (1999). Spliceosome-mediated RNA trans-splicing as a tool for gene therapy. *Nat Biotechnol* **17**, 246-52.

Puttaraju, M., DiPasquale, J., Baker, C. C., Mitchell, L. G. and Garcia-Blanco, M. A. (2001). Messenger RNA repair and restoration of protein function by spliceosome-mediated RNA trans-splicing. *Mol Ther* **4**, 105-14.

Radford, J. C., Davies, S. A. and Dow, J. A. (2002). Systematic G-protein-coupled receptor analysis in Drosophila melanogaster identifies a leucokinin receptor with novel roles. *J Biol Chem* **277**, 38810-7.

Randriamampita, C. and Tsien, R. Y. (1993). Emptying of intracellular Ca2+ stores releases

a novel small messenger that stimulates Ca2+ influx. *Nature* **364**, 809-14.

Reinhardt, T. A., Filoteo, A. G., Penniston, J. T. and Horst, R. L. (2000). Ca(2+)-ATPase protein expression in mammary tissue. *Am J Physiol Cell Physiol* **279**, C1595-602.

Reiter, L. T., Potocki, L., Chien, S., Gribskov, M. and Bier, E. (2001). A systematic analysis of human disease-associated gene sequences in Drosophila melanogaster. *Genome Res* **11**, 1114-25.

Rizzuto, R., Simpson, A. W., Brini, M. and Pozzan, T. (1992). Rapid changes of mitochondrial Ca2+ revealed by specifically targeted recombinant aequorin. *Nature* **358**, 325-7.

Rizzuto, R., Brini, M., Murgia, M. and Pozzan, T. (1993). Microdomains with high Ca2+ close to IP3-sensitive channels that are sensed by neighboring mitochondria. *Science* **262**, 744-7.

Rizzuto, R., Pinton, P., Carrington, W., Fay, F. S., Fogarty, K. E., Lifshitz, L. M., Tuft, R. A. and Pozzan, T. (1998). Close contacts with the endoplasmic reticulum as determinants of mitochondrial Ca2+ responses. *Science* **280**, 1763-6.

Robert, V., De Giorgi, F., Massimino, M. L., Cantini, M. and Pozzan, T. (1998). Direct monitoring of the calcium concentration in the sarcoplasmic and endoplasmic reticulum of skeletal muscle myotubes. *J Biol Chem* **273**, 30372-8.

Rogers, C. S., Vanoye, C. G., Sullenger, B. A. and George, A. L., Jr. (2002). Functional repair of a mutant chloride channel using a trans-splicing ribozyme. *J Clin Invest* **110**, 1783-9.

Rong, Y. S. and Golic, K. G. (2000). Gene targeting by homologous recombination in Drosophila. *Science* **288**, 2013-8.

Rong, Y. S. and Golic, K. G. (2001). A targeted gene knockout in Drosophila. *Genetics* **157**, 1307-12.

Rong, Y. S. (2002). Gene targeting by homologous recombination: a powerful addition to the genetic arsenal for Drosophila geneticists. *Biochem Biophys Res Commun* **297**, 1-5.

Rorth, P. (1996). A modular misexpression screen in Drosophila detecting tissue-specific phenotypes. *Proc Natl Acad Sci U S A* **93**, 12418-22.

Rorth, P., Szabo, K., Bailey, A., Laverty, T., Rehm, J., Rubin, G. M., Weigmann, K., Milan, M., Benes, V., Ansorge, W. et al. (1998). Systematic gain-of-function genetics in Drosophila. *Development* **125**, 1049-57.

Rosay, P., Davies, S. A., Yu, Y., Sozen, A., Kaiser, K. and Dow, J. A. (1997). Cell-type specific calcium signalling in a Drosophila epithelium. *J Cell Sci* **110 (Pt 15)**, 1683-92.

Rosay, P., Armstrong, J. D., Wang, Z. and Kaiser, K. (2001). Synchronized neural activity in the Drosophila memory centers and its modulation by amnesiac. *Neuron* **30**, 759-70.

Rubin, G. M. and Spradling, A. C. (1982). Genetic transformation of Drosophila with transposable element vectors. *Science* **218**, 348-53.

Rubin, G. M. (1988). Drosophila melanogaster as an experimental organism. *Science* **240**, 1453-9.

Rubin, G. M. and Lewis, E. B. (2000). A brief history of Drosophila's contributions to genome research. *Science* **287**, 2216-8.

Sakuntabhai, A., Ruiz-Perez, V., Carter, S., Jacobsen, N., Burge, S., Monk, S., Smith, M., Munro, C. S., O'Donovan, M., Craddock, N. et al. (1999). Mutations in ATP2A2, encoding a Ca2+ pump, cause Darier disease. *Nat Genet* **21**, 271-7.

Sandermann, H., Jr. and Strominger, J. L. (1972). Purification and properties of C 55 - isoprenoid alcohol phosphokinase from Staphylococcus aureus. *J Biol Chem* **247**, 5123-31.

Shimomura, O., Johnson, F. H. and Saiga, Y. (1962). Extraction, purification and properties of aequorin, a bioluminescent protein from the luminous hydromedusan, Aequorea. *J Cell Comp Physiol* **59**, 223-39.

Shimomura, O., Kishi, Y. and Inouye, S. (1993). The relative rate of aequorin regeneration from apoaequorin and coelenterazine analogues. *Biochem J* **296** (Pt 3), 549-51.

Smiley, S. T., Reers, M., Mottola-Hartshorn, C., Lin, M., Chen, A., Smith, T. W., Steele, G. D., Jr. and Chen, L. B. (1991). Intracellular heterogeneity in mitochondrial membrane potentials revealed by a J-aggregate-forming lipophilic cation JC-1. *Proc Natl Acad Sci U S A* **88**, 3671-5.

Somlyo, A. P., Urbanics, R., Vadasz, G., Kovach, A. G. and Somlyo, A. V. (1985). Mitochondrial calcium and cellular electrolytes in brain cortex frozen in situ: electron probe analysis. *Biochem Biophys Res Commun* **132**, 1071-8.

Sorin, A., Rosas, G. and Rao, R. (1997). PMR1, a Ca2+-ATPase in yeast Golgi, has properties distinct from sarco/endoplasmic reticulum and plasma membrane calcium pumps. *J Biol Chem* **272**, 9895-901.

Sozen, M. A., Armstrong, J. D., Yang, M., Kaiser, K. and Dow, J. A. (1997). Functional domains are specified to single-cell resolution in a Drosophila epithelium. *Proc Natl Acad Sci U S A* **94**, 5207-12.

Spradling, A. C. and Rubin, G. M. (1982). Transposition of cloned P elements into Drosophila germ line chromosomes. *Science* **218**, 341-7.

Srinivas, S. P., Ong, A., Goon, L. and Bonanno, J. A. (2002). Lysosomal Ca(2+) stores in bovine corneal endothelium. *Invest Ophthalmol Vis Sci* **43**, 2341-50.

Sudbrak, R., Brown, J., Dobson-Stone, C., Carter, S., Ramser, J., White, J., Healy, E., Dissanayake, M., Larregue, M., Perrussel, M. et al. (2000). Hailey-Hailey disease is caused by mutations in ATP2C1 encoding a novel Ca(2+) pump. *Hum Mol Genet* **9**, 1131-40.

Sullenger, B. A. and Cech, T. R. (1994). Ribozyme-mediated repair of defective mRNA by targeted, trans-splicing. *Nature* **371**, 619-22.

Tavernarakis, N., Wang, S. L., Dorovkov, M., Ryazanov, A. and Driscoll, M. (2000). Heritable and inducible genetic interference by double-stranded RNA encoded by transgenes. *Nat Genet* **24**, 180-3.

Terhzaz, S., O'Connell, F. C., Pollock, V. P., Kean, L., Davies, S. A., Veenstra, J. A. and Dow, J. A. (1999). Isolation and characterization of a leucokinin-like peptide of Drosophila melanogaster. *J Exp Biol* **202** **Pt 24**, 3667-76.

Thompson, J. D., Higgins, D. G. and Gibson, T. J. (1994). CLUSTAL W: improving the sensitivity of progressive multiple sequence alignment through sequence weighting, position-specific gap penalties and weight matrix choice. *Nucleic Acids Res* **22**, 4673-80.

Thummel, C. S., Boulet, A. M. and Lipshitz, H. D. (1988). Vectors for Drosophila P-element-mediated transformation and tissue culture transfection. *Gene* **74**, 445-56.

Ton, V. K., Mandal, D., Vahadji, C. and Rao, R. (2002). Functional expression in yeast of the human secretory pathway Ca(2+), Mn(2+)-ATPase defective in Hailey-Hailey disease. *J Biol Chem* **277**, 6422-7.

Toyoshima, C., Nakasako, M., Nomura, H. and Ogawa, H. (2000). Crystal structure of the calcium pump of sarcoplasmic reticulum at 2.6 A resolution. *Nature* **405**, 647-55.

Toyoshima, C. and Nomura, H. (2002). Structural changes in the calcium pump accompanying the dissociation of calcium. *Nature* **418**, 605-11.

Truong, K., Sawano, A., Mizuno, H., Hama, H., Tong, K. I., Mal, T. K., Miyawaki, A. and Ikura, M. (2001). FRET-based in vivo Ca2+ imaging by a new calmodulin-GFP fusion molecule. *Nat Struct Biol* **8**, 1069-73.

Tsien, R. Y. (1980). New calcium indicators and buffers with high selectivity against magnesium and protons: design, synthesis, and properties of prototype structures. *Biochemistry* **19**, 2396-404.

Tsien, R. Y. (1981). A non-disruptive technique for loading calcium buffers and indicators into cells. *Nature* **290**, 527-8.

Tsien, R. Y., Pozzan, T. and Rink, T. J. (1982). Calcium homeostasis in intact lymphocytes: cytoplasmic free calcium monitored with a new, intracellularly trapped fluorescent indicator. *J Cell Biol* **94**, 325-34.

Valera, S., Hussy, N., Evans, R. J., Adami, N., North, R. A., Surprenant, A. and Buell, G. (1994). A new class of ligand-gated ion channel defined by P2x receptor for extracellular ATP. *Nature* **371**, 516-9.

Van Baelen, K., Vanoevelen, J., Missiaen, L., Raeymaekers, L. and Wuytack, F. (2001). The Golgi PMR1 P-type ATPase of Caenorhabditis elegans. Identification of the gene and demonstration of calcium and manganese transport. *J Biol Chem* **276**, 10683-91.

Vashist, S., Frank, C. G., Jakob, C. A. and Ng, D. T. (2002). Two distinctly localized p-type ATPases collaborate to maintain organelle homeostasis required for glycoprotein processing and quality control. *Mol Biol Cell* **13**, 3955-66.

Veenstra, J. A. (2000). Mono- and dibasic proteolytic cleavage sites in insect neuroendocrine peptide precursors. *Arch Insect Biochem Physiol* **43**, 49-63.

Vizeacoumar, F. J., Torres-Guzman, J. C., Tam, Y. Y., Aitchison, J. D. and Rachubinski, R. A. (2003). YHR150w and YDR479c encode peroxisomal integral membrane proteins involved in the regulation of peroxisome number, size, and distribution in Saccharomyces cerevisiae. *J Cell Biol* **161**, 321-32.

Wang, L. and Wessler, S. R. (2001). Role of mRNA secondary structure in translational repression of the maize transcriptional activator Lc(1,2). *Plant Physiol* **125**, 1380-7.

Wang, J. W., Wong, A. M., Flores, J., Vosshall, L. B. and Axel, R. (2003). Two-photon calcium imaging reveals an odor-evoked map of activity in the fly brain. *Cell* **112**, 271-82.

Watanabe, T. and Sullenger, B. A. (2000). Induction of wild-type p53 activity in human cancer cells by ribozymes that repair mutant p53 transcripts. *Proc Natl Acad Sci U S A* **97**, 8490-4.

Watkins, N. J. and Campbell, A. K. (1993). Requirement of the C-terminal proline residue for stability of the Ca(2+)-activated photoprotein aequorin. *Biochem J* **293 (Pt 1)**, 181-5.

Wei, Y., Marchi, V., Wang, R. and Rao, R. (1999). An N-terminal EF hand-like motif modulates ion transport by Pmr1, the yeast Golgi Ca(2+)/Mn(2+)-ATPase. *Biochemistry* **38**, 14534-41.

Wei, Y., Chen, J., Rosas, G., Tompkins, D. A., Holt, P. A. and Rao, R. (2000). Phenotypic screening of mutations in Pmr1, the yeast secretory pathway Ca2+/Mn2+-ATPase, reveals residues critical for ion selectivity and transport. *J Biol Chem* **275**, 23927-32.

Weiss, J. L. and Burgoyne, R. D. (2002). Sense and sensibility in the regulation of voltage-gated Ca(2+) channels. *Trends Neurosci* **25**, 489-91.

Wiebel, F. F. and Kunau, W. H. (1992). The Pas2 protein essential for peroxisome biogenesis is related to ubiquitin-conjugating enzymes. *Nature* **359**, 73-6.

Wieczorek, H., Putzenlechner, M., Zeiske, W. and Klein, U. (1991). A vacuolar-type proton pump energizes K+/H+ antiport in an animal plasma membrane. *J Biol Chem* **266**, 15340-7.

Wodarz, A., Hinz, U., Engelbert, M. and Knust, E. (1995). Expression of crumbs confers apical character on plasma membrane domains of ectodermal epithelia of Drosophila. *Cell* **82**, 67-76.

Wuytack, F., Raeymaekers, L. and Missiaen, L. (2002). Molecular physiology of the SERCA and SPCA pumps. *Cell Calcium* **32**, 279-305.

Wuytack, F., Raeymaekers, L. and Missiaen, L. (2003). PMR1/SPCA Ca2+ pumps and the role of the Golgi apparatus as a Ca2+ store. *Pflugers Arch* **446**, 148-53.

Xu, X. Z., Li, H. S., Guggino, W. B. and Montell, C. (1997). Coassembly of TRP and TRPL produces a distinct store-operated conductance. *Cell* **89**, 1155-64.

Xu, C., Rice, W. J., He, W. and Stokes, D. L. (2002). A structural model for the catalytic cycle of Ca(2+)-ATPase. *J Mol Biol* **316**, 201-11.

Yagodin, S., Pivovarova, N. B., Andrews, S. B. and Sattelle, D. B. (1999). Functional characterization of thapsigargin and agonist-insensitive acidic Ca2+ stores in Drosophila melanogaster S2 cell lines. *Cell Calcium* **25**, 429-38.

Yoon, J., Ben-Ami, H. C., Hong, Y. S., Park, S., Strong, L. L., Bowman, J., Geng, C., Baek, K., Minke, B. and Pak, W. L. (2000). Novel mechanism of massive photoreceptor degeneration caused by mutations in the trp gene of Drosophila. *J Neurosci* **20**, 649-59.

Yu, D., Baird, G. S., Tsien, R. Y. and Davis, R. L. (2003). Detection of calcium transients in Drosophila mushroom body neurons with camgaroo reporters. *J Neurosci* **23**, 64-72.

Zha, X., Chandra, S., Ridsdale, A. J. and Morrison, G. H. (1995). Golgi apparatus is involved in intracellular Ca2+ regulation in epithelial LLC-PK1 cells. *Am J Physiol* **268**, C1133-40.

Zhao, J. J. and Pick, L. (1993). Generating loss-of-function phenotypes of the fushi tarazu gene with a targeted ribozyme in Drosophila. *Nature* **365**, 448-51.

Zimmerman, A. N. and Hulsmann, W. C. (1966). Paradoxical influence of calcium ions on the permeability of the cell membranes of the isolated rat heart. *Nature* **211**, 646-7.